THE LIGHTHILL CORRECTION TO THE MORISON EQUATION

by

Graham Ross Cook

A dissertation submitted to The Johns Hopkins University in conformity with the requirements for the degree of Doctor of Philosophy

Baltimore, Maryland

1987

ABSTRACT

THE LIGHTHILL CORRECTION TO THE MORISON EQUATION

When a hydrodynamic flow field is known, the in-line force on a submerged slender structural element is usually calculated using the Morison equation. According to this expression the total in-line force consists of two components: an inertia force of potential origin and a drag force due to viscosity effects.

Primarily, this report investigates a second order correction term to the Morison equation that is of potential origin and was proposed by Sir James Lighthill. This correction is due to the horizontal gradient of the in-line velocity, which causes the dynamic pressure to vary around the cylinder. The Lighthill correction is derived theoretically for the condition of finite water depth.

Two sets of data were used to determine the effect of the Lighthill correction quantitatively. The first set consisted of periodic wave data and the second set consisted of random wave data. Each set of data was analyzed to evaluate the drag and inertia coefficients used to calibrate the Morison equation and also to determine the effect of the Lighthill correction. It was found that the inertia coefficients based on the measured flow properties were in some cases significantly greater than the ideal potential flow value of 2.0. The theoretical calculation of the force coefficients was investigated for low Keulegan-Carpenter numbers, but it was found that the normally adopted procedure of

linearizing the boundary layer equation used in this calculation was not applicable for conditions experienced in these tests, and in general appears not to be applicable to ocean data. From the analysis of both the periodic and the random data it was found that the addition of the Lighthill correction term did not improve the Morison equation significantly; in most cases the Morison equation without the Lighthill correction provided a better fit to the measured forces.

Another correction, due to flow separation effects and based on Sarpkaya's 1981 work, is also investigated. The analysis suggests that a correction of the Sarpkaya type can be useful as a curve fitting device to improve the fit of the Morison equation to any given set of measured data.

BIOGRAPHICAL SKETCH

The author was born on September 21, 1954 in Melbourne, Australia. He graduated from Niddrie High School in December 1972.

In February 1973 the author started his studies in the Department of Civil Engineering at Footscray Institute of Technology. In December 1976 he graduated with a Bachelor of Engineering (Civil) with Distinction and won an award for obtaining the highest aggregate marks in the final year. In March 1977 he started his graduate studies at Melbourne University. In November 1978 he was awarded the degree of Master of Engineering Science with a major in Structural Engineering and a minor in Fluid Dynamics.

The author then worked at Melbourne University for one year as a Research Engineer. He then spent three years as a Design Engineer in a consulting office and one year as a Research Officer in a research organisation.

In September 1984 the author began his Ph.D. studies at The Johns Hopkins University studying Structural Engineering. His research for the Ph.D. degree was carried out while the author was both a Teaching Assistant at Johns Hopkins and a Guest Worker at the National Bureau of Standards in Gaithersburg, Maryland. All requirements for the degree were completed in August 1987.

ACKNOWLEDGEMENTS

The author is proud to have studied under Dr. Emil Simiu who served as his thesis advisor at the National Bureau of Standards (NBS). His sound advice, technical thoroughness, logical thinking and friendship are deeply appreciated.

Sincere thanks are extended to Professor Robert H. Scanlan, for providing guidance and encouragement throughout the author's time at Johns Hopkins.

Thanks are also due to the following establishments or people:
(i) The Delft Hydraulics Laboratory in the Netherlands which supplied the random data analysed by the author. The author would like to especially thank Mr. Jan Kostense of DHL for help in obtaining the data and his kind and effective cooperation.
(ii) Geraldine Dalton of NBS who translated the Delft tapes into a format that could be read on the NBS mainframe,
(iii) The Naval Civil Engineering Laboratory at Port Hueneme, California, and Mr. Jerry Dummer, who provided the periodic data analysed by the author.
(iv) Mr. Charles E. Smith, Research Program Manager, Technology Assessment and Research Branch, Minerals Management Service, U.S. Department of the Interior, which provided partial support for the work.

The author especially appreciates the continuing support and encouragement of his family in Australia. Their continuous presence in mind, if not body, was always a great help. In particular, thanks are due to the author's mother for the many years she gave to him. This thesis is dedicated to her as a small token of the author's gratitude.

This research and the author's Ph.D. studies at The Johns Hopkins University were funded by both Johns Hopkins and the National Bureau of Standards.

TABLE OF CONTENTS

LIST OF TABLES

LIST OF FIGURES

CHAPTER ONE

INTRODUCTION

Over the past fifteen years offshore platforms have increased by an order of magnitude in their size, complexity and cost. The loading imposed on slender cylindrical members of an offshore structure, subjected to forces induced by wave and current, represents one of the major design considerations and has been the focus of extensive experimental and theoretical research over the past 35 years.

Firstly, to evaluate the flow-induced forces on a structure it is required to know the surrounding hydrodynamic flow field. Once the appropriate flow field is defined the in-line force on a slender cylinder is usually calculated by using the well-known Morison equation.

According to this expression, proposed by Morison, O'Brien, Johnson and Schaaf in 1950, the total in-line force on a cylinder immersed in a fluctuating flow consists of two components: an inertia force, due to the effects of irrotational (potential) flow, and a drag force, due to viscosity (skin friction and flow separation) effects. The inertia force is analogous to the force a body experiences in uniformly accelerated flow, and is assumed to be proportional to the flow acceleration. The drag force is analogous to the drag on a body subjected to a steady flow and is assumed to be proportional to the square of the time dependent flow velocity, where the force has the same direction as the velocity.

The Morison equation is calibrated with two empirical coefficients which are referred to as the inertia and drag coefficient and which are functions of the flow conditions. A great deal of work, both theoretical and experimental, briefly reviewed in Chapter Two, has been performed to determine the values of the inertia and drag coefficients, and to seek possible improvements to the Morison equation. There appears to be a consensus that the Morison equation, though imperfect, is a good point of departure for modeling the hydrodynamic forces on cylinders, and that it would be better to improve the equation with correction terms rather than devise a completely new one.

Keulegan and Carpenter (1958) were the first researchers to propose a correction to the Morison equation. An analysis similar to but more elaborate than that of Keulegan and Carpenter was reported recently by Sarpkaya (1981a, 1981b). The corrections of Keulegan and Carpenter and Sarpkaya are aimed essentially at accounting for vorticity effects. It is only recently that the question of corrections associated with irrotational (potential) flow effects was raised. In his keynote address to the 1979 Conference on the Behaviour of Offshore Structures (BOSS), Sir James Lighthill showed that the force associated with the irrotational flow includes, in addition to the linear inertia term of the Morison equation, a nonlinear effect of potential origin due to the extensional motion (that is, the horizontal gradient of the the in-line component of the flow velocity). We refer to this effect as the Lighthill correction. Lighthill also noted that if the total force on a cylinder is expressed as a sum of the two

Morison equation terms only, then the Lighthill force, which is due to potential flow effects, is automatically incorporated into the nonlinear drag term, which is purportedly due solely to viscosity effects. Therefore, the Morison equation leads to an erroneous estimation of the force due to viscosity. The degree to which the error is significant depends upon the ratio between the Lighthill force and the actual Morison component associated with viscosity effects. This latter component is responsible for the bulk of the damping that controls the dynamic response of compliant offshore structures to fluctuating wind [Simiu and Leigh (1983) and Cook et al. (1986)]. The question of the extent to which corrections of the Lighthill type might affect the estimation of this component is therefore of significant practical interest in this context, and this provided the initial motivation for this work.

The primary object of this work is to investigate the significance of the Lighthill correction in quantitative terms. In Lighthill (1979) the theoretical developments pertaining to the Lighthill correction are presented for the case of flows with infinite water depths. Since the data used in this work for the quantitative assessment of the Lighthill correction are characterized by relatively high wave-height to water-depth ratios, derivations of the expression for the Lighthill correction in flows of finite depth are presented in Chapter Three. Also, Chapter Three presents the developments concerned with corrections for the effect of flow separation, along the lines of Sarpkaya's 1981 work.

Three sets of data were obtained for the purpose of investigating the quantitative significance of the Lighthill

correction. The first set was provided by the Naval Civil Engineering Laboratory (NCEL), and consisted of periodic flow force and flow measurements obtained in a wave tank. A second set was provided by the Delft Hydraulics Laboratory (DHL), and consisted of force and flow measurements obtained in a wave tank under random wave flow conditions. The third set consisted of full scale data obtained at the Christchurch Bay installation by the British Maritime Technology (BMT). Because the BMT data were not sufficiently complete to allow a conclusive analysis to be performed, they were not used in the investigation of the Lighthill correction. The experimental setup and data sets listed above are described in Chapter Four.

Chapters Five and Six, respectively, evaluate the magnitude of the Lighthill correction for both the NCEL and DHL data. In the case of the NCEL data, which corresponds to periodic wave flow, the variation of the the inertia and drag coefficients is investigated. In addition corrections for flow separation effects of the type described by Sarpkaya (1981a, 1981b) are evaluated and commented on. Because the Sarpkaya correction can be calculated only for periodic flows, it was not applicable to the DHL data.

Chapter Seven summarizes the main conclusions and discusses future work that is required to obtain a more complete answer to the wave loading problem.

CHAPTER TWO

LITERATURE REVIEW

2.1 Introduction

In the reviews on the fluid induced loadings on structural members [Hogben et al. (1977), Sarpkaya and Isaacson (1981), Wilson (1984), and McCormick (1973)] the process of finding the wave forces involves two distinct stages. The first stage is the description of the wave environment whereby the flow properties can either be measured or calculated using an appropriate wave theory. The second stage involves relating these wave flow properties to the forces acting on a body. This literature review deals with the broad subjects of waves and wave hydrodynamics before trying to describe the more specialized area of fluid loading.

A considerable amount of work has been done in theoretically describing the flow properties of wave motion. The theories vary from the relatively simple linear theory which gives approximate solutions and can be readily applied, to the more complex higher order theories, which lead to more accurate results but are computationally more involved.

The loading on structural elements has been of considerable interest since the first offshore facility was proposed. Morison et al. (1950) proposed a simple formula expressing the total force as the sum of a drag and inertia component with two semi-empirical coefficients calibrating the formula. Since then a substantial

amount of work has been done on evaluating the two empirical coefficients in the Morison equation.

The Morison equation has been criticized as oversimplifying the fluid mechanics of the loading but an alternative rigorous approach has not been developed to date. To represent the fluid mechanics more closely, rather than suggesting a completely new relationship, various authors have proposed the addition of correction terms to the Morison equation [for example, Lighthill (1979) and Sarpkaya (1981a, 1981b)]. This chapter reviews wave hydrodynamic fundamentals relevant to the application of the Morison equation; discusses the Morison equation and its limitations; describes experimental and theoretical work aimed at determining the Morison equation coefficients; reviews information on the treatment of the wave loading problem under random flow conditions and in the presence of current; and summarizes contributions by Lighthill (1979) and Sarpkaya (1981a, 1981b) on correction terms aimed at improving the Morison equation.

2.2 Wave Hydrodynamics

The pioneering work in wave hydrodynamics occurred in the latter half of the nineteenth century. The linear wave theory was first introduced in 1845 and in 1847 Stokes wrote an important paper (reprinted with a supplement in 1880) treating the subject in more detail.

Stokes assumed that the waves propagate with a constant velocity, without change of form and that the motion could be

described in two dimensions. It was further assumed that the fluid was homogeneous, incompressible, inviscid and of uniform depth.

The motion, being assumed to have been generated from rest, was set out as a solution of the Laplace equation (continuity equation) subject to a number of boundary conditions throughout the fluid. The first boundary condition is at the rigid bottom, on which the fluid sits, and imposes a no vertical flow condition on the fluid. Two further boundary conditions are applied at the free surface. One condition states that the fluid particles initially at the surface continue to be at the free surface throughout the motion. The other is that the pressure at the free surface, expressed in terms of Bernoulli's equation, is equal to the atmospheric pressure. These three boundary conditions are known as the bottom, kinematic free surface and dynamic free surface boundary conditions, respectively.

The problem was initially solved to first order by neglecting the slope of the free surface, as well as the velocity squared terms in Bernoulli's equation. In addition, due to the assumption of small amplitude waves the free surface boundary conditions were applied at the still water level rather than at the unknown free surface. This analysis is commonly known as small amplitude or linear wave theory. The derived velocity potential gives the result that the particles travel in closed elliptic orbits where the ellipticity depends upon the depth of the water (for example, in deep water the particle orbits are circular and in shallow water the orbits are ellipses) where the ratio of major axis to minor axis increases with decreasing depth. The boundary conditions yield

the dispersion relation which shows that the wave speed (the celerity, $c = \omega/k$) is a function of the wavenumber and water depth but is independent of the wave height. The linear theory forms the basis of ocean engineering practice as it is simple to apply and can be used for all water depths, whereas other theories generally only apply over limited depths. Stokes extended his analysis to the second order by substituting the first order result into the previously neglected second order terms. The free surface boundary conditions were applied at the actual free surface by expanding the actual conditions about the still water level using a Taylor series expansion, that is,

$$\phi(z) = 0 \qquad \text{at } z = \eta \qquad 2.1$$

may be expanded to

$$\phi(z) + \eta \frac{\partial \phi}{\partial z} + \frac{1}{2!} \eta^2 \frac{\partial^2 \phi}{\partial z^2} + \ldots = 0 \qquad \text{at } z = 0 \qquad 2.2$$

where $\phi(z)$ is the velocity potential a vertical distance z from the still water level and η is the vertical distance of the free surface from the still water level. The second order solution consists of the first order solution and a second order term with frequency equal to twice the frequency of the first order term. The second order solution has the same dispersion relation as the first order solution but instead of the fluid orbits being closed there is a gradual drift in the positive x direction.

By introducing a perturbation assumption where all the variables can be expanded in a perturbation parameter it is possible to extend the analysis to any higher order of approximation. However, at higher orders the analysis involves

increasingly lengthy mathematics. Skjelbreia and Hendrickson (1960) have given the Stokes expansion to the fifth order and explicit expressions for the coefficients are given in tabular form for various depth to wavelength ratios.

One problem with the Stokes expansion is the non-convergence of the series for steeper waves. Schwartz (1974) reformulated the problem using expansion variables different from those adopted by Stokes. He then obtained an accurate solution to the steep wave case using a computer to perform the requisite algebraic operations.

Korteweg and deVries (1895) developed the cnoidal wave theory, which is applicable to shallow water. Wave parameters are formulated in terms of the Jacobian elliptic function (cn) hence the term "cnoidal". A limiting case of the cnoidal wave corresponds to the case where the wavelength approaches infinity. This leads to the solitary wave which was first studied mathematically by Rayleigh (1876). Other wave theories include the linearized long wave theory [Gerstner (1802)] and the Stream Function Theory [Dean (1965)]. All these theories are discussed in considerable detail in Sarpkaya and Isaacson (1981).

A wave theory must be chosen so that it is appropriate to the wave conditions under consideration. LeMehaute (1969, 1976) produced a plot, see Figure 2.1 , that shows the approximate range of validity of various wave theories. The graph is not based on any quantitative investigation but can be helpful in initial calculations to determine whether a simple theory, such as linear theory, can be used.

2.3 Hydrodynamic Loads

2.3.1 The Morison Equation

The Morison equation [Morison et al. (1950)] is widely used in ocean engineering as an expression for wave-induced forces on structural members. In 1950 Morison et al. wrote: "The force exerted by unbroken surface waves on a cylindrical object, such as a pile, which extends from the bottom upward above the wave crest, is made up of two components, namely:

1. A drag force proportional to the square of the velocity which may be represented by a drag coefficient having substantially the same value as for steady flow, and
2. A virtual mass force proportional to the horizontal component of the acceleration force exerted on the mass of water displaced by the pile. These relationships follow directly from wave theory and have been confirmed by measurements in the Fluid Mechanics Laboratory of the University of California, Berkeley." The authors proposed the following expression for the force exerted on a differential section, dz in length,

$$dF = \left[Cm \frac{\rho \pi D^2}{4} \frac{\partial u}{\partial t} \pm Cd \frac{\rho D}{2} u^2\right] dz \qquad 2.3$$

where D = pile diameter

ρ = water mass density

Cm = coefficient of mass

Cd = coefficient of drag

u = horizontal component of the fluid velocity

$\partial u/\partial t$ = local acceleration of the water particle

The term u^2 was later changed to $u|u|$ to take into account the fact that the drag force is acting in the direction of the fluid velocity. Further generalization replaced the term $\pi D^2/4$ by a displaced volume per unit length V, and the term D by a projected frontal area per unit length A. Some authors have proposed the use in the Morison equation of the total acceleration of the flow

$$\frac{du}{dt} = \frac{\partial u}{\partial t} + u\frac{\partial u}{\partial x} + v\frac{\partial u}{\partial y} + w\frac{\partial u}{\partial z} \qquad 2.4$$

or in two dimensional flow

$$\frac{du}{dt} = \frac{\partial u}{\partial t} + u\frac{\partial u}{\partial x} + w\frac{\partial u}{\partial z} \qquad 2.5$$

in lieu of the local acceleration $\partial u/\partial t$.

To first and second order respectively, equation 2.5 becomes

$$\frac{du_1}{dt} = \frac{\partial u_1}{\partial t} \qquad 2.6$$

$$\frac{du_2}{dt} = \frac{\partial u_2}{\partial t} + u_1\frac{\partial u_1}{\partial x} + w_1\frac{\partial u_1}{\partial z} \qquad 2.7$$

Isaacson (1979) noted that the force due to the term $w\,\partial u/\partial z$ would not include any added mass effects. Therefore, the expression for the inertial force in the x direction is given by

$$F_x = \frac{\rho\pi D^2}{4}\left(Cm\frac{\partial u}{\partial t} + Cm\,u\frac{\partial u}{\partial x}\right) + \frac{\rho\pi D^2}{4}\frac{\partial u}{\partial z} \qquad 2.8$$

Generally, the convective acceleration term is negligible, [Ellix (1984), Sarpkaya and Isaacson (1981)], and this justifies the use for practical purposes of the local acceleration. When the generalizations are made to the Morison equation it can finally be written as

$$dF = [Cm\ \rho V \frac{du}{dt} + \frac{1}{2} Cd\ \rho A\ u\ |u|]dz \qquad 2.9$$

Morison et al. recognised that their equation was approximate and implied that it was calibrated with the two empirical constants Cm and Cd. The authors stated that "The reader is cautioned that these preliminary results are applicable only to single piles without bracing and are likely to be modified ..... This paper is essentially a preliminary report submitted at this time because of the current importance of wave forces in the design of offshore structures."

The Morison equation was very influential and many trusted it blindly. The limits and capabilities of the equation were not recognized until many years later. Some of the limitations of the Morison equation are:

1. It applies only to the prediction of in-line forces
2. It should be used only for cylinders with diameter to flow wavelength ratio less than about 0.2 so that the effects of the cylinder on the waves can be neglected.
3. It does not apply uniformly well for all ranges of Reynolds number (Re) and Keulegan-Carpenter number (KC) and seems to give the best results for flow regimes in the inertia dominated and drag dominated regions (that is, KC < 6 and KC > 20 respectively), where modeling problems associated with vorticity are less difficult. These limits vary and are approximate averages of values proposed by different researchers. Even in controlled laboratory conditions it has been found that there can be relatively large discrepancies between the measured forces and

forces given by the Morison equation in the region $6 < KC < 20$. This region was termed by Sarpkaya (1976c) the disturbance sensitive region of vortex formation where the flow and hence the in-line force is affected by fractional or incomplete vortex shedding. In deep water there is a depthwise variation of the Keulegan-Carpenter number. This can lead to a situation where if KC is high there is a well developed eddy structure near the surface, but there are relatively few eddies near the bottom. There will tend to be vertical diffusion of the eddies so that the forces acting near the bottom of the cylinder will be influenced by the conditions near the surface. Hence, under conditions that prevail in the ocean the use of drag data derived from simple two-dimensional situations cannot be expected to yield fully reliable results. Therefore, due to wake structure and the resulting interaction effects, studied by Bidde (1971), doubts about the reliablity of the Morison equation in deep water should be raised.

4. The effect of the axial pressure gradient nor the transverse force are taken into account.

5. It cannot adequately deal with the effects of orbital motion, omnidirectionality of the waves and/or current and it has no provision to deal with vortex and wake-return effects (history of the motion).

Finally, the Morison equation was proposed, and its validity was investigated, primarily on the basis of tests conducted for simple flow situations (standing waves in a rectangular basin as in Keulegan and Carpenter (1958), or sinusoidal planar flow in a U-shaped water tunnel as found in Sarpkaya (1976a, 1976b, 1976c,

1976d, 1981a, 1981b). It is only recently that careful and systematic attempts have been reported aimed at verifying, under controlled laboratory conditions, the validity of the Morison equation in random, as opposed to harmonic or almost harmonic waves [Vugts and Bouquet (1985) and Bearman et al. (1985)].

As mentioned earlier there appears to be a consensus that the Morison equation, though imperfect, is a good point of departure to model the hydrodynamic forces on cylinders, and that it would be better to improve the equation with correction terms rather than devisa a completely new one. Among the more notable attempts to improve upon the Morison equation by adding additional correction terms are those reported by Lighthill (1979) and Sarpkaya (1981a, 1981b).

With the widespread use of the Morison equation a great deal of work has been done on evaluating the appropriate values of the force coefficients. A review of the work is presented in the following two sections.

2.3.2 Experimental Work Concerning the Morison Equation Coefficients.

A comprehensive review of the work up until 1977 is given in BSRA Report No. W.278 (1976) and Hogben et al. (1977). The Appendices of the the BSRA Report contain summaries of all references that contain explicit values of Cd and Cm intended for use in the Morison equation, or that are otherwise relevant to the wave force problem. Only a few of these papers will be reviewed below.

Prior to 1975 the only data obtained under controlled laboratory conditions were those reported by Keulegan and Carpenter (1958), who performed a series of tests concerned with the experimental evaluation of the wave force coefficients. They did not detect any dependence of the drag and inertia coefficients Cd and Cm upon the Reynolds number but did note a dependence of the coefficients upon a period parameter. This period parameter was subsequently termed the Keulegan-Carpenter number, KC, and is a ratio of the measure of the path length of a fluid particle during a wave period, T, to the body diameter, D, ($KC = U\,T/D$).

The Keulegan-Carpenter number is an important parameter in determining the relative magnitudes of the inertia and drag forces. If the path length is large compared to the body diameter (high KC values) then the condition approaches that of a steady drag situation and drag dominates. Generally, at high KC values there is a continuous von Karman street of vortices being shed from alternate sides of the cylinder. The drag coefficient tends to be constant and approaches its steady flow value. At low values of KC drag development will be negligible in comparison to the inertia forces and the total force is inertia dominated. Keulegan and Carpenter's results indicate that, for a cylinder, there is a critical region around $KC \approx 15$ where the inertia coefficient is a minimum and the drag coefficient is a maximum. At very low KC values there is no separation and hence the drag coefficient is relatively low and the inertia coefficient should approach its ideal potential flow value of 2.0.

Keulegan and Carpenter could not find any dependence between the inertia or drag coefficient and Reynolds number. Sarpkaya (1976a) found that there is in fact a dependence on the viscosity. Since the effect of viscosity is relatively small and both Re and KC involve the velocity, Sarpkaya (1976a) recommended that a viscous frequency parameter, β, ($\beta = Re/KC = D^2/\nu T$) be used in lieu of the Reynolds number.

In a series of extensive experiments Sarpkaya (1976a,1976b) used a U-shaped tube to produce simple harmonic oscillations of water past a fixed circular cylinder. This type of flow has simpler flow properties than is the case in wave flow, in particular, horizontal spatial gradients are absent. From a fundamental research point of view the simplicity of the flow properties was viewed as being an advantage.This approach has allowed the force coefficients to be determined over a wide range of conditions. Sarpkaya's data show clearly that the force coefficients depend on the Keulegan-Carpenter number, the Reynolds number and the relative roughness of the cylinder surface. Figures 2.2 and 2.3 show the variation with KC of Cd and Cm respectively, for five different values of the viscous frequency parameter, β. Figures 2.4 and 2.5 show that Cd and Cm do not vary significantly for Re smaller than about 20,000. This may explain the conclusions reached by Keulegan and Carpenter.

Bearman et al. (1979) also measured the force coefficients due to plane oscillating flow in a U-tube. The results of their Cd values are at variance with those of Sarpkaya. The authors reported problems with their experimental setup which may account

for the difference between the two sets of data. The Cm values showed much less variation.

Garrison et al. (1977) studied the variation of the two force coefficients with Re in which the cylinder was oscillated through the water (that is, no Froude-Krylov force was present and the inertia force was due solely to added mass effects). An advantage of this setup was that the oscillation speed could be varied and the amplitude could be left unchanged. Hence, a range of Reynolds numbers could be obtained for constant values of KC. The results showing the variation of Cd and Cm with Re were essentially the same as those obtained by Sarpkaya.

Chakrabarti et al. (1976) and Chakrabarti (1980) performed a series of wave tank tests with fixed vertical cylinders. The forces were measured over 0.3048m (1 ft) sections and the wave properties were calculated using an appropriate wave theory. For the earlier tests the flow properties were calculated using linear wave theory and for the later tests it was found that the fifth order Stream Function Theory [Dean (1965)] gave the best fit to the surface profile. In each set of results the Keulegan-Carpenter number, Reynolds number and force coefficients were calculated. The results were compared to those obtained by Sarpkaya (1976b) for a smaller range of KC. Chakrabarti (1980) and Chakrabarti et al. (1976) found that the differences between the Cd values from their tests and those obtained by Sarpkaya were small in the range of $KC < 40$. However, the Cm values measured in the wave tests were generally higher than those obtained by Sarpkaya when $KC < 15$ and values were obtained that were considerably higher than the ideal potential

value of 2.0. In both cases there was a severe limitation associated with the Reynolds number. The range of the Reynolds number was too small and the scatter of the results too great for any conclusion to be drawn on the variation of the force coefficients with Re.

There have been several studies carried out to measure the forces exerted on a test structure under actual sea conditions. These have included the Ocean Test Structure of Exxon and the Christchurch Bay Tower of the British Maritime Technology (BMT), U.K. (formerly the National Maritime Institute).

The Exxon ocean test structure was a highly instrumented 20 x 40 x 120 ft platform which was installed in 66 ft of water in the Gulf of Mexico. Data obtained included local wave forces on clean and roughened sensors, the local wave properties and total loads on the structure [Heideman et al. (1979)]. Force coefficients were derived using two methods. The first was a least squares error procedure for each half cycle. The second was the evaluation of Cd over short time intervals where the flow was drag dominated and of Cm over short time intervals where the flow was inertia dominated. The coefficients exhibited large scatter particularly for $KC < 20$. The scatter decreased considerably in the range $20 < KC < 45$. It was not clear whether this was a genuine reduction in scatter or just the effect of the smaller number of data points obtained in the drag dominated region. Heideman et al. (1979) attributed the scatter in the drag and inertia coefficients to random wake encounters. One of the main conclusions they reached was that the Morison equation with time invariant coefficients could be made to

fit measured local forces satisfactorily over individual wave cycles.

The data from the Christchurch Bay tower has been analysed by Pearcey and Bishop (1979) and Standing (1980) using a mean square analysis. The inertia and drag coefficients were determined using one or more pairs of equations obtained from different samples of the measured histories. Pearcey and Bishop found that the force coefficients were quite stable for time intervals greater than about 4 minutes. Standing reported a wave by wave analysis of select sections of the data, and tentatively concluded that the Morison equation provided a good fit to the measured in-line force. The force coefficients obtained by Standing were similar to those obtained by Bishop (1978). It is noted that the Christchurch Bay results were plotted against an effective Keulegan-Carpenter number, proposed by Bishop (1978) for use with random waves, and defined as

$$KC^* = \frac{2\pi}{0.866D}\sqrt{\frac{u^4(t)}{a^2(t)}} \qquad 2.10$$

where u(t) is the velocity and a(t) is the acceleration. This reduces to the usual definition $KC = u_{max}T/D$ in periodic waves of form $u = u_{max} \cos \omega t$.

There appeared to be significant differences in the Christchurch Bay force coefficients due to the effect of current. Bishop (1979) noted that "the variations of the coefficients can be attributed to genuine hydrodynamic effects but also to imperfections in the experimental and analysis techniques. No attempt has been made to attribute the variations to individual

causes ....". Sarpkaya (1981b) stated that there did not seem to be any possibility of using the BMT (formerly the NMI) data in a meaningful way for a critical assessment and improvement of the Morison equation.

Similar problems of interpretation commonly arise with full scale data which may involve considerable uncertainty. The three-dimensionality of the flow and the fact that the conditions cannot be controlled or repeated adds to the difficulties of analysis and interpretation.

Sarpkaya (1976a,1976b) conducted a series of tests on sand-roughened cylinders in harmonic flow. The roughness was achieved by attaching sand grains to the cylinder surface. A range of relative roughness, defined as the ratio of mean sand particle size, k, to cylinder diameter, D, of 1/800 to 1/50 was used. The effect of the relative roughness on the force coefficients was very noticeable. The drag coefficients were found not to vary significantly from the smooth cylinder value at very low Reynolds number. The drag coefficient reached a maximum at a lower Reynolds number for the rough cylinders than for the smooth cylinders. Beyond this critical Reynolds number the drag coefficient increased rapidly until it reached a steady value which was considerably higher than for smooth cylinders. The inertia coefficient reached a maximum at the Reynolds number corresponding to the minimum Cd and then asymptotically decreased. Both the drag and inertia coefficients were independent of the relative roughness for roughness Reynolds numbers (defined as $Re_r = u D_r / \nu$ where D_r = diameter of the roughness element) larger than about 300. Sarpkaya

states that these results and conclusions are valid only for cylinders in harmonic flow with zero mean velocity within the range of variables Re_r, KC, k/D investigated.

Gaston and Ohmart (1979) conducted experiments to examine the effect of surface roughness on vertical cylinders under wave loading. The results obtained showed that the drag coefficient almost doubled in the change from smooth to rough cylinders. Most of the increase in Cd occurred for the initial transition between smooth and rough cylinders, a lesser effect was observed for increasing roughness. The inertia coefficient was found to be less sensitive to surface roughness, with the difference in Cm between the rough and smooth cylinders being only a few percent.

2.3.3 Theoretical and Experimental Work on the Morison Equation Coefficients for Low KC Numbers

Stokes (1851) was the first to show that the force on a sphere or cylinder in oscillatory, viscous, unseparated flow is dependent on both the Reynolds number and on a parameter that can be expressed in terms of the Keulegan-Carpenter number. His solution in which nonlinear terms in the Navier-Stokes equation are neglected is given in the form of a series expansion in powers of $\beta^{-1/2}$, where β is the viscous frequency parameter (β = Re/KC = $D^2/\nu T$). For a circular cylinder in flow with a spatially uniform velocity $u = U_m \cos \omega t$ the force F per unit length of cylinder is found to be

$$F = 0.25 \pi \rho D^2 \omega U_m (k \sin \omega t - k' \cos \omega t) \qquad 2.11$$

where $k = 1 + 4(\pi\beta)^{-1/2} + (\pi\beta)^{-3/2} + ..$ and

$$k' = 4(\pi\beta)^{-1/2} + 4(\pi\beta)^{-1} - (\pi\beta)^{-3/2} ..$$

As noted by Bearman et al. (1985) and Sarpkaya (1986) for a harmonic flow, over a flow cycle $|\cos \omega t| \cos \omega t$ may be approximated by $(8/3\pi)\cos \omega t$. Equating the inertia and drag coefficients in the Morison equation to k and k', respectively, yields the following expressions for the inertia and drag coefficients

$$Cm = 2 + 4(\pi\beta)^{-1/2} + O(\pi\beta)^{-3/2} \qquad 2.12$$

$$Cd = \frac{3\pi^3}{2\,KC}\,[(\pi\beta)^{-1/2} + (\pi\beta)^{-1} + O(\pi\beta)^{-3/2}] \qquad 2.13$$

Bearman et al. (1985) obtained the same result by adopting a modern boundary layer approach. Their analysis was based on the linearized boundary layer equations as given by Batchelor (1970), Lin (1957) and Schlichting (1960). The total non-steady boundary layer equations are obtained as follows. The velocity components u and v within the boundary layer, and the free stream velocity U(x,t) are separated into mean values and oscillatory components, that is,

$$U(x,t) = \bar{U}(x) + U_1(x,t) \qquad 2.14a$$

$$u(x,y,t) = \bar{u}(x,y) + u_1(x,y,t) \qquad 2.14b$$

$$v(x,y,t) = \bar{v}(x,y) + v_1(x,y,t) \qquad 2.14c$$

$$p(x,t) = \bar{p}(x) + p_1(x,t) \qquad 2.14d$$

These components are substituted into the Prandtl boundary layer equations and the total nonlinear non-steady boundary layer equation as given by Lin and Schlichting is

$$\frac{\partial u_1}{\partial t} + \bar{u}\frac{\partial u_1}{\partial x} + \bar{v}\frac{\partial u_1}{\partial y} + u_1\frac{\partial \bar{u}}{\partial x} + v_1\frac{\partial \bar{u}}{\partial y} + u_1\frac{\partial u_1}{\partial x} + v_1\frac{\partial u_1}{\partial y} +$$

$$\overline{u_1\frac{\partial u_1}{\partial x}} + \overline{v_1\frac{\partial u_1}{\partial y}} =$$

$$\frac{\partial U_1}{\partial t} + \bar{U}_1\frac{\partial U_1}{\partial x} + U_1\frac{\partial \bar{U}_1}{\partial x} + U_1\frac{\partial U_1}{\partial x} - \overline{U_1\frac{\partial U_1}{\partial x}} + \nu\frac{\partial^2 u_1}{\partial y^2} \qquad 2.15$$

Lin, Schlichting and Bearman et al. then simplify this equation by retaining only the three linear terms. This leads to

$$\frac{\partial u_1}{\partial t} = \frac{\partial U_1}{\partial t} + \nu\frac{\partial^2 u_1}{\partial y^2} \qquad 2.16$$

Schlichting (1960) showed that in practice this simplification restricts the theory to oscillatory flows with high frequencies. It should be noted that such flows are not representative of those experienced in experimental tests or in the ocean.

Wang (1968) extended Stokes' analysis using the method of inner and outer expansions to $O(\pi\beta)^{-3/2}$ and obtained a solution that is valid for $KC \ll 1$, $ReKC \ll 1$ and $\beta \gg 1$. While this solution is a refinement with respect to the solution of Stokes or Bearman et al. it is still restricted to flows with high frequency oscillations. Wang obtained the expressions

$$Cm = 2 + 4(\pi\beta)^{-1/2} + (\pi\beta)^{-3/2} \qquad 2.17$$

$$Cd = \frac{3\pi^3}{2KC}\left[(\pi\beta)^{-1/2} + (\pi\beta)^{-1} - 1/4(\pi\beta)^{-3/2}\right] \qquad 2.18$$

For real flow situations the terms $O(\pi\beta)^{-1}$ and $O(\pi\beta)^{-3/2}$ are extremely small. In all of the investigations done on this work the frequency parameter is assumed to be moderately high and further work needs to be done investigating the analysis for high β (low

frequency) flows. This is where the nonlinear terms, which are neglected in the previous work on the nonsteady boundary layer equations, become significant.

Up until the 1980's very little work had been done on the variation of Cm and Cd for small values of KC (less than 4). Sarpkaya (1986) states "Practically all the laboratory and ocean based experiments have been conducted for KC larger than about 4 and it is assumed that Cd for KC < 4 is unimportant and Cm has the theoretical potential flow value of the body shape tested."

Results of experimental investigations by Sarpkaya (1986) are shown in figures 2.6 and 2.7. Based on figure 2.6, Sarpkaya identified four different flow regimes:

1. $0 < KC < Kcr$ ($Kcr \simeq 0.75$ for $\beta = 1035$) where Kcr is the value corresponding to the transition from laminar to unstable boundary layer flow. This was referred to by Sarpkaya as the Stokes-Wang regime, and the flow is laminar, attached and stable.

2. $Kcr < KC < Kmd$ ($Kmd \simeq 1.6$ for $\beta = 1035$) where Kmd is the KC value corresponding to flow separation and the onset of turbulence. The minimum Cd occurs at this value. In this range the laminar flow becomes unstable though laminar. The instability corresponds to the formation of mushroom shaped vortices of the type discussed by Honji (1981). See figure 2.8. Hall (1984) presented a stability analysis motivated by Honji's observations and found that at and near the onset of the instability the flow remains laminar.

3. $Kmd < KC < K^*$. The effects of flow separation and vortex shedding become increasingly important and Cd increases with increasing KC.

4. KC > K^*. In this region Cd decreases as KC increases and the number of shed vortices and flow modes increase. Most of the data obtained up until the 1980's was in this region.

It is noted in figure 2.6 that for moderately high β (β = 1035), that is, for relatively high frequencies of the flow oscillations, the Wang prediction (solid line) appears to be reasonable for 0.35 < KC < 0.7. This suggests that for moderately high β the linearization in Bearman et al.'s work is acceptable. Figure 2.7 does not contain data at sufficiently low KC numbers to confirm (or invalidate) the existence of the 0 < KC < Kcr and Kcr < KC < Kmd regions in the case of the higher β value (β = 11240).

The question arises whether the Bearman et al. model, which neglects nonlinear terms in the boundary layer equation, or the Wang model is indeed realistic for flows with low frequency oscillations (high β numbers). This question is legitimate for the following reason. At low KC numbers, Bearman et al.'s model and Wang's model predicts Cm values that exceed the ideal potential flow value Cm = 2 by only negligible amounts. However, as mentioned earlier, according to Chakrabarti, for low KC numbers values of Cm as large as 2.5 were estimated. It may be surmised that such values could be predicted by a model that takes nonlinearities into account for flows where KC < 0.35, say. Such a model might thus predict Cd values different from those yielded by the Bearman et al. model or the Wang model. This suggests that research is warranted on the inertia and drag coefficients for nonlinear

boundary layer equations in flows with low frequency oscillations, such as are encountered in practice.

The practical value of dependable information concerning hydrodynamic damping at low KC numbers was noted in investigations of the dynamic response of compliant offshore structures to wind loads. Indeed, Simiu and Leigh (1983) and Cook et al. (1986) found that the bulk of damping that controls the dynamic response of compliant offshore platforms to fluctuating wind is due to the viscosity effects of the hydrodynamic loading. Numerical simulations of the response of a typical tension leg platform were performed for water depths of 600m and 150m. For 600m deep water, the equivalent linear damping ratios were found to be between 25 percent and 55 percent corresponding to Cd = 0.1 and Cd = 0.6, respectively. For 150m deep water the estimated equivalent linear damping ratios were found to be between 10 percent and 20 percent for Cd = 0.1 and Cd = 0.6, respectively. These papers showed that even for low drag coefficients the equivalent damping ratio is still significant enough to preclude dynamic amplification due to wind.

At present no data are available on the magnitude of Cd for the low KC numbers ($KC < 1$) and high Reynolds numbers ($Re \simeq 10^6$) typical of tension leg platforms columns. For this reason methods of estimating the drag coefficient from first principles by taking the nonlinearities into account are of potential practical interest.

2.4 Representation of Random Waves and Hydrodynamic Forces

Ocean waves are a complex phenomenon and the most recognizable feature is randomness in time and space. Statistical concepts have therefore been applied to their analysis and description [Sarpkaya and Isaacson (1981) and Wilson (1984)].

Numerous one dimensional frequency spectral models have been proposed to describe ocean waves. The Pierson-Moskowitz and the Bretschneider spectra, which fundamentally are similar, are the most commonly used. Both the Bretschneider and Pierson-Moskowitz are based on theoretical arguments. However, they depend on constants (that must be determined from experimental data) and are semi-empirical. Another spectral model was obtained experimentally from the analysis of an extensive wave measurement program known as the Joint North Sea Wave Project (JONSWAP). The JONSWAP spectrum is an extension of the Pierson-Moskowitz spectrum and has a much sharper peak.

The standard form of the JONSWAP spectrum uses fetch F and wind speed U_{10} (wind velocity at an elevation of 10m) as the two basic input parameters and defines a non-dimensional fetch

$$\bar{F} = \frac{g\ F}{U_{10}^{\ 2}} \qquad 2.19$$

and a non-dimensional frequency

$$\bar{f}_m = 2.84\ \bar{F}^{-0.3} \qquad 2.20$$

The JONSWAP spectrum has the expression

$$S_{\eta\eta}(f) = \frac{\alpha\ g^2}{(2\pi)^4\ f^5} \exp\ [-5/4\ (f/f_m)^{-4}]\ \gamma^a \qquad 2.21$$

where $f_m = g\,\overline{f_m} / U_{10}$ is the peak frequency at which $S_{\eta\eta}(f)$ is a maximum,

$$a = \exp\left[\frac{-(f-f_m)^2}{2\sigma^2 f_m^2}\right] \qquad 2.22$$

σ describes the width of the spectrum on either side of the peak and is specified as follows:

$$\sigma = \begin{cases} \sigma_a = 0.07 & \text{for } f \le f_m \\ \sigma_b = 0.09 & \text{for } f > f_m \end{cases}$$

$\alpha = 0.0662\,(\overline{f_m} / 2.84)^{0.66}$ is dependent on the fetch parameter and γ is a shape parameter with the following typical values

$$\gamma = \begin{cases} 7.0 \text{ for a very peaked spectrum} \\ 3.3 \text{ for the mean from selected JONSWAP data} \\ 1.0 \text{ for the Pierson-Moskowitz spectrum} \end{cases}$$

Houmb and Overvik (1976) give a table of γ values to be used for different wave conditions (that is, varying wave height and wave period).

A random sea can be simulated from a known spectrum using numerical techniques. A numerical model of a random sea can be based on a summation of a number of first order waves derived from the surface elevation spectrum $S_{\eta\eta}(f)$ in the following way

$$\eta(x,t) = \sum_{j=1}^{m} a_j \cos(k_j x - \omega_j t + \varphi_j) \qquad 2.23$$

where $a_j = \sqrt{2}\, S_{\eta\eta}(\omega_j)\Delta\omega_j$ 2.24

k_j is the wavenumber and is related to the frequency and water depth, d, by the dispersion relation

$$\omega_j^2 = g\, k_j \tanh(k_j d) \qquad 2.25$$

φ_j is the phase angle and is selected from an independent and uniform probability distribution between 0 and 2π.

Outlines of methods used to determine the variables in equation 2.23 are given by Borgman (1969) and Shinozuka and Jan (1972). Wave generators have been developed in which the input is obtained by simulation in accordance with equation 2.23. See Funke and Mansard (1979,1984) for details.

If it is assumed that linear wave theory applies then the velocities and accelerations can be expressed in terms of the wave spectrum. The velocity and acceleration of a wave are given in complex form, using linear wave theory, as

$$u_x(t) = \mathrm{Re}\ (H_{ux}(f)\ \eta(t)) \qquad 2.26$$

$$a_x(t) = \mathrm{Re}\ (H_{ax}(f)\ \eta(t)) \qquad 2.27$$

$$u_z(t) = \mathrm{Im}\ (H_{uz}(f)\ \eta(t)) \qquad 2.28$$

$$a_z(t) = \mathrm{Im}\ (H_{az}(f)\ \eta(t)) \qquad 2.29$$

where

$$H_{ux}(f) = 2\pi f \frac{\cosh k(z+d)}{\sinh kd} \qquad 2.30$$

$$H_{ax}(f) = -i\ 4\pi^2\ f^2 \frac{\cosh k(z+d)}{\sinh kd} \qquad 2.31$$

$$H_{uz}(f) = 2\ \pi\ f \frac{\sinh k(z+d)}{\sinh kd} \qquad 2.32$$

$$H_{az}(f) = -i\ 4\pi^2\ f^2 \frac{\sinh k(z+d)}{\sinh kd} \qquad 2.33$$

and $$\eta(t) = a\ e^{i(kx-wt)} \qquad 2.34$$

where a is the wave amplitude. H_{ux}, H_{ax}, H_{uz} and H_{az} are transfer functions. Since the frequency are related to the wavenumber by the

dispersion relation the transfer functions may be expressed as functions of the wavenumber. Equations 2.26 to 2.29 are just linear systems relating the output to the input [Bendat (1983) and Bendat and Piersol (1982, 1986)]. We can thus obtain the power spectra of the horizontal and vertical velocity and acceleration as functions of the wave elevation spectrum as follows

$$S_{ux}(f) = | H_{ux}(f) |^2 S_{\eta\eta}(f) \qquad 2.35$$

$$S_{ax}(f) = | H_{ax}(f) |^2 S_{\eta\eta}(f) \qquad 2.36$$

$$S_{uz}(f) = | H_{uz}(f) |^2 S_{\eta\eta}(f) \qquad 2.37$$

$$S_{az}(f) = | H_{az}(f) |^2 S_{\eta\eta}(f) \qquad 2.38$$

Other quantities can be derived in exactly the same manner. Now that the spectral properties of the wave properties have been determined the spectral properties of the force on a cylinder, using the Morison equation can be evaluated. The force per unit length of cylinder is

$$F(t) = Cd \frac{\rho D}{2} u_x(t) \, | u_x(t) | + Cm \frac{\rho \pi D^2}{4} a_x(t) \qquad 2.39$$

If Kd and Ki are defined as

$$Kd = Cd \frac{\rho D}{2} \qquad 2.40$$

and

$$Ki = Cm \frac{\pi D^2}{4} \qquad 2.41$$

then equation 2.39 becomes

$$F(t) = Kd \, u_x(t) \, |u_x(t)| + Ki \, a_x(t) \qquad 2.42$$

The spectral density of the force can be obtained from the latter's autocorrelation function. Borgman (1967a,1967b) has shown that when the velocity and acceleration are assumed to be

independent Gaussian processes the autocorrelation function can be written as

$$R_F(\tau) = Kd^2\ \sigma_{ux}{}^4\ G\left(\frac{R_{ux}(\tau)}{\sigma_{ux}{}^2}\right) + Ki^2\ R_{ax}(\tau) \qquad 2.43$$

where σ_{ux} is the standard deviation of the horizontal velocity and

$G(r) = [(4r^2 + 2)\ \arcsin\ r + 6r\ (1-r^2)^{1/2}\ ]/\pi$

or, in an expanded power series,

$$G(r) = (1/\pi)[8r + 4r^3/3 + r^5/15 + r^7/70 + \ldots] \qquad 2.44$$

The spectral density for F is the Fourier transform of the autocorrelation function. Hence,

$$S_F(f) = \int_{-\infty}^{\infty} R_F(\tau)\ e^{-i2\pi f\tau} d\tau \qquad 2.45$$

Borgman (1969) showed that for u_x less than approximately $2\sigma_{ux}$ the linear approximation is reasonable. Using this approximation the autocorrelation function becomes

$$R_F(\tau) = 8\ \frac{Kd^2\ \sigma_{ux}{}^2}{\pi}\ R_{ux}(\tau) + Ki^2\ R_{ax}(\tau) \qquad 2.46$$

and the spectral density is

$$S_F(f) = 8\ \frac{Kd^2\ \sigma_{ux}{}^2}{\pi}\ S_{ux}(f) + Ki^2\ S_{ax}(f) \qquad 2.47$$

If the expressions in equations 2.35 and 2.36 are adopted, then the spectral density can be written directly in terms of $S_{\eta\eta}(f)$ as

$$S_F(f) = 8\left[\ \frac{Kd^2\ \sigma_{ux}{}^2}{\pi}\ |\ H_{ux}(f)|^2 + Ki^2\ |\ H_{ax}(f)|^2\right] S_{\eta\eta}(f) \qquad 2.48$$

If the flow regime is inertia dominated then the first term in equation 2.48 is negligible and the force spectral density becomes

$$S_F(f) = Ki^2\ |H_{ax}(f)|^2\ S_{\eta\eta}(f) \qquad 2.49$$

A comprehensive summary of methods for estimating the force coefficients using spectral methods has been given by Borgman (1972). Generally, if time series are available it is easiest to determine the drag and inertia coefficients using a least squares method.

2.5 Effect of Current

A comprehensive review of current-wave interaction can be found in Peregrine (1976). The salient features of this interaction are summarized in this section.

When a wave encounters a current it is known that the wave characteristics change. If the current opposes the wave then the wave becomes steeper and shorter. If the current is in the direction of the wave the wave becomes flatter and longer. This changing of the waveform may lead to the breaking of the wave.

The current can substantially affect the wake and eddy formation and transport. For example, a current perpendicular to wave propagation will tend to sweep the vortices produced by the wave motion, away from the structure. Very little information exists on the effect of current wave interaction on the hydrodynamic loading of offshore structures and the effects on the values of Cd and Cm. In the 1976 BSRA W.278 report, of the twenty-five papers reviewed on the evaluation of Cd and Cm, only three papers mentioned current effects.

A common, though approximate way of accounting for the effects of current is to sum vectorily the wave- and current-induced particle velocities. Since the drag force is proportional to the

interaction between the irrotational flow field and the structure. This assumption forces the user of the Morison equation to interpret all nonlinear effects reflected in the experimental data as being associated with the vorticity and hence with the drag force. Lighthill argues that for real structures in real waves there is a significant nonlinear force arising from the irrotational flow component and that to ignore these nonlinear forces can lead to misleading estimates for the drag coefficient.

As stated previously, it is the hydrodynamic drag that controls the amplification of wind effects on compliant offshore platforms. Therefore, accounting correctly for nonlinear effects may in principle be of significant practical importance in this context.

Lighthill derived two main second order correction terms due to the nonlinear interaction between a surface piercing cylinder and the irrotational flow field. The flow was assumed to consist of sinusoidal waves propagating in the positive x direction. In his derivation linear, deep water wave theory was assumed. The first of the correction terms is a waterline force due to the integration of the pressure between the still water level and the instantaneous free surface. The second of the correction forces is due to the horizontal gradient of the velocity (the extensional motions) and is given by the resultant of the dynamic pressure acting over the body's surface. Lighthill found that for a moderately steep wave the second order forces amounted to approximately 20% of the inertia force. In this case attributing all nonlinearities to the drag force leads to a doubling of the drag coefficient. For a

Ellix proposed an additional correction term based on a model suggested by Verley (1975) and associated with a third-order drag force in the waterline region. In the writer's opinion further work would be needed to justify the use of this correction.

2.7 The Sarpkaya Correction Term

Sarpkaya (1976a) stated that "the difference between the measured and calculated forces is primarily the fractional shedding of vortices and vortex-induced oscillations in the in-line forces".

The work of Sarpkaya (1981a, 1981b) was aimed at developing an improved form of the Morison equation. This did not involve completely modifying the Morison equation but rather finding additional correction terms to account for vorticity. Sarpkaya did an extensive study of the calculated and measured forces obtained using a U-tube similar to that used in his 1976 work. Following various attempted approaches that did not prove satisfactory, Sarpkaya performed a Fourier analyses of the force residues (that is, of the differences between the measured and calculated forces). This approach was based on the residual analysis performed by Keulegan and Carpenter for the case of sinusoidally oscillating flow with velocity $u = U_m \cos \omega t$. It was assumed that the force is a summation of odd harmonics of ωt. The force can then be written as

$$\frac{F}{\rho D U_m^2} = A_1 \sin \omega t + A_3 \sin 3\omega t + A_5 \sin 5\omega t + \ldots$$

$$+ B_1' \cos \omega t|\cos \omega t| + B_3' \cos 3\omega t + B_5' \cos 5\omega t + \ldots \quad 2.51$$

This equation can be reconciled with the Morison equation by expressing it as

$$\frac{F}{\rho D U_m^2} = A_1 \sin \omega t + B_1' \cos \omega t|\cos \omega t| + \Delta R \qquad 2.52$$

where $\Delta R = A_3 \sin 3\omega t + A_5 \sin 5\omega t + \ldots$

$$+ B_3' \cos 3\omega t + B5' \cos 5\omega t + \ldots$$

or

$$\frac{F}{\rho D U_m^2} = \frac{\pi}{4} Cm \frac{D\omega}{U_m} \sin \omega t - \frac{Cd}{2} \cos \omega t|\cos \omega t| + \Delta R \qquad 2.53$$

where

$$\frac{\pi}{4} Cm \frac{D\omega}{U_m} = A_1 + A_3 \frac{\sin 3\omega t}{\sin \omega t} + A_5 \frac{\sin 5\omega t}{\sin \omega t} + \ldots$$

and $$\frac{Cd}{2} = -B_1' - B_3' \frac{\cos 3\omega t}{\cos \omega t \, |\cos \omega t|} - B_5' \frac{\cos 5\omega t}{\cos \omega t \, |\cos \omega t|} + \ldots$$

Sarpkaya (1976a) found that the third harmonic of the residue was significant. Therefore, Sarpkaya and Isaacson (1981) said that the ΔR term could be expressed approximately as $A_3 \cos \omega t + B_3 \sin \omega t$ or $C_3 \cos (3\omega t - \Phi_3)$. The Sarpkaya and Isaacson work was significantly expanded and improved upon in Sarpkaya (1981a, 1981b). In his analysis of the new experimental data Sarpkaya found that all the harmonics from two through fifteen appeared in the spectral analysis but that the third and fifth harmonics were by far the most important. With this new analysis the residual grew from one to two additional terms. The Morison equation was therefore changed from a two term equation with two unknowns to a four term equation with six unknowns.

The analysis of the data showed that all the additional constants were functions of the deviation of Cm from its ideal potential value of 2.0 (for circular cylinders). All the constants had a maximum or a minimum for KC ≈ 12.5. Plots of two of the variables are given in Figures 2.10 and 2.11. The form of the four term Morison equation proposed by Sarpkaya is

$$F = Cd \frac{\rho D}{2} u(t) |u(t)| + Cm \frac{\rho \pi D^2}{4} \frac{\partial u(t)}{\partial t}$$
$$+ \rho D U_m^2 C_3 \cos(3\omega t - \Phi_3)$$
$$+ \rho D U_m^2 C_5 \cos(5\omega t - \Phi_5) \qquad 2.54$$

or in final form the four term Morison equation is written as

$$F = Cd \frac{\rho D}{2} u(t) |u(t)| + Cm \frac{\rho \pi D^2}{4} \frac{\partial u(t)}{\partial t}$$
$$+ \frac{\rho D U_m^2}{2\Lambda^{1/2}} [A_{C3} + B_{C3} \exp(C_{C3}(KC-12.5)^2)] x$$
$$\cos(3\omega t - \Lambda^{-1/2}[A_{\Phi 3} + B_{\Phi 3} \exp(C_{\Phi 3}(KC-12.5)^2)]$$
$$+ \frac{\rho D U_m^2}{2\Lambda^{1/2}} [A_{C5} + B_{C5} \exp(C_{C5}(KC-12.5)^2)] x$$
$$\cos(5\omega t - \Lambda^{-1/2}[A_{\Phi 5} + B_{\Phi 5} \exp(C_{\Phi 5}(KC-12.5)^2)] \qquad 2.55$$

where $\Lambda = (Cm^* - Cm)/(KC\ Cd)$ and $Cm^* = 2$ is the ideal value of the inertia coefficient for a cylinder in potential flow. The universal constants are independant of KC, Re and β and are equal to

$A_{C3} = 0.01$	$B_{C3} = 0.10$	$C_{C3} = -0.08$
$A_{\Phi 3} = -0.05$	$B_{\Phi 3} = -0.35$	$C_{\Phi 3} = -0.04$
$A_{C5} = 0.0025$	$B_{C5} = 0.053$	$C_{C5} = -0.06$
$A_{\Phi 5} = 0.25$	$B_{\Phi 5} = 0.60$	$C_{\Phi 5} = -0.02$

From equation 2.55 the residue as represented by the last two terms approaches zero for KC < 7 and KC > 20. Therefore, the four term equation reduces to the two term Morison equation outside the drag inertia region. The additional terms reflect the role played by the growth and convection of vortices on the in-line force.

When comparing the two term equation to the three and four term equation Sarpkaya found that the differences between the calculated and measured forces were reduced significantly. Subsequent investigations by Hudspeth and Nath (1985) yielded values of the universal constants that differed from those given by Sarpkaya. It appears therefore that additional work is needed to obtain correction terms associated with vorticity that are applicable to all flow cases.

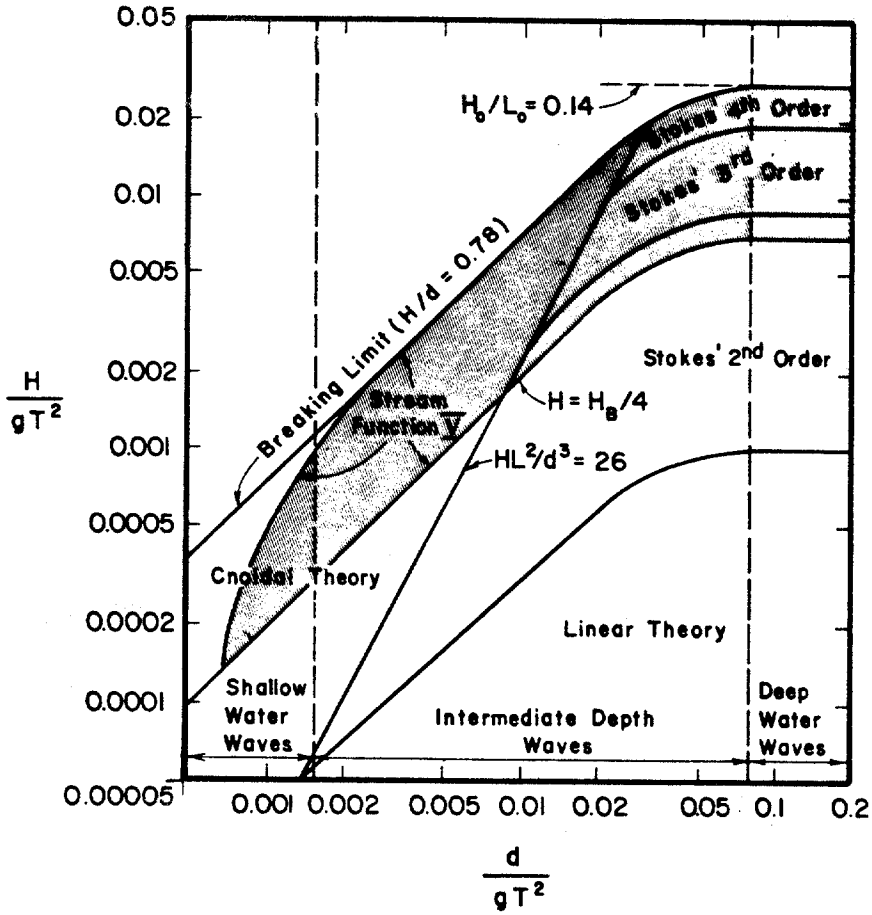

Figure 2.1. Ranges of suitability for various wave theories. [Le Mehaute (1976)].

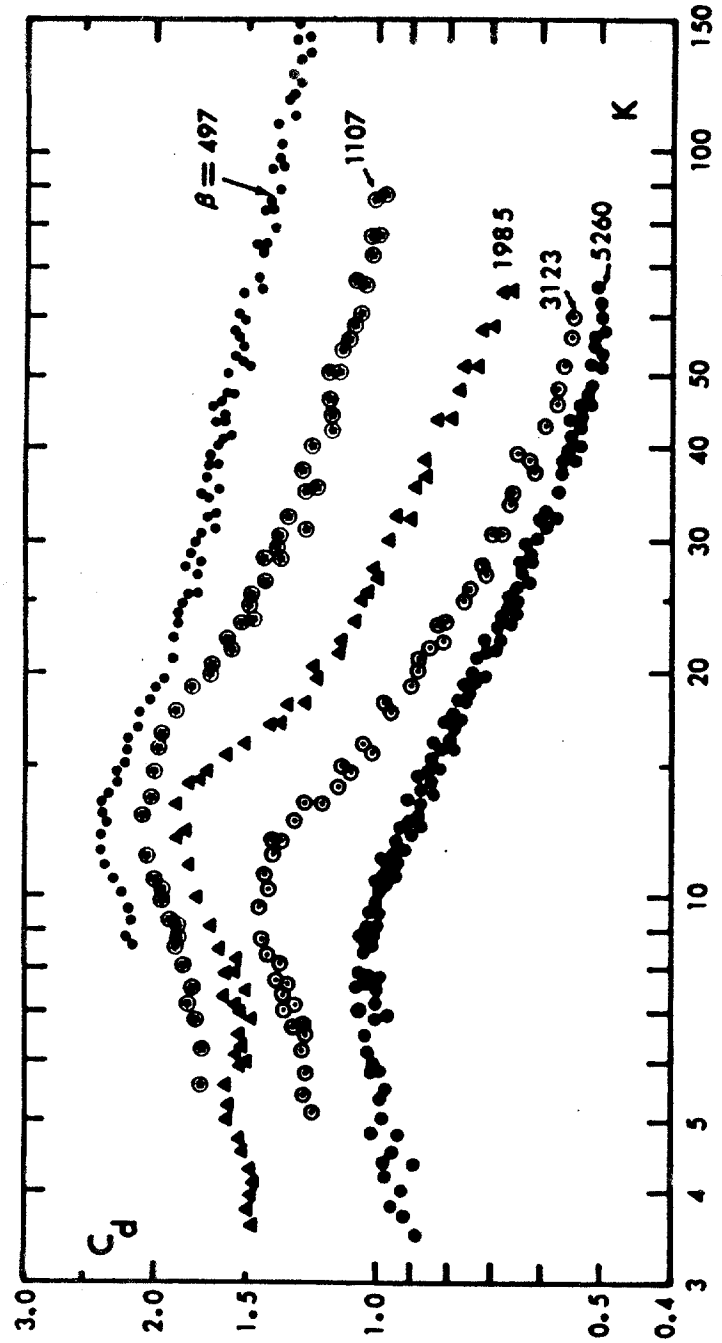

Figure 2.2. Drag coefficients versus Keulegan-Carpenter number (K) for constant values of β (β = Re/K). [Sarpkaya (1976b)].

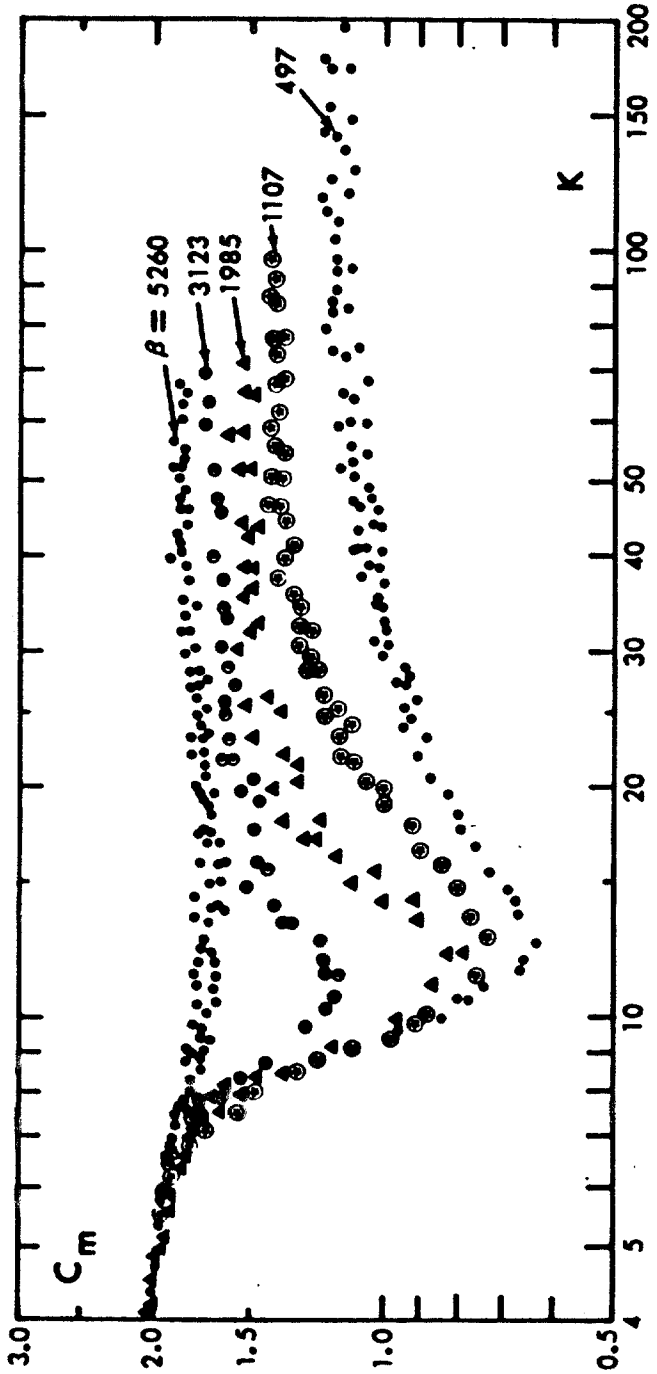

Figure 2.3. Inertia coefficients versus Keulegan-Carpenter number (K) for constant values of β (β = Re/K). [Sarpkaya (1976b)].

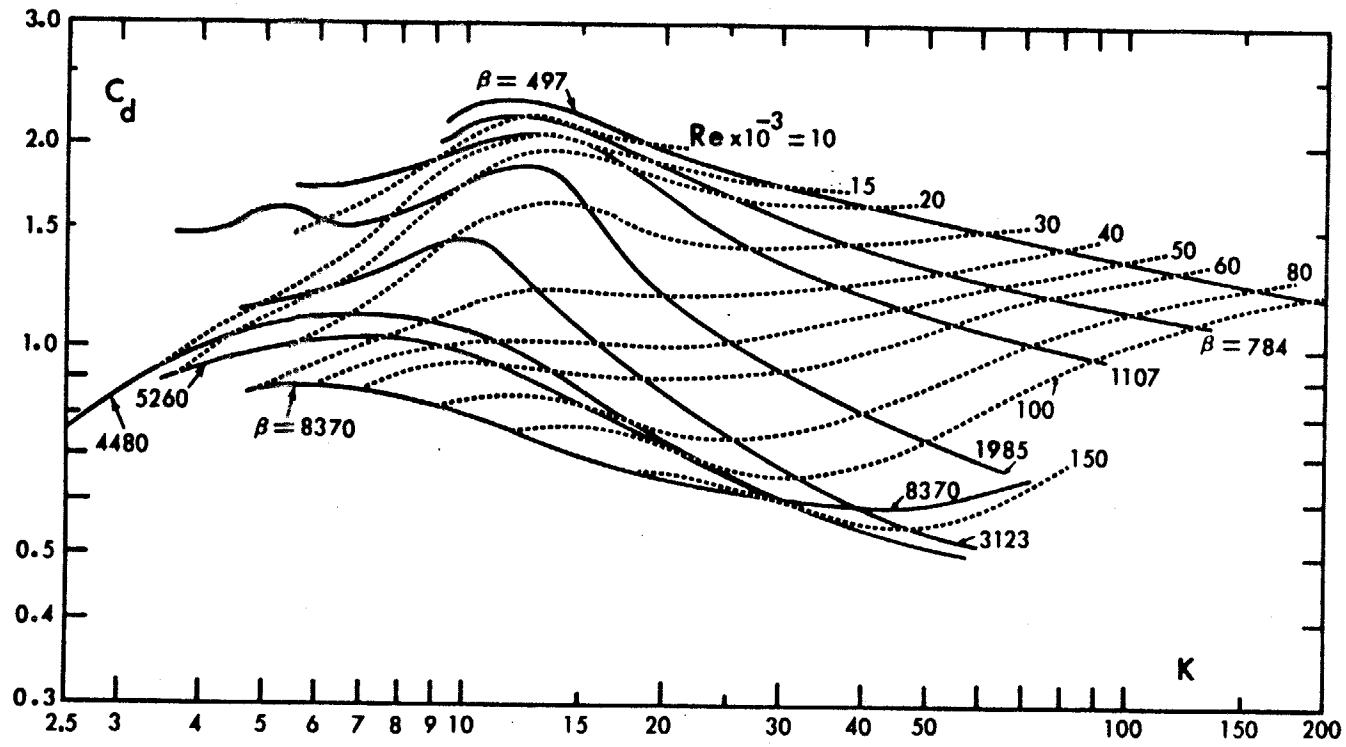

Figure 2.4. Drag coefficient versus Keulegan-Carpenter number (K) for constant values of β and Re. [Sarpkaya (1976b)].

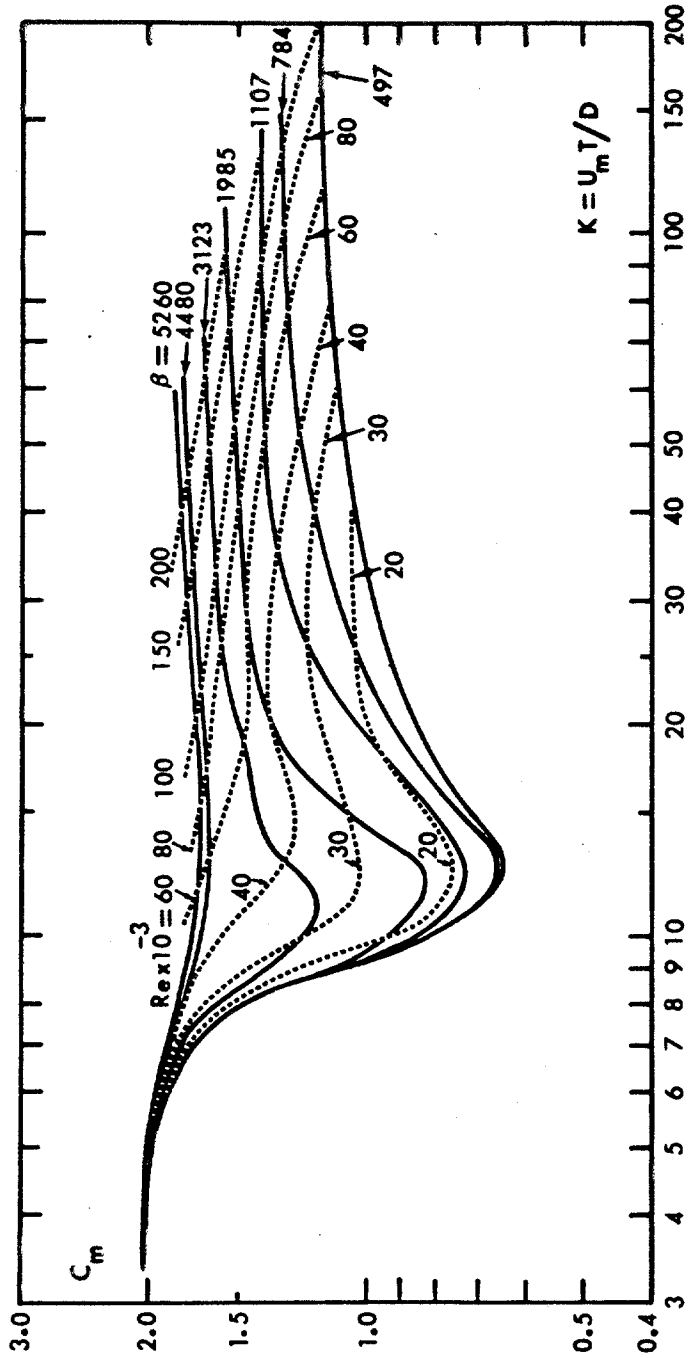

Figure 2.5. Inertia coefficient versus Keulegan-Carpenter number (K) for constant values of β and Re. [Sarpkaya (1976b)].

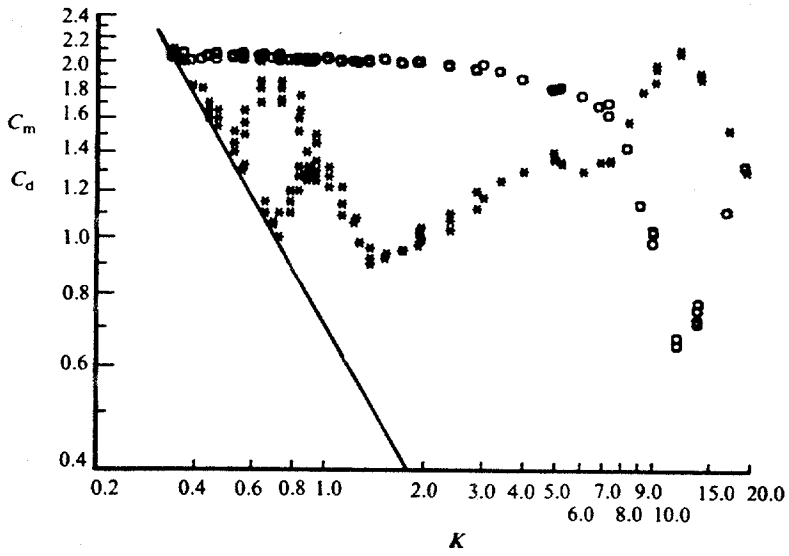

Figure 2.6. Drag and inertia coefficients versus Keulegan-Carpenter number: Experimental, ∘ Cm; * Cd; theory, ——; β=1380. [Sarpkaya (1986)].

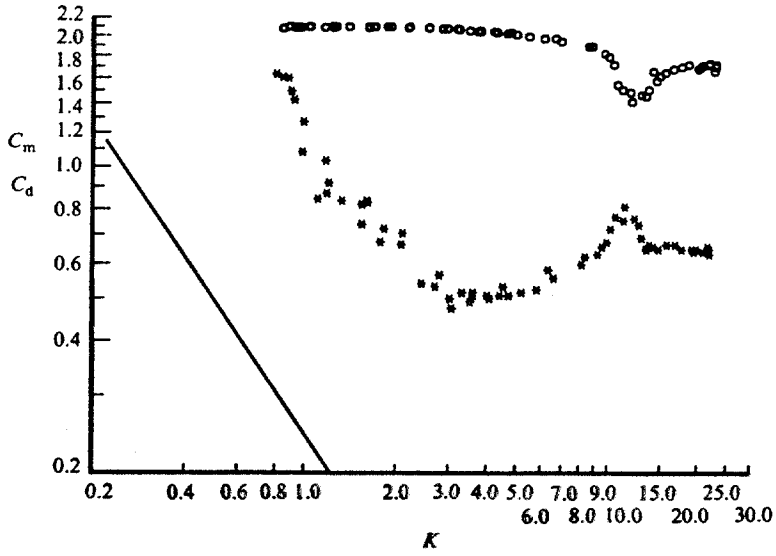

Figure 2.7. Drag and inertia coefficients versus Keulegan-Carpenter number: Experimental, ∘ Cm; * Cd; theory, ——; β=11240. [Sarpkaya (1986)].

Figure 2.8. Mushroom shaped vortices. [Honji (1981)].

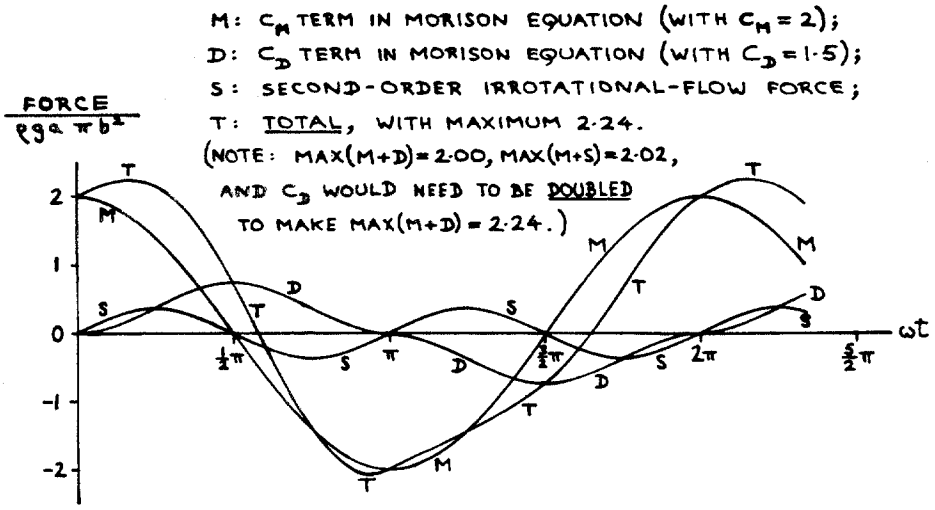

FORCE ON VERTICAL CYLINDER OF RADIUS b IN DEEP-WATER WAVES: PLOT FOR KEULEGAN-CARPENTER NUMBER 10 (WAVE AMPLITUDE $\pm 3{\cdot}2b$), WITH WAVE STEEPNESS $ka = 0{\cdot}3$ (WAVELENGTH $67b$).

Figure 2.9. Lighthill correction terms. [Lighthill (1979)].

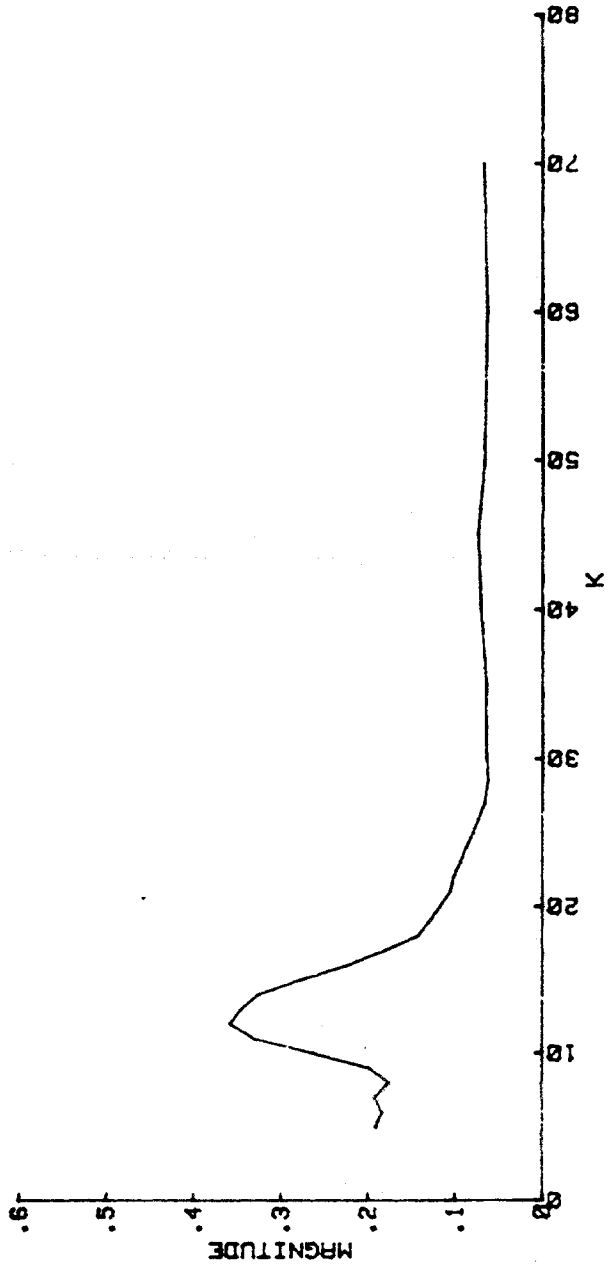

Figure 2.10. Coefficient C_3 versus Keulegan-Carpenter number (K) (averaged over each K). [Sarpkaya (1981a)].

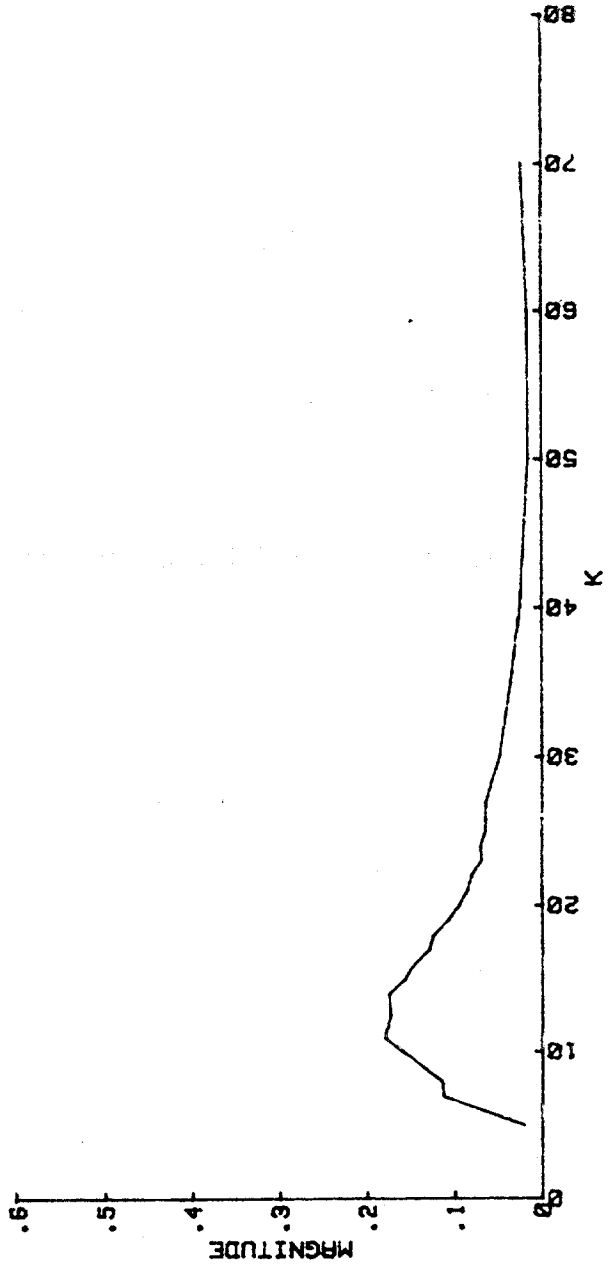

Figure 2.11. Coefficient C_5 versus Keulegan-Carpenter number (K) (averaged over each K). [Sarpkaya (1981a).

CHAPTER THREE

MODELING OF WAVE FORCES ON CYLINDERS

3.1 Governing Equations of Motion

This section briefly reviews the equations of motion and the boundary conditions needed for the development of Stokes' second order theory which in turn is used in this chapter to derive theoretical expressions for wave forces on cylinders.

Consider a free, simple harmonic plane wave as shown in figure 3.1 propagating in the positive x direction. If we assume incompressible, irrotational flow then we require that the fluid motion be described by a velocity potential, ϕ, such that

$$u = \frac{\partial \phi}{\partial x} \quad , \quad v = \frac{\partial \phi}{\partial z} \tag{3.1}$$

The equation of continuity states that the rate of flow into a control volume equals the rate of flow out. Assuming two dimensional flow the continuity equation is

$$\frac{\partial u}{\partial x} + \frac{\partial w}{\partial z} = 0 \quad \text{for all } (x,z) \tag{3.2a}$$

or

$$\frac{\partial^2 \phi}{\partial x^2} + \frac{\partial^2 \phi}{\partial z^2} = 0 \tag{3.2b}$$

The boundary condition to be satisfied at the bottom is that there is no flow through the boundary on which the fluid sits, that is, the vertical velocity must be equal to zero at z = -d;

$$\frac{\partial \phi}{\partial z} = 0 \qquad \text{at } z = -d \tag{3.3}$$

The kinematic free surface condition states that any particle on the surface remains on the surface. "Actually this property is a consequence of the basic assumption in continuum mechanics that the motion of a fluid particle can be described mathematically as a topological deformation which depends continuously on time t" [Stoker (1957)]. The condition is imposed by noticing that the surface moves with the fluid and that (for a particle on the surface)

$$\frac{d\,(z - \eta(x,y,t))}{dt} = 0 \qquad \text{at } z = \eta \tag{3.4a}$$

or

$$\frac{dz}{dt} = \frac{d\eta(x,y,t)}{dt} \qquad \text{at } z = \eta \tag{3.4b}$$

The operation of taking a particle derivative d/dt is defined as

$$\frac{d()}{dt} = u\frac{\partial()}{\partial x} + v\frac{\partial()}{\partial y} + w\frac{\partial()}{\partial z} + \frac{\partial()}{\partial t} \tag{3.5}$$

Equation 3.4b becomes

$$\frac{\partial\phi}{\partial z} = \frac{\partial\eta}{\partial t} + \frac{\partial\phi}{\partial x}\frac{\partial\eta}{\partial x} + \frac{\partial\phi}{\partial y}\frac{\partial\eta}{\partial y} \tag{3.6}$$

For two-dimensional flow, which is assumed in this report, equation 3.6 is

$$\frac{\partial\phi}{\partial z} = \frac{\partial\eta}{\partial t} + \frac{\partial\phi}{\partial x}\frac{\partial\eta}{\partial x} \tag{3.7}$$

The second free surface boundary condition is the dynamic boundary condition. It is a consequence of the unsteady Bernoulli law which states that the pressure on the free surface is equal to the atmospheric pressure (taken as zero), and can be written as

$$g\eta + \frac{\partial \phi}{\partial t} + \frac{1}{2}\left(\frac{\partial \phi}{\partial x}\right)^2 + \frac{1}{2}\left(\frac{\partial \phi}{\partial z}\right)^2 = 0 \quad \text{at } z = \eta \qquad 3.8$$

where g = acceleration due to gravity

ρ = fluid density

Implicit in equations 3.7 and 3.8 are the assumptions that there is no underlying current, the depth is constant and the wave is two dimensional and of permanent form.

3.2 Stokes Second Order Wave Theory

To obtain higher order terms in accordance with Stokes wave theory we assume that the velocity potential, ϕ, and surface elevation, η, can be expanded in power series with respect to the perturbation parameter, ϵ, taken as equal to the wave steepness ak, that is,

$$\phi = \epsilon\,\phi_1 + \epsilon^2\,\phi_2 + \epsilon^3\,\phi_3 + \ldots \qquad 3.9$$

and $$\eta = \epsilon\,\eta_1 + \epsilon^2\,\eta_2 + \epsilon^3\,\eta_3 + \ldots \qquad 3.10$$

Substituting equation 3.9 in the Laplace equation gives

$$\nabla^2 \phi_k = 0 \qquad (k = 1,2,\ldots) \qquad 3.11$$

The boundary condition of no flow through the ocean floor gives

$$\frac{\partial \phi_k}{\partial z} = 0 \qquad (k = 1,2,\ldots) \qquad 3.12$$

Both the kinematic and the dynamic free surface boundary conditions are applied at the free surface, $z = \eta$, which itself is an unknown. The problem involves transforming the boundary conditions at the unknown $z = \eta$ to conditions at $z = 0$ (Still Water

Level). This can be done by using a Taylor series expansion such that the boundary condition

$$f(z) = 0 \qquad \text{at } z = \eta \tag{3.13}$$

is written as

$$f(z) = \eta \frac{\partial f}{\partial z} + \frac{1}{2!}\eta^2 \frac{\partial^2 f}{\partial z^2} + \frac{1}{3!}\eta^3 \frac{\partial^3 f}{\partial z^3} + \ldots = 0 \tag{3.14}$$

where the derivatives of the function f are evaluated at $z = 0$ (rather than at the unknown elevation η). By expanding equations 3.7 and 3.8 in the Taylor series expansion and collecting ϵ and ϵ^2 terms we obtain the first and second order boundary conditions:

(i) to first order

$$\frac{\partial \phi_1}{\partial t} + g\eta_1 = 0 \qquad \text{at } z = 0 \tag{3.15}$$

$$\frac{\partial \eta_1}{\partial t} - \frac{\partial \phi_1}{\partial z} = 0 \qquad \text{at } z = 0 \tag{3.16}$$

The value of η_1 in equation 3.15 is substituted in 3.16 to obtain the following condition in terms of ϕ_1 only

$$\frac{\partial^2 \phi_1}{\partial t^2} + g\frac{\partial \phi_1}{\partial z} = 0 \qquad \text{at } z = 0 \tag{3.17}$$

(ii) to second order

$$\frac{\partial \phi_2}{\partial t} + \eta_1 \frac{\partial^2 \phi_1}{\partial t \partial z} + \frac{1}{2}(\nabla \phi_1)^2 + g\eta_2 = 0 \qquad \text{at } z = 0 \tag{3.18}$$

$$\frac{\partial \eta_2}{\partial t} - \frac{\partial \phi_2}{\partial z} - \eta_1 \frac{\partial^2 \phi_1}{\partial z^2} + \frac{\partial \phi_1}{\partial x}\frac{\partial \eta_1}{\partial x} + \frac{\partial \phi_1}{\partial y}\frac{\partial \eta_1}{\partial y} = 0 \text{ at } z = 0 \tag{3.19}$$

Using results for η_1 from equation 3.15 and combining equations 3.18 and 3.19 we get equation 3.20 which is in terms of ϕ_1 and ϕ_2 only.

$$\frac{\partial^2\phi_2}{\partial t^2} + g\frac{\partial\phi_2}{\partial z} = g\frac{\partial\phi_1}{\partial x}\frac{\partial\eta_1}{\partial x} - g\eta_1\frac{\partial^2\phi_1}{\partial z^2} - \eta_1\frac{\partial^3\phi_1}{\partial z\,\partial t^2}$$

$$- 2\frac{\partial\phi_1}{\partial z}\frac{\partial^2\phi_1}{\partial z\,\partial t} - \frac{\partial\phi_1}{\partial x}\frac{\partial^2\phi_1}{\partial x\partial t} \quad \text{or}$$

$$\frac{\partial^2\phi_2}{\partial t^2} + g\frac{\partial\phi_2}{\partial z} = -\frac{\partial}{\partial t}(\nabla\phi_1)^2$$

$$+ \frac{\partial\phi_1}{\partial x}\frac{\partial}{\partial z}\left(\frac{\partial\phi_1}{\partial z} + \frac{1}{g}\frac{\partial^2\phi_1}{\partial t^2}\right) \quad \text{at } z = 0 \qquad 3.20$$

where the subscripts 1 and 2 denote the first and second order quantities, respectively.

The boundary conditions can be expanded to any order required but at the higher orders they become increasingly difficult to formulate, for this reason this is usually done on a computer. The solution of the Laplace equation subject to the boundary conditions 3.15 and 3.16 is given by the linear (Airy) wave theory. The theory is valid when the wave height is very much smaller than the wave length and the still water depth, and the solution is

$$\eta_1 = \frac{1}{k}\cos(kx - \omega t) \qquad 3.21$$

$$\phi_1 = \frac{g}{k\omega}\frac{\cosh k(z+d)}{\cosh kd}\sin(kx-\omega t) \qquad 3.22$$

where k = wavenumber

d = water depth

The actual elevation and potential can then be obtained by multiplying 3.21 and 3.22 by the perturbation parameter ϵ (see equations 3.9 and 3.10).

Consideration of the kinematic condition yields the linear dispersion relation

$$\omega^2 = gk \tanh kd \qquad 3.23$$

This shows that the wave speed (celerity, $c = \omega/k$) only depends on the wavenumber and water depth and is independent of the wave height.

The water particle velocities can be obtained by differentiating the potential in accordance with equations 3.1 to yield

$$u_1 = \frac{\partial \phi}{\partial x} = \frac{g\ a\ k}{\omega} \frac{\cosh k(z+d)}{\cosh kd} \cos (kx-\omega t) \qquad 3.24$$

$$w_1 = \frac{\partial \phi}{\partial z} = \frac{g\ a\ k}{\omega} \frac{\sinh k(z+d)}{\cosh kd} \sin (kx-\omega t) \qquad 3.25$$

Once the first order solutions ϕ_1 and η_1 are determined they can be substituted in the boundary conditions 3.17 and 3.18 to yield conditions for ϕ_2 and η_2, so that solutions for ϕ_2 and η_2 can be obtained. The results of the second order analysis are

$$\eta_2 = \frac{g}{4\omega^2} \frac{1}{\sinh^2 kd} (\cosh 2kd + 2) \cos 2(kx-\omega t) \qquad 3.26$$

$$\phi_2 = \frac{3}{8} \frac{g}{k\omega} \frac{\cosh 2k(z+d)}{\sinh^3 kd \cosh kd} \sin 2(kx-\omega t) \qquad 3.27$$

and the actual second order elevation and potential can be obtained by multiplying these results above by the perturbation parameter ϵ^2. Note that the second order components of η and ϕ have frequencies that are twice the frequency of the first order components. The corresponding second order horizontal and vertical velocities, respectively, are

$$u_2 = \frac{3}{4} \frac{ga^2k^2}{\omega} \frac{\cosh 2k(z+d)}{\sinh^3 kd \cosh kd} \cos 2(kx-\omega t) \qquad 3.28$$

$$w_2 = \frac{3}{4} \frac{ga^2k^2}{\omega} \frac{\sinh 2k(z+d)}{\sinh^3 kd \cosh kd} \sin 2(kx-\omega t) \qquad 3.29$$

An important result of the second order analysis is that the dispersion relation equation 3.23 is valid and hence it simplifies the application of the theory. For third and higher orders the celerity does depend on the wave height and the calculation of the wave properties becomes much more complex.

One feature of the second order theory is that the particle paths are not closed and there is a net drift of fluid in the wave motion. One consequence of the orbits not being closed is that in a closed system such as a wave flume this drift would imply a gradual buildup of water at one end. Since this does not occur the net mass transfer is assumed to be counteracted by a uniform current flowing in the opposite direction.

3.3 Expression of the Morison Equation Force Based on Second Order Stokes Theory

To use the Morison equation corresponding to periodic flow with given amplitude a (a = H/2 where H = wave height), and period T, it is necessary in practice to evaluate the in-line velocity and acceleration corresponding to a and T. This can be done by using Stokes theory. This section presents an approximation to the Morison equation based on the second order Stokes theory.

The total force acting on a surface piercing cylinder is obtained by considering an infinitesimal element, δy, of the

cylinder at some depth below the still water level. The cylinder is assumed small with respect to the wavelength and diffraction effects are negligible. Morison et al. (1950) proposed an expression for the force exerted by the surface waves on the element which consists of the sum of two components. The first of the components is the inertia force, Fi. This force is the product of the so called virtual inertia and the acceleration, $\partial u/\partial t$, of the undisturbed fluid relative to the body. The virtual inertia is the sum of the displaced mass (fluid density, ρ, times the body volume, V) and the added mass, Ma, therefore the inertia force is

$$Fi = (\rho V + Ma) \frac{\partial u}{\partial t} \qquad 3.30$$

In ideal potential flow Ma is equal to ρV. In real flows around bluff bodies $Ma \neq \rho V$ and the inertia force is usually specified in terms of a parameter called the mass coefficient Cm (also known as the inertia coefficient). It should be noted that the mass coefficient is concerned only with the fluid forces on the boundary of the body and has no relation to any actual mass. It is a function of the body shape and has been theoretically calculated for many standard geometric shapes such as spheres, circular cylinders, disks and other bodies. In practice Cm is obtained by measurement. With this notation equation 3.30 can be written as

$$Fi = Cm\ \rho V \frac{\partial u}{\partial t} \qquad 3.31$$

The second component is the drag force. This force acts over the frontal area of the element, is proportional to the square of the velocity and has the same direction as the velocity u. The drag

force is due to the effects of viscosity. In particular, at sufficiently large Keulegan-Carpenter numbers, separation of the flow occurs which creates a low pressure region behind the body. The drag force is then influenced by the point of flow separation on the body and the nature of the flow wake. A major difference between uniform flow and a harmonically oscillating flow, such as a wave, is that in the latter case, the wake is swept back past the cylinder each time the flow reverses. All the effects associated with viscosity are accounted for by the drag coefficient Cd. The drag force is written as

$$Fd = \frac{1}{2} \rho \, Cd \, A \, u \, |u| \qquad 3.32$$

The total force as expressed by the Morison equation is equal to the sum of the inertia force (equation 3.31) and the drag force (equation 3.32). To second order, by using the horizontal velocity and acceleration given by Stokes' theory (Section 3.2), the inertia and drag forces become

$$\begin{aligned} Fi &= Cm \frac{\rho\pi D^2}{4} \left\{ -g \, a \, k \frac{\cosh k(z+d)}{\cosh kd} \sin \omega t - \right. \\ &\qquad \left. \frac{3}{2} g \, a^2 \, k^2 \frac{\cosh 2k(z+d)}{\cosh kd \sinh^3 kd} \sin 2\omega t \right. \\ &= -Cm \frac{\rho\pi D^2}{4} g \, a \, k \frac{\cosh k(z+d)}{\cosh kd} \sin \omega t - \\ &\qquad \frac{3}{8} Cm \, \rho\pi D^2 \, g \, a^2 \, k^2 \frac{\cosh 2k(z+d)}{\cosh kd \sinh^3 kd} \sin 2\omega t \end{aligned} \qquad 3.33$$

$$Fd = \frac{1}{2} Cd \, \rho D \left\{ \frac{g \, a \, k}{\omega} \frac{\cosh k(z+d)}{\cosh kd} \cos \omega t + \right.$$

$$\left.\frac{3}{4}\,\frac{g\,a^2\,k^2}{\omega}\,\frac{\cosh 2k(z+d)}{\cosh kd\,\sinh^3 kd}\cos 2\omega t\right\}\times$$

$$\left|\frac{g\,a\,k}{\omega}\,\frac{\cosh k(z+d)}{\cosh kd}\cos\omega t+\right.$$

$$\left.\frac{3}{4}\,\frac{g\,a^2\,k^2}{\omega}\,\frac{\cosh 2k(z+d)}{\cosh kd\,\sinh^3 kd}\cos 2\omega t\right| \qquad 3.34$$

If the upper and lower limits of integration are located at vertical distances s and r below the still water level (see figure 3.2), respectively, then

$$Ft = Cm\,\frac{\rho\pi D^2}{4}\int_{-r}^{-s}\frac{\partial u}{\partial t}\,dz +$$

$$\frac{1}{2}\,Cd\,\rho D\int_{-r}^{-s} u\,|u|\,dz \qquad 3.35$$

If s does not differ significantly from r (so that the velocities u at these two levels would not differ by more than 10% or so) then it may be assumed approximately that the coefficients Cd and Cm are almost constant along the element and can therefore be placed outside the integral. We then obtain the expression for the Morison equation based on Stokes' second order theory:

$$Ft = -Cm\,\frac{\rho\pi D^2}{4}\,g\,a\,\frac{\sinh k(-s+d)-\sinh k(-r+d)}{\cosh kd}\sin\omega t -$$

$$\frac{3}{16}\,Cm\;\rho\pi D^2\,g\,a^2\,k\,\frac{\sinh 2k(-s+d)-\sinh 2k(-r+d)}{\cosh kd\,\sinh^3 kd}\sin\omega t +$$

$$\frac{1}{2}\,Cd\,\rho\,D\,\frac{g^2\,a^2\,k^2}{\omega^2}\,\frac{\sinh 2k(-s+d)-\sinh 2k(-r+d)}{4k\,\cosh^2 kd}\cos^2\omega t$$

$$+\frac{3}{8}\,Cd\,\rho D\,\frac{g^2\,a^3\,k^3}{\omega^2}\times$$

$$\left\{ \frac{\sinh 3k(-s+d)+3\sinh k(-s+d)-\sinh 3k(-r+d)-3\sinh k(-r+d)}{\cosh^2 kd \sinh^3 kd} \right\} x$$

$$2\cos wt \cos 2wt +$$

$$\frac{9}{32} Cd \rho D \frac{g^2 a^4 k^4}{\omega^2} x$$

$$\left\{ \frac{\sinh 4k(-s+d) - \sinh 4k(-r+d) -4k(s-r)}{8k \cosh^2 kd \sinh^6 kd} \right\} \cos^2 2\omega t \qquad 3.36$$

If the value of u from Stokes second order analysis is negative then the drag force will be the negative of the value calculated above.

3.4 Lighthill's Second Order Correction Term

The force on a section of a cylinder is given by the sum of the pressures integrated around the cylinder and along the cylinder span.

At any point in a fluid, if the velocity potential ϕ is known, the fluid pressure is determined by Bernoulli's equation

$$p = -p_s - \rho g z - \rho \frac{\partial \phi}{\partial t} - \frac{1}{2}\rho(\nabla\phi)^2 + C(t) \qquad 3.37$$

p_s and C(t) may be taken equal to zero without loss of generality, see Stoker (1957).

Expanding the pressure p and the right hand side of equation 3.37 with respect to the perturbation parameter ϵ we obtain, to second order,

$$p_0 + \epsilon p_1 + \epsilon^2 p_2 = - \rho g z - \epsilon \rho \frac{\partial \phi_1}{\partial t} - \epsilon^2 \rho \frac{\partial \phi_2}{\partial t} - \epsilon^2 \frac{1}{2} \rho \left(\frac{\partial \phi_1}{\partial x}\right)^2 - \epsilon^2 \frac{1}{2} \rho \left(\frac{\partial \phi_1}{\partial z}\right)^2 \qquad 3.38$$

When like terms in powers of ϵ are equated we get

$$p_0 = - \rho g z \qquad 3.39$$

$$p_1 = -\rho \frac{\partial \phi_1}{\partial t} \qquad 3.40$$

$$p_2 = -\rho \frac{\partial \phi_2}{\partial t} - \frac{1}{2} \rho (\nabla \phi_1)^2 \qquad 3.41$$

To obtain p_1 and p_2 it is necessary to evaluate the first and second order potentials ϕ_1 and ϕ_2.

Consider a potential flow with velocity u in the far field. The presence of a circular cylinder results in a modified flow field (see figure 3.3) whose potential ϕ_d corresponds to a dipole (Milne-Thomson (1960), p. 154), that is

$$\phi_d = u \left(r + \frac{b^2}{r}\right) \cos \theta \qquad 3.42$$

Using this potential it can be shown that the term in the right hand side of equation 3.40 and the first term in the right hand side of equation 3.41 lead to the first and second order inertia forces, respectively. The inertia force can be calculated by evaluating the integral

$$Fi = \int -\rho \frac{\partial \phi}{\partial t} n_x \, ds \qquad 3.43$$

where n_x is the direction cosine between the outward normal and the direction of the force component and ds is an elemental length on the perimeter of the body. Substituting 3.42 in the integral (equation 3.43) gives

$$Fi = \int -\rho \frac{\partial u}{\partial t}\left(r + \frac{b^2}{r}\right) \cos\theta \; r \cos\theta \; d\theta \qquad 3.44$$

Evaluating 3.44 at r = b gives

$$Fi = \int_0^{2\pi} -\rho \frac{\partial u}{\partial t} \; 2 \; b^2 \cos^2\theta \; d\theta$$

$$= -2\rho\pi b^2 \frac{\partial u}{\partial t} \qquad 3.45$$

which is the ideal potential value of the inertia force.

Strictly speaking, equation 3.42 would be valid if the cylinder response is due to the fluctuating velocity only. However, in the case of a wave flow the in-line velocity has a nonzero horizontal gradient (extension) denoted by $E = \partial u/\partial x$. This extension can be expressed as a sum of a pure dilatation and a dilatationless strain (figure 3.4). The cylinder responds to a variable extension because the cylinder itself impedes the local extensional motion of the fluid that would occur if the element were absent. This in turn sets up a local compensating addition to the irrotational flow field. This corresponds to a field, and a potential, that may be expressed as sums of two terms:

a) a monopole field associated with the pure dilatation to which there corresponds the potential, ϕ_m, is [Lighthill (1979), p. 19],

$$\phi_m = \frac{E}{4}\left(r^2 - 2b^2 \ln\frac{r}{b}\right) \qquad 3.46$$

where E = Extension = $\partial u/\partial x$ or $\partial w/\partial x$

r = radius to point being considered

b = cylinder radius

b) a quadrupole field associated with the dilatationless strain to which there corresponds the potential, ϕ_q, is [Paterson (1983), p. 217]

$$\phi_q = \frac{E}{4}\left(r^2 + \frac{b^4}{r^2}\right)\cos 2\theta \qquad 3.47$$

where θ = angle between the axis and the point being considered. Therefore, the total potential for the fluctuating extension is given as the sum of equations 3.46 and 3.47, that is,

$$\phi_e = \frac{E}{4}\left(r^2 - 2b^2 \ln\frac{r}{b}\right) + \frac{E}{4}\left(r^2 + \frac{b^4}{r^2}\right)\cos 2\theta \qquad 3.48$$

To include the response to the fluctuating extension in the dynamic pressure, the extension needs to be expanded in a power series

$$E = \epsilon E_1 + \epsilon^2 E_2 + \ldots\ldots \qquad 3.49$$

where $E_1 = \dfrac{\partial^2 \phi_1}{\partial x^2}$ and $E_2 = \dfrac{\partial^2 \phi_2}{\partial x^2}$

The extension potential, ϕ_e, expanded in the power series 3.49 gives

$$\phi_e = \epsilon\left\{\frac{E_1}{4}\left(r^2 - 2b^2 \ln\frac{r}{b}\right) + \frac{E_1}{4}\left(r^2 + \frac{b^4}{r^2}\right)\cos 2\theta\right\}$$

$$+ \epsilon^2\left\{\frac{E_2}{4}\left(r^2 - 2b^2 \ln\frac{r}{b}\right) + \frac{E_2}{4}\left(r^2 + \frac{b^4}{r^2}\right)\cos 2\theta\right\} \qquad 3.50$$

The basic fluctuating velocity potential, ϕ_d, can be expanded as

$$\phi_d = \epsilon u_1 \left(r + \frac{b^2}{r}\right) \cos\theta + \epsilon^2 u_2 \left(r + \frac{b^2}{r}\right) \cos\theta \qquad 3.51$$

Using polar coordinates the horizontal and vertical velocities, on the cylinder surface (r = b), are, respectively

$$v_\theta = \frac{1}{r}\frac{\partial\phi}{\partial\theta} = \frac{1}{r}\frac{\partial}{\partial\theta}(\epsilon\,\phi_1 + \epsilon^2\,\phi_2) \qquad 3.52$$

$$= \epsilon\,(-E_1\, b \sin 2\theta - 2\frac{\partial\phi_1}{\partial x}\sin\theta) +$$

$$\epsilon^2\,(-E_2\, b \sin 2\theta - 2\frac{\partial\phi_2}{\partial x}\sin\theta)$$

and

$$v_z = \frac{\partial\phi}{\partial z} = \frac{\partial}{\partial z}(\epsilon\,\phi_1 + \epsilon^2\,\phi_2) \qquad 3.53$$

$$= \epsilon\left(\frac{\partial\phi_1}{\partial z} + 2\frac{\partial^2\phi_1}{\partial x\partial z} b\cos\theta + \frac{1}{4}\frac{\partial E_1}{\partial z} b^2 + \frac{1}{2}\frac{\partial E_1}{\partial z} b^2 \cos 2\theta\right)$$

$$+ \epsilon^2\left(\frac{\partial\phi_2}{\partial z} + 2\frac{\partial^2\phi_2}{\partial x\partial z} b\cos\theta + \frac{1}{4}\frac{\partial E_2}{\partial z} b^2 + \frac{1}{2}\frac{\partial E_2}{\partial z} b^2 \cos 2\theta\right)$$

We can now calculate the total second order dynamic pressure, $p_{2d} = (1/2\rho(\nabla\phi_1)^2)$,

$$p_{2d} = -\frac{\rho}{2}\left\{ E_1^2\, b^2 \sin^2 2\theta + 4\frac{\partial\phi_1}{\partial x} E_1\, b \sin 2\theta \sin\theta \right.$$

$$+ 4\left(\frac{\partial\phi_1}{\partial x}\right)^2 \sin^2\theta + \left(\frac{\partial\phi_1}{\partial z}\right)^2 + 4\frac{\partial\phi_1}{\partial z}\frac{\partial^2\phi_1}{\partial x\partial z} b\cos\theta$$

$$+ \frac{1}{2}\frac{\partial\phi_1}{\partial z}\frac{\partial E_1}{\partial z} b^2 + \frac{\partial\phi_1}{\partial z}\frac{\partial E_1}{\partial z} b^2 \cos 2\theta + 4\left(\frac{\partial^2\phi_1}{\partial x\partial z}\right)^2 b^2 \cos^2\theta$$

$$\left. + \frac{\partial^2\phi_1}{\partial x\partial z}\frac{\partial E_1}{\partial z} b^3 \cos\theta + 2\frac{\partial E_1}{\partial z}\frac{\partial^2\phi_1}{\partial x\partial z} b^3 \cos\theta \cos 2\theta \right.$$

$$+ \frac{1}{16}\left(\frac{\partial E_1}{\partial z}\right)^2 b^4 + \frac{1}{4}\left(\frac{\partial E_1}{\partial z}\right)^2 b^4 \cos 2\theta$$

$$+ \frac{1}{4}\left(\frac{\partial E_1}{\partial z}\right)^2 b^4 \cos^2 2\theta \Bigg\} \qquad 3.54$$

The dynamic force around the cylinder is calculated as follows

$$F_{dy} = \int \frac{1}{2} \rho \, (\nabla \phi_1)^2 \, n_x \, ds$$

$$= \rho\pi b^2 \, u_{1x} \, E_1 + 2\rho\pi b^2 \, u_{1z} \frac{\partial u_{1z}}{\partial x} + 2\rho\pi b^4 \frac{\partial u_{1z}}{\partial x} \frac{\partial E_1}{\partial z} \qquad 3.55$$

where ρ = fluid density

u_{1x} = first order velocity in the x direction = $\partial\phi_1/\partial x$

E_1 = first order extension in the x direction = $\partial^2\phi_1/\partial x^2$

u_{1z} = first order velocity in the z direction = $\partial\phi_1/\partial z$

and the total force on the section being considered is

$$F_{2d} = \int F_{dy} \, dz \qquad 3.56$$

For slender cylinders the last term in equation 3.55 turns out to be insignificant compared to the first two. If we consider deep water waves ($kh > \pi$) and Stokes first order theory [as in Lighthill (1979)], we obtain

$$u_{1x} \, E_1 \simeq - \, u_{1z} \frac{\partial u_{1z}}{\partial x} \qquad 3.57$$

and

$$F_{dy} = -\rho\pi b^2 \, u_{1x} \, E_1 \qquad 3.58$$

which is the same as the result obtained by Lighthill (1979) for deep water waves.

For the effect of a current to be included, we write the velocity potential of the current as

$$\phi_c = U_c \left(r + \frac{b^2}{r}\right) \cos\theta \qquad 3.59$$

and the horizontal velocity is

$$v_{c\theta} = -\frac{1}{r}\frac{\partial \phi_c}{\partial \theta} = -2\, U_c \sin\theta \qquad 3.60$$

where U_c is the current velocity and is assumed to be constant. The total velocity is then calculated and substituted into the equation for the dynamic pressure to obtain a total perimeter force equal to

$$F_{dyc} = \rho\pi b^2 \left\{ u_{1x}\, E_1 + 2u_{1z} \frac{\partial u_{1z}}{\partial x} + 2\rho\pi b^2 \frac{\partial u_{1z}}{\partial x}\frac{\partial E_1}{\partial z} + \frac{U_c E_2}{2} \right\} \qquad 3.61$$

The second order extension E_2 is usually much smaller than E_1. If the first order velocity is much greater than the current, the correction term due to the current is small compared to the first two terms in equation 3.61 and can be ignored.

The resultant total force on the element, due to the dynamic pressure, is found by integrating the perimeter force (equation 3.55) over the section being considered. For the case of an elemental section always below the free surface (such as the force sleeve of figure 3.2) the force acting on that section is given by equation 3.56, that is

$$F_{2d} = \int_{-r}^{-s} F_{dy}\, dz \qquad 3.62$$

Therefore, the total Lighthill second order force acting over the elemental section is

$$F_{2d} = \rho\pi b^2 \int_{-r}^{-s} \left(u_{1x}\, E_1 + 2\, u_{1z} \frac{\partial u_{1z}}{\partial x} + 2\, b^2 \frac{\partial u_{1z}}{\partial x}\frac{\partial E_1}{\partial z}\right) dz \qquad 3.63$$

When the results from Stokes second order wave theory are substituted in equation 3.63 we obtain

$$F_{2d} = \left\{ -\rho \frac{\pi b^2 g^2 k}{4\omega^2} \frac{\left(\frac{\sinh 2k(-s+d)}{2k} - s\right) - \left(\frac{\sinh 2k(-r+d)}{2k} - r\right)}{\cosh^2 kd} \right.$$

$$+ \rho \frac{\pi b^2 g^2 k}{2\omega^2} \frac{\left(\frac{\sinh 2k(-s+d)}{2k} + s\right) - \left(\frac{\sinh 2k(-r+d)}{2k} + r\right)}{\cosh^2 kd}$$

$$\left. - \rho \frac{\pi b^4 g^2 k^3}{2\omega^2} \frac{\left(\frac{\sinh 2k(-s+d)}{2k} + s\right) - \left(\frac{\sinh 2k(-r+d)}{2k} + r\right)}{\cosh^2 kd} \right\} x$$

$$a^2 k^2 \sin 2(kx-\omega t) \qquad 3.64$$

In addition to the second order force due to the dynamic pressure an additional nonlinear force is present due to the integration of the pressure up to $z = 0$ rather than $z = \eta$ [Lighthill (1979)]. This is a horizontal force which acts at the still water level, $z = 0$. This term does not come into effect in the analysis in this work as we are only determining the load over a small section of the cylinder that is always below the free surface, for which the effect of integration up to $z = \eta$ has been taken into account in the derivation of the velocity potential ϕ.

According to Lighthill (1979) the analysis for the second order corrections is equally relevant in random wave fields. If the analysis is to be performed in the time domain then the velocity is simply the local fluctuating velocity and the extension is the local fluctuating extension in the wave field.

3.5 Relations Between Flow Properties and Their First Order Components

The first order quantities of equation 3.61 were expressed in equation 3.64 in terms of wave amplitude, a, and period, T, using Stokes second order theory.

The periodic flow data obtained from the Naval Civil Engineering Laboratory include measurements of the flow velocities near the cylinder as well as measurements of the wave amplitude and period. To take advantage of the availability of the velocity data relations must be developed to obtain the requisite first order components of equation 3.61. Initially the following approach was attempted. Let the first and second order components of the total measured velocity u_m be denoted by u_{1m} and u_{2m}, respectively, so that

$$u_{1m} + u_{2m} = u_m \tag{3.65}$$

We require

$$\frac{u_{1m}}{u_{2m}} = \frac{u_{1St}}{u_{2St}} \tag{3.66}$$

where u_{1St} and u_{2St} are the first and second order components calculated by Stokes' second order theory. It follows that

$$u_{1m}\left(1 + \frac{u_{2St}}{u_{1St}}\right) = u_m \tag{3.67}$$

or

$$u_{1m} = \frac{u_m\, u_{1St}}{(u_{1St} + u_{2St})} \tag{3.68}$$

It can be seen from equation 3.68 that this approach is not workable because at points where $u_{1St} \simeq u_{2St}$ (see figures 3.5 and

3.6), u_{1m} as calculated by equation 3.68 becomes very large. In the case of figure 3.6, this occurs over a sizeable time interval. To eliminate this problem the following relations were used:

$$u_{1m} = u_{1St} + (u_m - (u_{1St} + u_{2St})) \frac{|u_{1St}|}{|u_{1St} + u_{2St}|} \qquad 3.69$$

$$u_{2m} = u_{2St} + (u_m - (u_{1St} + u_{2St})) \frac{|u_{2St}|}{|u_{1St} + u_{2St}|} \qquad 3.70$$

Relations of this type were applied to all the measured wave kinematics: horizontal velocity, vertical velocity, horizontal acceleration and vertical acceleration.

The extension E and the spatial derivatives of the vertical velocity u_z and of E, which are also needed in equation 3.61, were not measured, since such measurements cannot be carried out in practice. To estimate E_{1m}, $\partial u_{1zm}/\partial x$ and $\partial E_{1m}/\partial z$, we make use of the following relations based on Stokes' theory.

$$E_1 = -\frac{k}{\omega} \frac{\partial u_{1x}}{\partial t} \qquad 3.71$$

$$\frac{\partial u_{1z}}{\partial x} = \frac{k}{\omega} \frac{\partial u_{1z}}{\partial t} \qquad 3.72$$

$$\frac{\partial E_1}{\partial z} = -k^2 u_{1z} \qquad 3.73$$

Thus

$$E_{1m} = -\frac{k}{\omega} \frac{\partial u_{1xm}}{\partial t} \qquad 3.74$$

and so forth, where u_{1xm} is the calculated first order velocity. All the required first order components based on the measured data

can be calculated and the Lighthill force equation 3.61 can be evaluated.

3.6 Wave Flow Representation by Fourier Series

Consider a sample record x(t) of finite length T. Assume that the record is sampled at an even number, N, equally spaced points a distance f = T/N apart. The time series x_{m+1}, where x_{m+1} is the value of x(t) at $t_{m+1} = (m+1)f$ (m = 0,1,2..), can be regenerated by a Fourier series as follows

$$x_{m+1} = a_1/2 + a_{N/2+1}/(2N(-1)^m) + \sum_{n=1}^{N/2+1} \left(a_{n+1} \cos \frac{2\pi mn}{N} + b_{n+1} \sin \frac{2\pi mn}{N}\right) \qquad 3.75$$

where

$$a_{n+1} = \frac{2}{N} \sum_{m=0}^{N-1} x_{m+1} \cos \frac{2\pi mn}{N} \; ; \quad n = 0,\ 1,\ 2\ldots,\ N/2 \qquad 3.76$$

$$b_{n+1} = \frac{2}{N} \sum_{m=0}^{N-1} x_{m+1} \sin \frac{2\pi mn}{N} \; ; \quad n = 0,\ 1,\ 2\ldots,\ N/2 \qquad 3.77$$

Equations 3.75, 3.76 and 3.77 can be used to smooth the measured time history. This is done by truncating the Fourier series representing the time history, so that high frequency components due to noise are eliminated. Equation 3.75 will thus become

$$x_{m+1} = \frac{a_1}{2} + \sum_{n=1}^{NFC} \left(a_{n+1} \cos \frac{2\pi mn}{N} + b_{n+1} \sin \frac{2\pi mn}{N}\right) \qquad 3.78$$

where NFC is the number of Fourier components in the truncated series. This smoothing procedure can be used for both random and periodic waves.

A Fourier analysis can be used to obtain the time series of the extension, $\partial u/\partial x$. If in equation 3.78 the variable x represents the velocity u and the extension E, respectively, then

$$u_{m+1} = \frac{a_1}{2} + \sum_{n=1}^{NFC} \left(a_{n+1} \cos \frac{2\pi mn}{N} + b_{n+1} \sin \frac{2\pi mn}{N} \right) \qquad 3.79$$

and

$$E_{m+1} = \sum_{n=1}^{NFC} \left(a_{n+1} k_n \cos \frac{2\pi mn}{N} + b_{n+1} k_n \sin \frac{2\pi mn}{N} \right) \qquad 3.80$$

where k_n is the wavenumber determined from the dispersion relation. The frequency used for the calculation of the wavenumber is

$$\omega_n = \frac{2\pi n}{Nf} \qquad 3.81$$

This method for estimating the extension will be used to calculate the extensional time history for the random data. It is noted that for the periodic data Stokes second order theory may be used directly for calculating the requisite values of E, that is, the use of equations 3.79 and 3.80 is not needed in this case.

3.7 Frequency Composition of the Residual Force

In the residue analysis by Keulegan and Carpenter (1958) and by Sarpkaya (1981a, 1981b) it was required when calculating the drag force to simplify the trigonometric expressions that arise from the u|u| term. If Stokes second order theory is used, then this term is of the form

$$(a \cos \omega t + b \cos 2\omega t) \, |a \cos \omega t + b \cos 2\omega t| \qquad 3.82$$

Ellix (1984) has shown that if (1) $b \ll a$ such that $b^2 \cos^2 2\omega t$ is

negligible, (2) cos ωt and cos $2\omega t$ are of opposite sign, and (3) $|b \cos 2\omega t| < |a \cos \omega t|$,

then

$$(a \cos \omega t + b \cos 2\omega t)\ |a \cos \omega t + b \cos 2\omega t| \simeq$$

$$a^2 \cos \omega t\ |\cos \omega t| + 2ab \cos 2\omega t\ |\cos \omega t| \qquad 3.83$$

Ellix found that the approximation in equation 3.83 is very close.

Using a Fourier analysis approach Keulegan and Carpenter (1958) have shown that

$$\cos \omega t\ |\cos \omega t| =$$

$$\frac{8}{3\pi} \cos \omega t + \frac{8}{15\pi} \cos 3\omega t - \frac{8}{105\pi} \cos 5\omega t + \ldots$$

Using a similar approach, the following result is obtained for the second term on the right hand side of equation 3.83

$$\cos 2\omega t\ |\cos \omega t| =$$

$$\frac{2}{3\pi} + \frac{28}{15\pi} \cos 2\omega t + \frac{76}{105\pi} \cos 4\omega t + \ldots \qquad 3.84$$

Therefore,

$$a^2 \cos \omega t\ |\cos \omega t| + 2ab \cos 2\omega t\ |\cos \omega t| \simeq$$

$$a^2 \left\{ \frac{8}{3\pi} \cos \omega t + \frac{8}{15\pi} \cos 3\omega t - \frac{8}{105\pi} \cos 5\omega t + \ldots \right\} +$$

$$2ab \left\{ \frac{2}{3\pi} + \frac{28}{15\pi} \cos 2\omega t + \frac{76}{105\pi} \cos 4\omega t + \ldots \right\}$$

$$\simeq \frac{4}{3\pi} ab + \frac{8}{3\pi} a^2 \cos \omega t + \frac{56}{15\pi} ab \cos 2\omega t + \frac{8}{15\pi} a^2 \cos 3\omega t$$

$$\frac{152}{105\pi} ab \cos 4\omega t - \frac{8}{105\pi} a^2 \cos 5\omega t + \ldots \qquad 3.85$$

For perfectly harmonic flow, Keulegan and Carpenter and Sarpkaya showed that the force residual comprises only odd harmonics. However, equation 3.85 shows clearly that in an actual wave flow the residual will comprise all harmonics rather than just odd harmonics. This result is used later in the analysis of the Naval Civil Engineering Laboratory data (Section 5.5).

3.8 Evaluation of the Force Coefficients

Sarpkaya and Isaacson (1981) give some of the most frequently used methods to evaluate the force coefficients Cd and Cm. In this study the time invariant coefficients are calculated using the method of least squares. This procedure involves minimizing the sum of the squares of the errors between the measured and the calculated forces, that is, the coefficients Cd and Cm were chosen to minimize the quantity

$$\overline{R^2} = \frac{1}{N} \sum_{i=1}^{N} R_i^2 \qquad 3.86$$

where $R_i = \left(f_i - Cm \frac{\rho \pi D^2}{4} \frac{\partial u_i}{\partial t} - Cd \frac{\rho D}{2} u_i \, |u_i|\right)$

f_i is the measured in-line force, and

N is the number of data points

By making $\overline{R^2}$ stationary with respect to variations in both Cd and Cm (that is, setting $\partial\overline{R^2}/\partial Cm = \partial\overline{R^2}/\partial Cd = 0$), the required solution is obtained:

$$Cm = \frac{F_1 A_{22} - F_2 A_{12}}{A_{11} A_{22} - A_{21} A_{12}} \qquad 3.87$$

$$Cd = \frac{F_2\ A_{11} - F_1\ A_{21}}{A_{11}\ A_{22} - A_{21}\ A_{12}} \qquad 3.88$$

where

$$F_1 = \overline{f_i\ u_i}$$

$$F_2 = \overline{f_i\ u_i\ u_i}$$

$$A_{11} = \frac{\rho\pi D^2}{4}\ \overline{u_i^{\,2}}$$

$$A_{12} = \frac{\rho D}{2}\ \overline{u_i\ u_i\ u_i}$$

$$A_{21} = \frac{\rho\pi D^2}{4}\ \overline{u_i\ u_i\ u_i}$$

$$A_{22} = \frac{\rho D}{2}\ \overline{(u_i\ u_i)^2}$$

If the hydrodynamic force depends upon the coefficients Cm^I (associated with the inertia force in the Morison equation), Cm^{II} (associated with the Lighthill correction term), and Cd (associated with the drag force in the Morison equation) it is necessary to minimize equation 3.86 where

$$R_i = (f_i - Cm^I\ X - Cm^{II}\ Y - Cd\ Z) \qquad 3.89$$

where $$X = \frac{\rho\pi D^2}{4}\left(\frac{\partial u_{1x}}{\partial t} + \frac{\partial u_{2x}}{\partial t}\right)$$

$$Y = \frac{\rho\pi D^2}{8}\left(u_{1x}\ E_1 + 2\ u_{1z}\ \frac{\partial u_{1z}}{\partial x} + \frac{D^2}{2}\ \frac{\partial u_{1z}}{\partial x}\ \frac{\partial E_1}{\partial z}\right)$$

$$Z = \frac{\rho D}{2}\ u_{1x}\ |u_{1x}|$$

For the condition

$$\frac{\partial \overline{R^2}}{\partial Cd} = \frac{\partial \overline{R^2}}{\partial Cm^I} = \frac{\partial \overline{R^2}}{\partial Cm^{II}} = 0 \qquad 3.90$$

we obtain

$$Cd = \frac{E_1 D_2 - D_1 E_2}{D_3 E_2 - E_3 D_2} \qquad 3.91$$

$$Cm^I = \frac{F_3 G_1 - F_1 G_3}{F_2 G_3 - G_2 F_3} \qquad 3.92$$

$$Cm^{II} = \frac{D_1 E_3 - D_3 E_1}{D_3 E_2 - E_3 D_2} \qquad 3.93$$

where $A_1 = \overline{f_i Z}$ $B_1 = \overline{f_i X}$ $C_1 = \overline{f_i Y}$

$A_2 = \overline{X Z}$ $B_2 = \overline{X^2}$ $C_2 = \overline{X Y}$

$A_3 = \overline{Y Z}$ $B_3 = \overline{X Y}$ $C_3 = \overline{Y_2}$

$A_4 = \overline{Z^2}$ $B_4 = \overline{X Z}$ $C_4 = \overline{Y Z}$

$D_1 = (-A_1 B_2 + B_1 A_2)$ $E_1 = (C_1 B_2 - B_1 C_2)$

$D_2 = (A_3 B_2 - A_2 B_3)$ $E_2 = (B_3 C_2 - C_3 B_2)$

$D_3 = (A_4 B_2 - B_4 A_2)$ $E_3 = (B_4 C_2 - C_4 B_2)$

These results (equations 3.87, 3.88, 3.91, 3.92 and 3.93) are used to obtain time invariant coefficients required when modeling the fluid forces on a cylinder using either the Morison equation or the Morison equation with the Lighthill correction. Time invariant coefficients are used with either periodic flow (such as the NCEL data) or random flow (such as the Delft data).

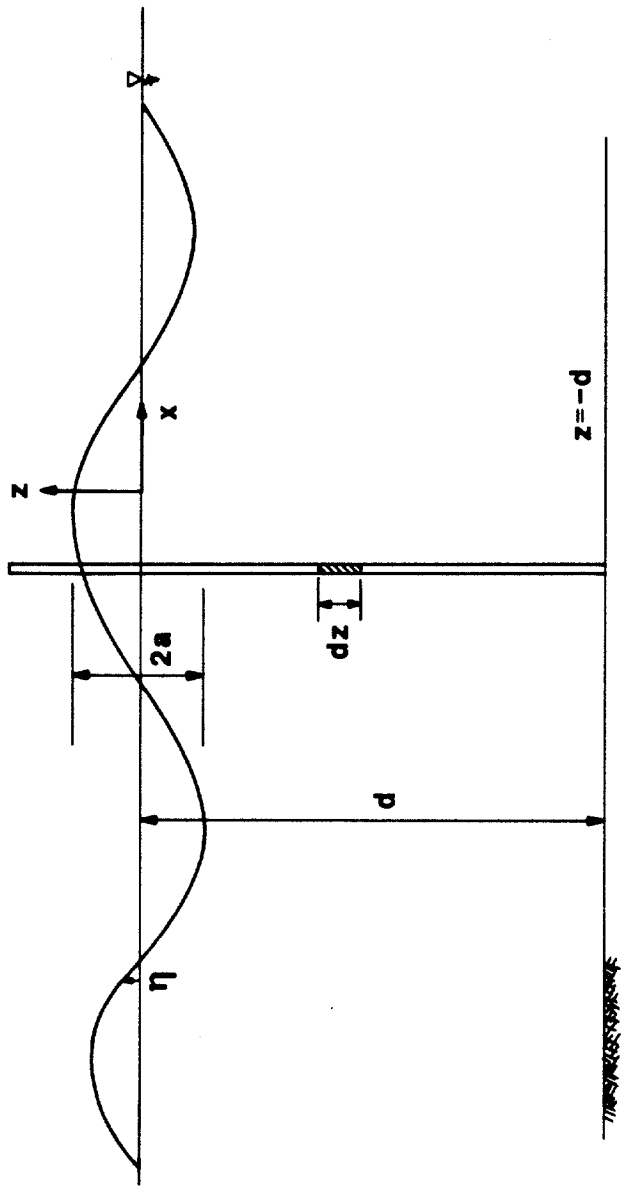

Figure 3.1. Definition of a progressive wave.

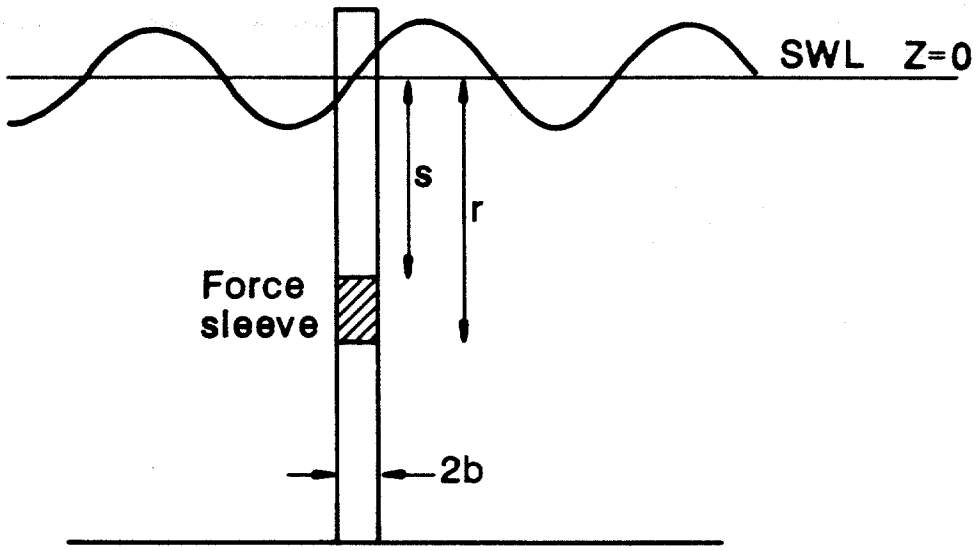

Figure 3.2. Integration limits for the force element.

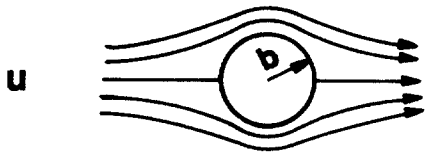

Basic flow

$$\Phi = u\left(r + \frac{b^2}{r}\right)\cos\theta$$

Figure 3.3. Basic potential fluid flow around a cylinder.

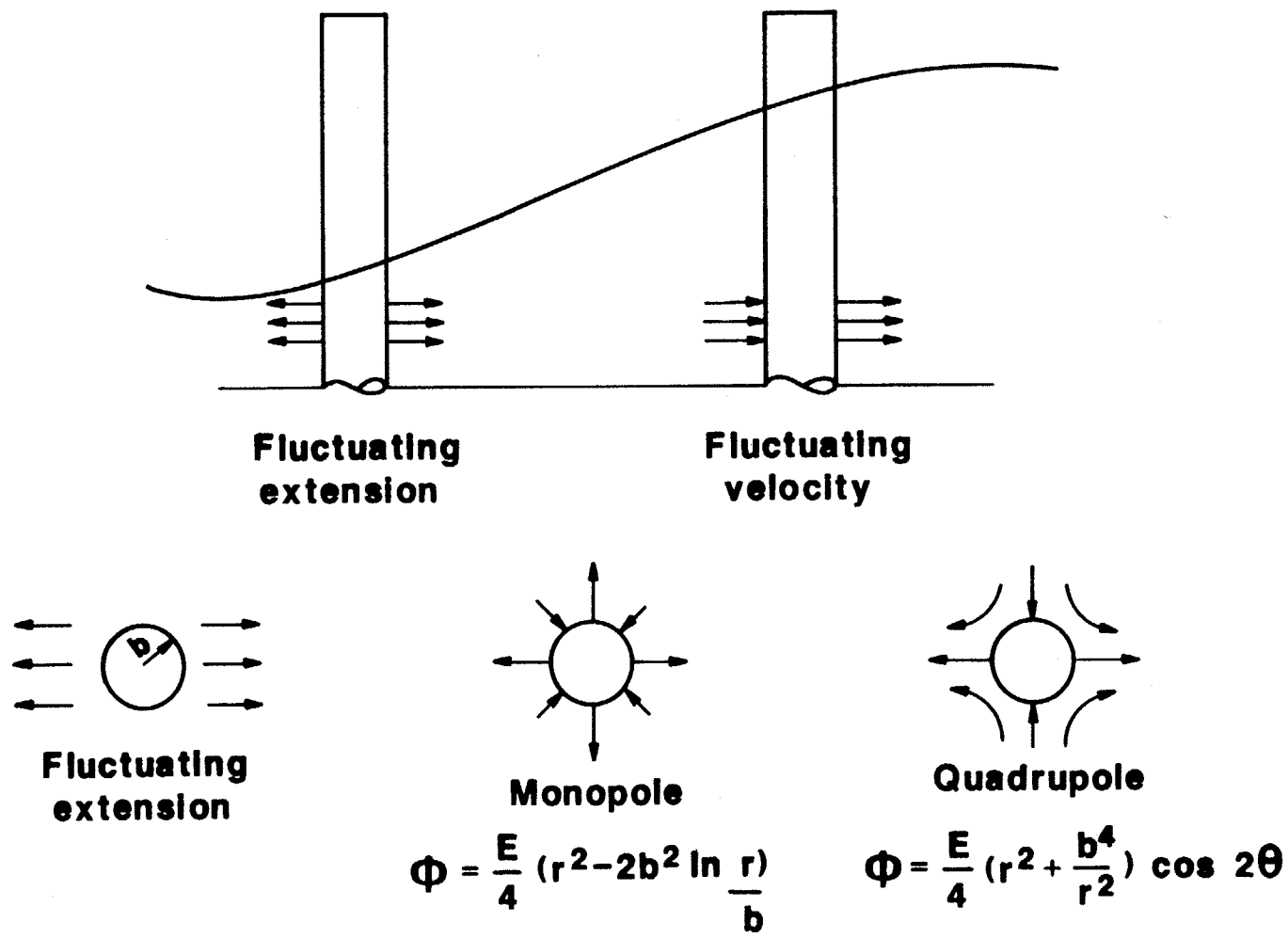

Figure 3.4. Fluctuating extensions.

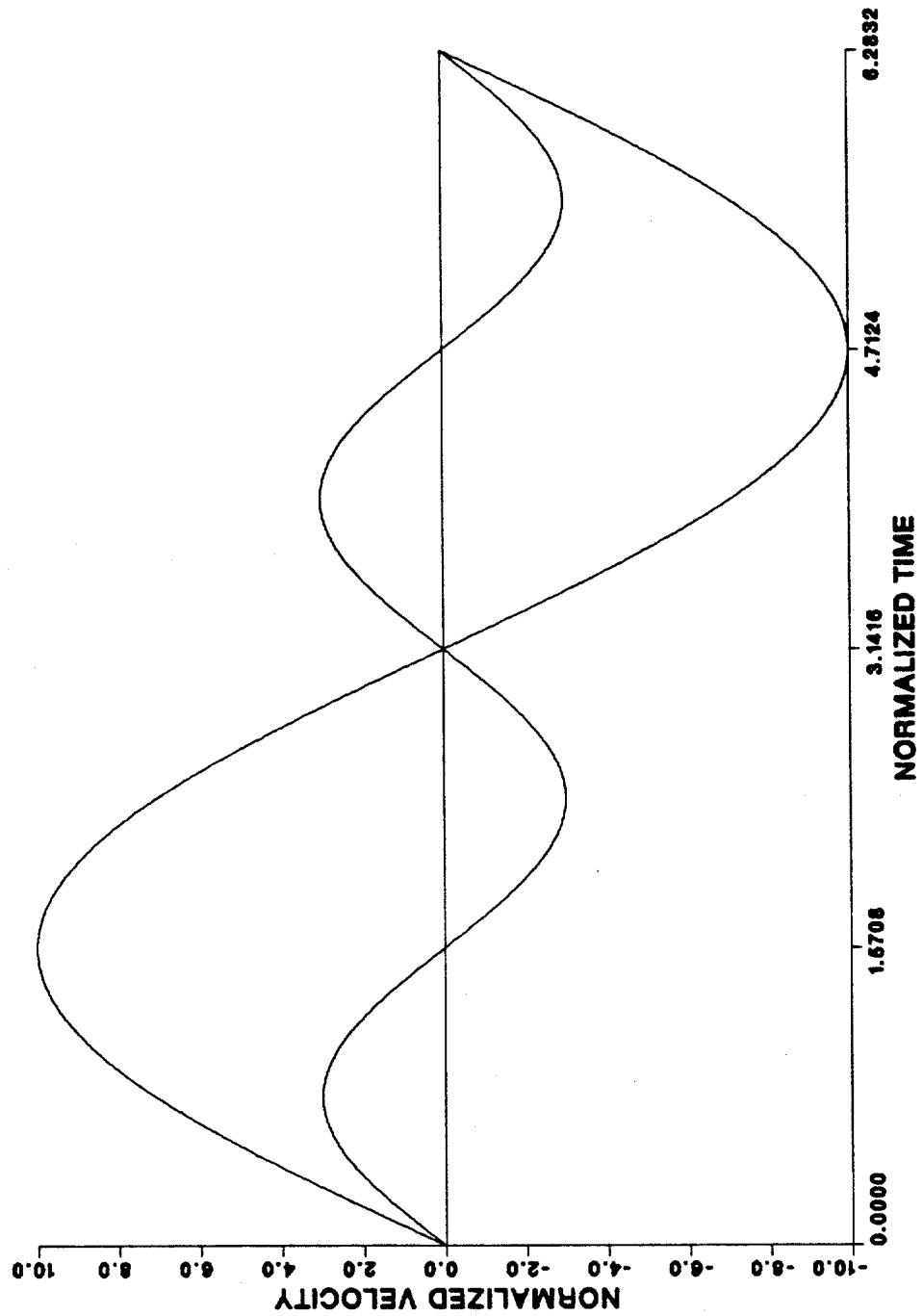

Figure 3.5. Comparison of first and second order velocities.

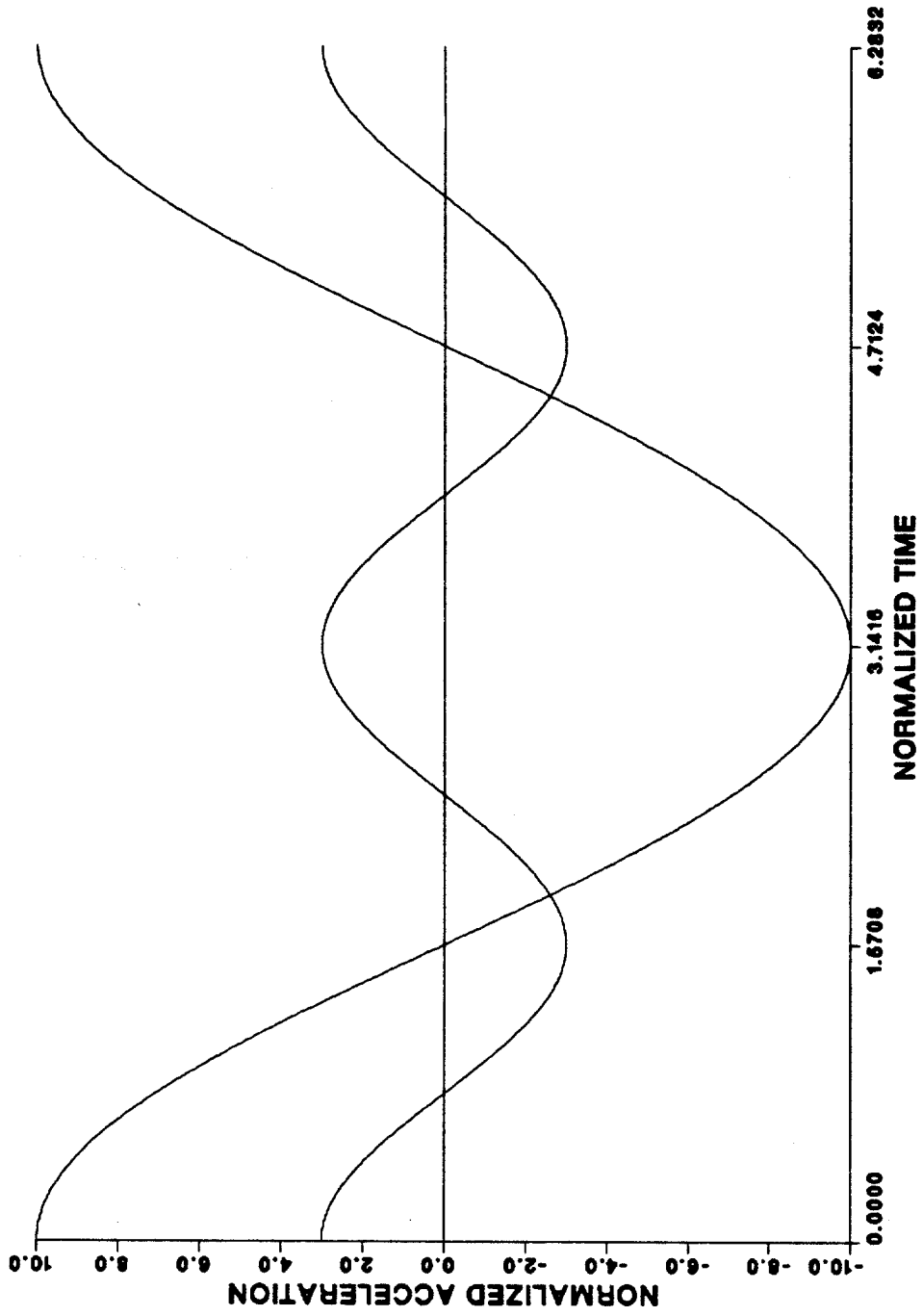

Figure 3.6. Comparison of first and second order accelerations.

CHAPTER FOUR

EXPERIMENTAL DATA

This chapter presents a summary and basic analyses of the experimental data from the following three sources:

1. The British Maritime Technology (BMT), U.K. which supplied full-scale random data from the Christchurch Bay Tower.
2. Naval Civil Engineering Laboratory (NCEL), California, which supplied data obtained in periodic waves from a series of 28 tests conducted at the Oregon State University (OSU).
3. Delft Hydraulics Laboratory, Netherlands, which supplied data obtained in random waves from laboratory tests.

4.1 British Maritime Technology

The Christchurch Bay wave force experiment involved the measuring of wave forces on two vertical circular columns which formed part of a structure placed in Christchurch Bay. The test setup is shown in figure 4.1 [from Standing (1980)]. The forces were measured using force sleeves of 0.48m diameter and 0.54m height. The particle velocities were measured at points adjacent to the elements to avoid uncertainties associated with having to deduce the particle properties indirectly. Two sets of data, Runs Nos. 35 and 54 were obtained. The data included the force in the X and Y direction and the velocity in the X, Y, and Z directions, for four levels of the column. According to the BMT analysis the two records were to have the following properties:

Record 54; Surface elevation rms = 0.68m (corresponding to approximately 20 minutes maximum waveheight = 5.3m); current = 0.83 m/sec.

Record 35; Surface elevation rms = 0.51m (corresponding to approximately 20 minutes maximum waveheight = 4.0m); current = 0.54 m/sec.

The data received from BMT were analyzed, and figures 4.2 to 4.7 give typical time histories and spectra for the force, velocity and acceleration in the x direction at the first level. These results are representative of the four levels. None of the time histories has been smoothed, but the means have been subtracted. Although the time histories have zero mean it can be observed that the spectral densities of the force and mean are not zero at zero frequency. This may be attributed to the time series having non-zero autocorrelations at small time increments and/or to drift in the measuring devices. Figure 4.8 shows the velocity spectrum that corresponds to figure 4.7 but with the mean included in the analysis. It can be seen that the inclusion of the mean gives a larger spectral density at zero frequency than that calculated with the mean removed. The mean can be viewed as a trend with infinite period, hence zero frequency.

The effective Keulegan-Carpenter numbers proposed by Standing are for Run 35, KC^* = 11.76 for level 2, KC^* = 12.76 for level 3, KC^* = 12.37 for level 4 and KC^* = 11.71 for level 5. For Run 54 KC^* = 14.87 for level 2, KC^* = 22.32 for level 3, KC^* = 21.53 for level 4 and KC^* = 21.87 for level 5.

From the analysis, basic statistical properties of the data were obtained which are summarized in Table 4.1. All the horizontal velocity spectra give a spectral peak at approximately 0.125 Hz (period T = 8.0s). Using this representative period and maximum velocities from Table 4.1, for any particular run and level, maximum Keulegan-Carpenter numbers can be determined. The KC values based on a zero mean velocity are:

for Run 35	level 2	KC = 24.10
	level 3	KC = 23.25
	level 4	KC = 20.20
	level 5	KC = 18.57
for Run 54	level 2	KC = 32.53
	level 3	KC = 34.79
	level 4	KC = 32.21
	level 5	KC = 32.24

Because they are based on the maximum velocity these values are considerably higher than the effective KC values which are based on averages.

From the mean velocities given in Table 4.1 the direction and amplitude of the current can be determined. These are given in Table 4.2. The data supplied by BMT did not include a current direction because of apparent malfunction of the current directional meter (Personal communication from J.C. Shipway, BMT). From Table 4.2 it can be seen that the calculated current velocity varies considerably over the depth of the test. In addition, Standing (1980) found that in some tests the current decreased and changed direction during the course of a run. It is concluded that

the data were affected by currents whose values and variations are poorly measured. Such currents would also significantly affect the analysis and therefore introduce uncertainties in the latter. For this reason it was decided not to pursue the analysis of the BMT data.

4.2 Naval Civil Engineering Laboratory

Tests were conducted in the Oregon State University (OSU) wave flume to determine wave forces on a vertical cylinder. The flume has an overall length of 104m, of which 39.3m constitutes the length in which tests can be performed without any effect from the wave board. According to OSU good, repeatable waves can be produced ranging from a high frequency of 1.0 Hz to a low of approximately 0.12 Hz. The cylinder was smooth, 0.324m in diameter and the forces were measured over a 0.305m section 2.377m from the bottom. The still water depth was 3.505m. The wave flume and cylinder setup are shown in figures 4.9 and 4.10 respectively [Hudspeth and Nath (1985)].

The data obtained from NCEL includes the wave profile, in-line force and velocity measurements for a reasonable range of wave heights and wave periods, and hence, of the Keulegan-Carpenter number. Twenty eight different tests were obtained and a summary of the wave properties, for each test, is given in Table 4.3. The Reynolds number was calculated on the basis of the measured water temperature of 10^{o} C (50^{o} F). The kinematic viscosity was therefore 1.307×10^{-6} m^2/sec. Each of the twenty eight runs consisted of eight waves. The runs were divided into seven individual waves,

each wave being defined as starting and ending at points of maximum velocity (or zero acceleration). In this manner startup and end irregularities were eliminated. It was found from the time histories that the points of maximum velocity coincided with points of zero acceleration extremely well. The wave properties for each of the individual waves are given in Table 4.4. Note from Table 4.3 that for periodic waves the effective Keulegan-Carpenter number, as proposed by Standing, is a good estimate of the KC value based on the maximum velocity when KC is less than approximately 8.

The first fifty Fourier components of all the time histories were calculated and after inspection it was decided to smooth all time histories using the first 20 components. This eliminated the high frequency noise and allowed numerical differentiation of the velocities to obtain the accelerations. It was observed that the second order components obtained by Fourier decomposition of the measured time histories were significantly greater than the second order components based on Stokes' second order wave theory, especially for flows with low KC numbers. A series of unsmoothed and smoothed time histories are given in figures 4.11 to 4.22. All the histories are for Run NCEL08 and are typical of the results. All of the runs were tested according to LeMehautes criterion (see figure 2.1) to evaluate the appropriate wave theory to be used for describing the wave properties. In all cases either Stokes 2nd or 3rd order theory were found to be suitable.

The first and second order components of the measured quantities were obtained using the approach described in Section 3.5. Some typical plots of the first and second order components

of the velocity are given in figures 4.23 to 4.25. Figure 4.23 shows the first and second order components for the horizontal velocity for a record with very low KC number (KC = 0.31). For this situation the second order component is negligible. Figure 4.24 shows the components for a moderate KC of 9.56. In this situation the second order component is more significant and cannot be ignored. Finally, figure 4.25 shows the components for the highest KC of 16.19. In this case the second order component is greater than 20% of the total value.

Plots of the horizontal extension for the same low, moderate and high KC values are given in figures 4.26 to 4.28. As with the velocities, the second order values for the higher KC values are considerable and play a significant part in the total effect.

The effect of using just the local acceleration in the Morison equation was evaluated by plotting the local and total accelerations for different wave steepnesses. The value of the wave steepness varied between a low value of 0.025 to a high value of 0.324. Figures 4.29 to 4.32 show the difference between the local and total accelerations for wave steepnesses 0.024 (wave height = 0.21m), 0.120 (wave height = 1.09m), 0.215 (wave height = 1.25m) and 0.324 (wave height = 0.97m). These figures show that the difference between the local and total acceleration is negligible. According to Sarpkaya and Isaacson (1981) the larger errors occur at the higher wave steepnesses. However, in the case of figures 4.29 to 4.32 the larger error occurs at the higher values of wave height and not necessarily at the higher wave steepnesses. The largest difference between the local and total acceleration occurs

in figure 4.30 and is less than 4%. From these typical comparisons it is seen that the effect of the convective acceleration is negligible and that the Morison equation inertia force can be evaluated accurately using the local acceleration (see Section 2.3.1).

A comprehensive analysis of the NCEL data is given in the next chapter.

4.3 Delft Hydraulics Laboratory

This section gives a summary of the random laboratory data supplied by the Delft Hydraulics Laboratory (DHL). The test was conducted in a Delta flume which is located in DHL's De Voorst Laboratory. The flume is 230m long, 5m wide and 7m deep and is equipped with a programmable, hydraulically driven piston type wavemaker. At the end of the flume was a 1:6 slope installed for wave damping. The maximum reflection coefficient expected was 10%. To prevent reflection from the paddle a device was developed to absorb the wave [Bearman et al. (1985)]. The tests involved a 7m long, 0.5m diameter smooth vertical cylinder under random loads. The water had a mean depth of 5m and the waves were generated from a JONSWAP spectrum with a significant wave height of 0.8m and a spectral peak frequency of 0.167 Hz. The duration of the test was 189 minutes and the sampling frequency was 10 Hz.

From the peak spectral frequency an average wavenumber can be determined using the dispersion relation. The wavenumber calculated is $k = 0.165$. The product kd, where d = depth, is therefore 0.825. This value of kd does not fall in the shallow water or deep water

range. Therefore, the approximation of the hyperbolic functions in Stokes theory, applicable to these two regions could not be used. Also, the Lighthill correction term cannot be reduced to a single term as it can when the fluid flow is in the deep water range.

The instrumentation consisted of a force sleeve for simultaneous force measurements in two directions, 26 pressure transducers equally spaced in one cylinder cross section, two wave gauges, two Colnbrook electromagnetic flow meters and two perforated ball flow meters.

The measured quantities that were used in the analysis were the in-line force, the horizontal and vertical velocity, all measured at 2.5m (the lower level) and 3.5m (the upper level) above the bottom of the tank and wave elevations which were measured before and after the cylinder. The locations of all the measuring equipment are shown in figure 4.33.

When the time histories were first plotted there was visible noise in most of the measured quantities so it was decided to smooth the relevant time histories. To determine the degree to which the time histories should be smoothed the total error for varying number of Fourier components was determined. Figure 4.34 shows a plot of the root mean square error (that is, $\sqrt{((F_{measured} - F_{smoothed})^2/\text{number of points})}$) versus the number of Fourier components used to smooth the time history, for the horizontal velocity at the lower level. All of the other variables produced a similar result. From this figure it can be seen that to eliminate the noise and still provide a reasonable representation of the time series we need to use between 5000 and 22000 Fourier components.

The ratio of rms error to variance gives that the error difference between 6500 Fourier components and 20000 Fourier components is rather small therefore, the time histories were smoothed using 6500 Fourier components. This corresponds to an approximate cutoff frequency, f_c = 0.572 Hz (f_c = 5x6500/56832 where 56832 is the total number of Fourier components needed to completely regenerate the time history and 5 is the cut-off frequency for the total time history). Typical time histories of the horizontal velocity before and after smoothing are given in figures 4.35 and 4.36, respectively. If the high frequency noise had not been eliminated from the velocity time history, instabilities would have occurred when numerically differentiating to obtain the acceleration.

Typical time histories of all the relevant smoothed quantities, that is, wave elevation, horizontal and vertical velocity, horizontal and vertical acceleration and in-line force for the two different measuring positions, are given in figures 4.37 to 4.48. All forces are per meter length of cylinder and the time histories are plotted starting from t = 150s to eliminate any errors due to the startup of the experiment. Following the time histories in figures 4.49 to 4.60 are the spectra of the measured quantities given in figures 4.37 to 4.48. Some of the statistical properties of the time histories are given in Table 4.5.

The effective Keulegan-Carpenter number as defined by Standing (equation 2.10) was KC^* = 5.75 for the lower level and KC^* = 6.00 for the upper level. From the analysis of the NCEL data it was seen that the effective Keulegan-Carpenter number was a reasonable estimate of the actual Keulegan-Carpenter number especially for

KC < 8. Since the Keulegan-Carpenter numbers for the data are relatively low, it would be expected that the dominant part of the total Morison force is due to the inertia term. The region of low KC numbers is also one in which Lighthill's correction is, in principle, most applicable. Using the ranges of suitability of various wave theories suggested by LeMehaute it can be seen from the data ($H/gT^2 = 0.0023$, $d/gT^2 = 0.0142$, where H = wave height, g = acceleration due to gravity, T = wave period and d = water depth) that Stokes second order theory should be applicable. Also from the NCEL analysis it was seen that for KC < 7 the second order components of velocity and acceleration were small compared to the first order values. Hence the Lighthill force can be calculated based on the total properties rather than just the first order components.

The calculation of the horizontal extensional motion involved determining the partial derivative of the velocity with respect to horizontal (x) and vertical (z) distance. Owing to the absence of direct measurements (these would be extremely difficult to obtain), the extensional motions were obtained by differentiating the Fourier series of the velocities with respect to x or z (Section 3.6). Typical time histories of the horizontal gradient of the horizontal and vertical velocity are given in figures 4.61 and 4.62 respectively. The spectra of these horizontal gradients are given in figures 4.63 and 4.64.

Generally, in spectral representations of the Morison equation the nonlinear drag term is linearized to ensure that the velocity component at one frequency affects only the drag component of the

same frequency, so that a transfer function can be used. This linearization was reviewed in Section 2.4. The term u|u| (full line) and its linearized counterpart (dashed line) are given in figures 4.65 and 4.66 for the lower and upper levels, respectively. It is seen that differences between the spectra of the original and the linearized terms are negligible.

QUANTITY	RUN NUMBER							
	RUN 35				RUN 54			
	MEAN	STD. DEV.	MIN.	MAX.	MEAN	STD. DEV.	MIN.	MAX.
FX2	-0.0049	0.0924	-0.504	0.379	0.0286	0.1372	-0.438	0.965
FY2	-0.0409	0.0740	-0.477	0.265	0.0414	0.0913	-0.479	0.768
VX2	0.1103	0.5299	-1.296	1.556	0.6021	0.5623	-1.177	2.554
VY2	-0.2636	0.2301	-0.949	0.646	0.3026	0.2520	-0.635	1.306
VZ2	-0.0716	0.4279	-1.453	1.469	-0.0288	0.5103	-1.590	2.054
FX3	-0.0131	0.0750	-0.417	0.271	-0.0053	0.1260	-0.556	0.741
FY3	-0.0344	0.0458	-0.379	0.087	0.0449	0.0646	-0.246	0.486
VX3	-0.0229	0.4425	-1.624	1.101	0.1794	0.7402	-1.908	2.267
VY3	-0.3751	0.1559	-0.822	0.209	0.5286	0.2659	-0.449	1.634
VZ3	0.0252	0.2596	-0.802	0.946	-0.0015	0.3670	-1.351	1.624
FX4	-0.0101	0.0532	-0.403	0.211	0.0036	0.0947	-0.299	0.499
FY4	-0.0314	0.0323	-0.642	0.083	0.0248	0.0463	-0.263	0.329
VX4	-0.1971	0.3933	-1.409	0.951	0.1527	0.6652	-1.780	1.872
VY4	-0.3687	0.1324	-0.748	0.084	0.5137	0.2365	-0.457	1.196
VZ4	0.0293	0.1638	-0.516	0.626	-0.0069	0.2423	-0.772	1.041
FX5	0.0002	0.0382	-0.148	0.172	0.0216	0.0808	-0.254	0.446
FY5	-0.0288	0.0248	-0.181	0.064	0.0186	0.0398	-0.245	0.357
VX5	-0.1458	0.3201	-1.260	0.838	0.1395	0.6690	-1.795	1.847
VY5	-0.7237	0.0637	-1.012	-0.550	0.3197	0.2751	-0.478	1.041
VZ5	0.0331	0.0727	-0.217	0.295	-0.0266	0.1791	-0.531	0.642

Table 4.1. Statistical properties of the BMT data.

LEVEL	RECORD			
	RUN 35		RUN 54	
	VELOCITY	DIRECTION FROM +Y	VELOCITY	DIRECTION FROM +Y
	m/s	degrees	m/s	degrees
2	0.286	157.3	0.674	63.3
3	0.439	211.4	0.558	71.3
4	0.418	208.1	0.536	73.4
5	0.738	191.4	0.349	66.4

Table 4.2. Current magnitude and direction for each level of BMT data

RUN NUMBER	WAVE HEIGHT m	WAVE PERIOD secs	MAX. VELOCITY m/s	WAVE LENGTH m	KEULEGAN CARPENTER NUMBER	EFFECTIVE KC	REYNOLDS NUMBER
NCEL01	0.325	1.998	0.170	6.221	1.049	0.965	42135
NCEL02	0.109	2.001	0.051	6.254	0.319	0.286	12752
NCEL03	0.309	2.483	0.189	9.446	1.453	1.364	46947
NCEL04	0.569	2.490	0.332	9.494	2.551	2.455	82207
NCEL05	0.974	2.494	0.573	9.525	4.411	4.173	141850
NCEL06	0.290	2.704	0.207	18.007	2.369	2.284	51322
NCEL07	0.757	3.694	0.522	17.937	5.952	5.687	129300
NCEL08	1.277	3.700	0.924	17.979	10.559	10.108	228970
NCEL09	0.193	4.617	0.128	24.086	1.830	1.698	31793
NCEL10	0.435	4.608	0.300	24.019	4.271	4.137	74383
NCEL11	1.054	4.610	0.848	24.036	12.068	11.534	210030
NCEL12	1.292	4.615	0.951	24.070	13.558	12.858	235680
NCEL13	0.229	5.291	0.147	28.427	2.395	2.218	36328
NCEL14	0.366	5.282	0.283	28.371	4.611	4.138	70040
NCEL15	0.769	5.270	0.603	28.294	9.811	8.086	149360
NCEL16	1.024	5.288	0.815	28.409	13.303	10.439	210850
NCEL17	1.089	5.285	0.891	28.389	14.538	11.146	220730
NCEL18	0.852	5.987	0.793	32.832	14.652	11.621	196350
NCEL19	1.432	4.193	1.056	21.297	13.675	13.394	261680
NCEL20	1.098	5.291	0.937	28.428	15.309	11.983	232190
NCEL21	1.283	4.608	0.941	24.019	13.391	12.747	233160
NCEL22	1.294	3.694	0.899	17.937	10.259	9.797	222850
NCEL23	0.991	2.490	0.621	9.495	4.773	4.758	153770
NCEL24	0.835	5.979	0.802	32.791	14.807	11.901	198690
NCEL25	1.252	3.689	0.887	17.909	10.103	9.493	219730
NCEL26	1.070	4.607	0.792	24.019	11.273	10.831	196280
NCEL27	0.582	5.979	0.530	32.789	9.788	8.525	131360
NCEL28	0.699	5.979	0.658	32.789	12.147	10.067	163000

Table 4.3. Wave properties for each of the 28 NCEL runs.

RUN	WAVE	WAVE HEIGHT	CIRCULAR FREQUENCY	WAVE PERIOD	WAVE NUMBER	WAVE LENGTH	KEULEGAN-CARPENTER NUMBER	REYNOLDS NUMBER
		m	s^{-1}	s	m^{-1}	m		
	1	0.372	3.179	1.976	1.032	6.088	1.171	47544
	2	0.317	3.166	1.985	1.024	6.136	0.989	39998
	3	0.315	3.058	2.055	0.956	6.572	1.119	43714
NCEL01	4	0.321	3.179	1.976	1.032	6.088	1.033	41932
	5	0.318	3.179	1.976	1.032	6.088	1.028	41716
	6	0.319	3.117	2.016	0.992	6.334	1.022	40688
	7	0.316	3.142	2.000	1.008	6.233	0.981	39358
	1	0.114	3.081	2.039	0.971	6.471	0.302	11881
	2	0.107	3.323	1.891	1.127	5.575	0.310	13172
	3	0.107	2.883	2.179	0.851	7.383	0.330	12164
NCEL02	4	0.112	3.283	1.914	1.099	5.717	0.281	11759
	5	0.109	2.979	2.109	0.908	6.920	0.390	14832
	6	0.107	3.229	1.946	1.065	5.900	0.308	12719
	7	0.108	3.256	1.930	1.082	5.807	0.306	12737
	1	0.319	2.563	2.451	0.681	9.226	1.484	48558
	2	0.306	2.513	2.500	0.657	9.563	1.414	45379
	3	0.313	2.503	2.510	0.652	9.637	1.476	47193
NCEL03	4	0.308	2.523	2.490	0.662	9.491	1.527	49204
	5	0.308	2.523	2.490	0.662	9.491	1.453	46806
	6	0.304	2.494	2.519	0.648	9.696	1.471	46859
	7	0.305	2.594	2.422	0.697	9.015	1.347	44605
	1	0.562	2.523	2.490	0.662	9.491	2.596	83652
	2	0.565	2.533	2.481	0.667	9.420	2.486	80402
	3	0.577	2.484	2.529	0.643	9.772	2.551	80911
NCEL04	4	0.569	2.523	2.490	0.662	9.491	2.712	87388
	5	0.569	2.563	2.451	0.681	9.226	2.558	83722
	6	0.566	2.484	2.529	0.643	9.772	2.512	79667
	7	0.574	2.553	2.461	0.676	9.295	2.444	79667

Table 4.4. Properties of seven individual waves from each of the 28 NCEL tests.

RUN	WAVE	WAVE HEIGHT	CIRCULAR FREQUENCY	WAVE PERIOD	WAVE NUMBER	WAVE LENGTH	KEULEGAN-CARPENTER NUMBER	REYNOLDS NUMBER
		m	s^{-1}	s	m^{-1}	m		
	1	0.972	2.533	2.481	0.667	9.420	4.482	144962
	2	0.981	2.523	2.490	0.662	9.491	4.577	147448
	3	1.007	2.503	2.510	0.652	9.637	4.579	146346
NCEL05	4	0.879	2.484	2.529	0.643	9.772	4.453	141238
	5	1.004	2.574	2.441	0.686	9.159	4.170	137049
	6	0.992	2.484	2.529	0.643	9.772	4.329	137313
	7	0.981	2.533	2.481	0.667	9.420	4.284	138560
	1	0.289	1.659	3.787	0.338	18.589	2.403	50900
	2	0.292	1.685	3.729	0.346	18.159	2.475	53245
	3	0.293	1.739	3.613	0.361	17.405	2.398	53247
NCEL06	4	0.289	1.692	3.713	0.347	18.107	2.359	50966
	5	0.287	1.692	3.713	0.347	18.107	2.371	51224
	6	0.286	1.698	3.700	0.349	18.003	2.362	51206
	7	0.292	1.712	3.670	0.353	17.799	2.218	48496
	1	0.737	1.698	3.700	0.349	18.003	5.957	129164
	2	0.738	1.712	3.670	0.353	17.799	5.763	125995
	3	0.735	1.692	3.713	0.348	18.055	5.831	125994
NCEL07	4	0.745	1.712	3.670	0.353	17.799	5.801	126823
	5	0.787	1.698	3.700	0.349	18.003	6.241	135318
	6	0.769	1.698	3.700	0.349	18.003	6.241	135318
	7	0.791	1.698	3.700	0.349	18.003	5.836	126533
	1	1.241	1.685	3.729	0.346	18.159	10.521	226371
	2	1.281	1.692	3.713	0.348	18.055	10.915	235840
	3	1.259	1.692	3.713	0.348	18.055	10.573	228450
NCEL08	4	1.287	1.725	3.642	0.357	17.600	10.433	229821
	5	1.299	1.692	3.713	0.347	18.107	10.708	231364
	6	1.286	1.712	3.670	0.353	17.799	10.227	223577
	7	1.285	1.692	3.713	0.348	18.055	10.537	227674

Table 4.4. Properties of seven individual waves from each of the 28 NCEL tests (cont.)

RUN	WAVE	WAVE HEIGHT	CIRCULAR FREQUENCY	WAVE PERIOD	WAVE NUMBER	WAVE LENGTH	KEULEGAN-CARPENTER NUMBER	REYNOLDS NUMBER
		m	s^{-1}	s	m^{-1}	m		
	1	0.185	1.393	4.511	0.269	23.358	1.851	32921
	2	0.189	1.345	4.672	0.257	24.448	2.037	34988
	3	0.184	1.329	4.728	0.253	24.835	2.067	35087
NCEL09	4	0.188	1.393	4.511	0.269	23.358	1.850	32911
	5	0.197	1.335	4.707	0.255	24.640	1.785	30430
	6	0.196	1.377	4.563	0.265	23.710	1.697	29839
	7	0.211	1.355	4.637	0.259	24.259	1.524	26367
	1	0.429	1.371	4.583	0.263	23.890	4.326	75731
	2	0.429	1.366	4.600	0.262	23.982	4.418	77071
	3	0.422	1.361	4.617	0.261	24.074	4.534	78797
NCEL10	4	0.439	1.371	4.583	0.263	23.890	4.095	71698
	5	0.445	1.345	4.672	0.257	24.448	4.243	72868
	6	0.438	1.388	4.527	0.267	23.533	4.078	72284
	7	0.441	1.345	4.672	0.257	24.448	4.208	72268
	1	1.092	1.345	4.672	0.257	24.448	11.738	201603
	2	1.078	1.366	4.600	0.262	23.982	12.495	217951
	3	1.082	1.388	4.527	0.267	23.533	11.705	207465
NCEL11	4	1.062	1.335	4.707	0.255	24.640	12.327	210153
	5	1.014	1.361	4.617	0.261	24.074	12.417	215798
	6	1.021	1.355	4.637	0.259	24.259	12.256	212071
	7	1.029	1.393	4.511	0.269	23.358	11.542	205306
	1	1.311	1.339	4.692	0.256	24.544	14.842	253777
	2	1.314	1.371	4.583	0.263	23.890	14.504	253933
	3	1.311	1.371	4.583	0.263	23.890	13.051	228481
NCEL12	4	1.283	1.361	4.617	0.261	24.074	12.970	225409
	5	1.285	1.366	4.600	0.262	23.982	13.080	228156
	6	1.227	1.329	4.728	0.253	24.835	13.503	229166
	7	1.316	1.393	4.511	0.269	23.358	12.962	230569

Table 4.4. Properties of seven individual waves from each of the 28 NCEL tests (cont.)

RUN	WAVE	WAVE HEIGHT	CIRCULAR FREQUENCY	WAVE PERIOD	WAVE NUMBER	WAVE LENGTH	KEULEGAN-CARPENTER NUMBER	REYNOLDS NUMBER
		m	s^{-1}	s	m^{-1}	m		
	1	0.211	1.214	5.176	0.227	27.679	2.425	37595
	2	0.221	1.191	5.276	0.222	28.303	2.413	36698
	3	0.222	1.199	5.240	0.224	28.050	2.338	35798
NCEL13	4	0.232	1.176	5.343	0.219	28.690	2.384	35806
	5	0.231	1.172	5.361	0.218	28.822	2.336	34955
	6	0.241	1.985	3.165	0.223	28.176	2.291	58060
	7	0.247	1.167	5.384	0.217	28.955	2.583	38497
	1	0.355	1.191	5.276	0.222	28.303	4.427	67335
	2	0.356	1.181	5.320	0.219	28.690	4.673	70475
	3	0.357	1.195	5.258	0.223	28.176	4.619	70478
NCEL14	4	0.366	1.191	5.276	0.222	28.303	4.797	72951
	5	0.376	1.191	5.276	0.222	28.303	4.797	72951
	6	0.375	1.199	5.240	0.224	28.050	4.465	68363
	7	0.377	1.181	5.320	0.219	28.690	4.500	67871
	1	0.773	1.204	5.219	0.225	27.925	9.410	144684
	2	0.725	1.195	5.258	0.223	28.176	9.726	148417
	3	0.752	1.195	5.258	0.223	28.176	10.118	154393
NCEL15	4	0.781	1.176	5.343	0.219	28.690	10.277	154331
	5	0.808	1.204	5.219	0.225	27.925	9.631	148077
	6	0.777	1.171	5.366	0.218	28.822	9.899	148019
	7	0.767	1.199	5.240	0.224	28.050	9.623	147332
	1	1.017	1.191	5.276	0.222	28.303	12.999	197701
	2	1.014	1.194	5.262	0.223	28.176	13.547	206553
	3	1.023	1.191	5.276	0.222	28.303	13.600	206845
NCEL16	4	1.034	1.191	5.276	0.222	28.303	13.700	208362
	5	1.042	1.176	5.343	0.219	28.690	13.861	208159
	6	1.029	1.191	5.276	0.222	28.303	12.772	194248
	7	1.009	1.186	5.298	0.221	28.431	12.645	191514

Table 4.4. Properties of seven individual waves from each of the 28 NCEL tests (cont.)

RUN	WAVE	WAVE HEIGHT	CIRCULAR FREQUENCY	WAVE PERIOD	WAVE NUMBER	WAVE LENGTH	KEULEGAN-CARPENTER NUMBER	REYNOLDS NUMBER
		m	s^{-1}	s	m^{-1}	m		
	1	1.086	1.191	5.276	0.222	28.303	13.712	208536
	2	1.092	1.204	5.219	0.225	27.925	15.105	232241
	3	1.064	1.186	5.298	0.221	28.431	15.345	232400
NCEL17	4	1.108	1.191	5.276	0.222	28.303	14.789	224916
	5	1.141	1.167	5.384	0.217	28.955	14.659	218456
	6	1.094	1.199	5.240	0.223	28.176	13.943	213483
	7	1.041	1.186	5.298	0.221	28.431	14.218	215325
	1	0.871	1.027	6.118	0.187	33.600	14.932	195826
	2	0.845	1.055	5.956	0.193	32.555	14.585	196495
	3	0.839	1.051	5.978	0.192	32.725	14.643	196521
NCEL18	4	0.868	1.051	5.978	0.192	32.725	15.175	203669
	5	0.856	1.039	6.047	0.189	33.244	15.354	203712
	6	0.845	1.059	5.933	0.194	32.388	13.874	187616
	7	0.841	1.064	5.905	0.194	32.388	14.005	190285
	1	1.416	1.484	4.234	0.291	21.592	13.571	257168
	2	1.443	1.502	4.183	0.296	21.227	14.031	269122
	3	1.451	1.514	4.150	0.299	21.014	12.850	248429
NCEL19	4	1.446	1.491	4.214	0.293	21.444	13.535	257709
	5	1.421	1.508	4.167	0.297	21.156	13.519	260328
	6	1.428	1.479	4.248	0.289	21.741	14.072	265780
	7	1.417	1.514	4.150	0.299	21.014	14.148	273523
	1	1.084	1.172	5.361	0.218	28.822	14.661	219425
	2	1.081	1.191	5.276	0.222	28.303	14.690	223419
	3	1.091	1.209	5.197	0.226	27.802	15.869	245003
NCEL20	4	1.068	1.186	5.298	0.221	28.431	16.186	245130
	5	1.105	1.186	5.298	0.221	28.431	15.461	234162
	6	1.123	1.172	5.361	0.218	28.822	15.643	234110
	7	1.136	1.199	5.240	0.224	28.050	14.657	224419

Table 4.4. Properties of seven individual waves from each of the 28 NCEL tests (cont.)

RUN	WAVE	WAVE HEIGHT	CIRCULAR FREQUENCY	WAVE PERIOD	WAVE NUMBER	WAVE LENGTH	KEULEGAN-CARPENTER NUMBER	REYNOLDS NUMBER
		m	s^{-1}	s	m^{-1}	m		
	1	1.302	1.355	4.637	0.259	24.259	12.971	224439
	2	1.305	1.371	4.583	0.263	23.890	13.549	237208
	3	1.316	1.361	4.617	0.261	24.074	13.655	237324
NCEL21	4	1.276	1.377	4.563	0.265	23.710	13.587	238912
	5	1.224	1.351	4.651	0.258	24.353	13.854	239015
	6	1.277	1.355	4.637	0.259	24.259	13.605	235404
	7	1.281	1.377	4.563	0.265	23.710	12.510	219974
	1	1.291	1.698	3.700	0.349	18.003	10.082	218605
	2	1.304	1.705	3.685	0.351	17.901	9.695	211081
	3	1.299	1.725	3.642	0.357	17.600	10.120	222911
NCEL22	4	1.337	1.698	3.700	0.349	18.003	10.280	222905
	5	1.315	1.705	3.685	0.351	17.901	10.473	228022
	6	1.329	1.698	3.700	0.349	18.003	10.514	227976
	7	1.184	1.678	3.744	0.344	18.265	10.656	228340
	1	0.969	2.533	2.481	0.667	9.420	4.795	155105
	2	0.981	2.513	2.500	0.657	9.563	4.996	160319
	3	0.992	2.533	2.481	0.667	9.420	4.891	158199
NCEL23	4	1.005	2.484	2.529	0.643	9.772	5.002	158671
	5	0.982	2.543	2.471	0.671	9.364	4.617	149926
	6	1.019	2.475	2.539	0.639	9.833	4.748	150071
	7	0.991	2.584	2.432	0.692	9.080	4.367	144093
	1	0.845	1.047	6.001	0.191	32.896	13.943	186422
	2	0.838	1.055	5.956	0.193	32.555	14.874	200391
	3	0.826	1.051	5.978	0.192	32.725	14.933	200417
NCEL24	4	0.848	1.047	6.001	0.191	32.896	15.125	202220
	5	0.823	1.051	5.978	0.192	32.725	15.066	202200
	6	0.815	1.055	5.956	0.193	32.555	14.869	200316
	7	0.849	1.047	6.001	0.191	32.896	14.845	198480

Table 4.4. Properties of seven individual waves from each of the 28 NCEL tests (cont.)

RUN	WAVE	WAVE HEIGHT	CIRCULAR FREQUENCY	WAVE PERIOD	WAVE NUMBER	WAVE LENGTH	KEULEGAN-CARPENTER NUMBER	REYNOLDS NUMBER
		m	s^{-1}	s	m^{-1}	m		
	1	1.223	1.685	3.729	0.346	18.159	9.563	205777
	2	1.288	1.698	3.700	0.349	18.003	9.831	213174
	3	1.179	1.705	3.685	0.351	17.901	10.018	218121
NCEL25	4	1.286	1.725	3.642	0.357	17.600	10.220	225126
	5	1.266	1.712	3.670	0.353	17.799	10.301	225203
	6	1.268	1.698	3.700	0.349	18.003	10.304	223428
	7	1.254	1.698	3.700	0.349	18.003	10.484	227320
	1	1.099	1.355	4.637	0.259	24.259	11.549	199825
	2	1.086	1.366	4.600	0.262	23.982	11.614	202591
	3	1.099	1.371	4.583	0.263	23.890	10.665	186713
NCEL26	4	1.058	1.361	4.617	0.261	24.074	11.326	196847
	5	1.058	1.361	4.617	0.261	24.074	10.918	189744
	6	1.039	1.299	4.837	0.246	25.541	12.129	201198
	7	1.051	1.439	4.366	0.279	22.520	10.717	196939
	1	0.605	1.035	6.071	0.188	33.421	9.598	126851
	2	0.582	1.043	6.024	0.191	32.896	9.972	132812
	3	0.559	1.064	5.905	0.194	32.388	9.778	132851
NCEL27	4	0.558	1.047	6.001	0.191	32.896	9.507	127103
	5	0.569	1.051	5.978	0.192	32.725	9.817	131757
	6	0.591	1.059	5.933	0.194	32.388	9.905	133947
	7	0.611	1.055	5.956	0.193	32.555	9.944	133968
	1	0.732	1.027	6.118	0.187	33.600	11.984	157171
	2	0.696	1.055	5.956	0.193	32.555	11.907	160413
	3	0.689	1.051	5.978	0.192	32.725	12.495	167696
NCEL28	4	0.694	1.055	5.956	0.193	32.555	12.446	167674
	5	0.686	1.047	6.001	0.191	32.896	12.406	165872
	6	0.684	1.064	5.905	0.194	32.388	11.880	161416
	7	0.709	1.055	5.956	0.193	32.555	11.913	160492

Table 4.4. Properties of seven individual waves from each of the 28 NCEL tests (cont.)

MEASURING DEVICE	UNITS	MEAN	STD. DEV.	MIN.	MAX.
WAVE GAUGE 1	meter	-0.006	0.212	-0.810	1.036
WAVE GAUGE 2	meter	0.001	0.210	-0.820	0.859
FORCE SLEEVE 1X	Newton	18.400	102.300	-379.600	378.100
FORCE SLEEVE 1Y	Newton	4.580	9.860	-139.900	149.500
FORCE SLEEVE 2X	Newton	-5.110	136.500	-524.900	546.000
FORCE SLEEVE 2Y	Newton	1.890	15.820	-284.600	230.300
VELOCITY 1X	meter/sec	0.001	0.250	-1.039	1.020
VELOCITY 1Z	meter/sec	0.010	0.111	-0.520	0.456
VELOCITY 2X	meter/sec	0.019	0.277	-1.066	1.176
VELOCITY 2Z	meter/sec	-0.003	0.149	-0.706	0.588

Table 4.5. Statistics for the Delft data.

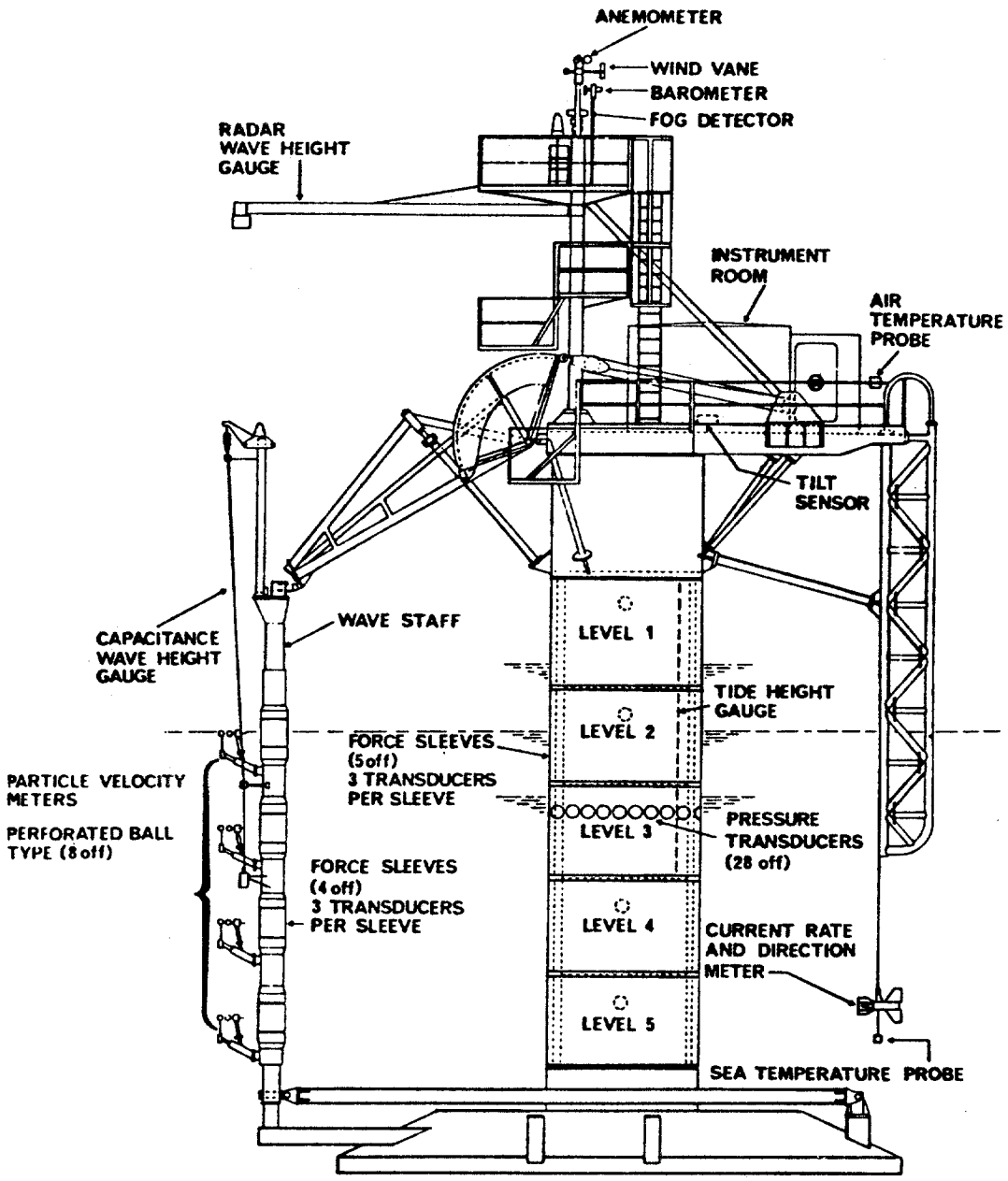

Figure 4.1. Force measuring elements on the Christchurch Bay Facility [Standing (1980)].

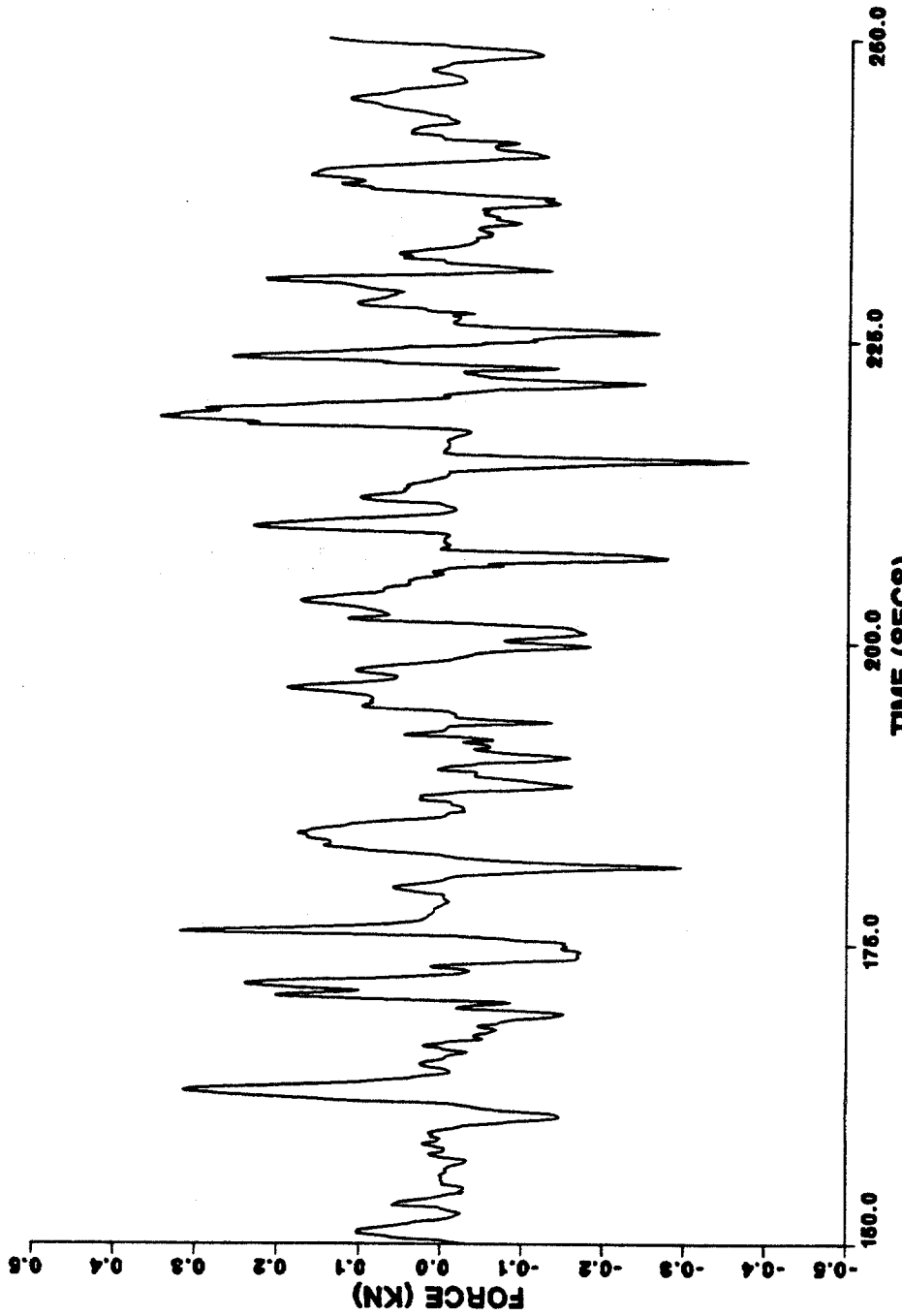

Figure 4.2. Force in X direction at level 2, Run 35.

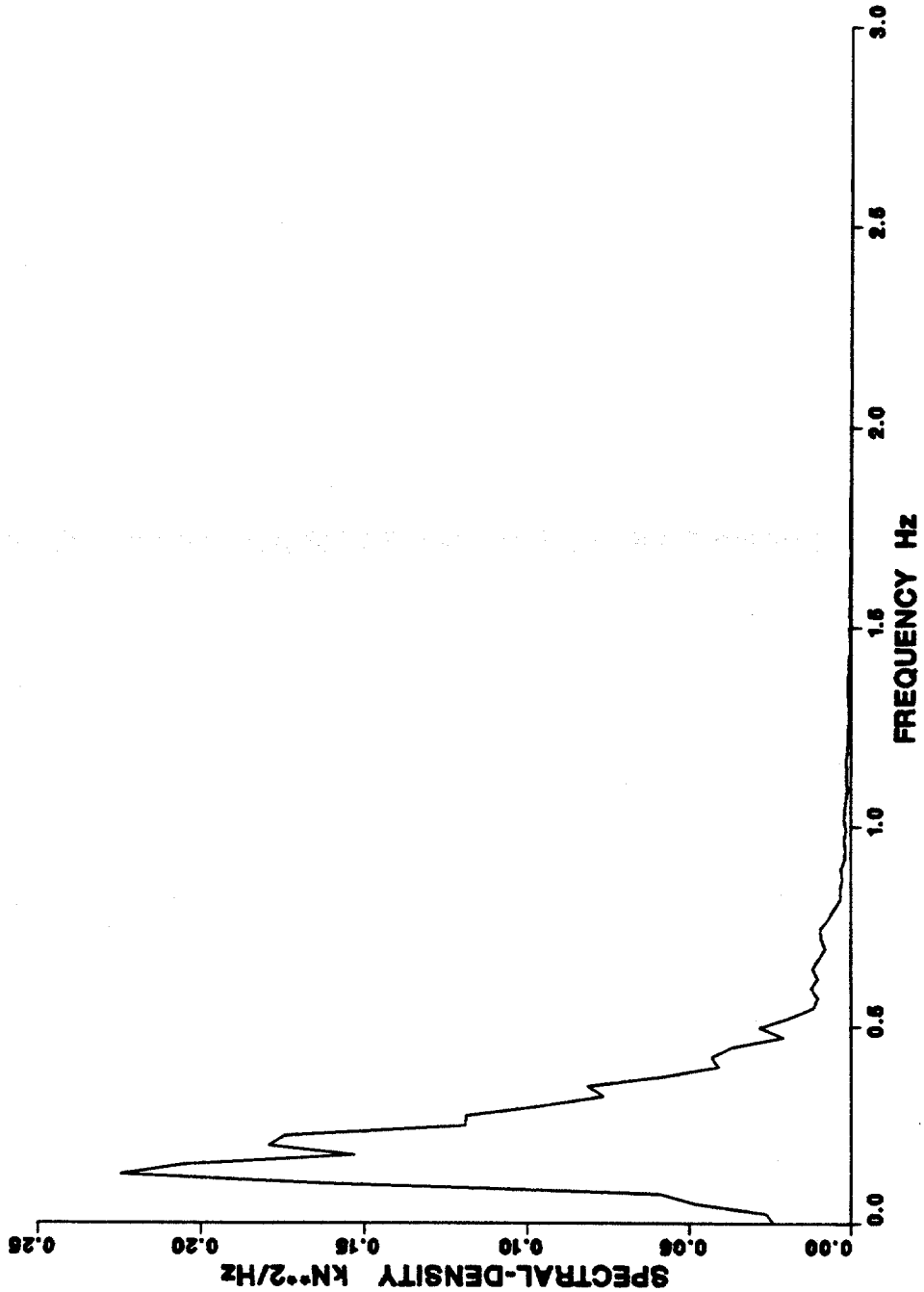

Figure 4.3. Spectral density of force in X direction at level 2, Run 35.

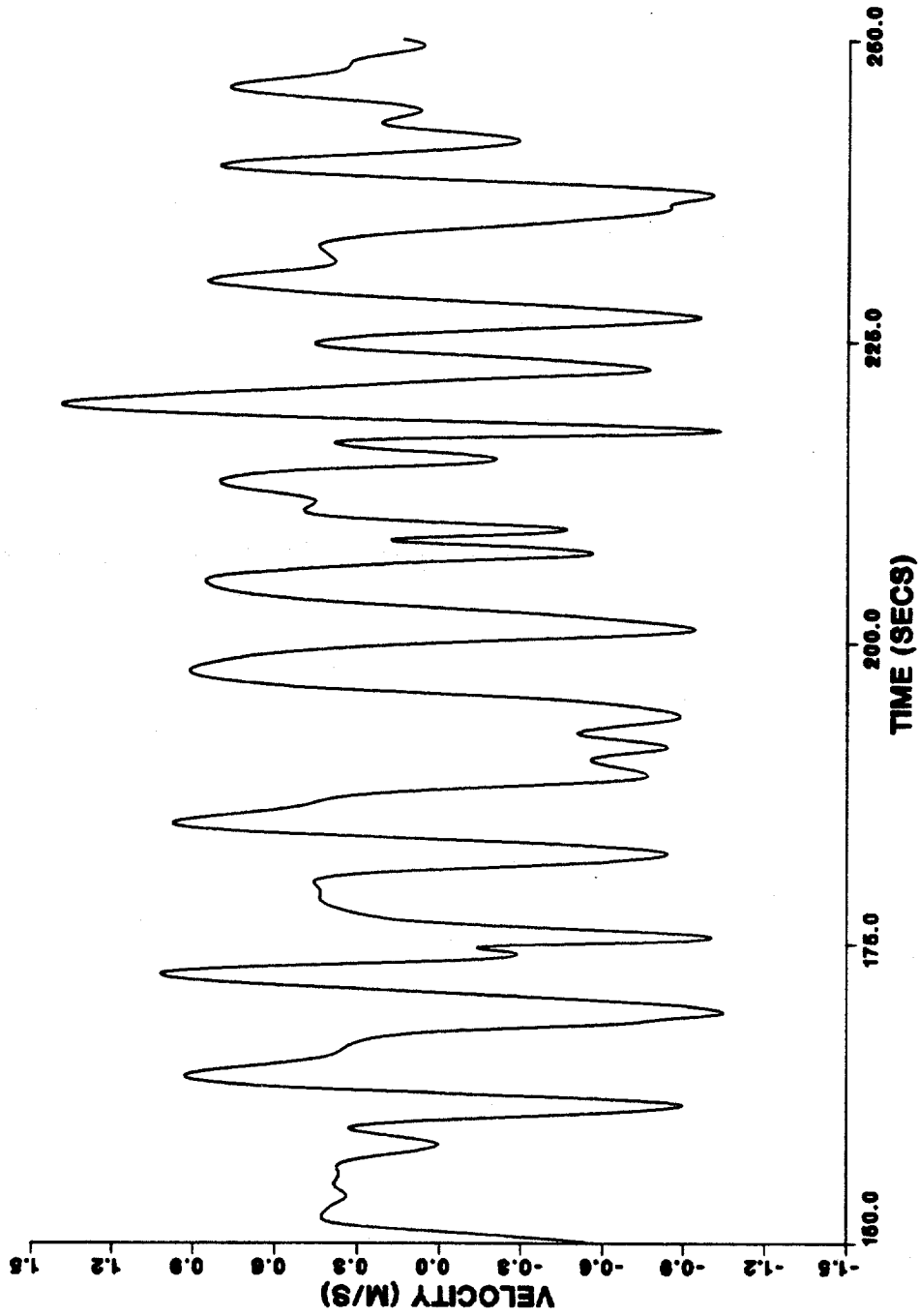

Figure 4.4. Velocity in X direction at level 2, Run 35.

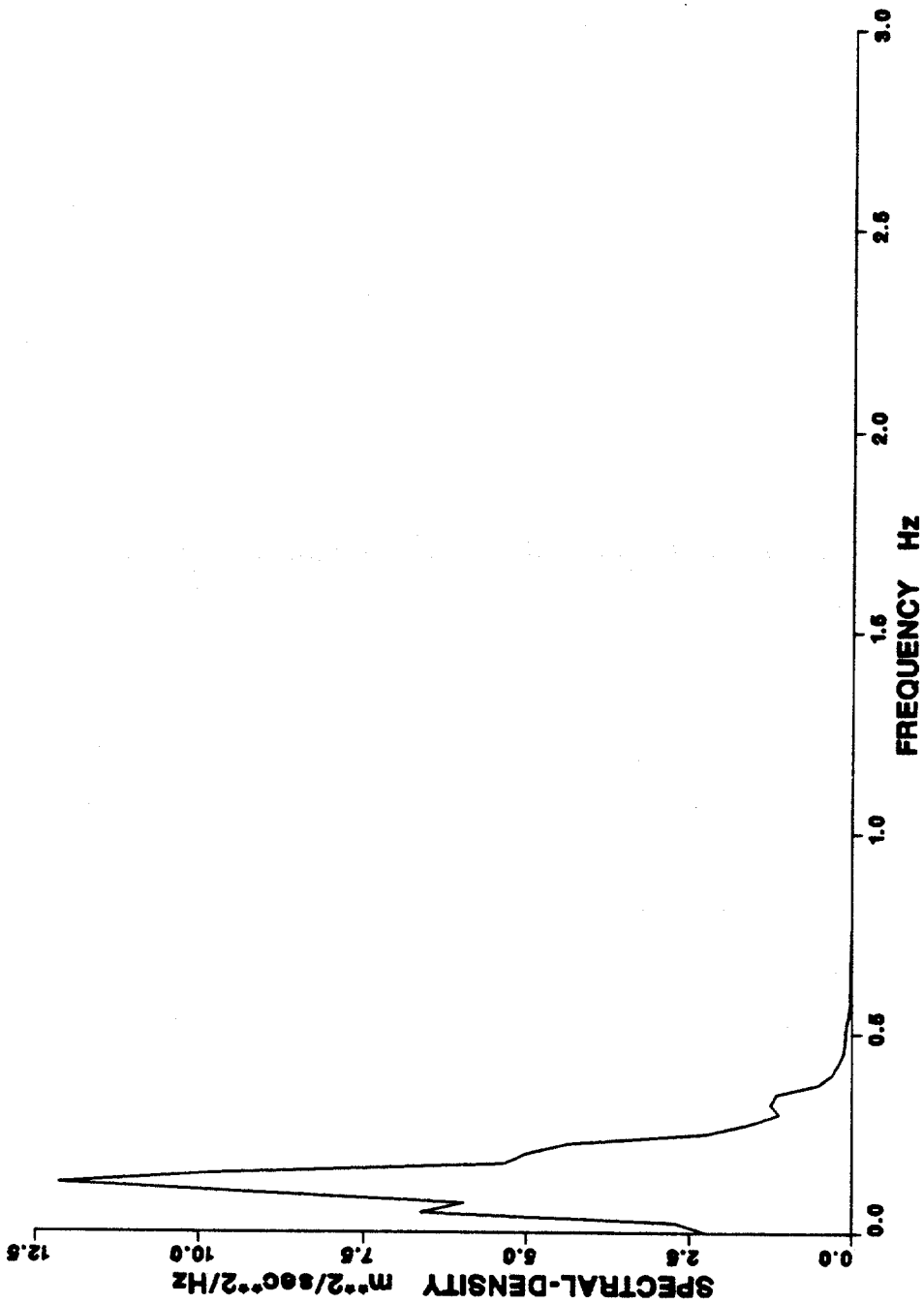

Figure 4.5. Spectral density of velocity in X direction at level 2, Run 35.

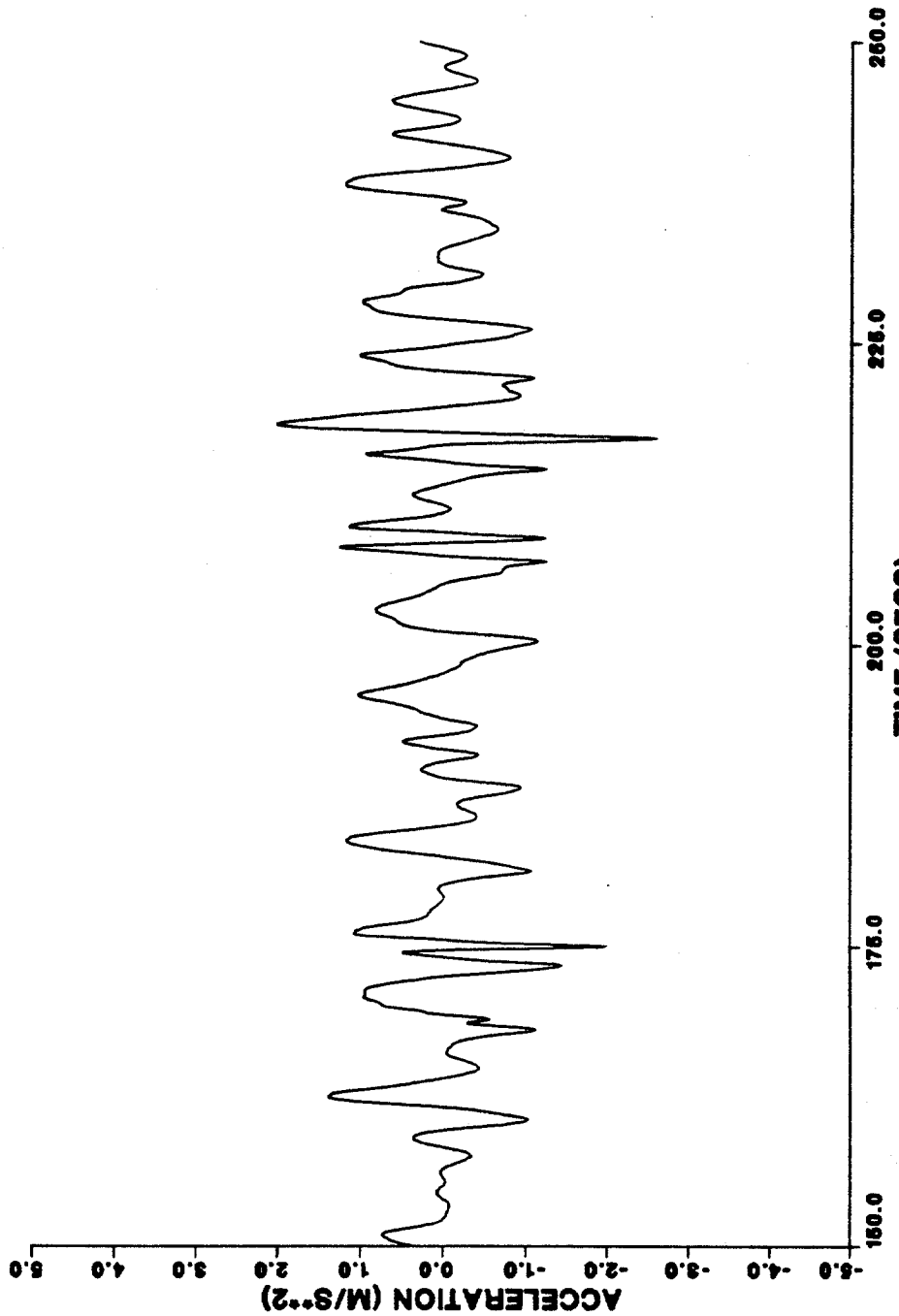

Figure 4.6. Acceleration in X direction at level 2, Run 35.

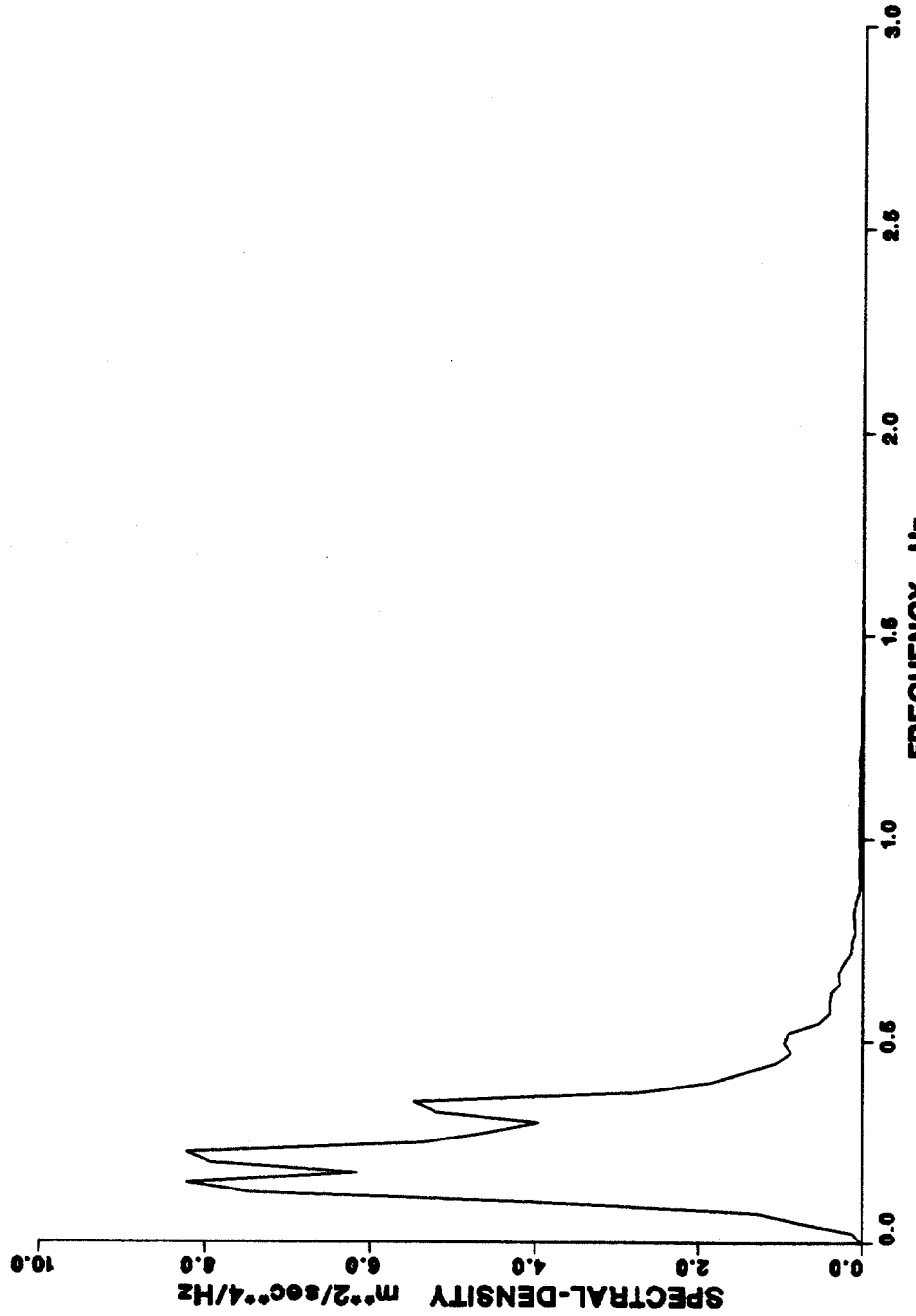

Figure 4.7. Spectral density of acceleration in X direction at level 2, Run 35.

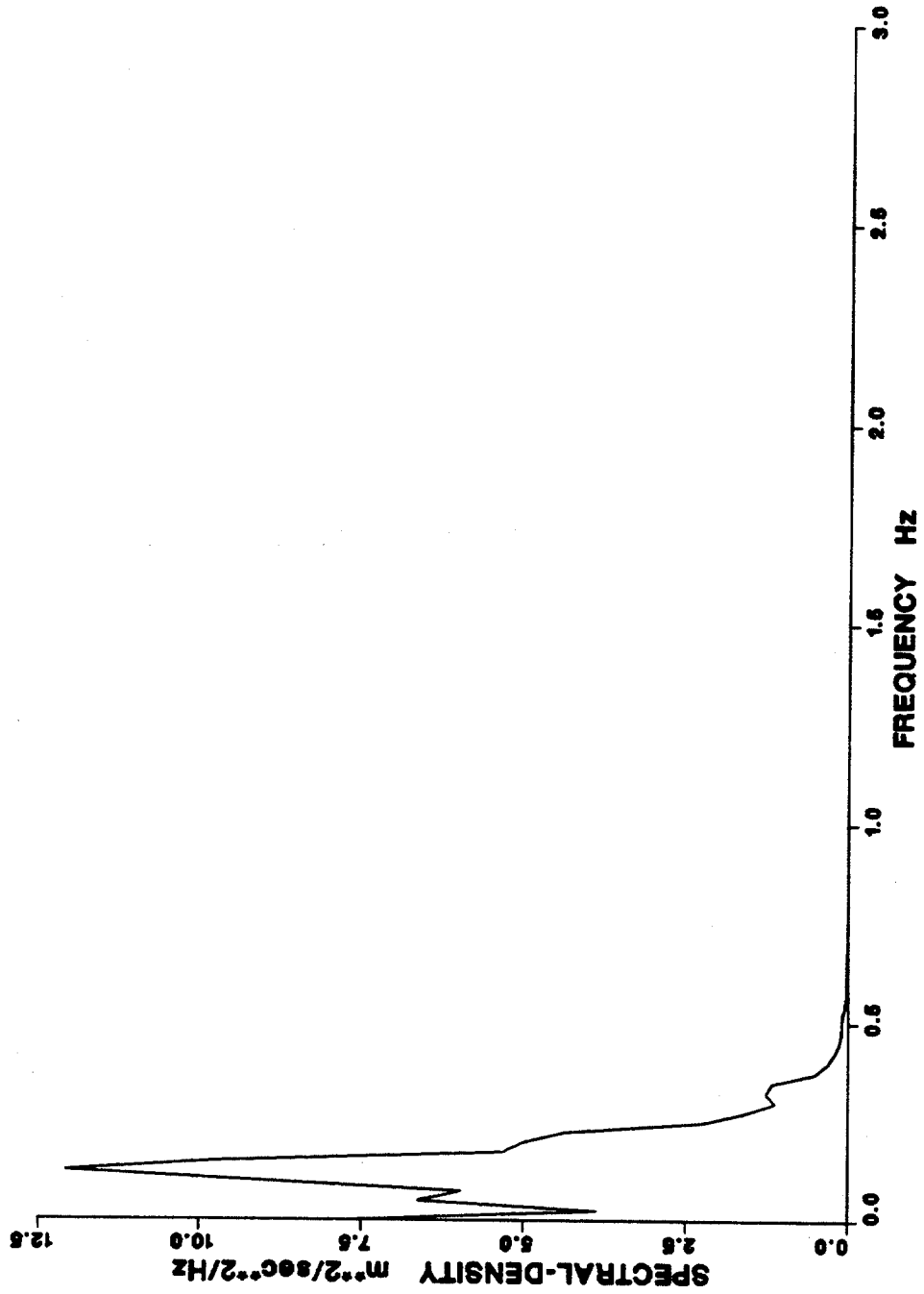

Figure 4.8. Spectral density of velocity with mean included, level 2, Run 35.

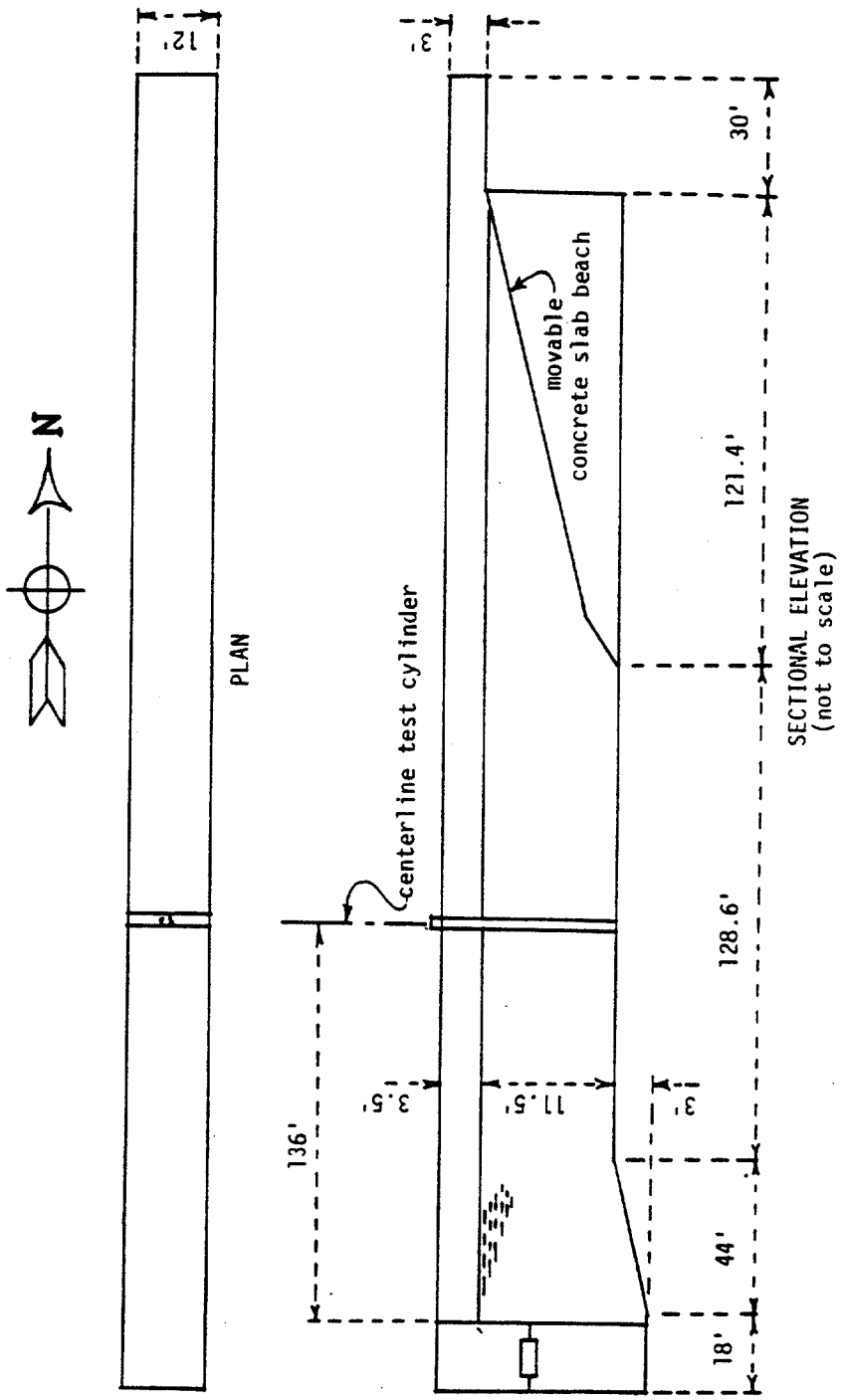

Figure 4.9. Oregon State University wave flume [Hudspeth and Nath (1985)].

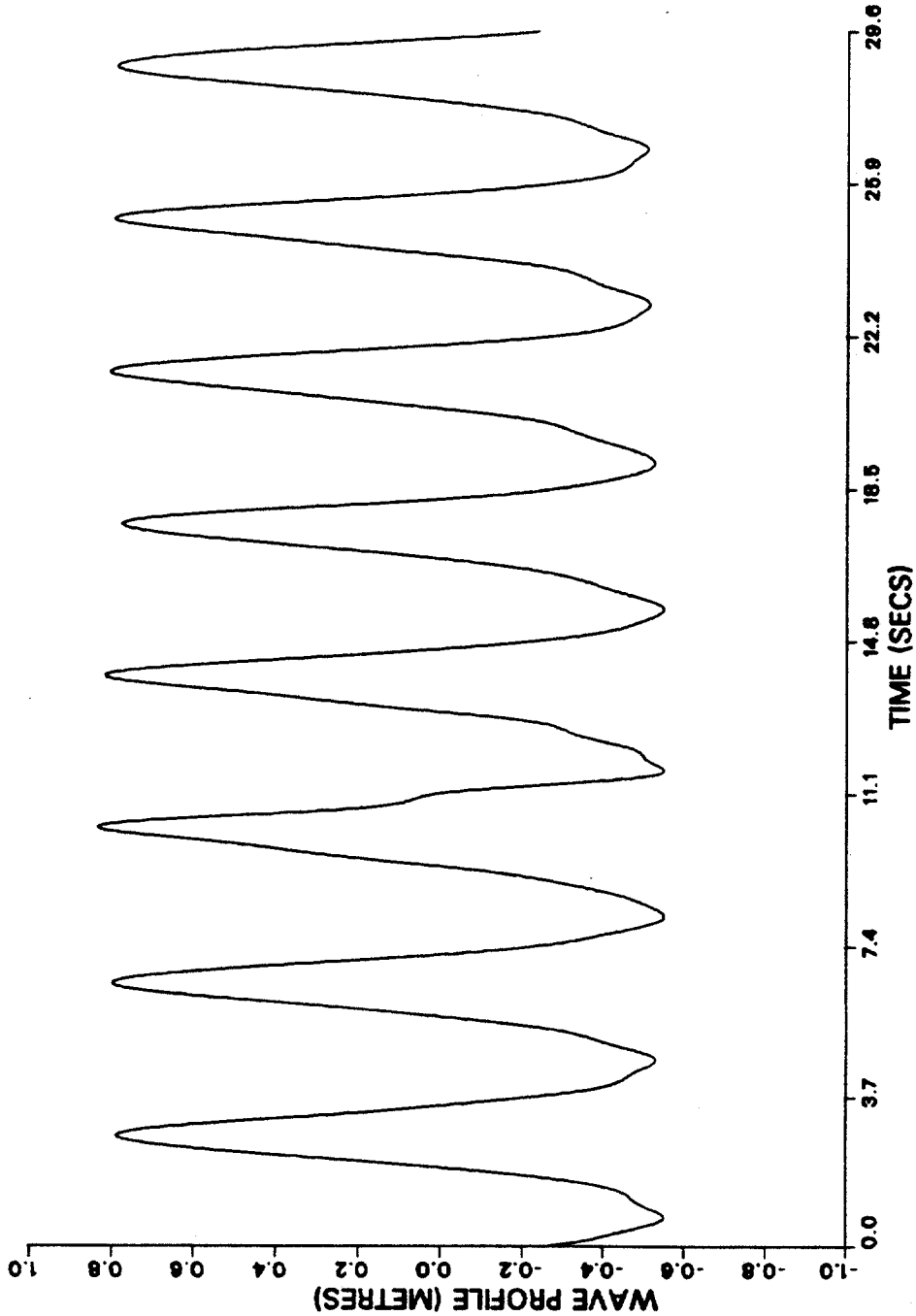

Figure 4.11. Unsmoothed wave profile time history - Run NCEL08.

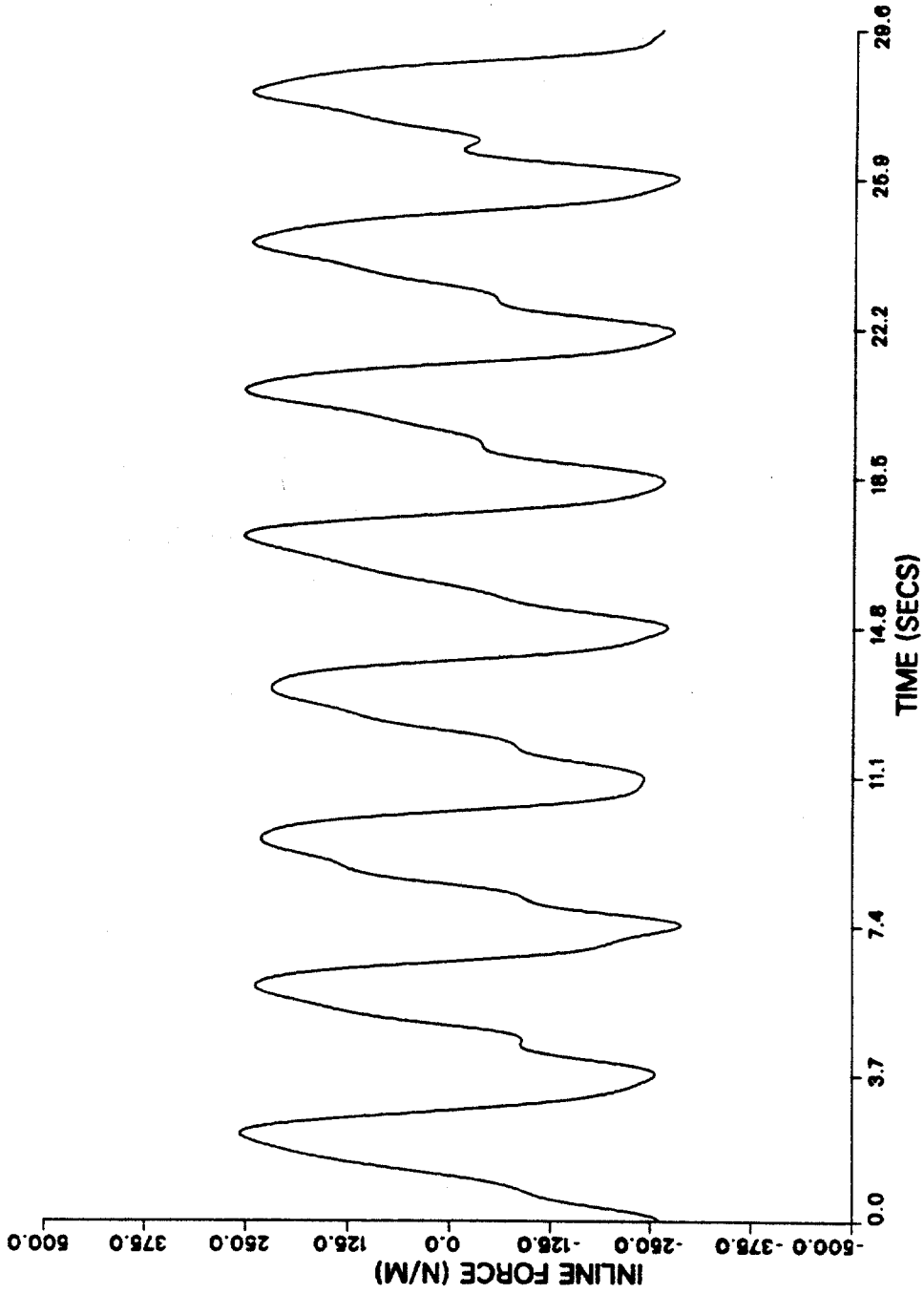

Figure 4.13. Unsmoothed in-line force time history - Run NCEL08.

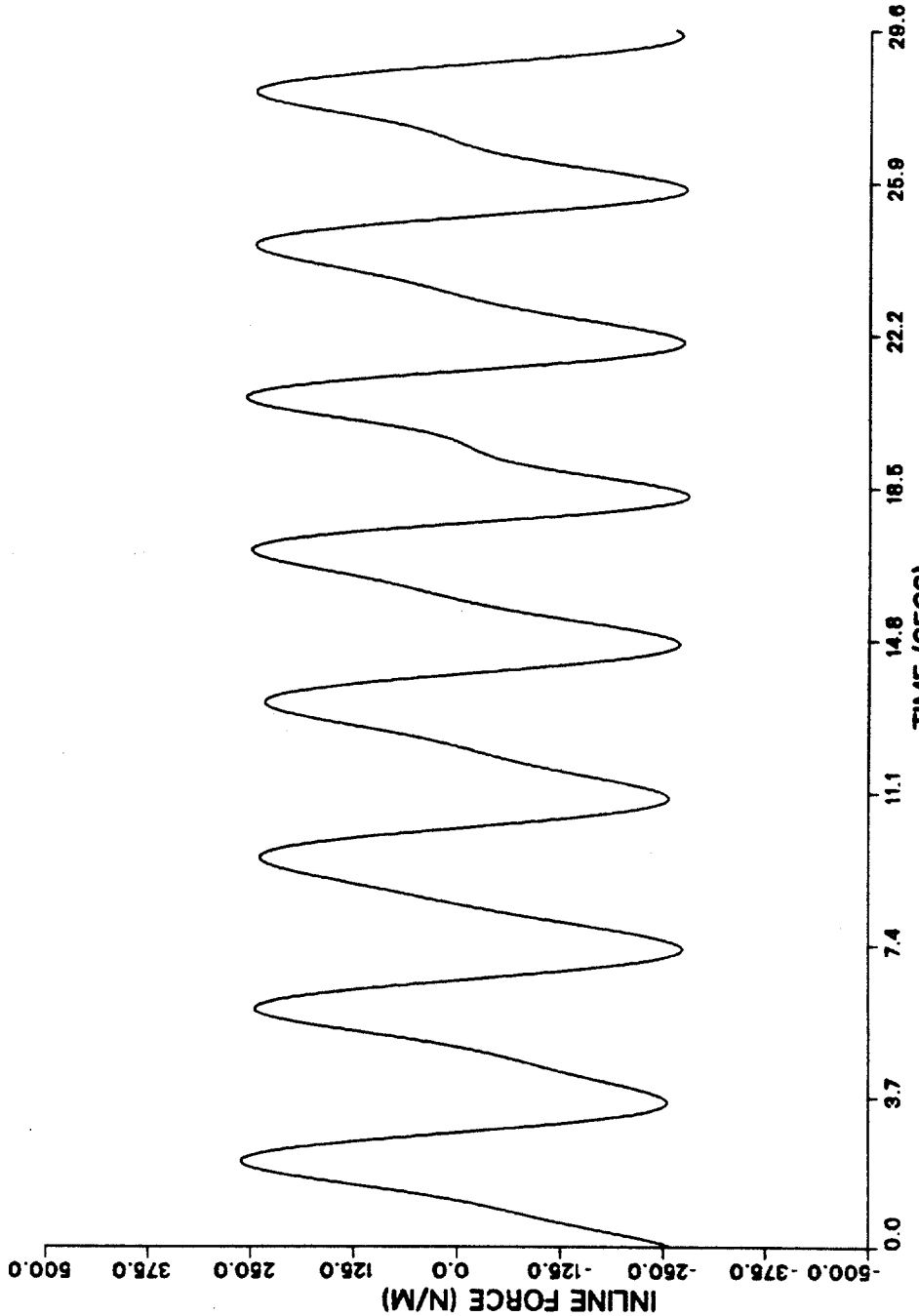

Figure 4.14. Smoothed in-line force time history - Run NCEL08.

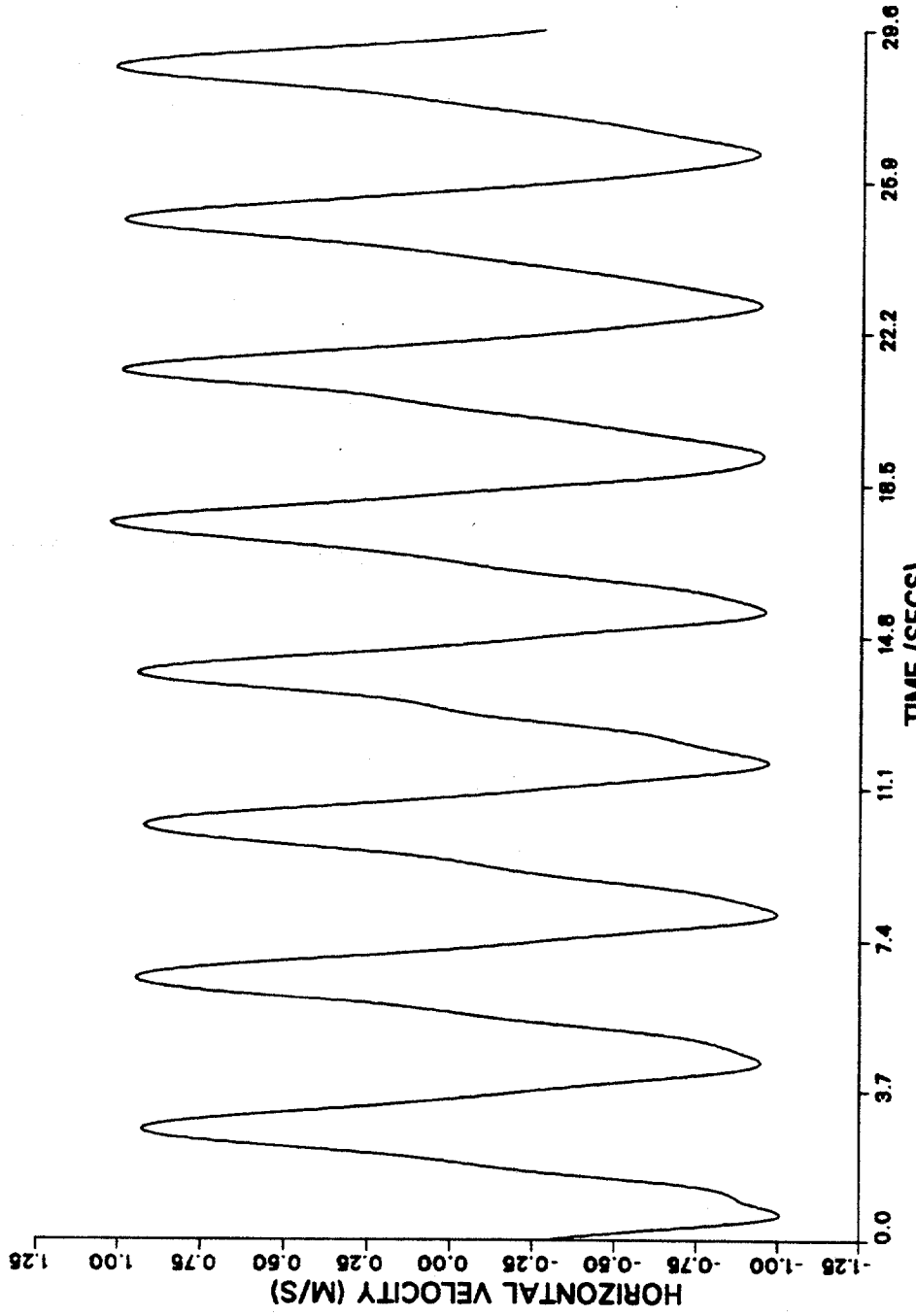

Figure 4.15. Unsmoothed horizontal velocity time history - Run NCEL08.

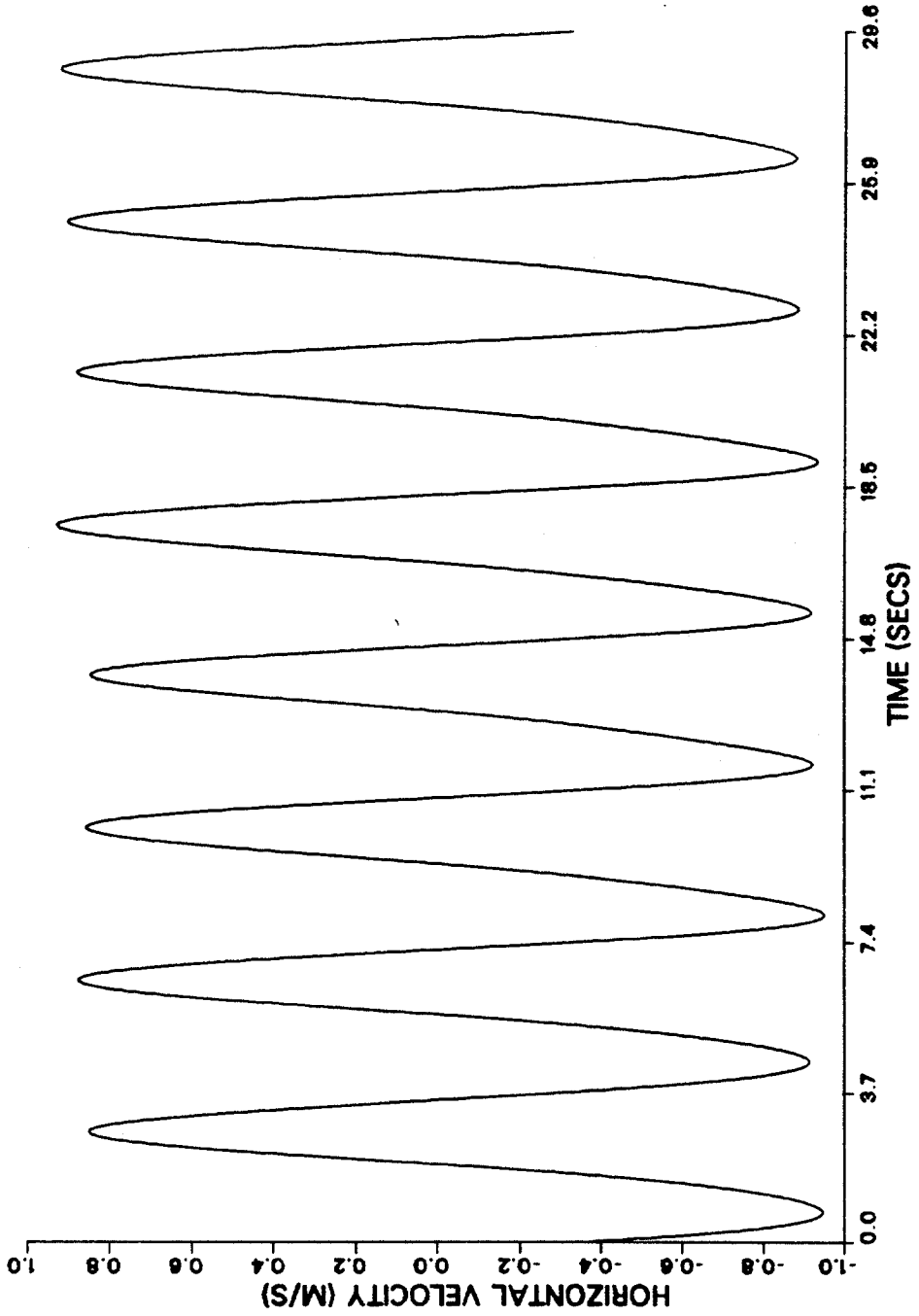

Figure 4.16. Smoothed horizontal velocity time history - Run NCEL08.

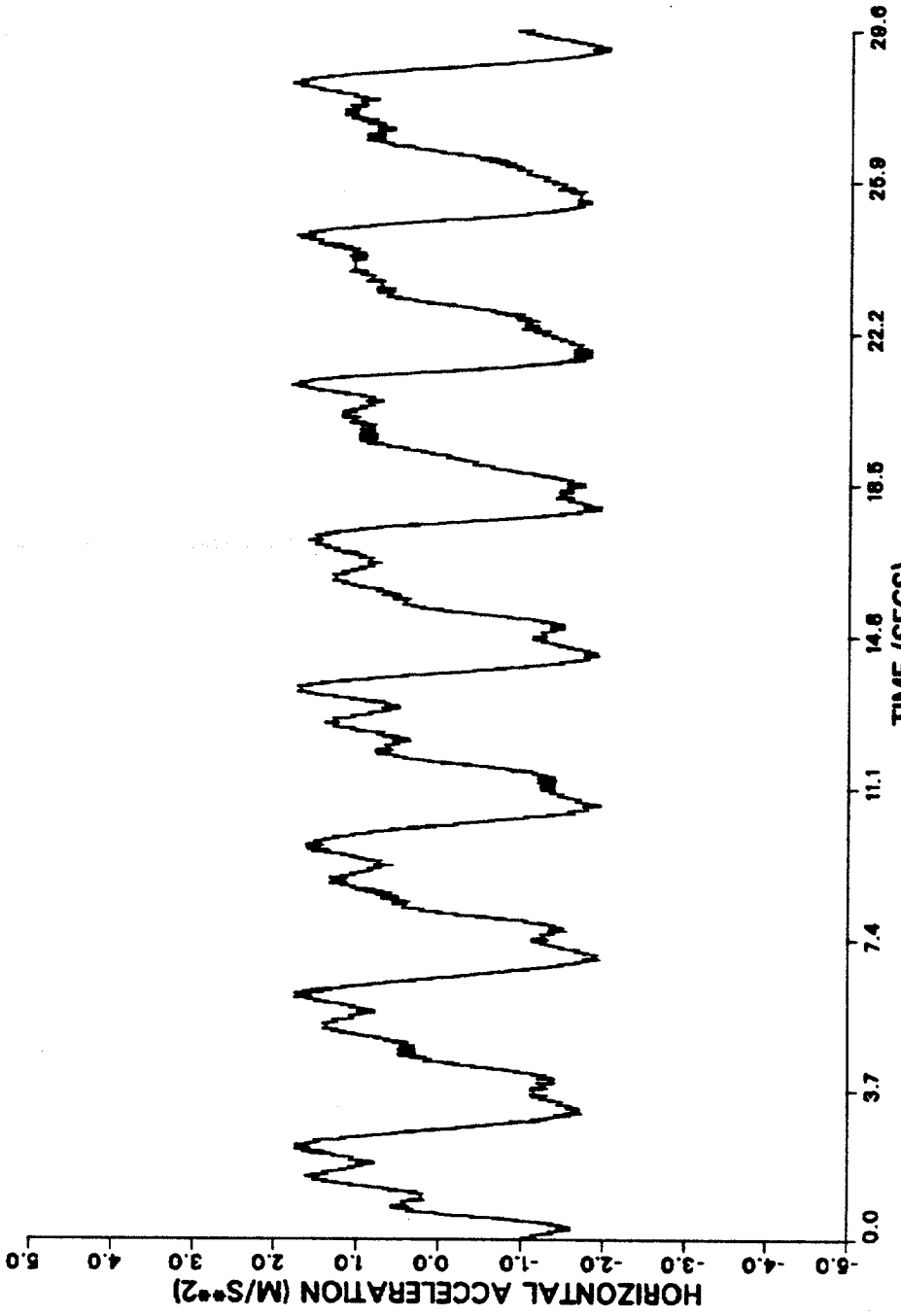

Figure 4.17. Unsmoothed horizontal acceleration time history - Run NGEL08.

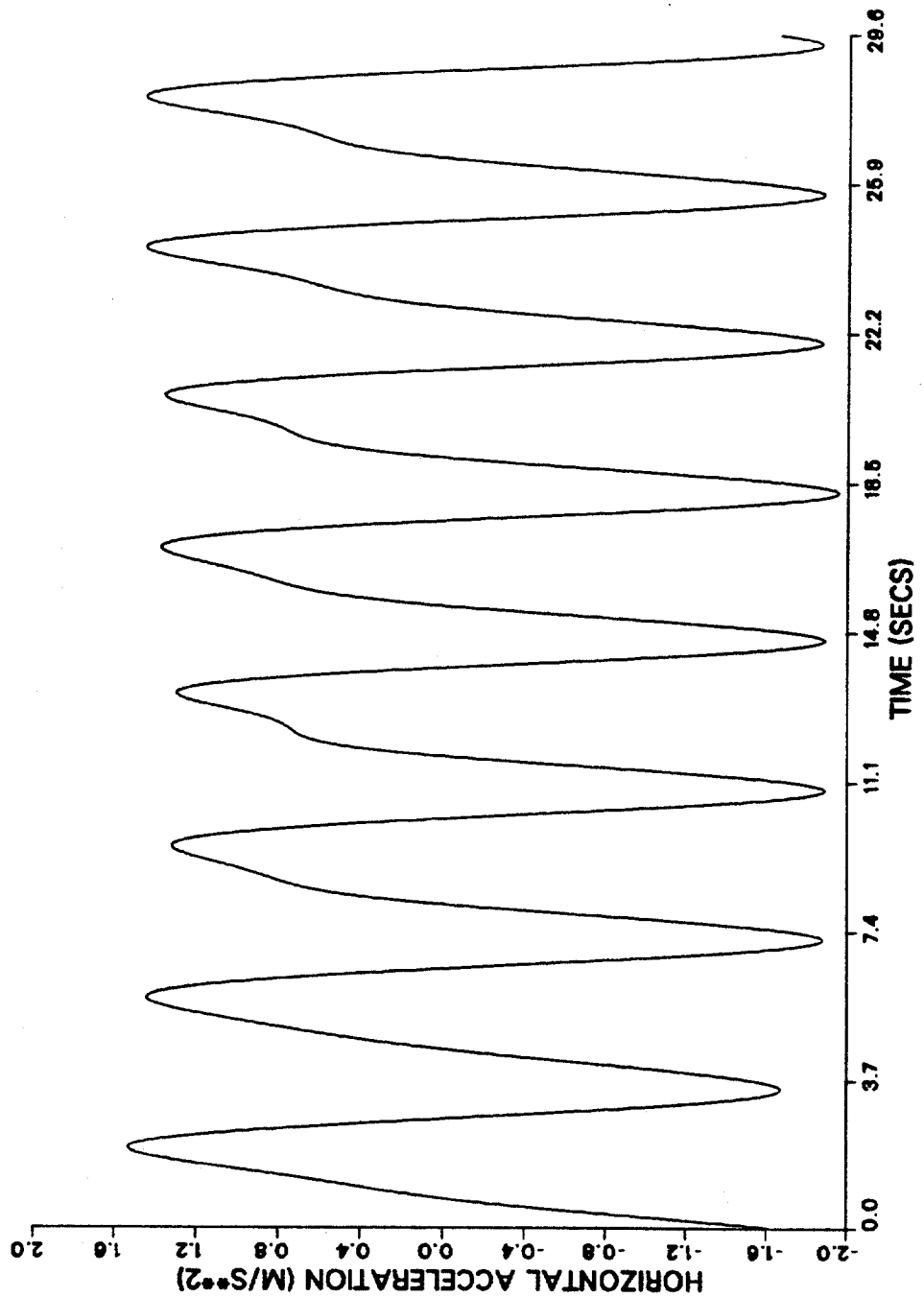

Figure 4.18. Smoothed horizontal acceleration time history - Run NCEL08.

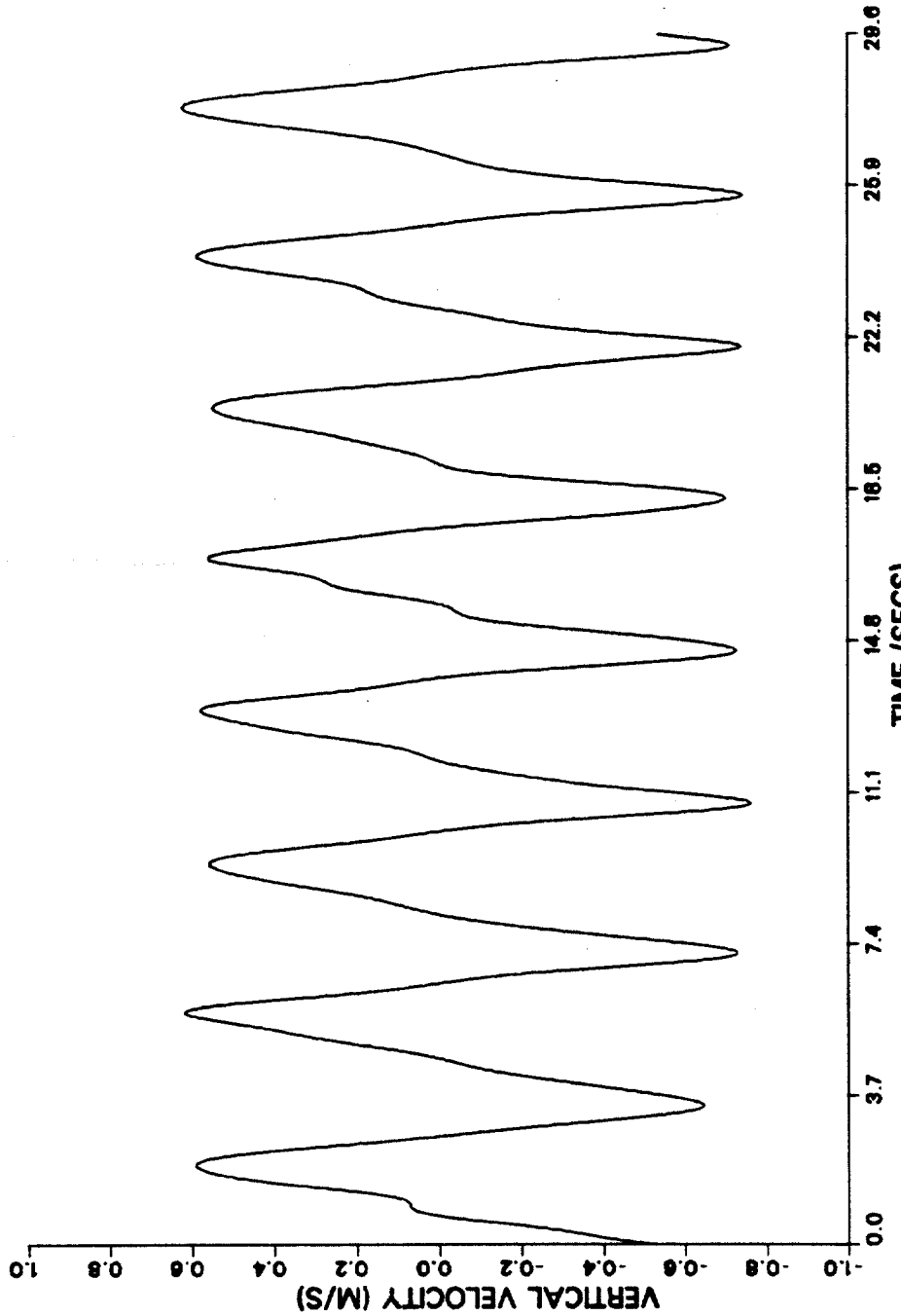

Figure 4.19. Unsmoothed vertical velocity time history - Run NCEL08.

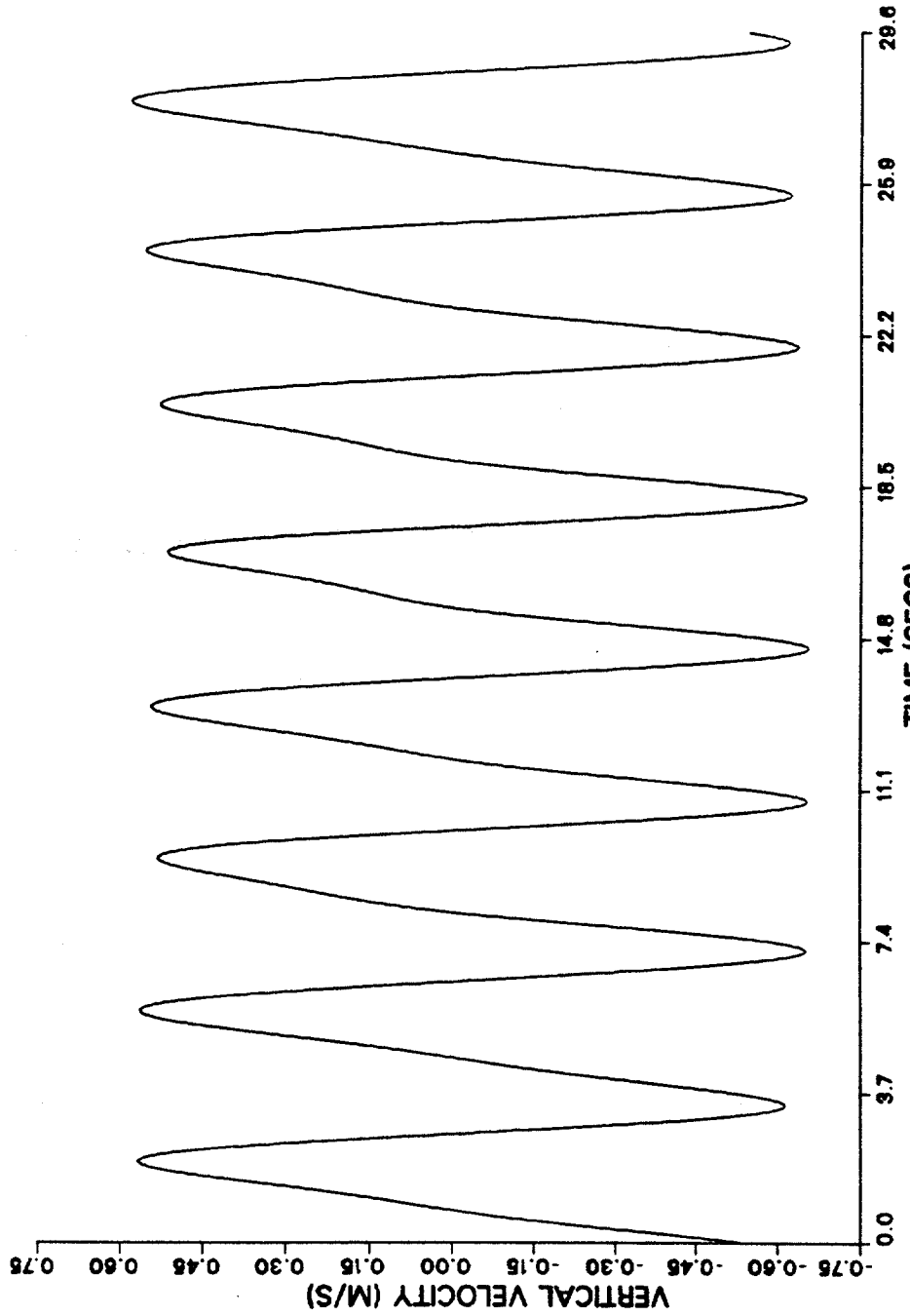

Figure 4.20. Smoothed vertical velocity time history - Run NCEL08.

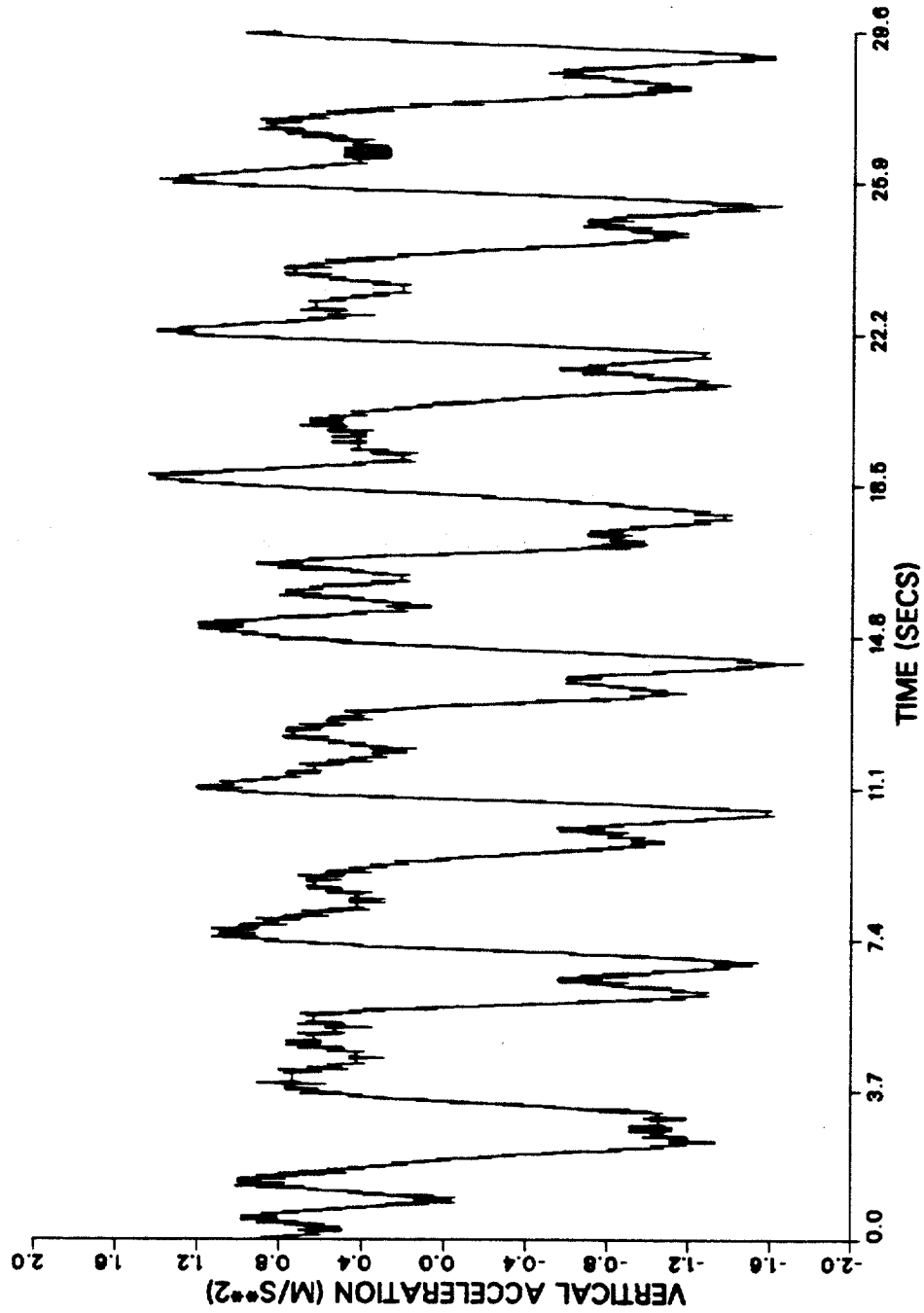

Figure 4.21. Unsmoothed vertical acceleration time history - Run NGEL08.

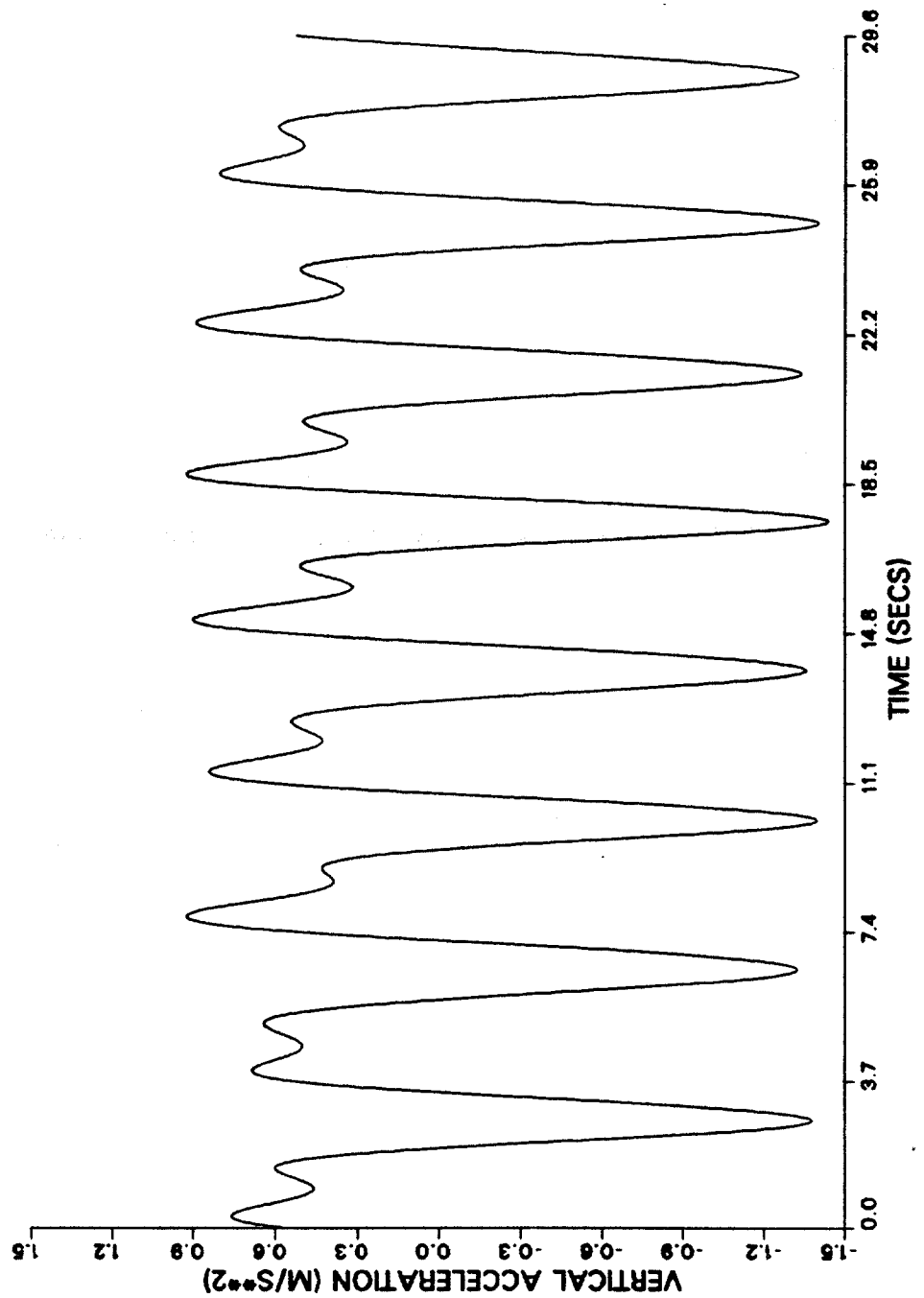

Figure 4.22. Smoothed vertical acceleration time history - Run NCEL08.

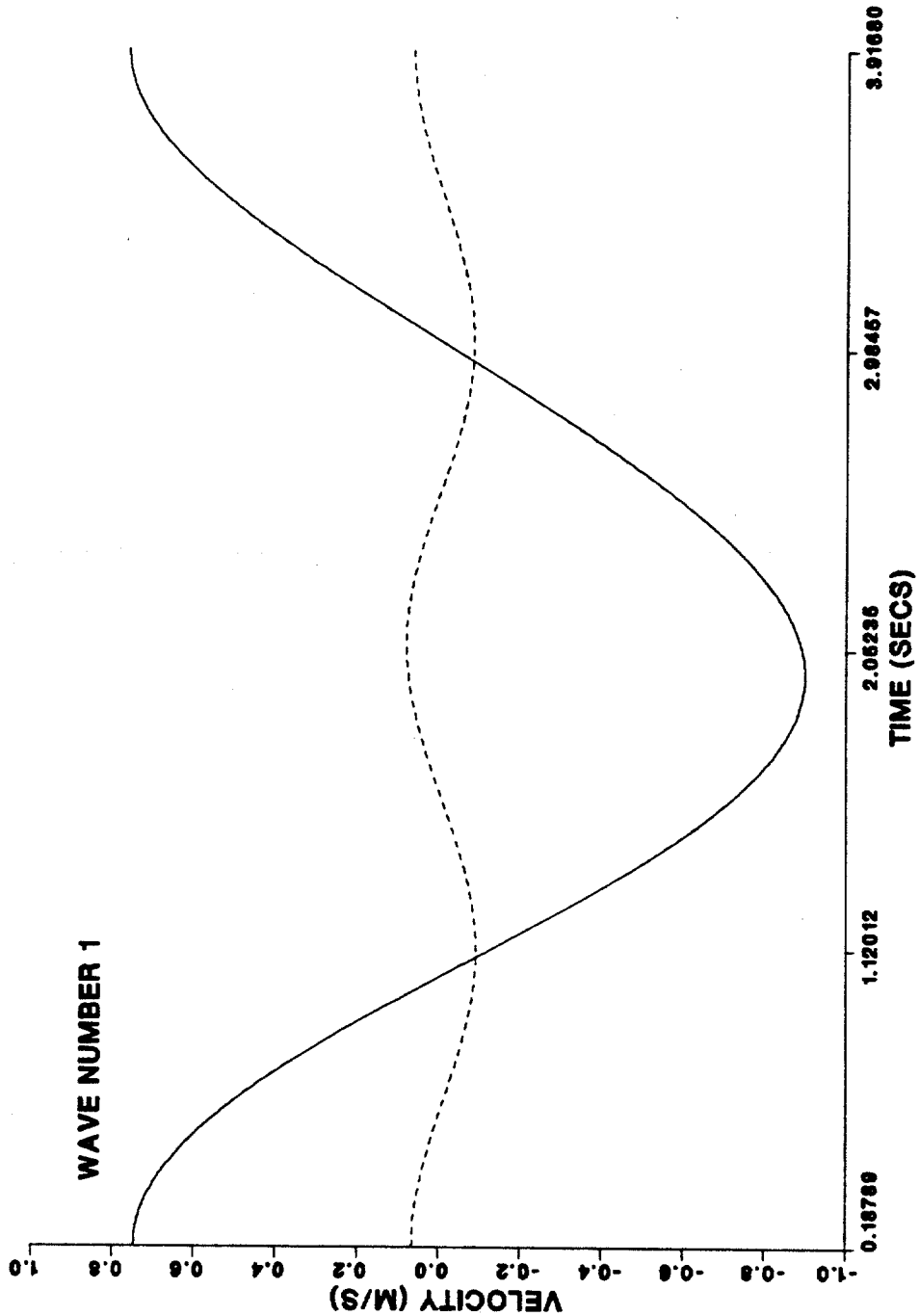

Figure 4.24. First and second order measured velocity for KC = 9.56.
[First order component ——; second order component - - -].

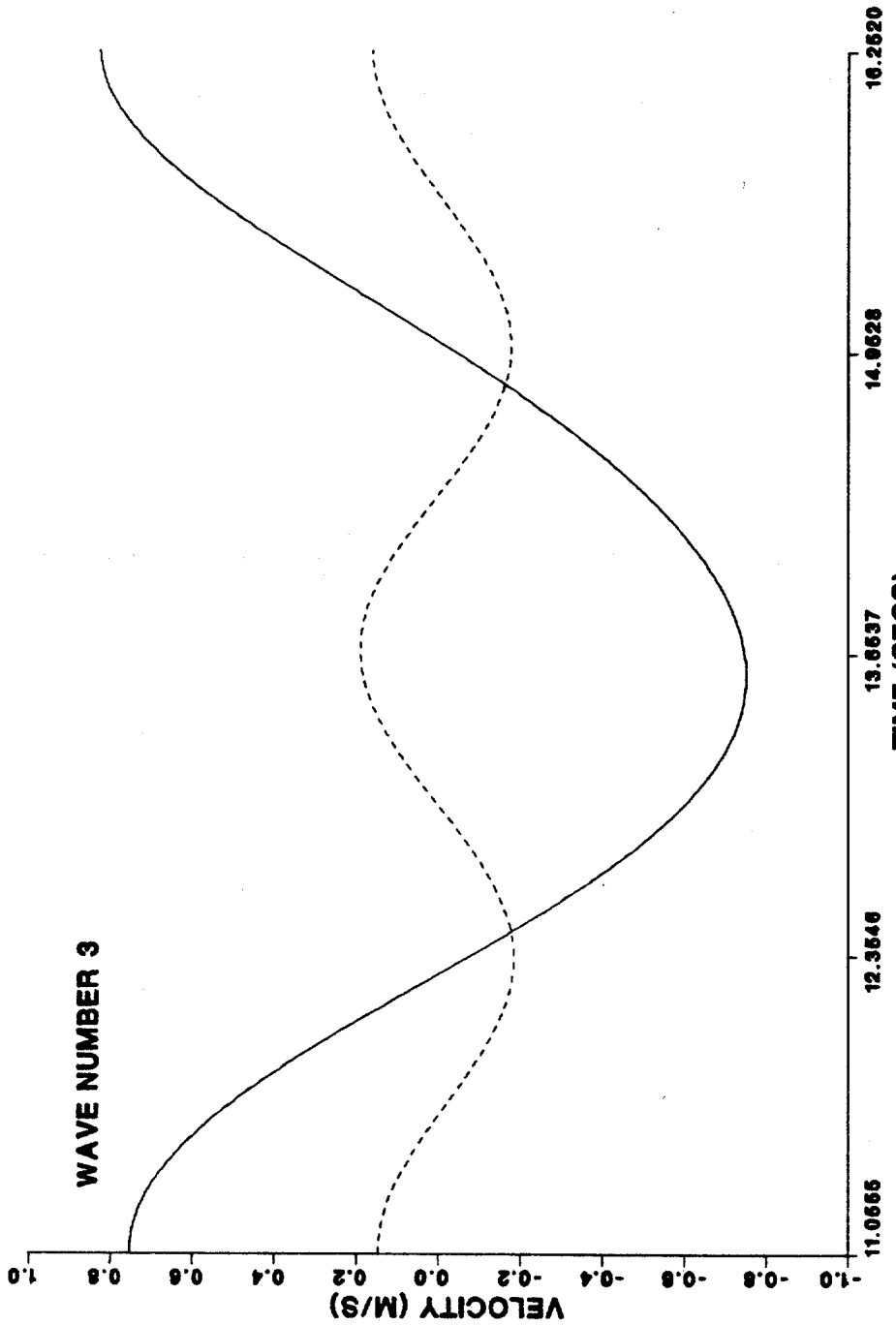

Figure 4.25. First and second order measured velocity for KC = 16.19.
[First order component ——; second order component - - -].

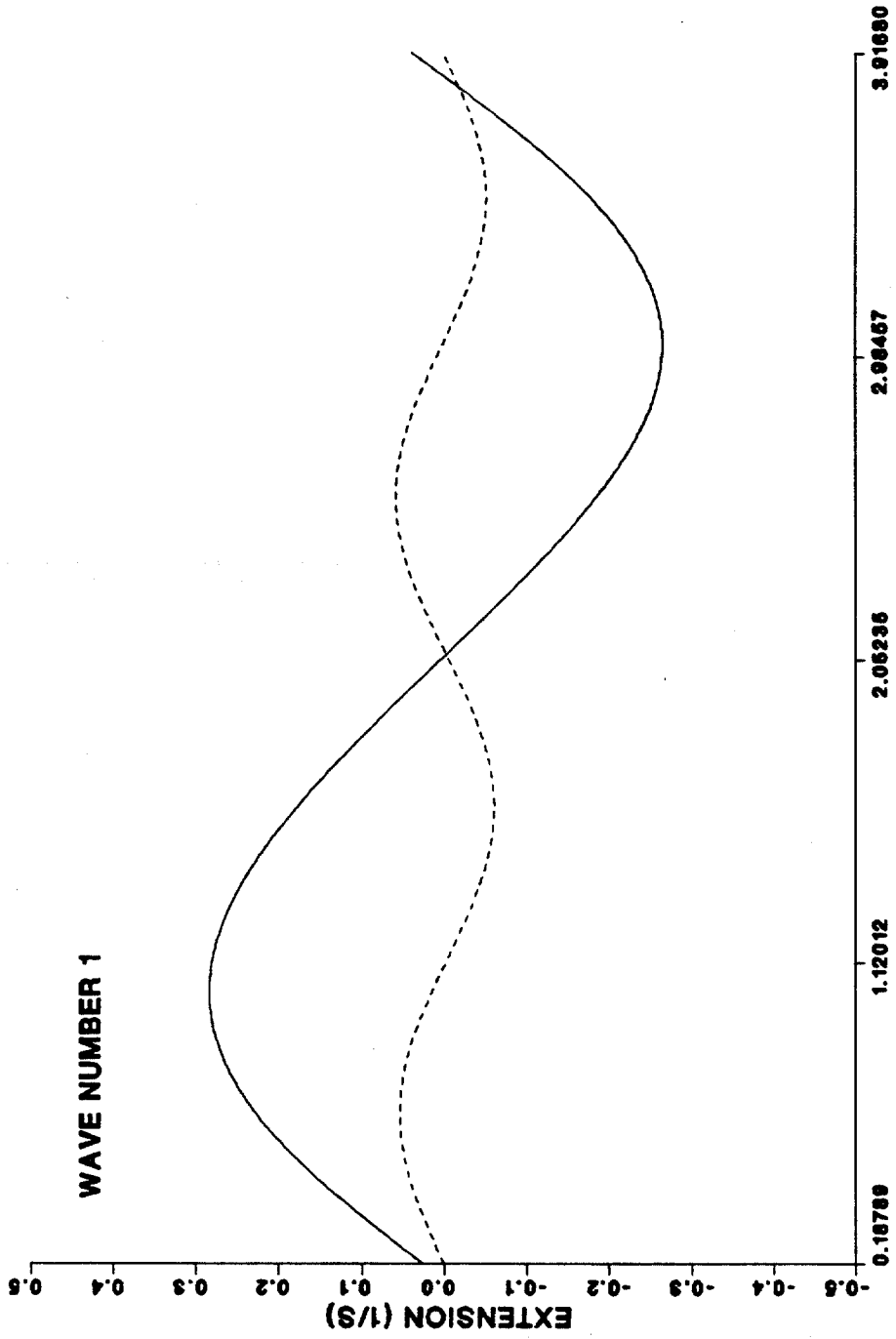

Figure 4.27. First and second order measured extension for KC = 9.56.
[First order component ——; second order component ---].

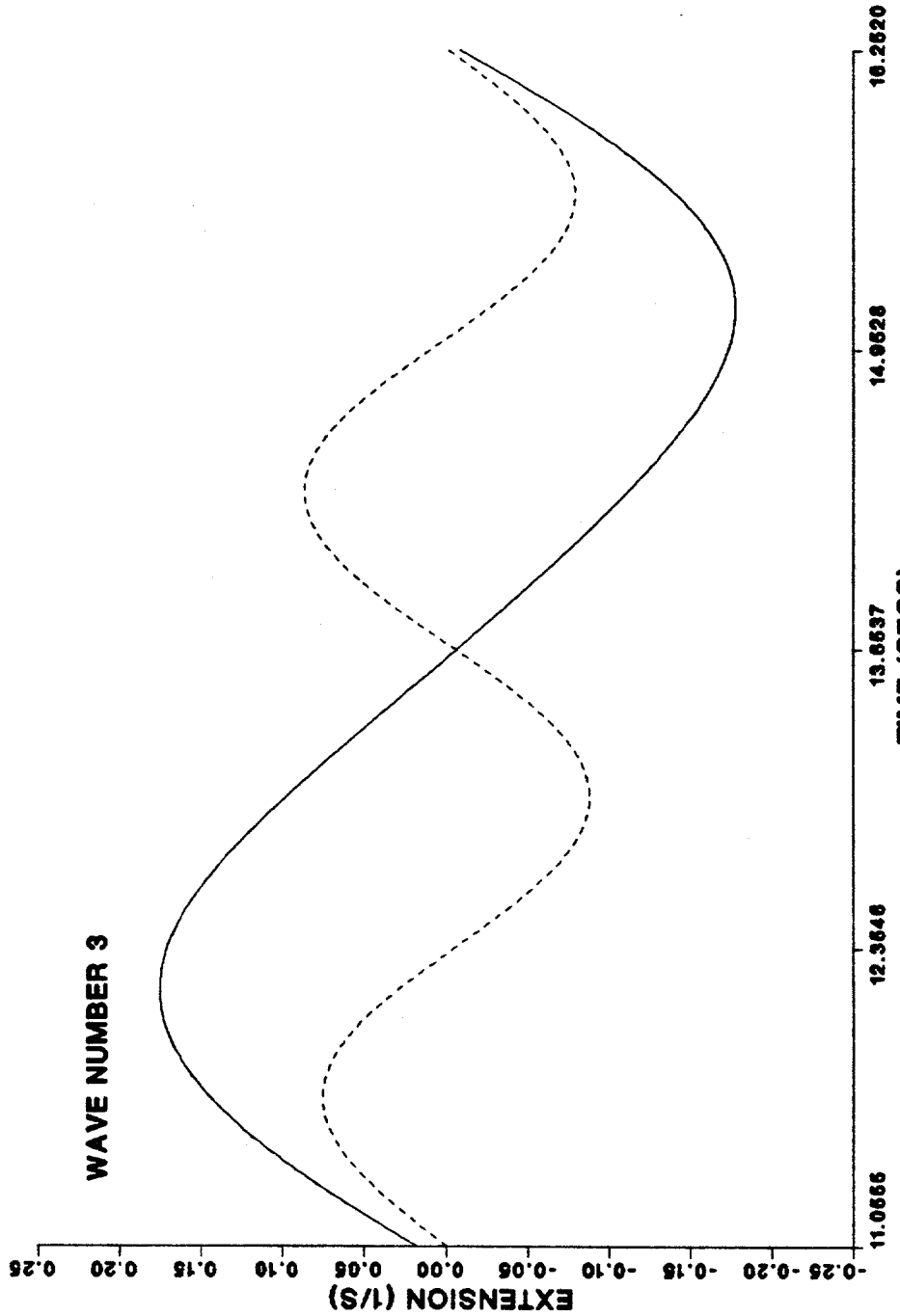

Figure 4.28. First and second order measured extension for KC = 16.19
[First order component ——; second order component ---].

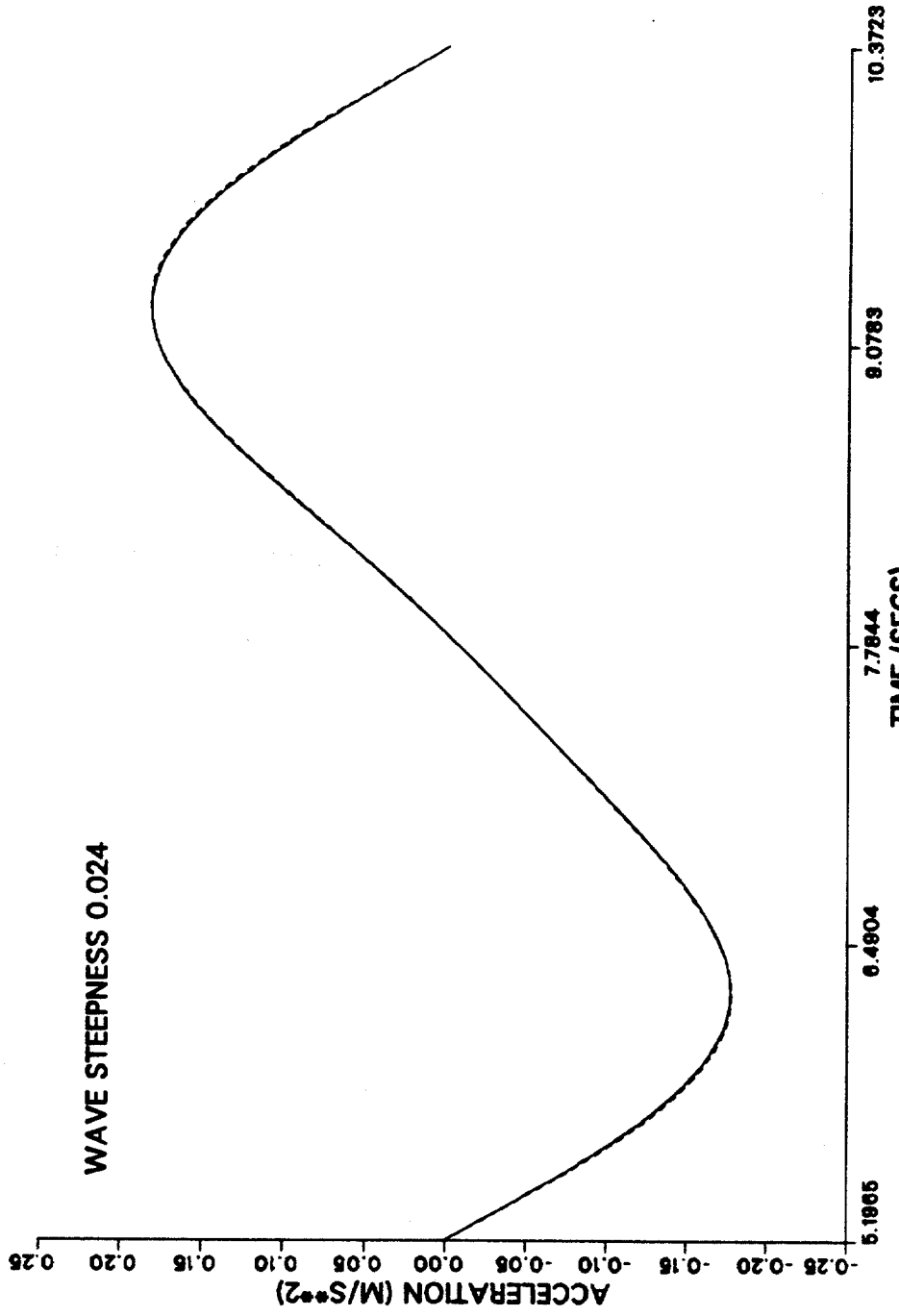

Figure 4.29. Comparison of local and total acceleration for wave steepness, ak = 0.024. [Local ——; Total - - -].

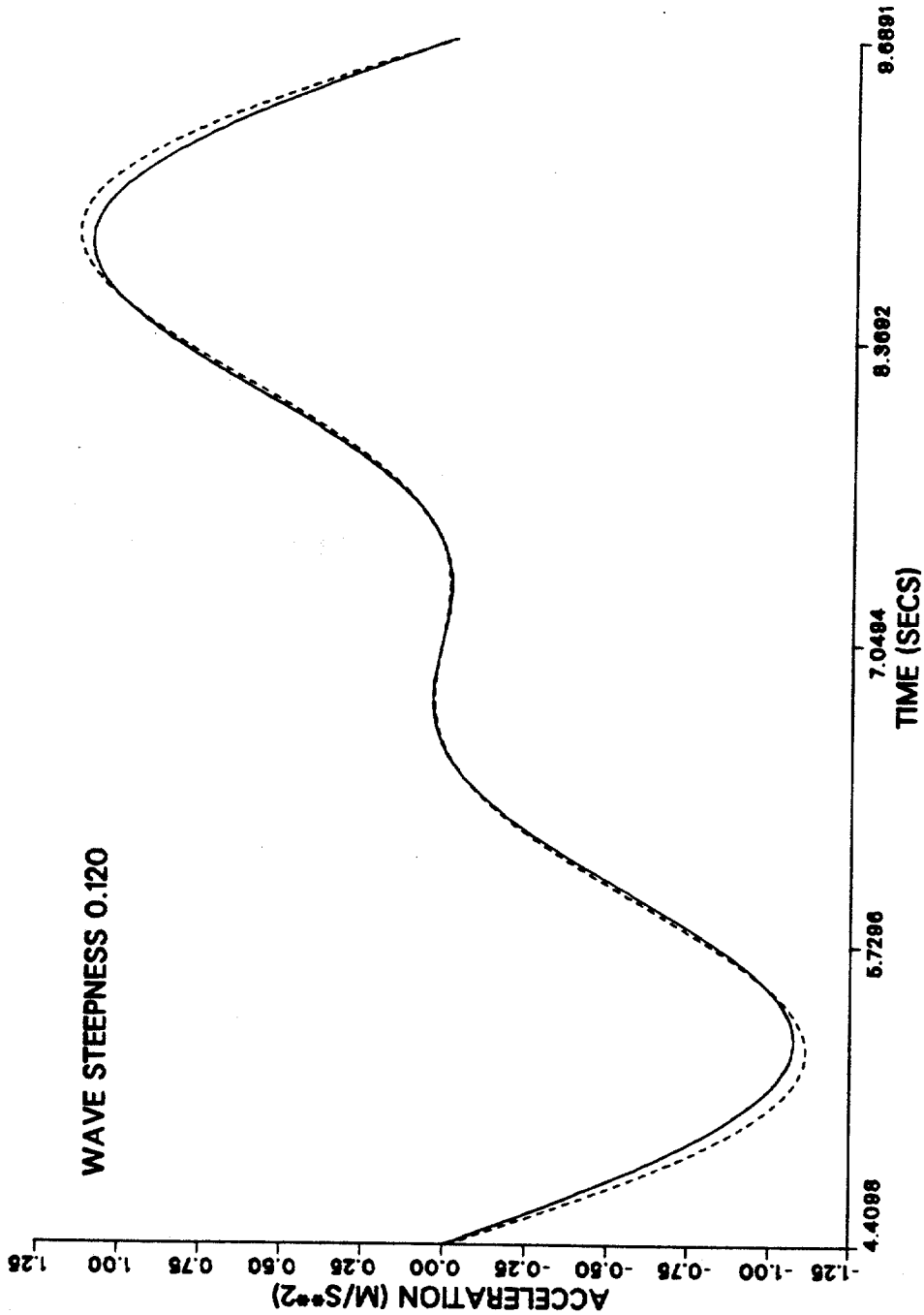

Figure 4.30. Comparison of local and total acceleration for wave steepness, ak = 0.120. [Local ——; Total - - -].

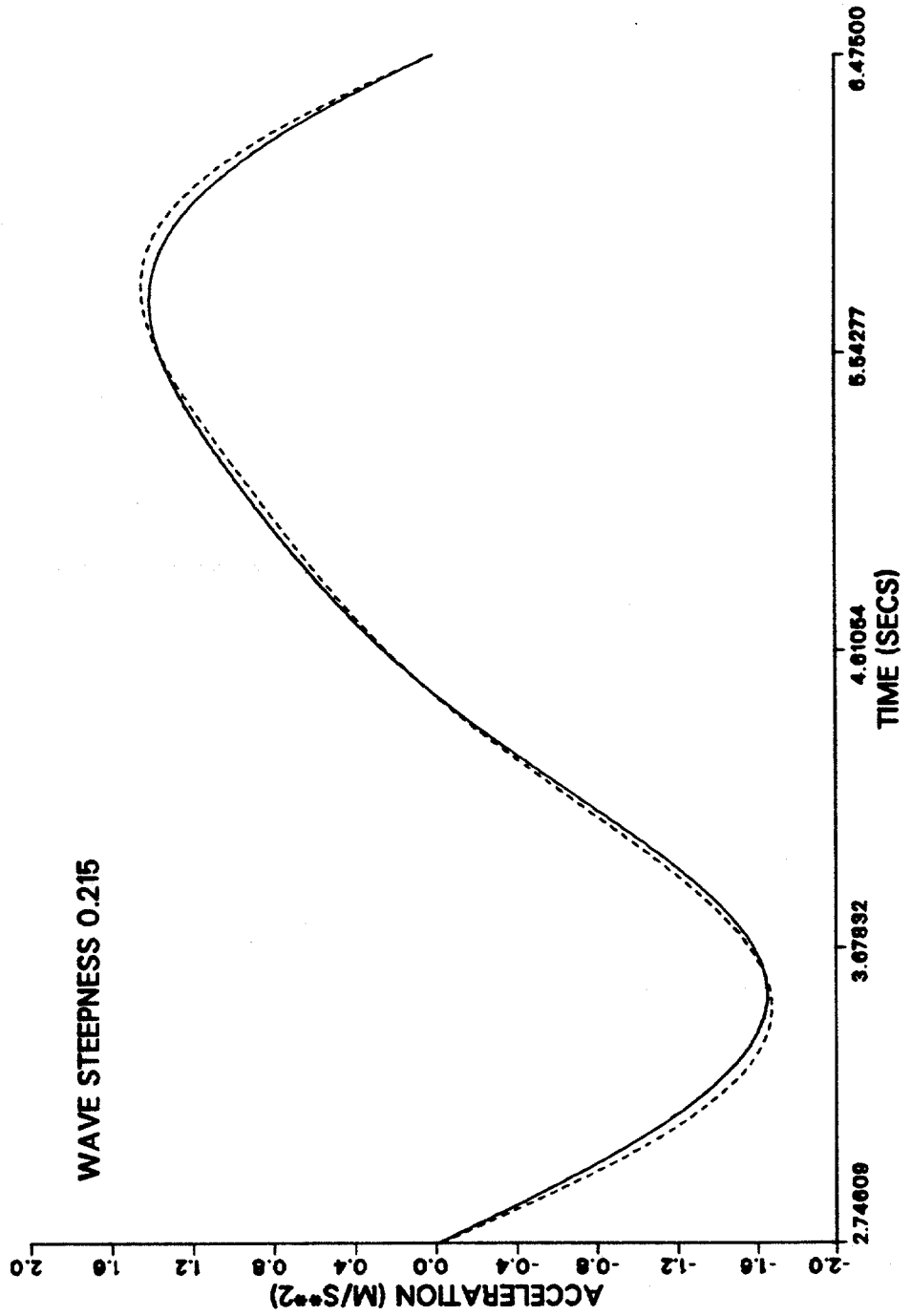

Figure 4.31. Comparison of local and total acceleration for wave steepness, ak = 0.215. [Local ——; Total ---].

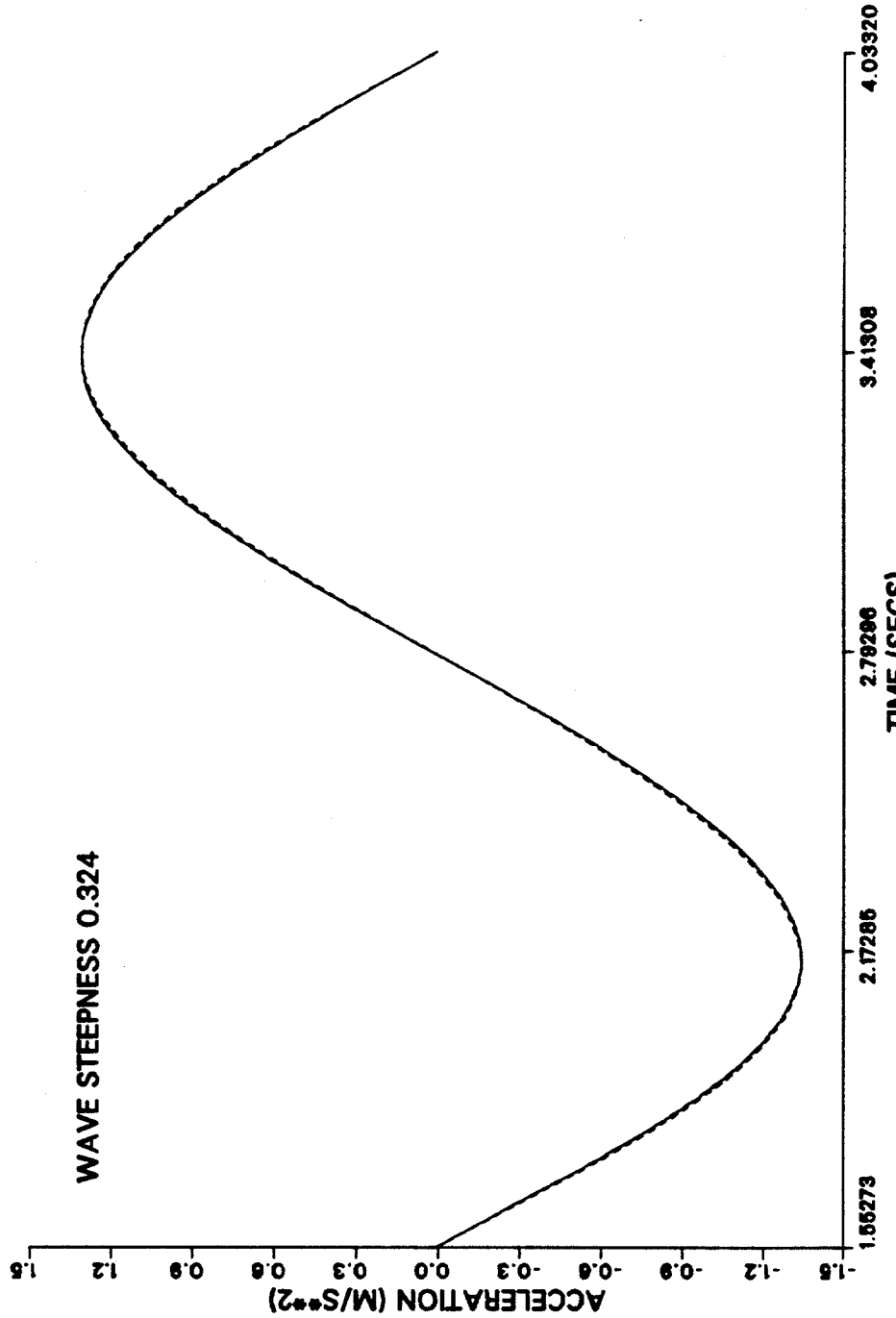

Figure 4.32. Comparison of local and total acceleration for wave steepness, ak = 0.324. [Local ——; Total - - -].

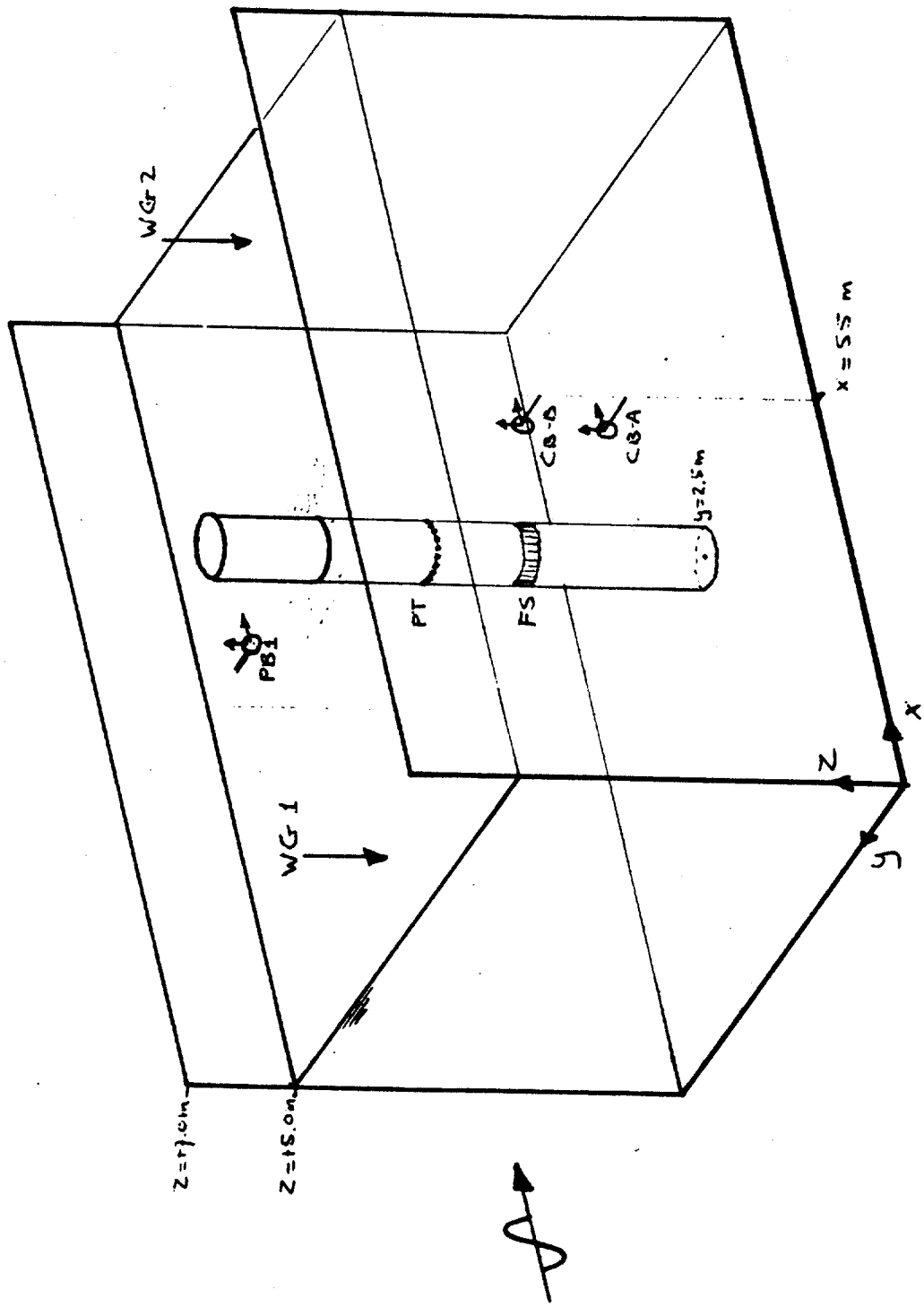

Figure 4.33. Location of measuring equipment for Delft data.

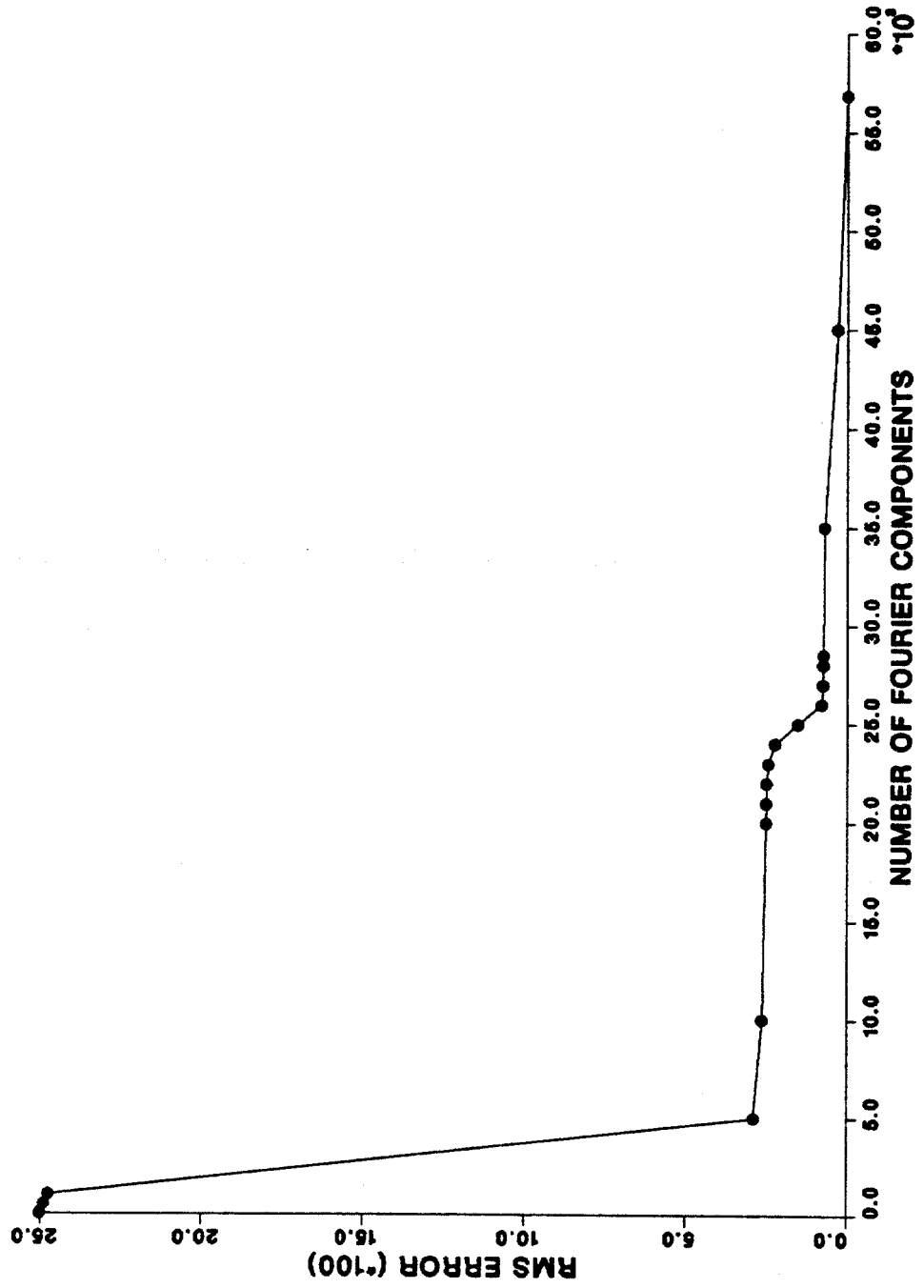

Figure 4.34. RMS error versus number of Fourier components used to smooth the time history.

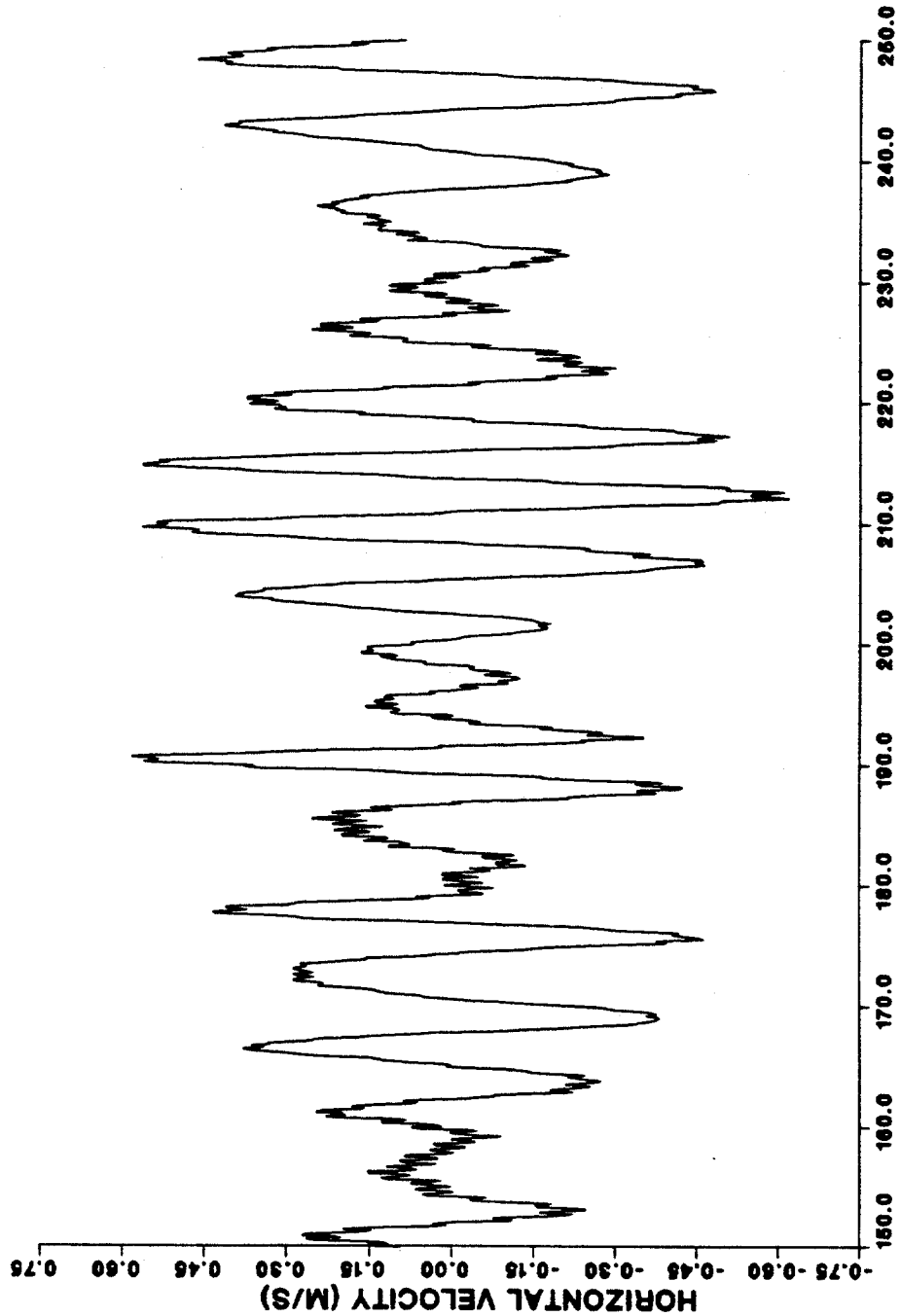

Figure 4.35. Horizontal velocity time history, unsmoothed, lower level.

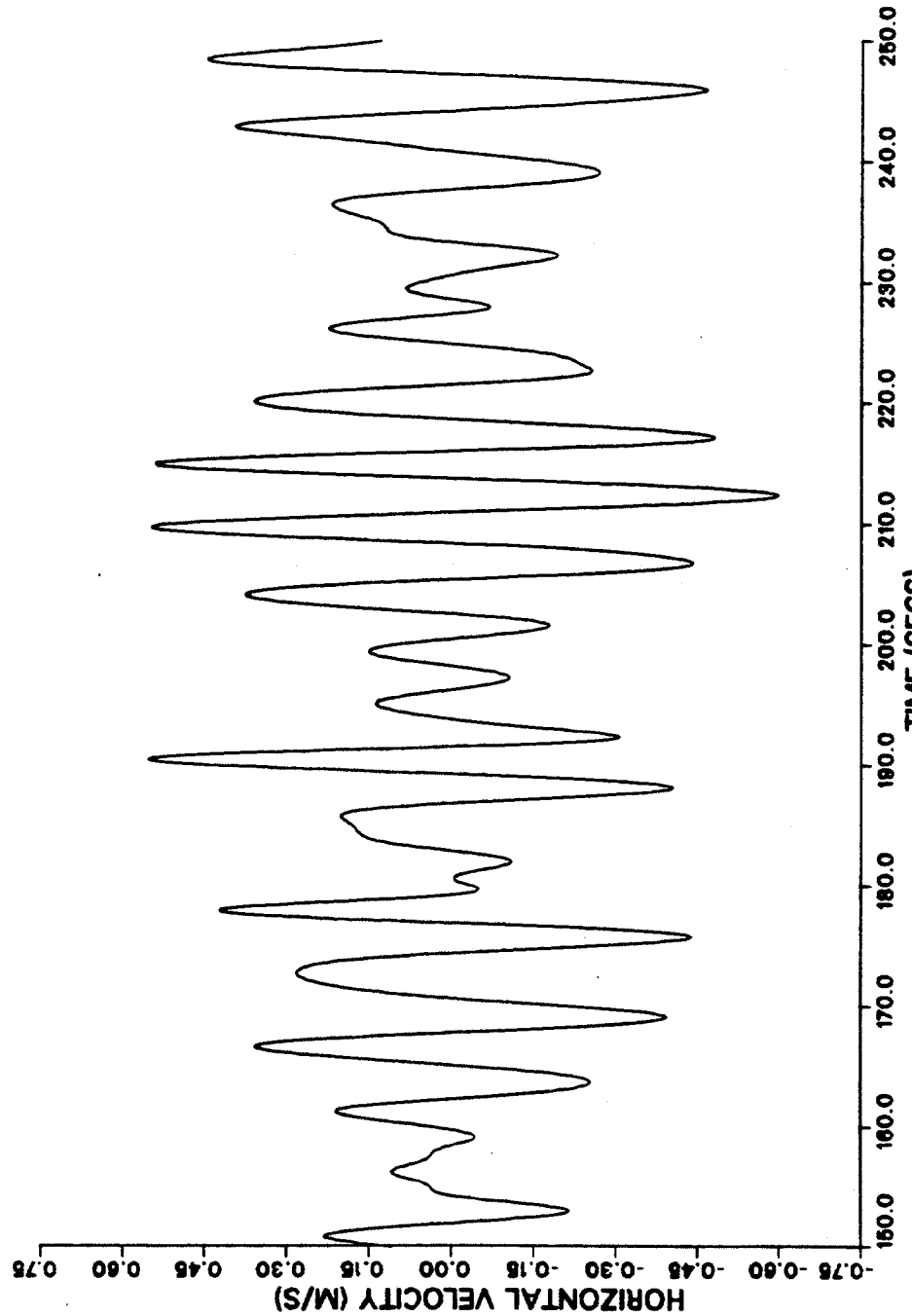

Figure 4.36. Horizontal velocity time history, smoothed, lower level.

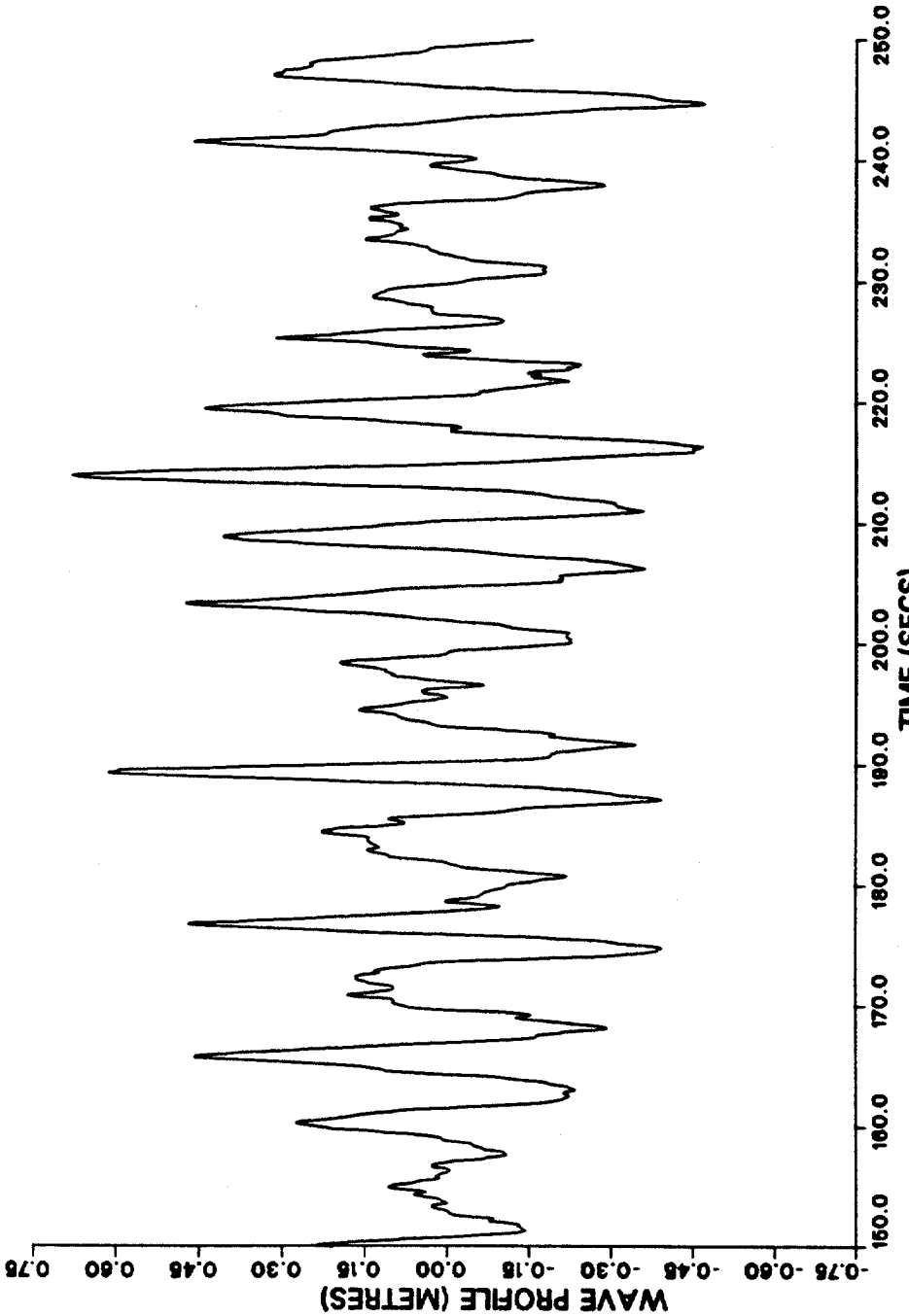

Figure 4.37. Wave elevation time history, smoothed, position 1.

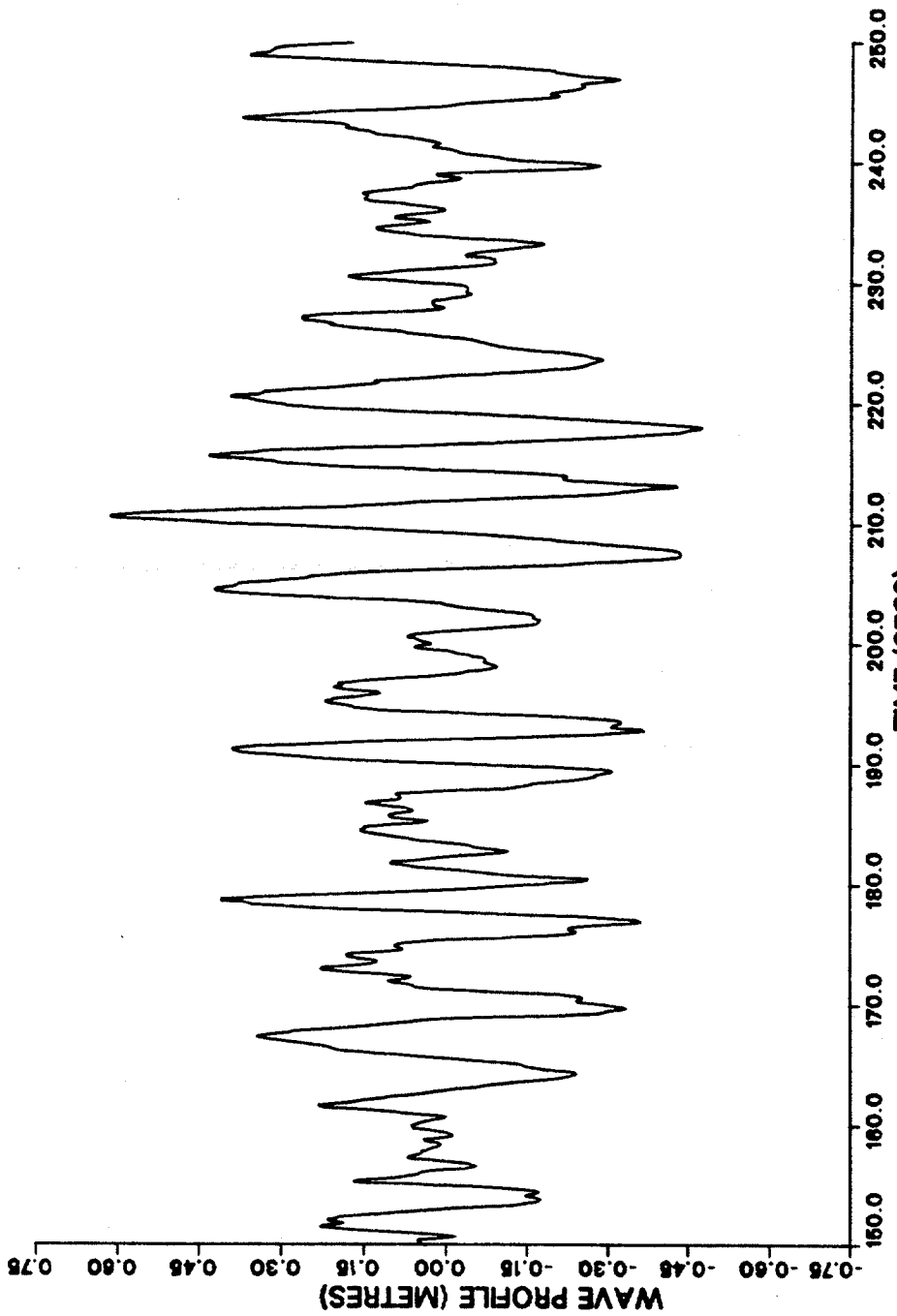

Figure 4.38. Wave elevation time history, smoothed, position 2.

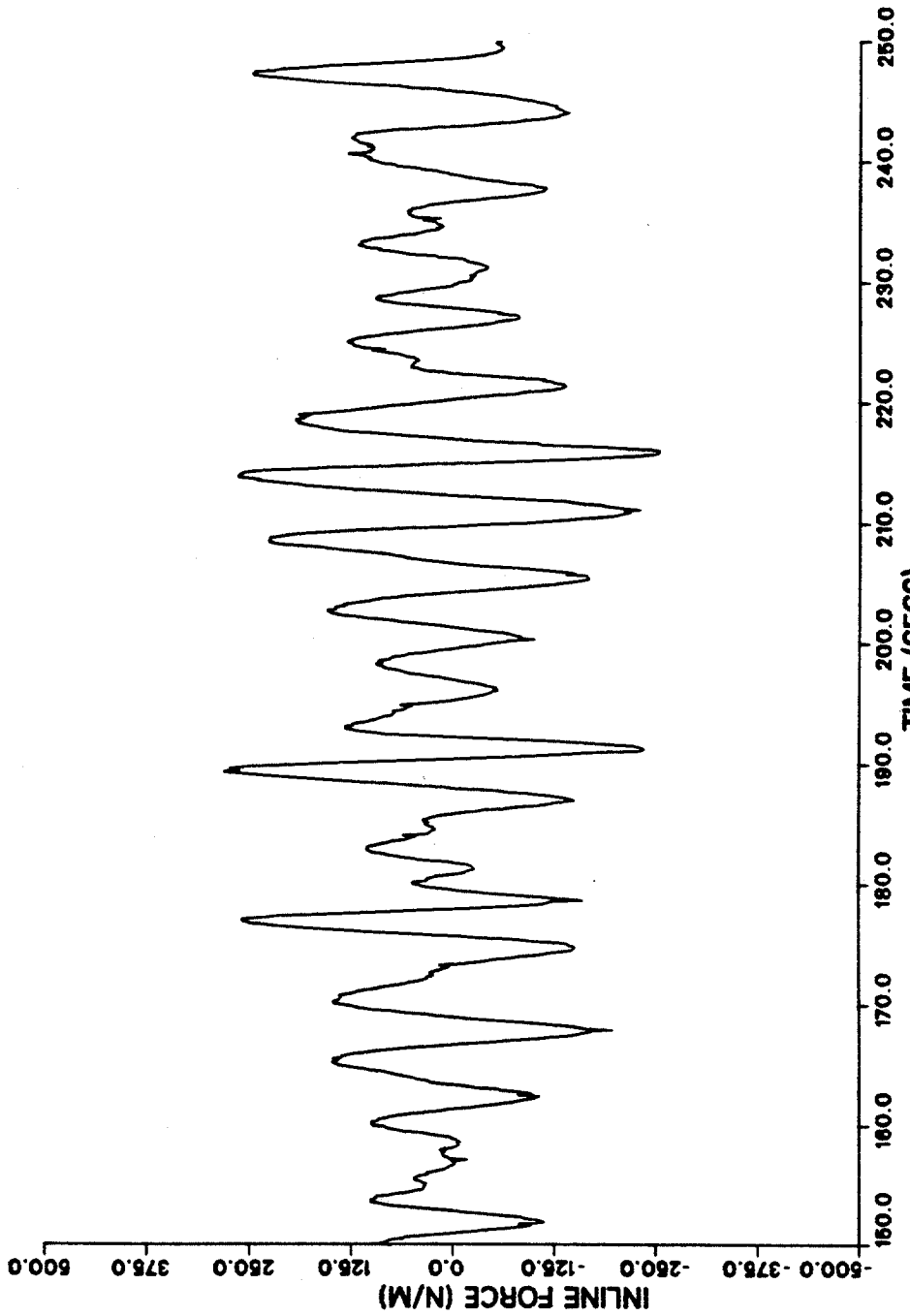

Figure 4.39. In-line force time history, smoothed, lower level.

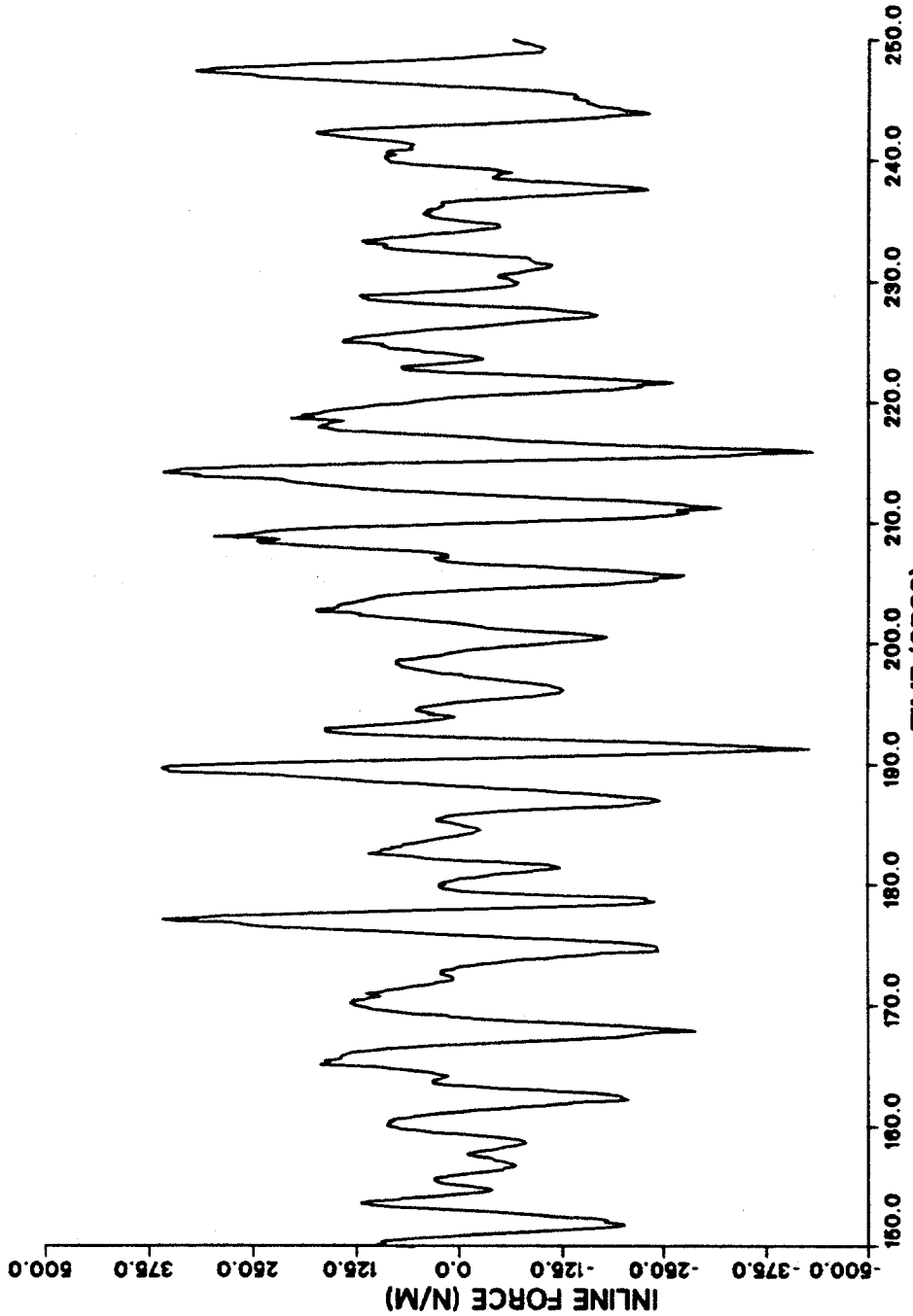

Figure 4.40. In-line force time history, smoothed, lower level.

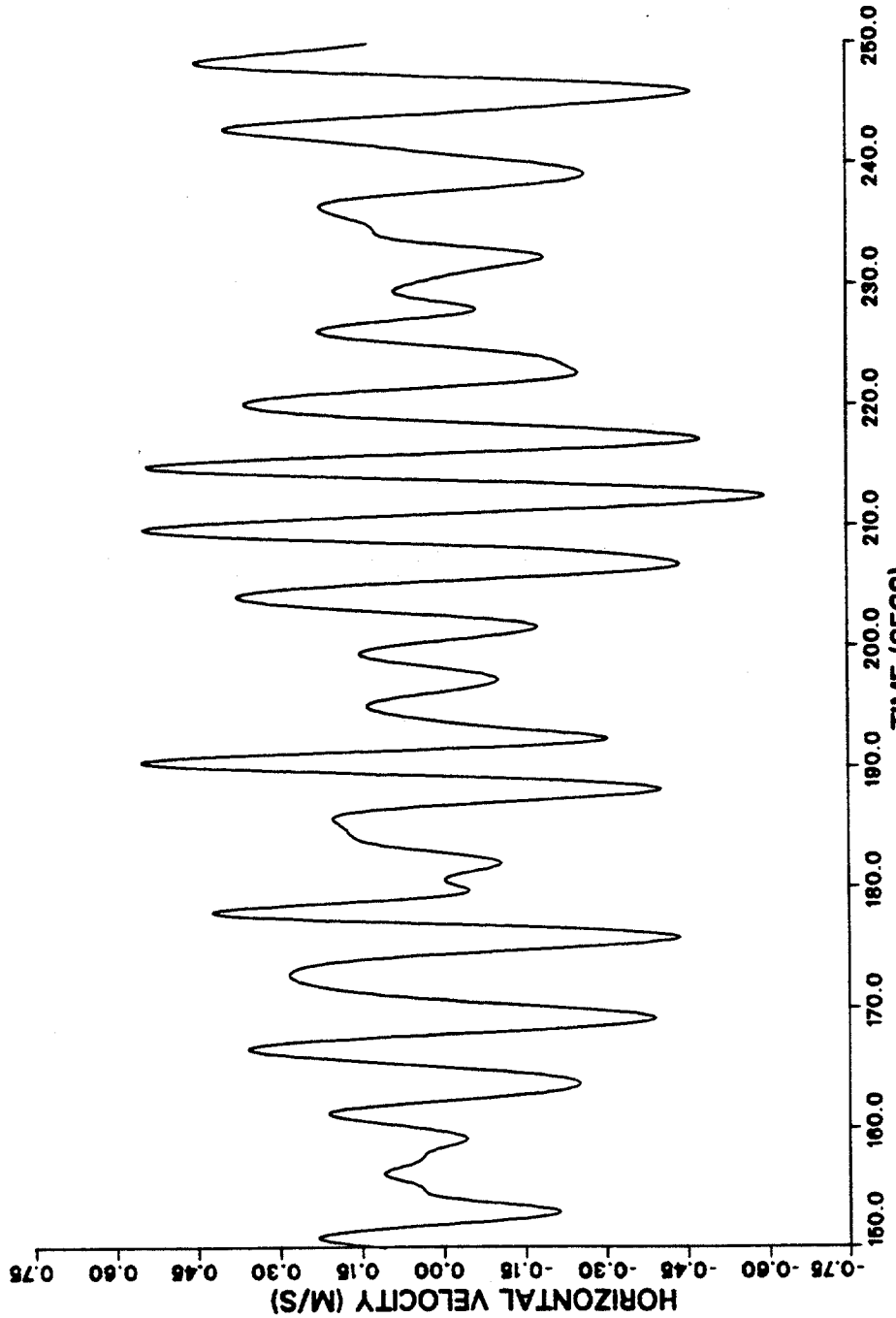

Figure 4.41. Horizontal velocity time history, smoothed, lower level.

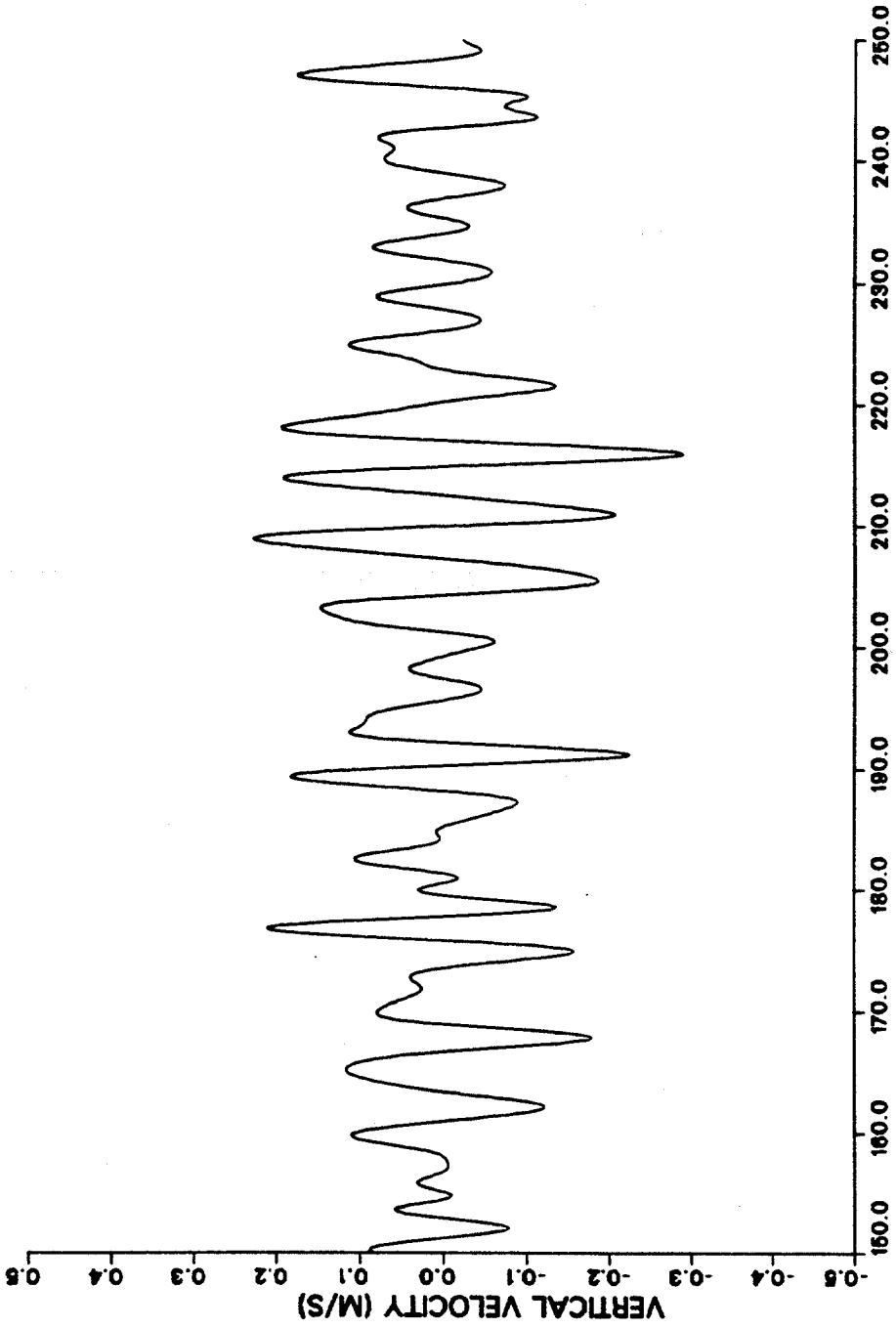

Figure 4.42. Vertical velocity time history, smoothed, lower level.

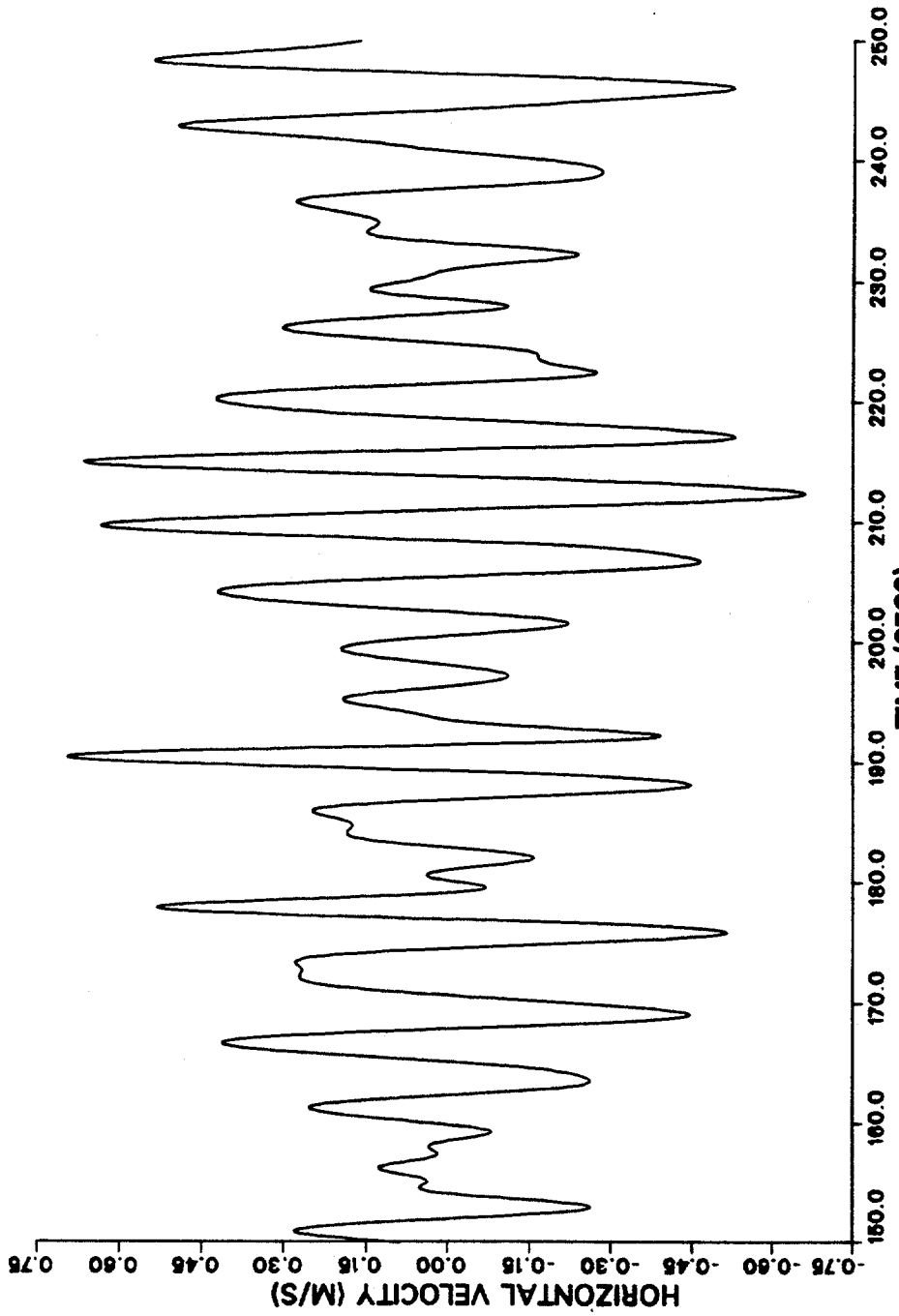

Figure 4.43. Horizontal velocity time history, smoothed, upper level.

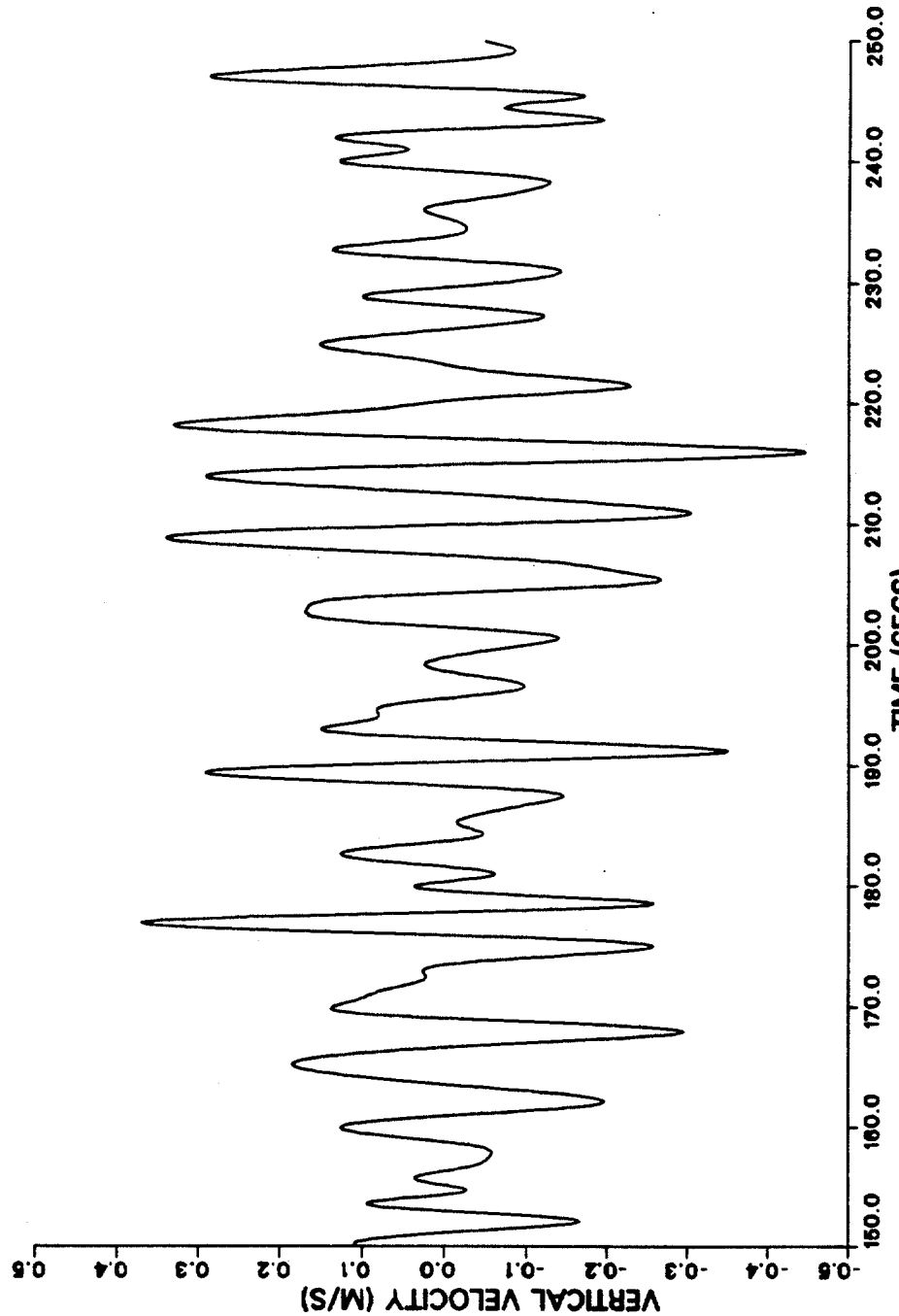

Figure 4.44. Vertical velocity time history, smoothed, upper level.

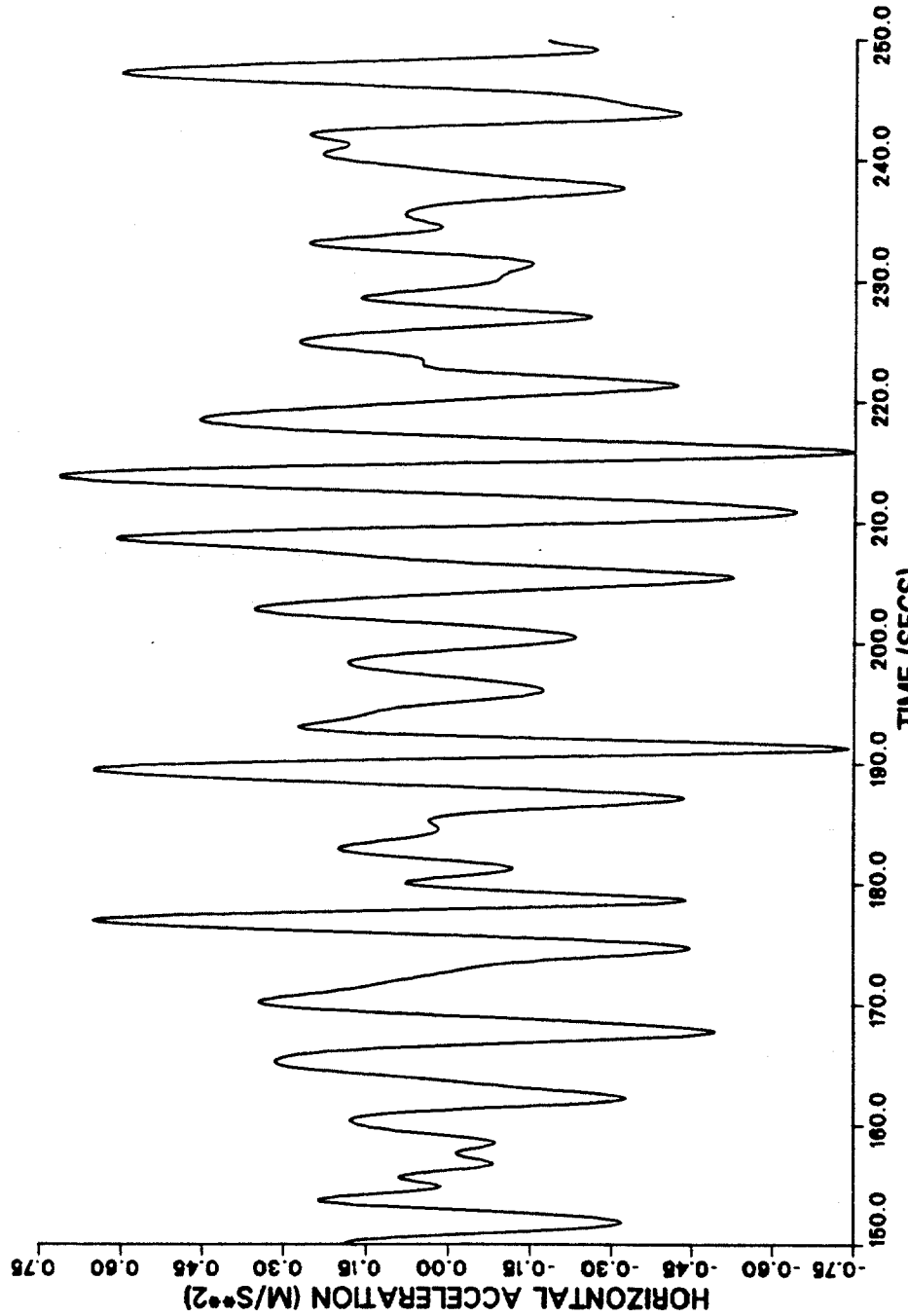

Figure 4.45. Horizontal acceleration time history, smoothed, lower level.

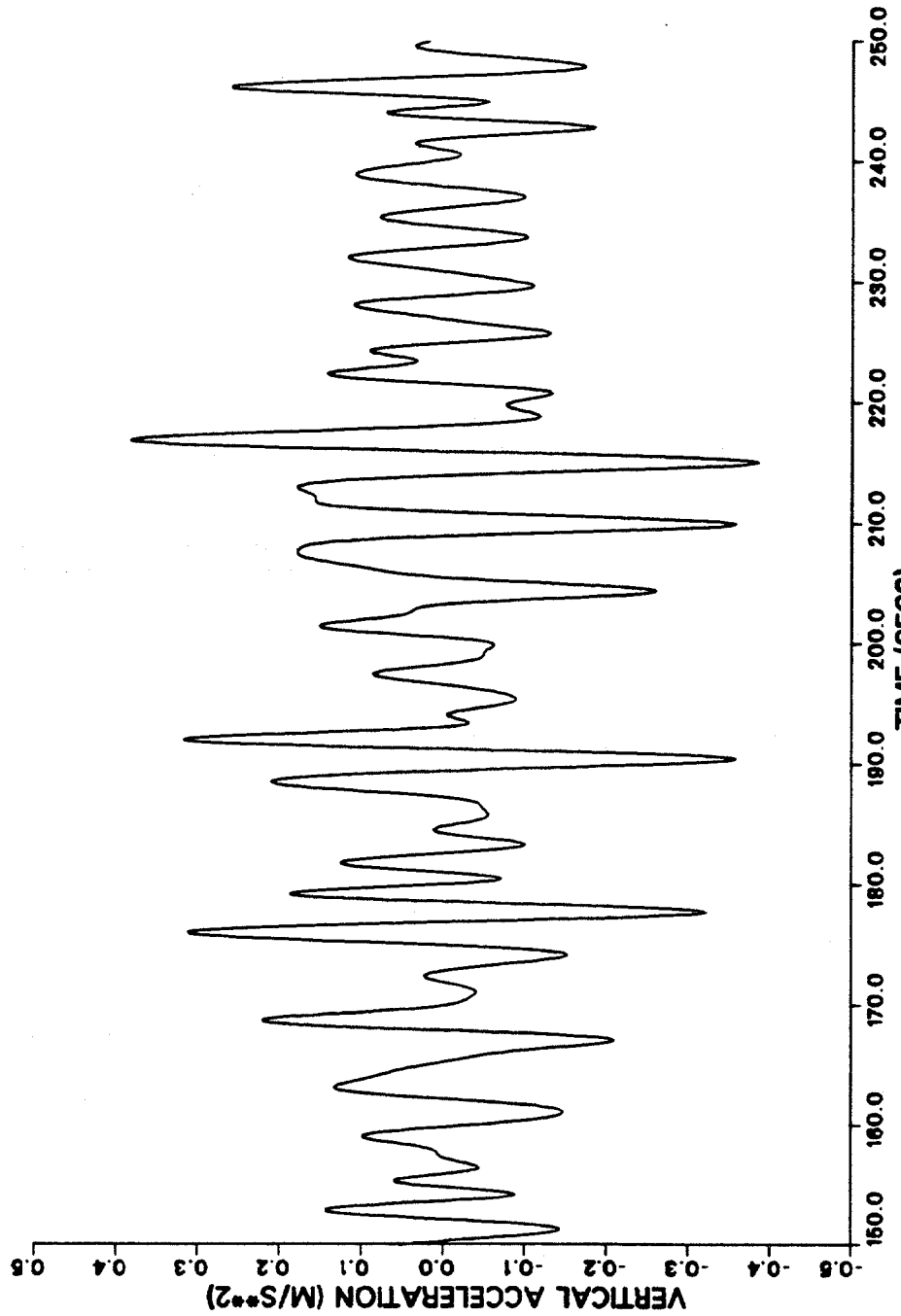

Figure 4.46. Vertical acceleration time history, smoothed, lower level.

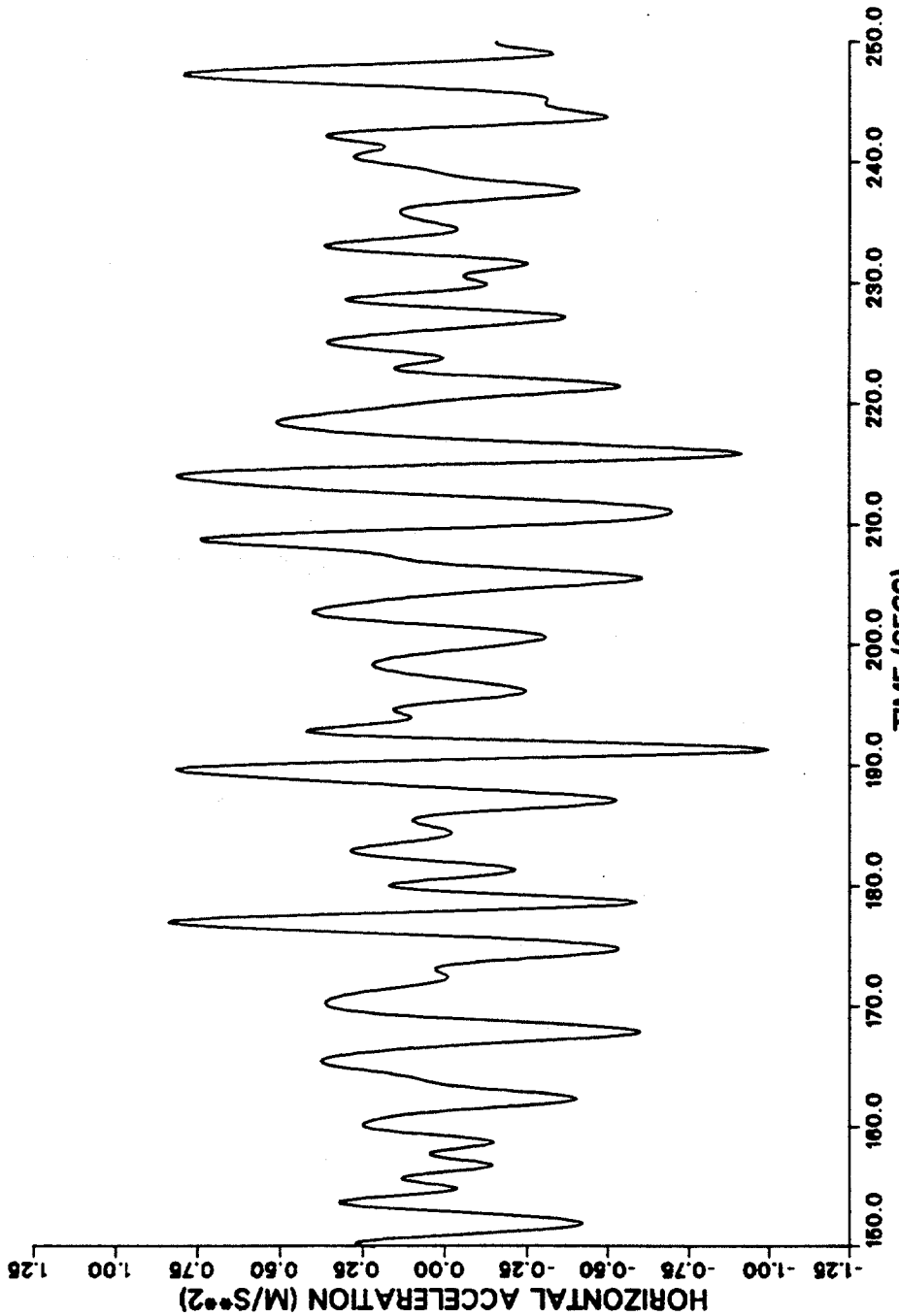

Figure 4.47. Horizontal acceleration time history, smoothed, upper level.

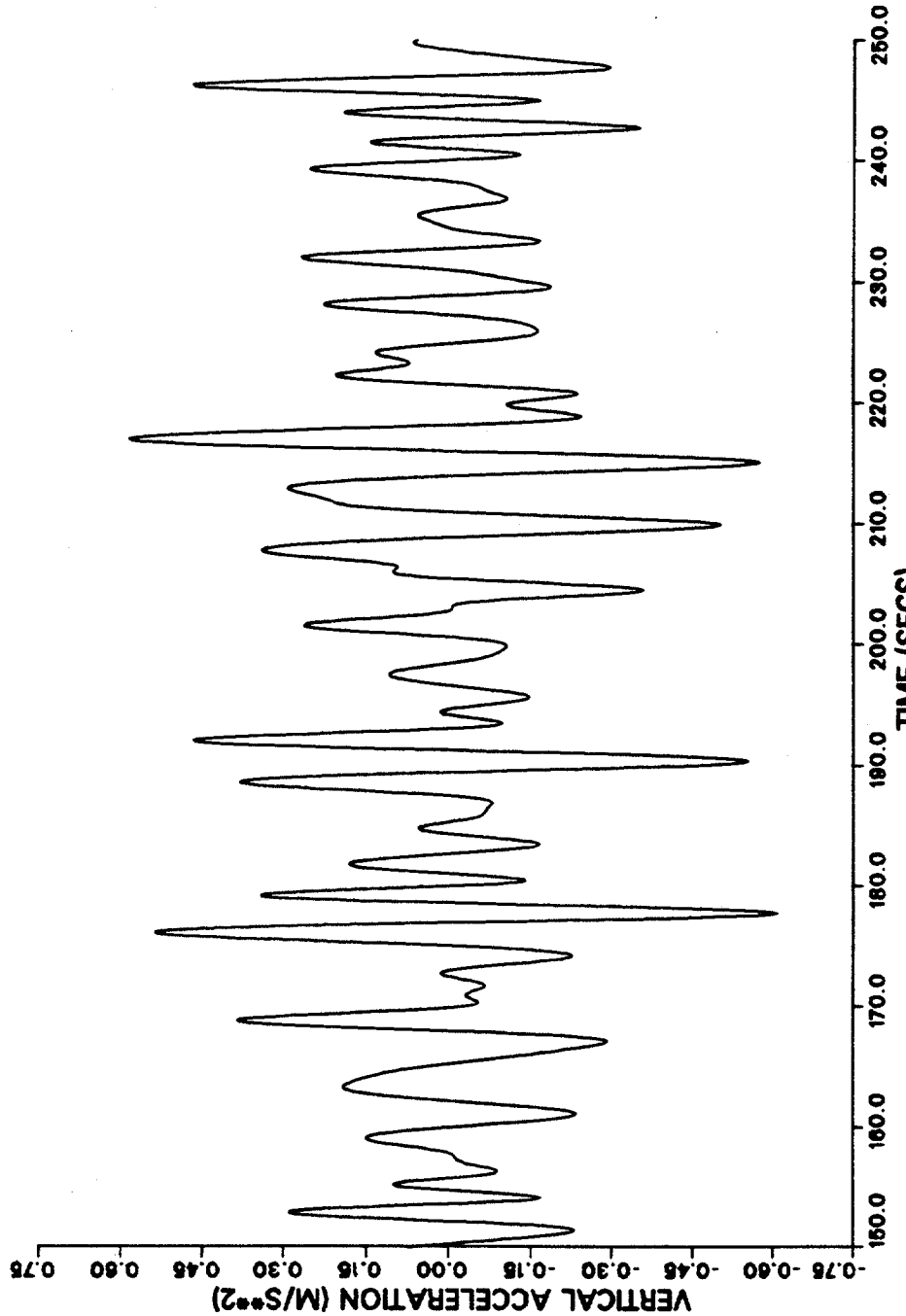

Figure 4.48. Vertical acceleration time history, smoothed, upper level.

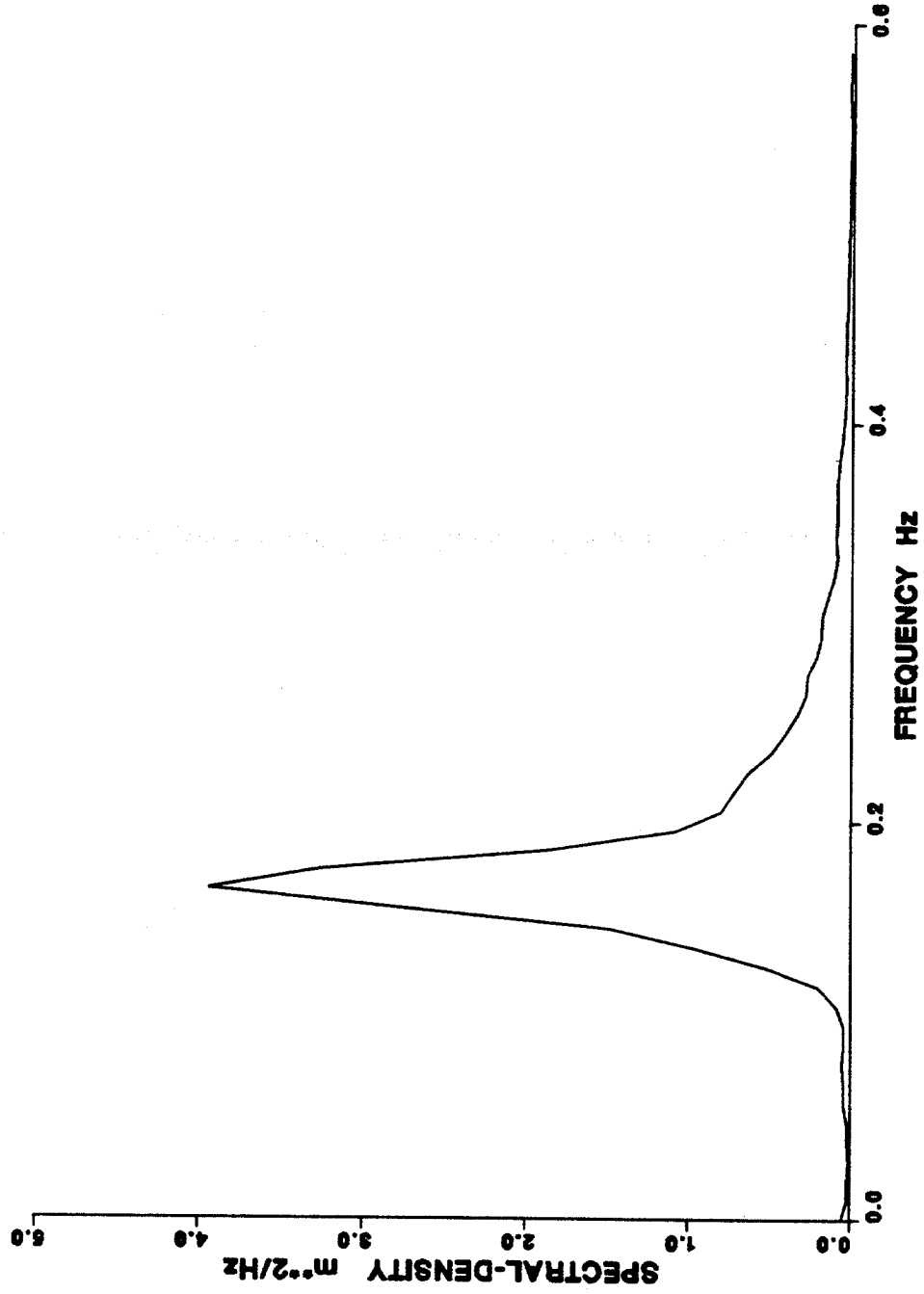

Figure 4.49. Spectrum of wave elevation, position 1.

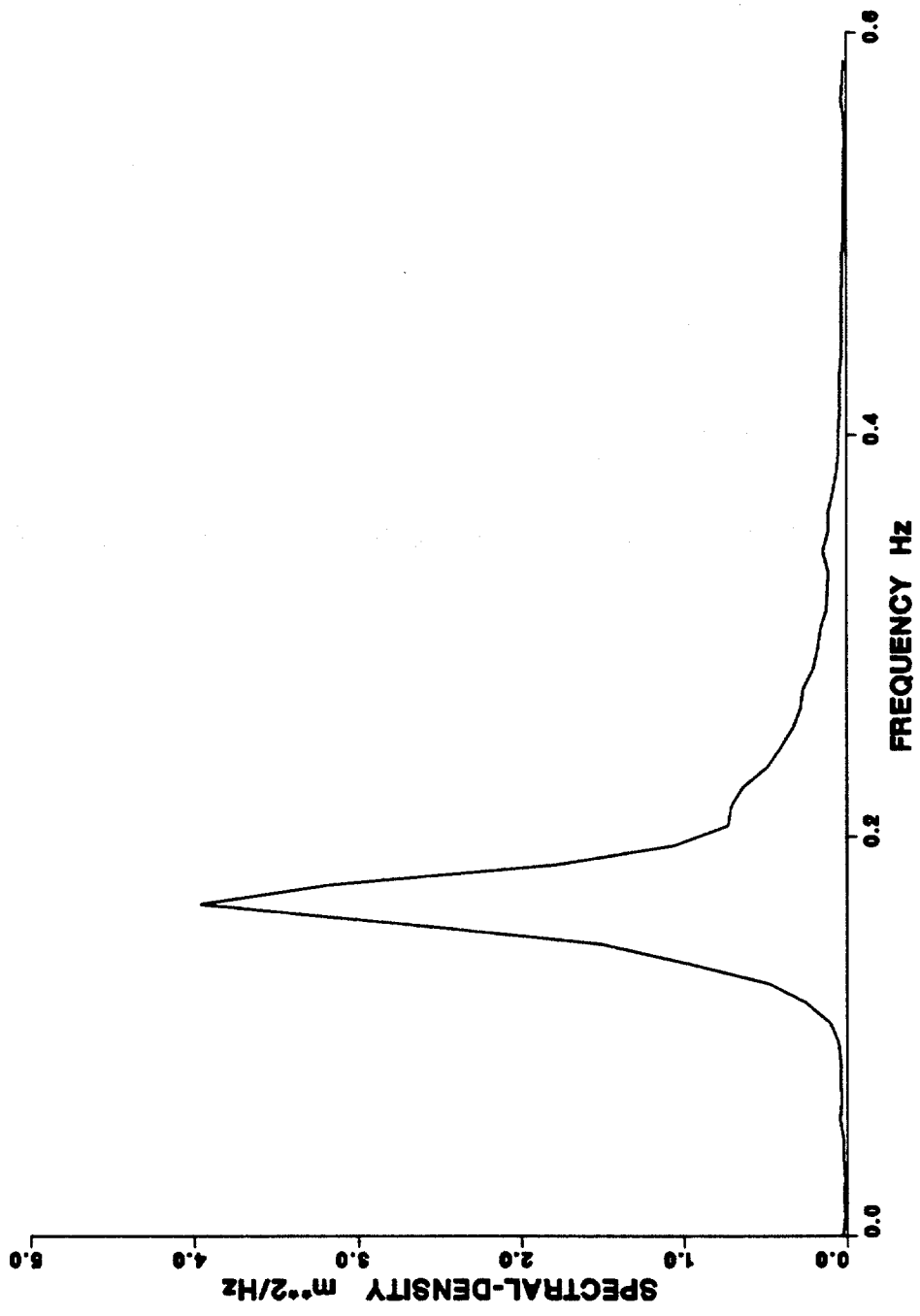

Figure 4.50. Spectrum of wave elevation, position 2.

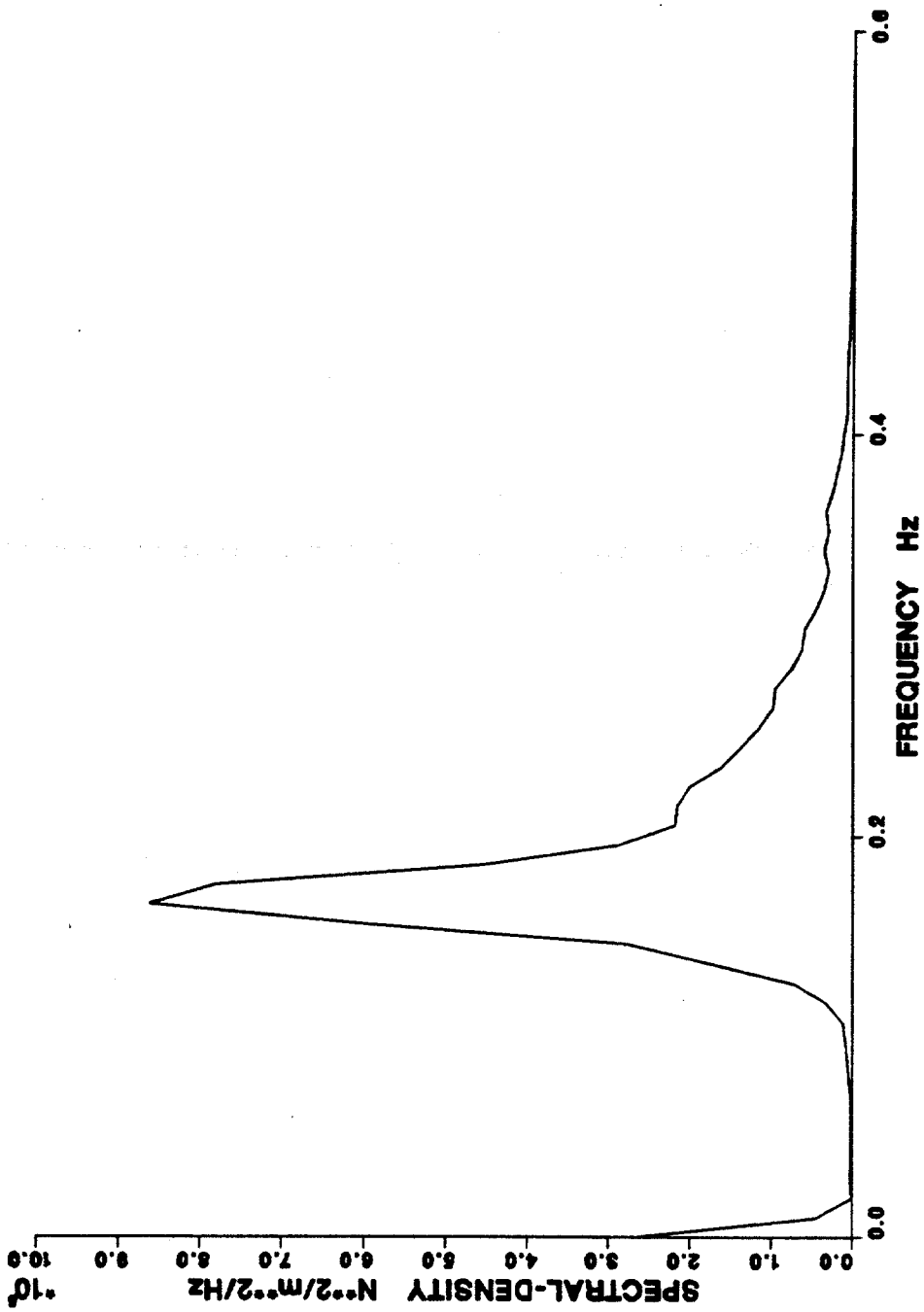

Figure 4.51. Spectrum of inline force, lower level.

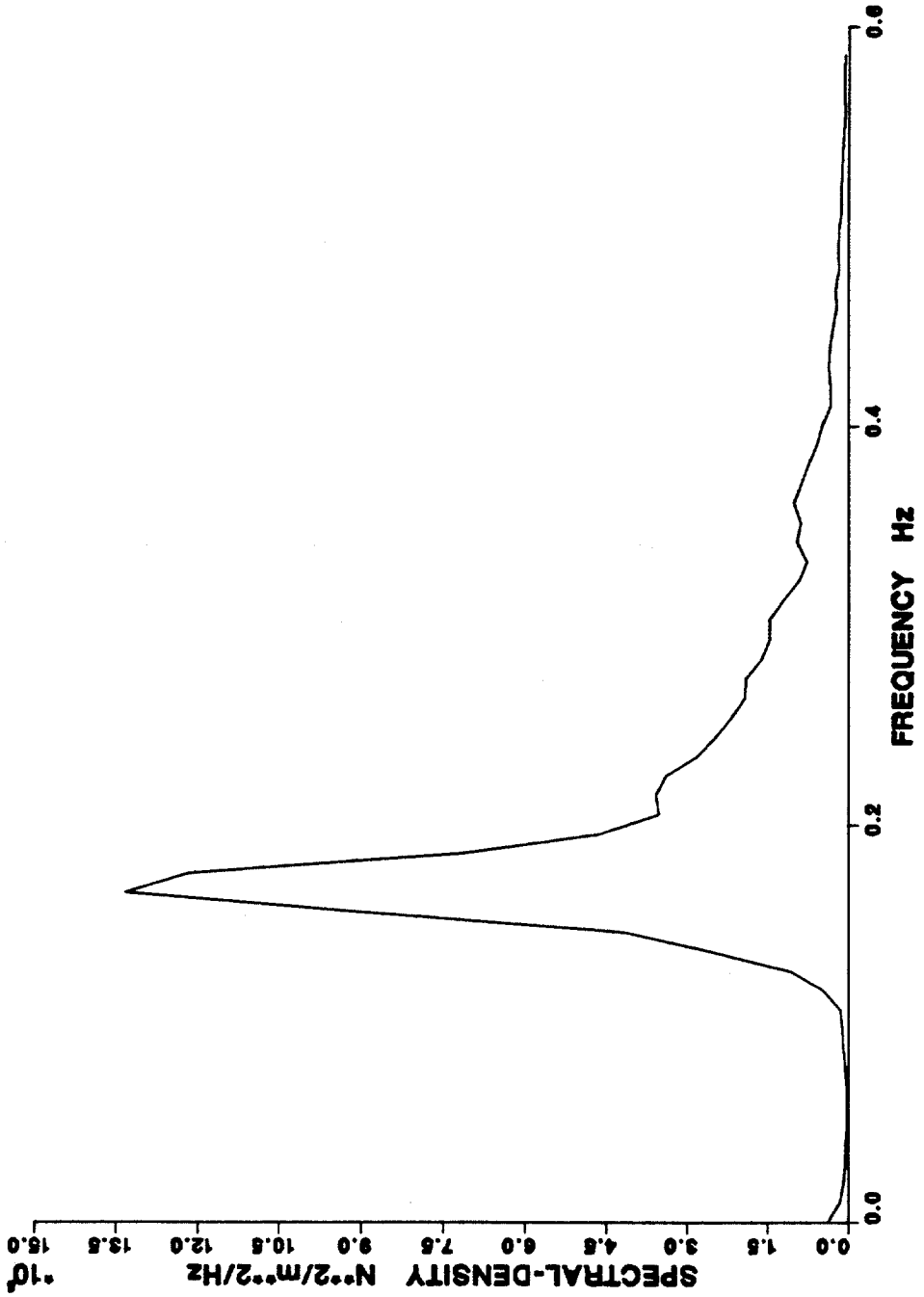

Figure 4.52. Spectrum of inline force, upper level.

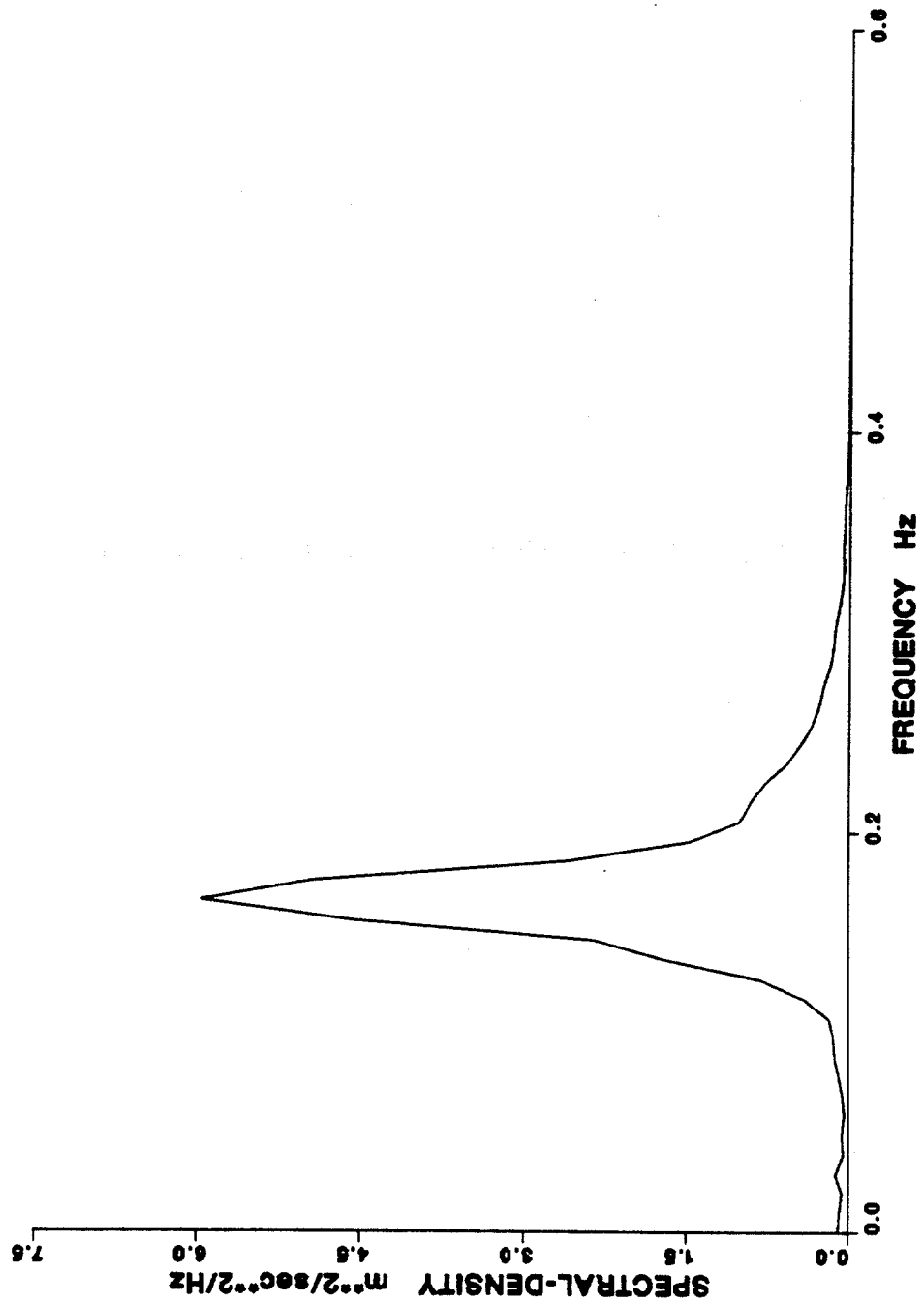

Figure 4.53. Spectrum of horizontal velocity, lower level.

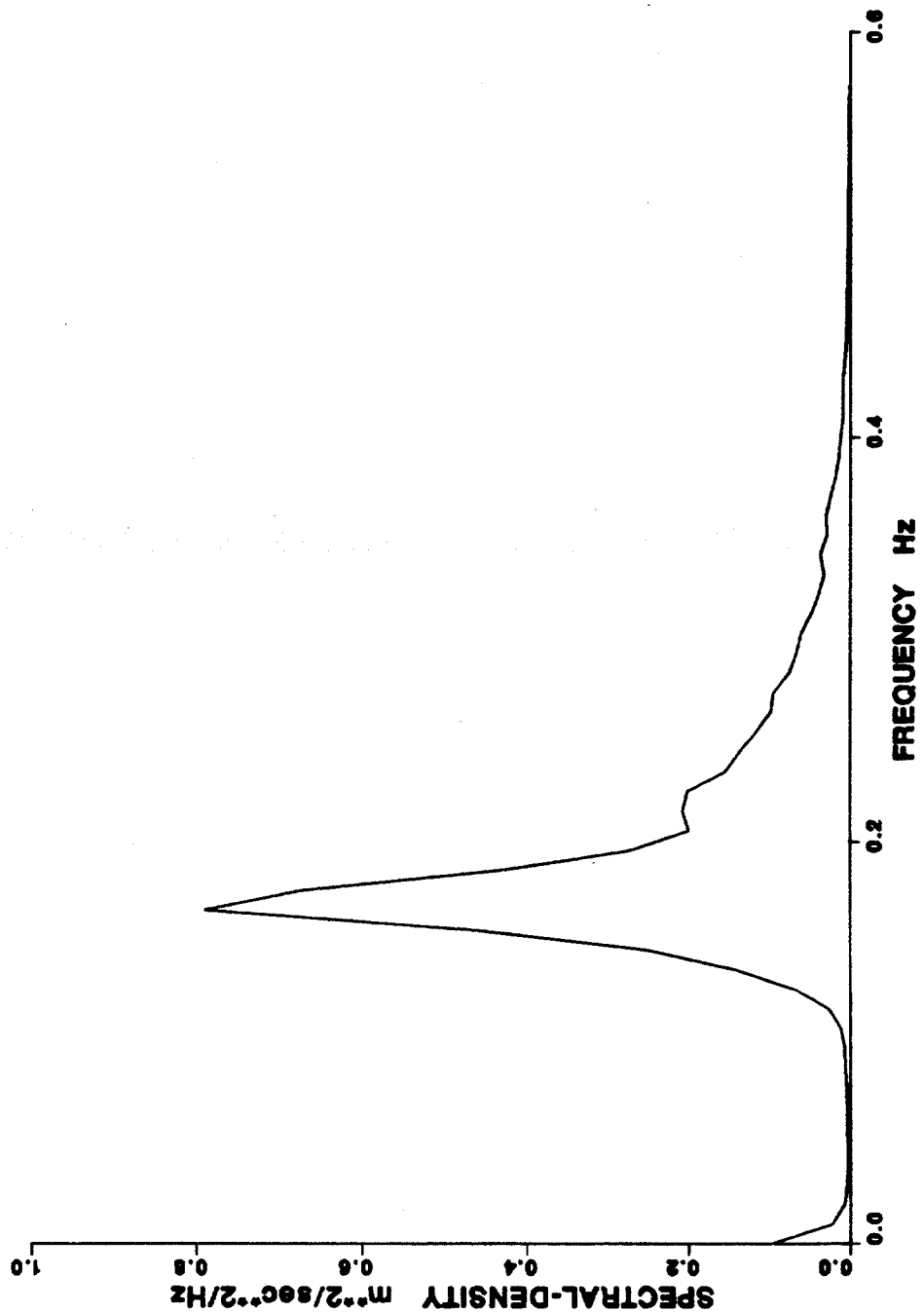

Figure 4.54. Spectrum of vertical velocity, lower level.

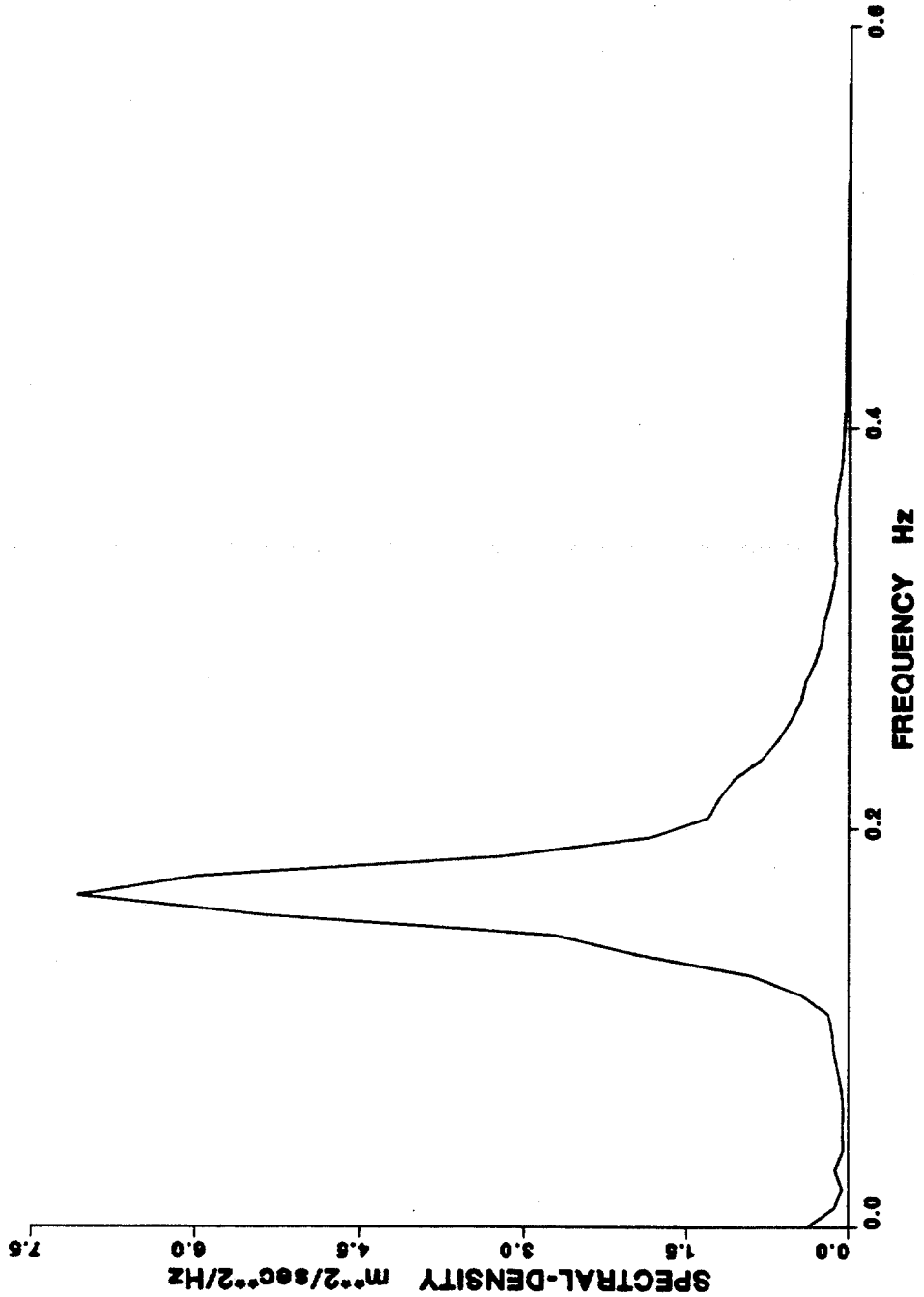

Figure 4.55. Spectrum of horizontal velocity, upper level.

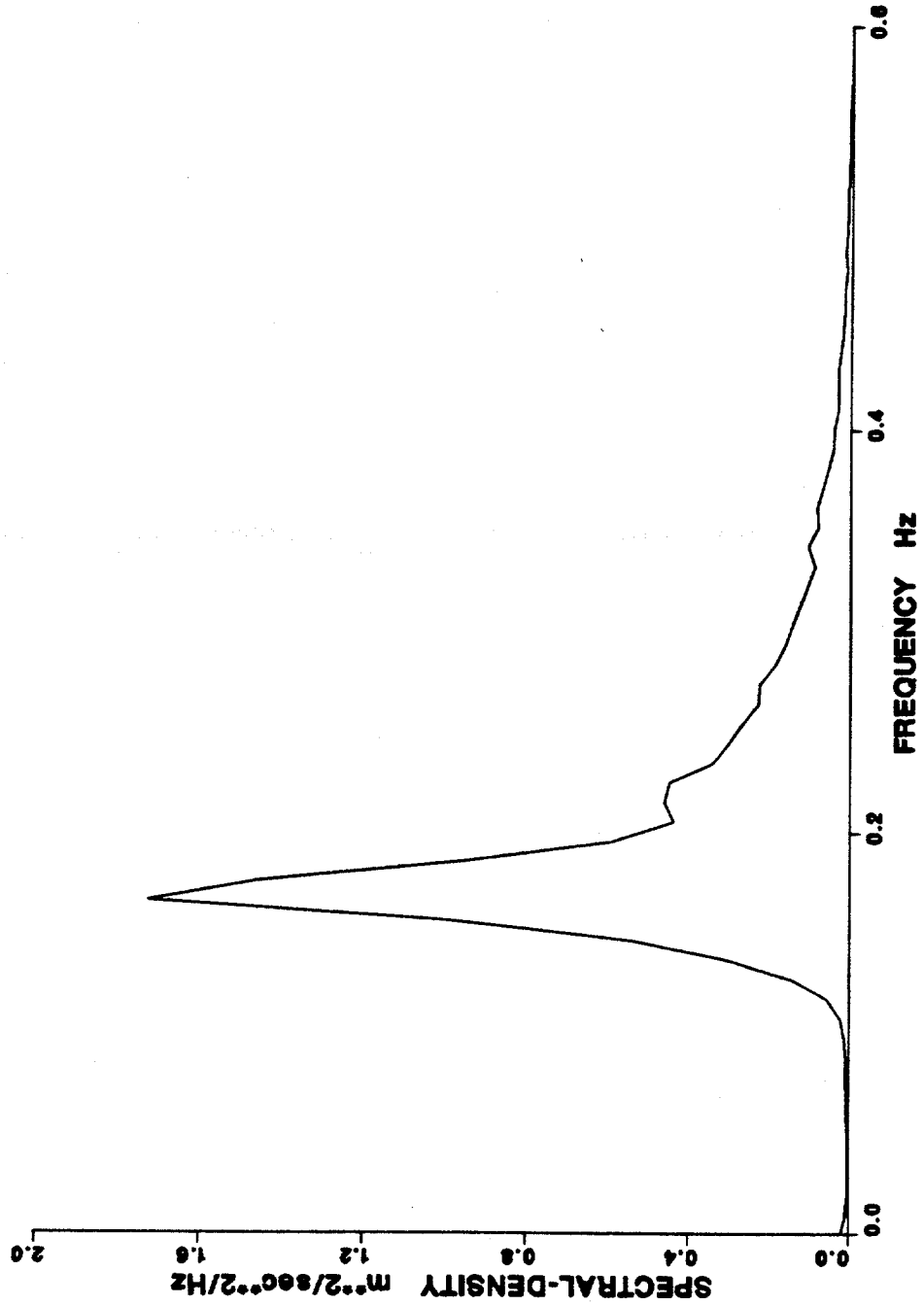

Figure 4.56. Spectrum of vertical velocity, upper level.

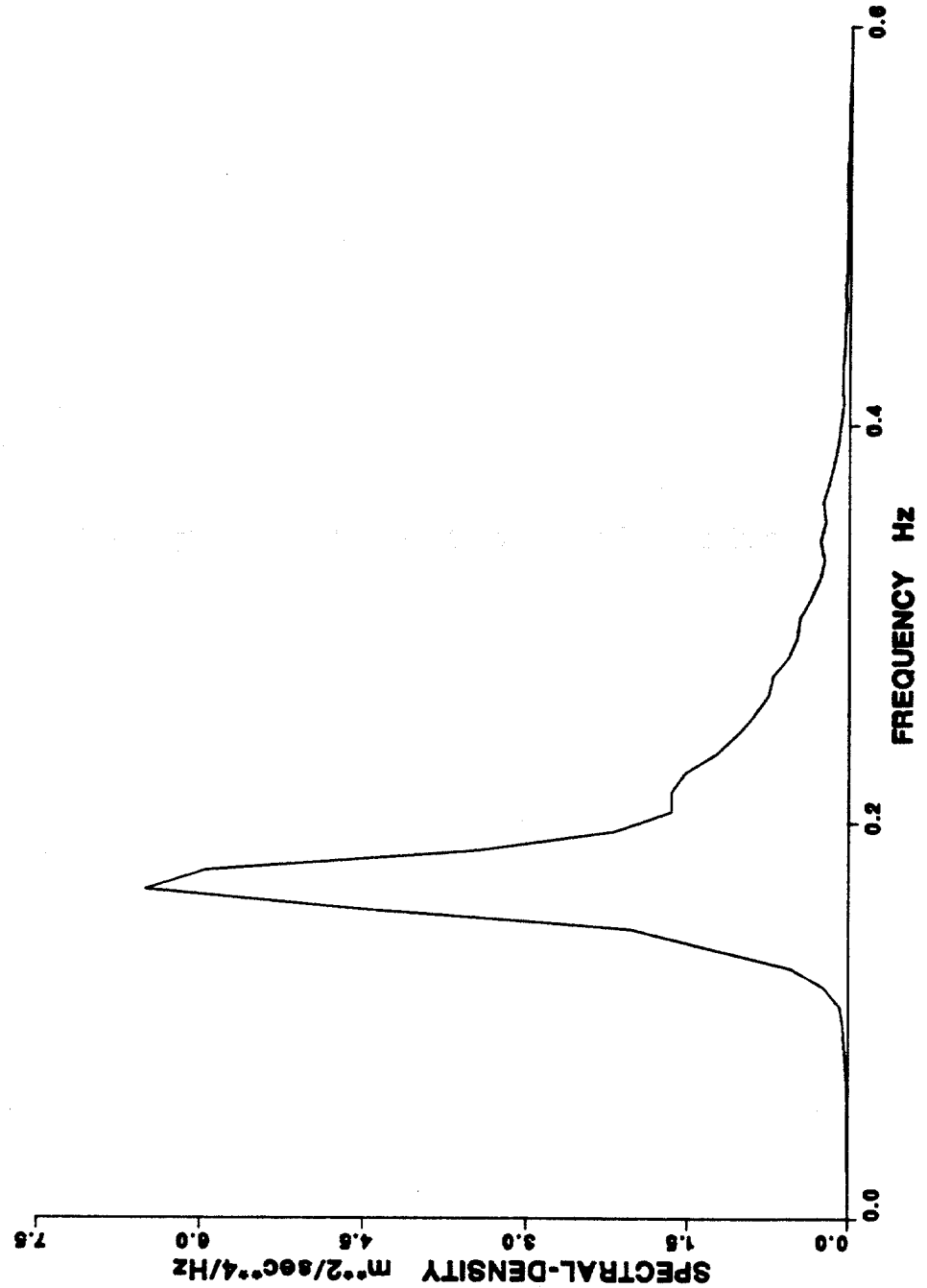

Figure 4.57. Spectrum of horizontal acceleration, lower level.

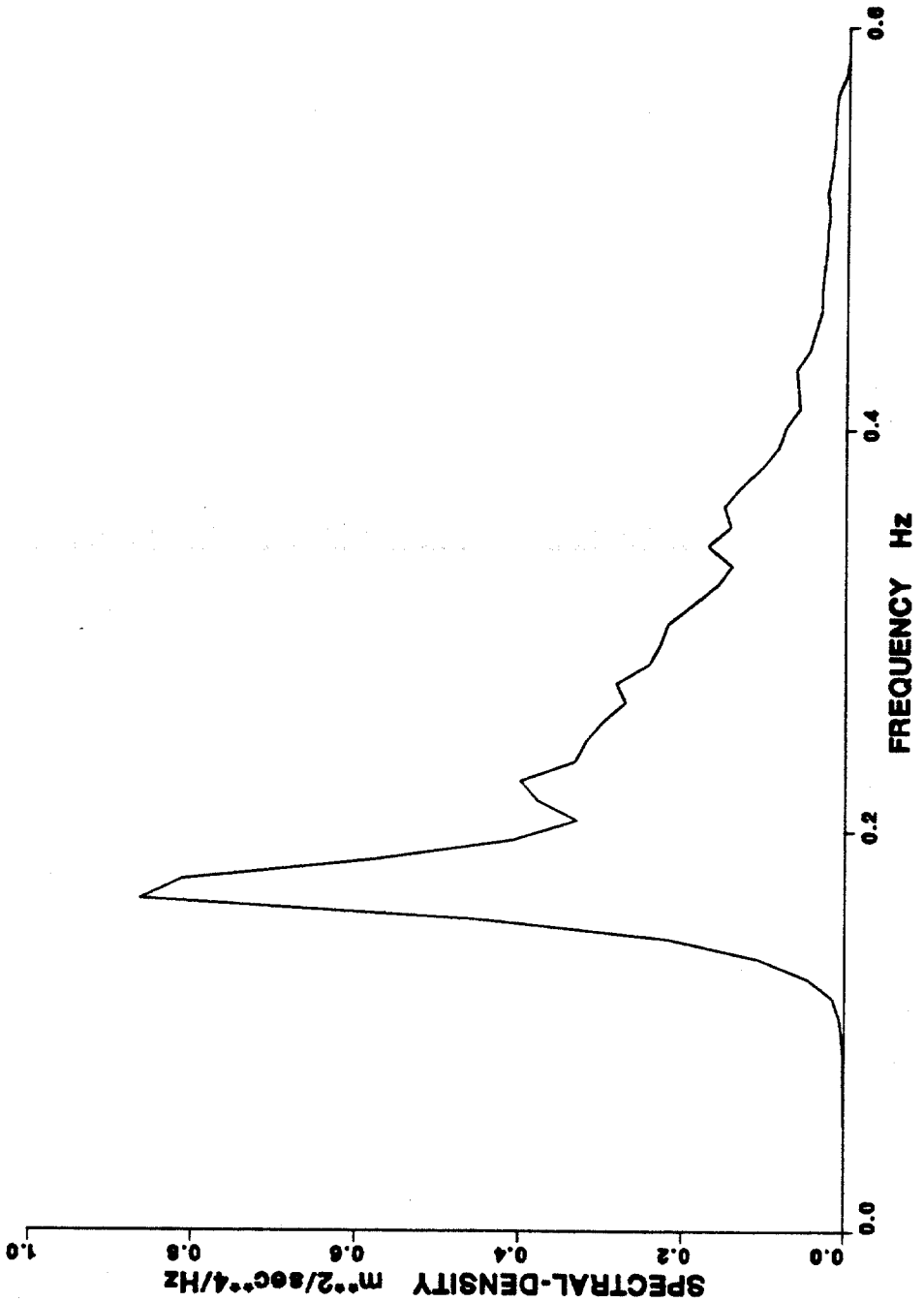

Figure 4.58. Spectrum of vertical acceleration, lower level.

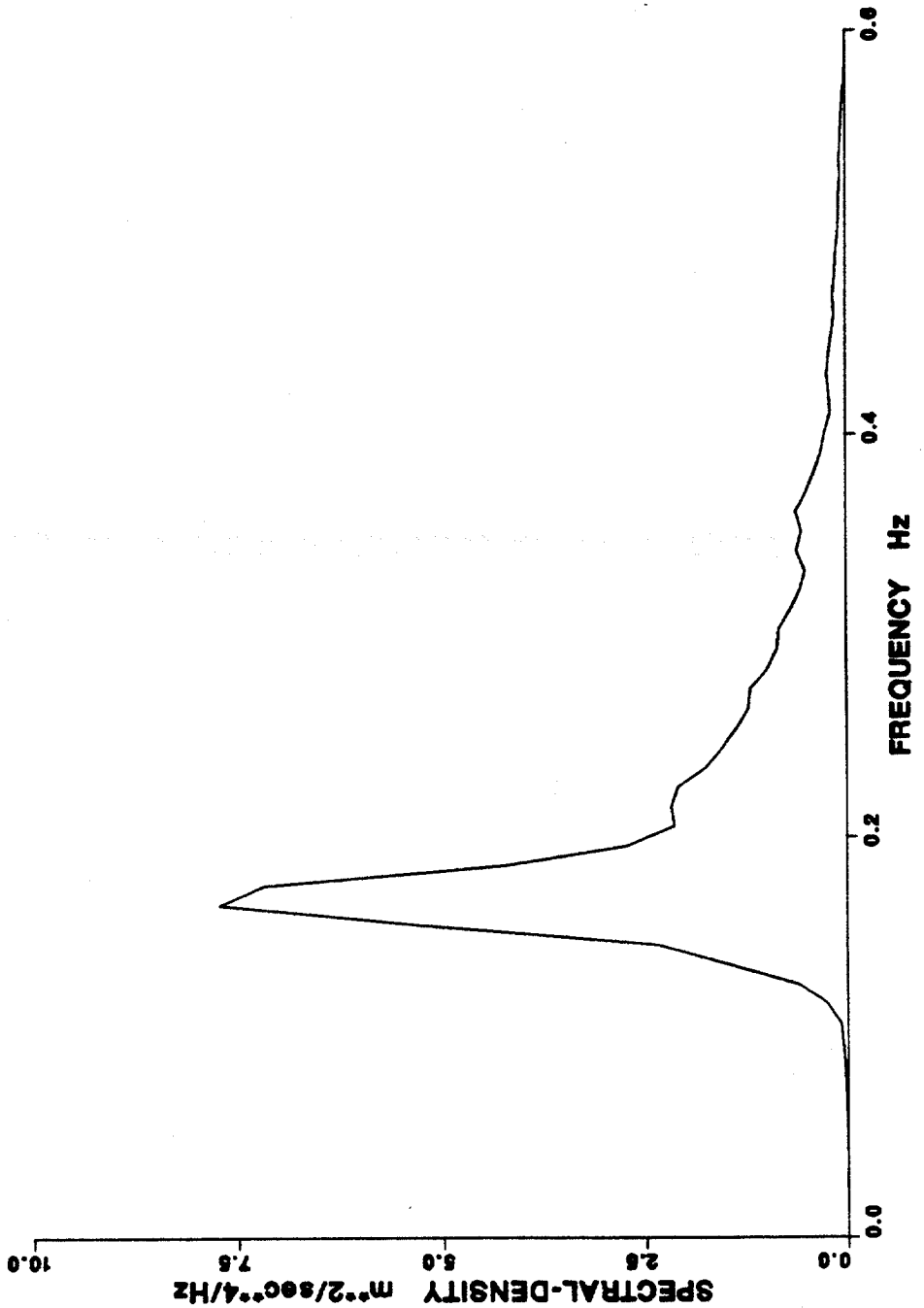

Figure 4.59. Spectrum of horizontal acceleration, upper level.

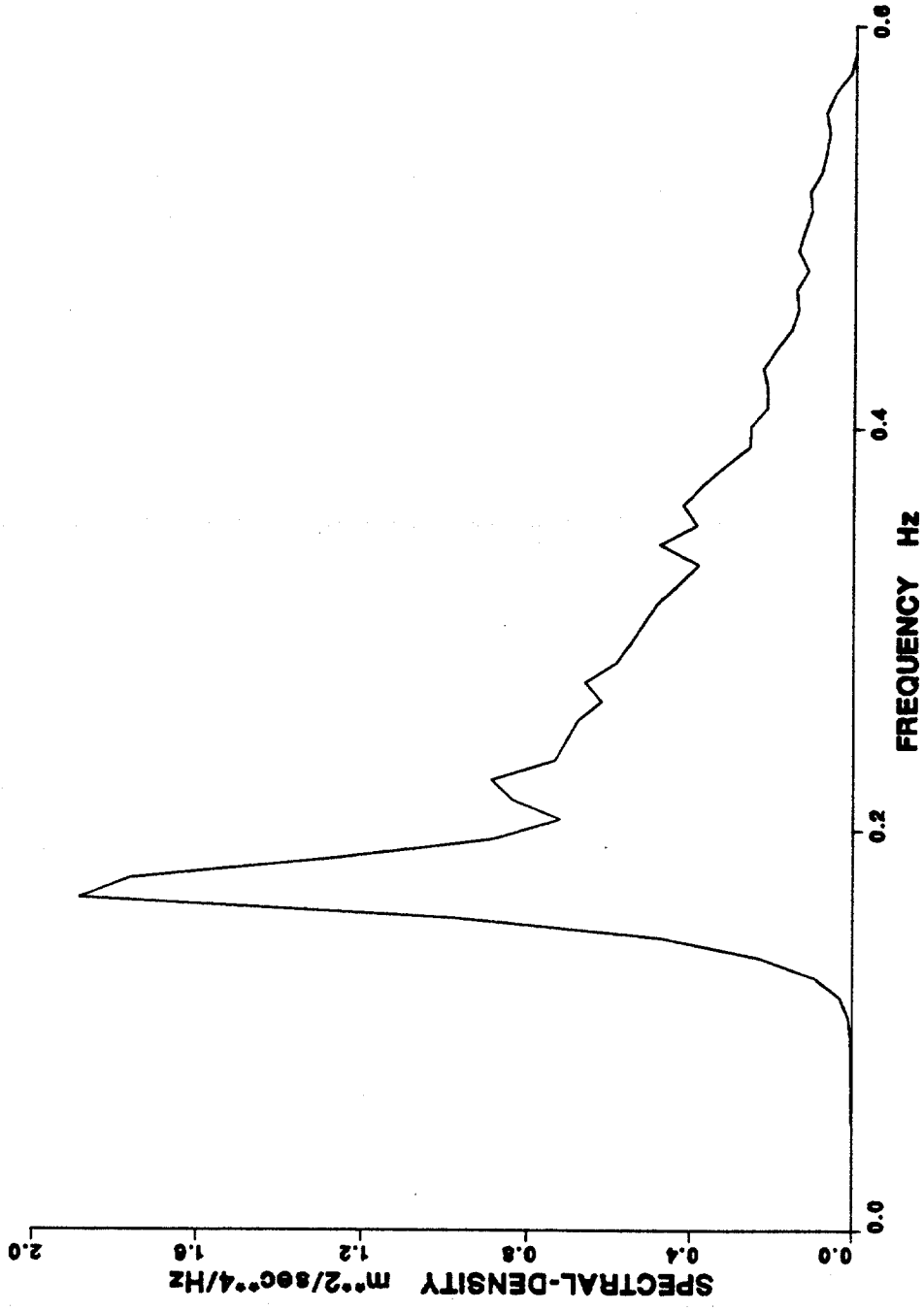

Figure 4.60. Spectrum of vertical acceleration, upper level.

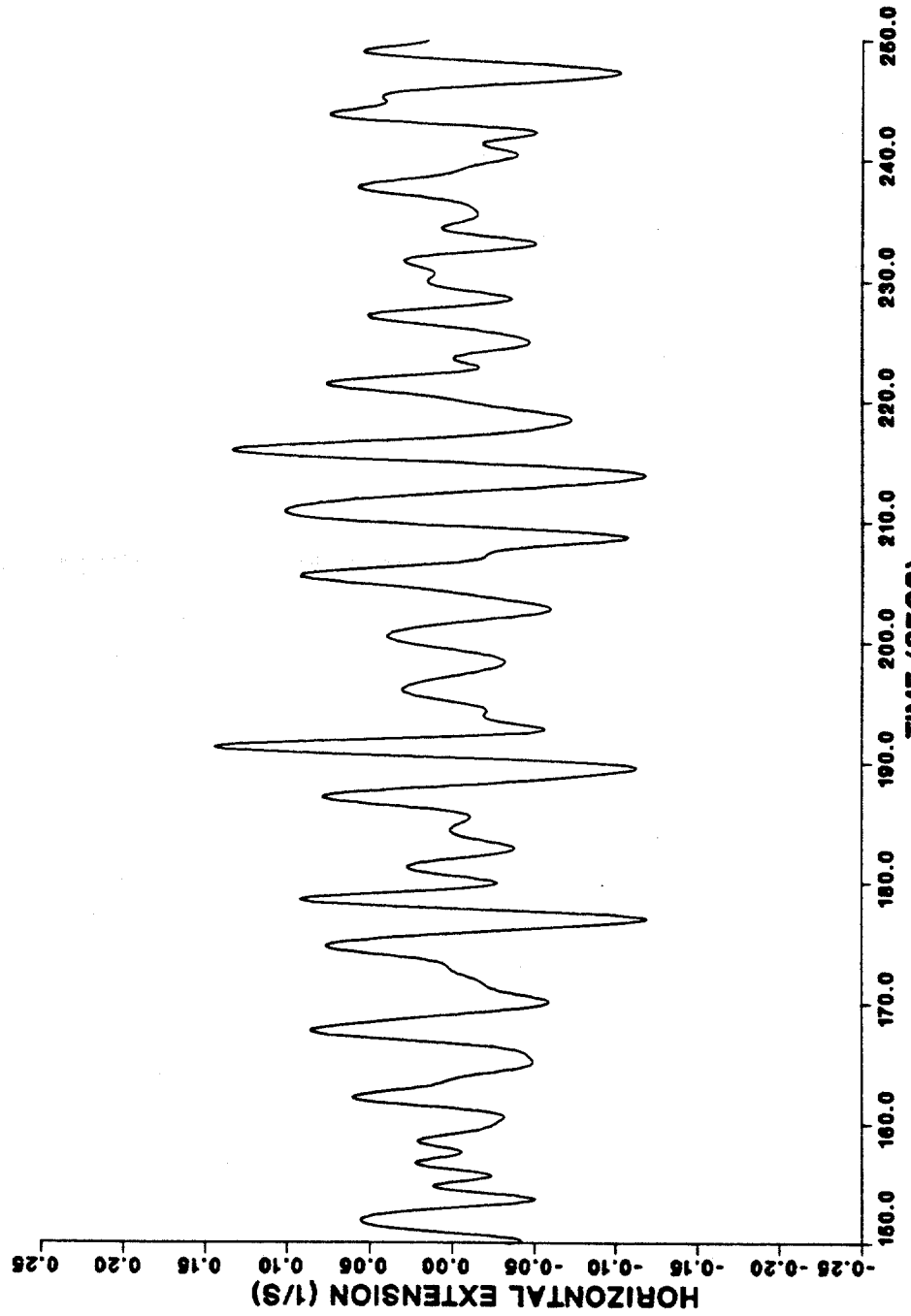

Figure 4.61. Horizontal gradient of the horizontal velocity time history, lower level.

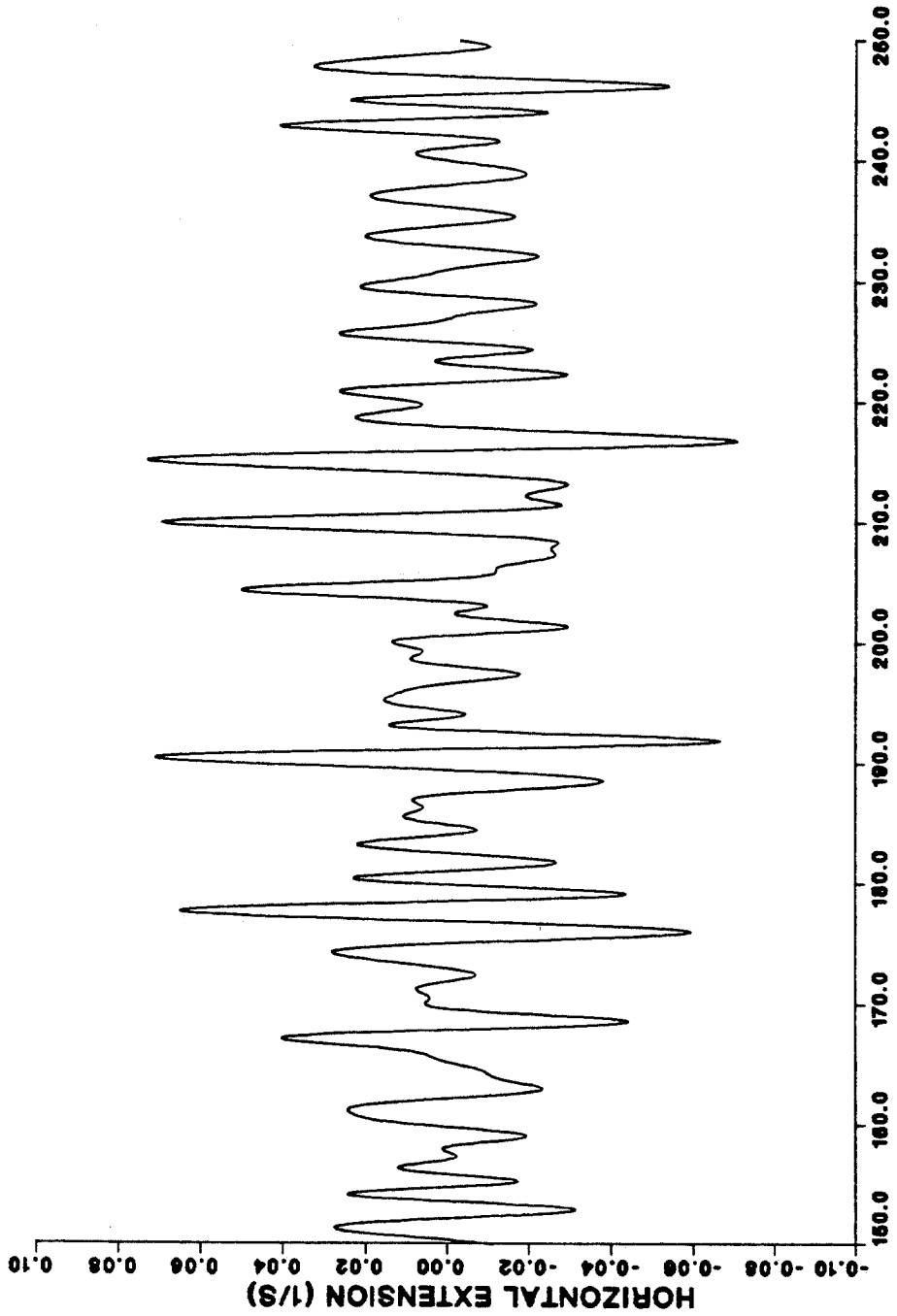

Figure 4.62. Horizontal gradient of the vertical velocity time history, lower level.

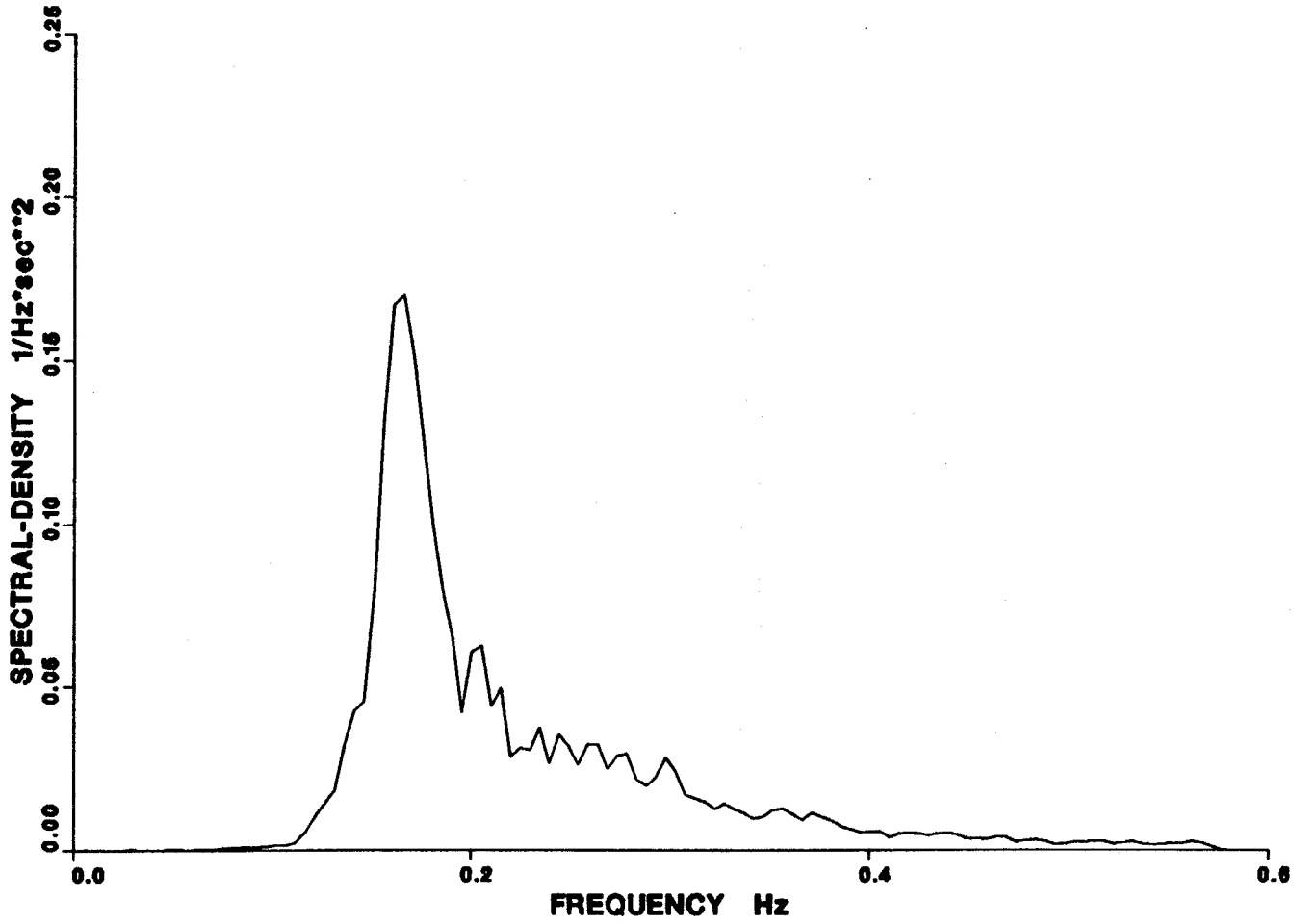

Figure 4.63. Spectrum of the horizontal gradient of the horizontal velocity.

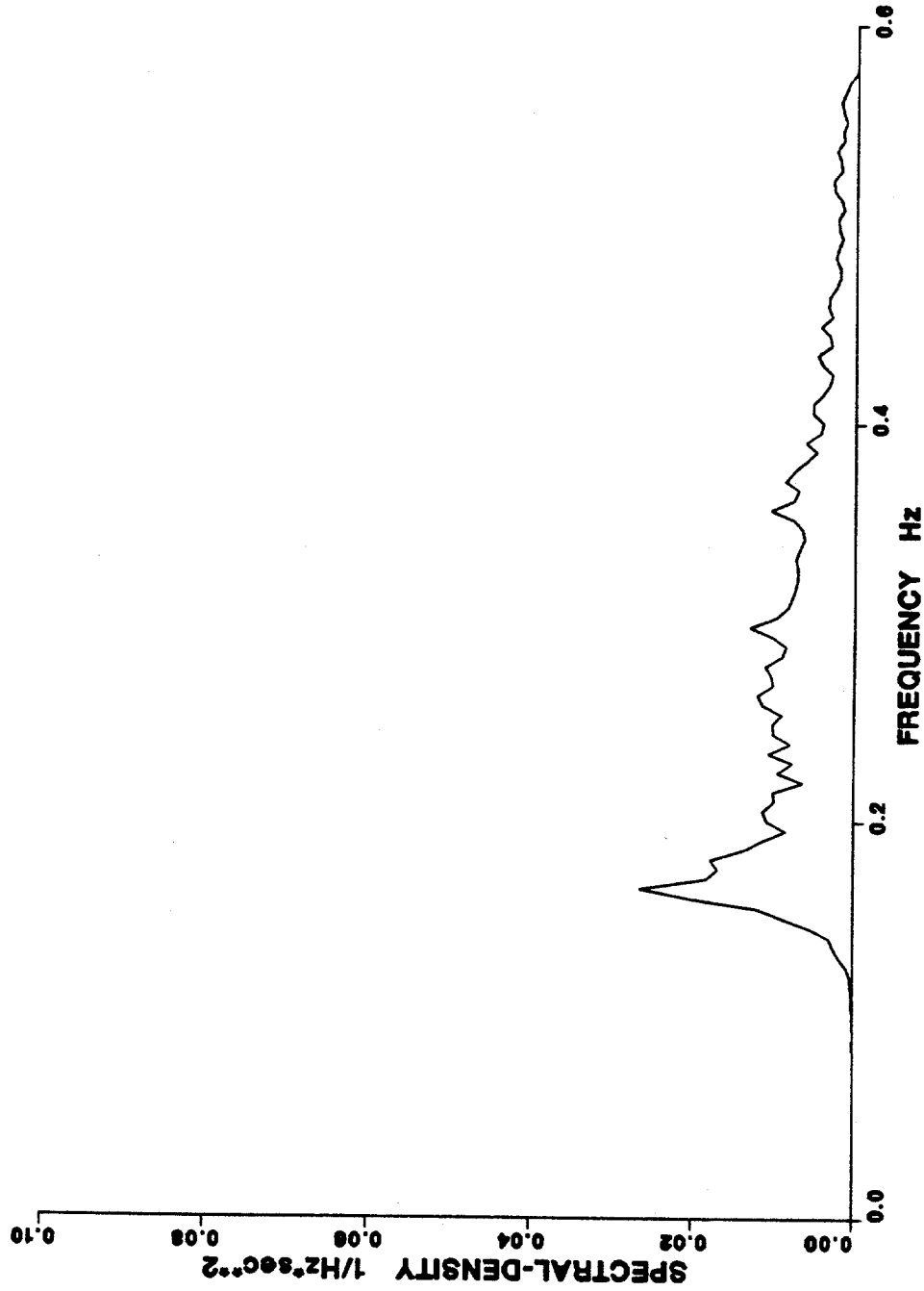

Figure 4.64. Spectrum of the horizontal gradient of the vertical velocity.

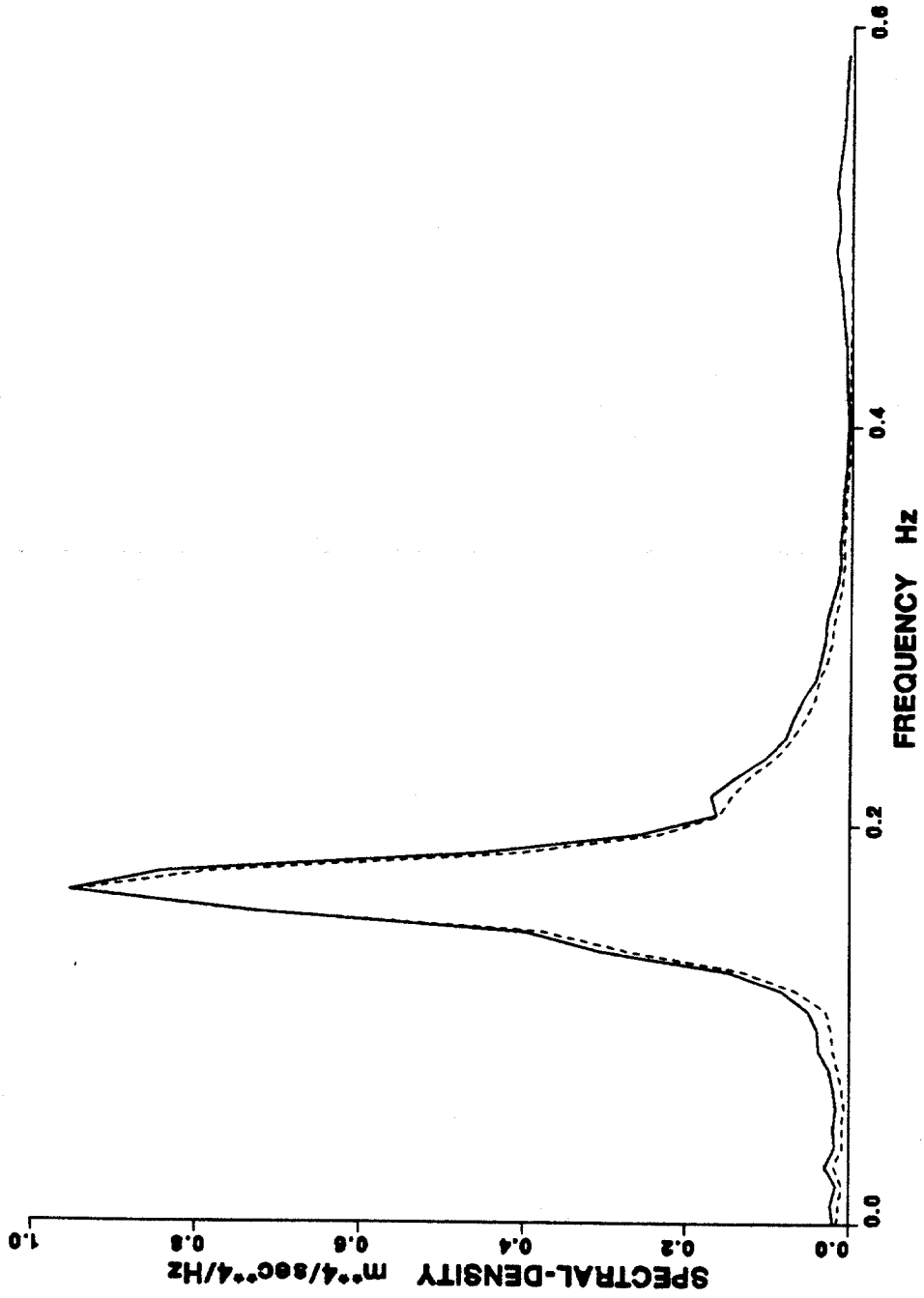

Figure 4.65. Comparison of nonlinear and linearized u|u|, lower level.
[Linearized ——, nonlinear - - -].

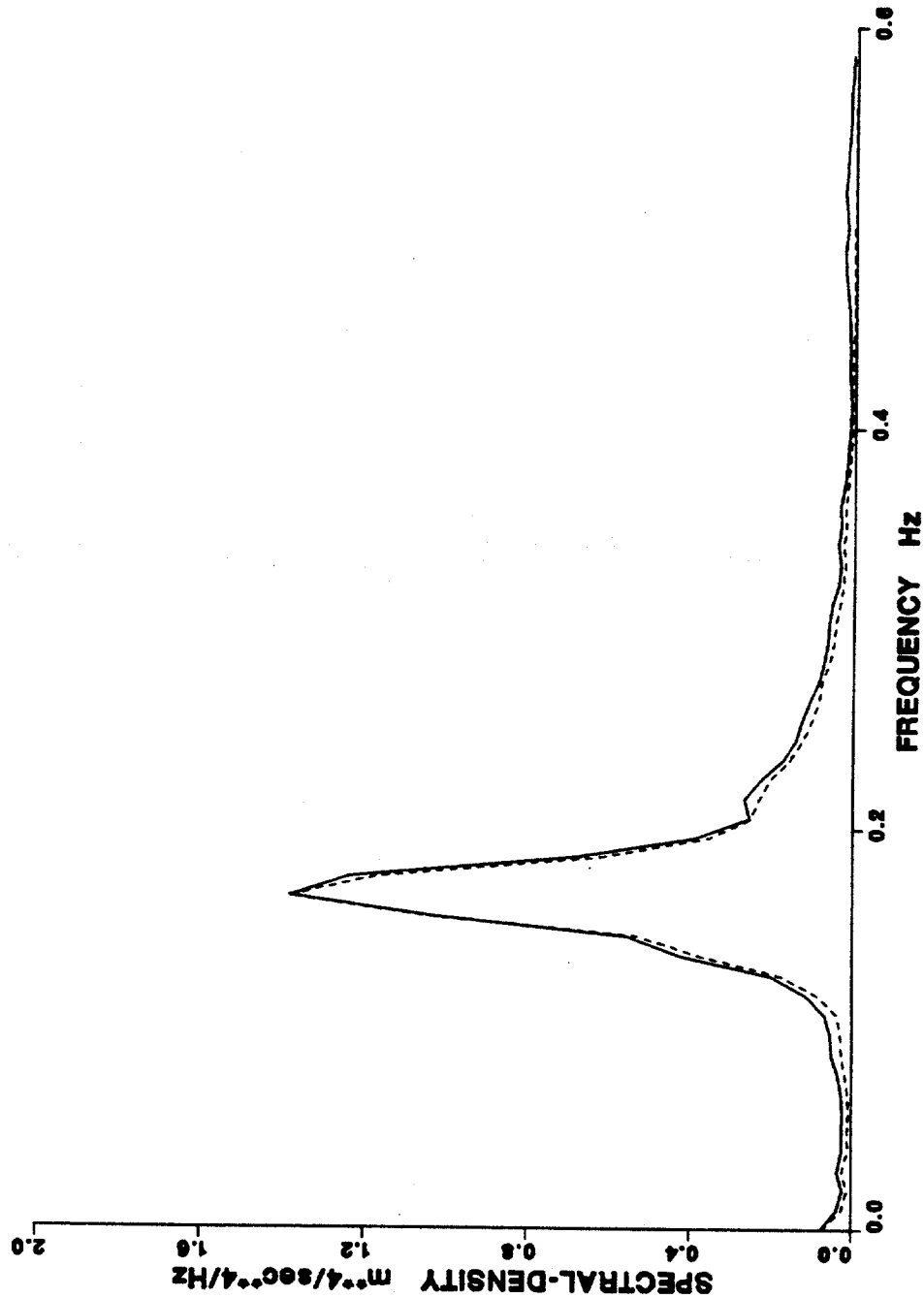

Figure 4.66. Comparison of nonlinear and linearized u|u|, upper level. [Linearized ——, nonlinear ---].

CHAPTER FIVE

DATA ANALYSIS AND ESTIMATION OF CORRECTION TERMS FOR THE PERIODIC FLOW

This chapter deals with the analysis of the experimental data for the periodic flow described in Section 4.2 and the evaluation of the Lighthill and Sarpkaya correction terms (see sections 3.4 and 2.7, respectively) for these data.

5.1 Estimates of the Inertia and Drag Coefficients in the Morison Equation.

The Morison equation, as applied to periodic flows, uses horizontal flow velocities and accelerations at various elevations to calculate forces on vertical cylinders. The flow properties being used are obtained on the basis of assumed or measured properties of the flow. For example, the flow properties can be calculated from the measured or assumed wave amplitude and period using an appropriate wave theory (for example, linear or second order).

It is of interest to compare the estimated inertia and drag coefficients obtained by using measured flow properties or flow properties based on various models for the wave flow. In this section, inertia and drag coefficients are estimated that correspond to the measured in-line forces on the cylinder, and to the description of the wave properties based on:

1. Measured horizontal velocity and accelerations. The force has the expression:

$$F_1 = \rho \frac{\pi D^2}{4} Cm_1 \frac{\partial u_m}{\partial t} + \frac{\rho D}{2} Cd_1 |u_m| u_m$$

where u_m = total measured velocity.

2. Horizontal velocities and accelerations calculated using the linear wave theory, the flow properties being based on the measured wave amplitude and period. The force in this case has the expression

$$F_2 = \rho \frac{\pi D^2}{4} Cm_2 \frac{\partial u_1}{\partial t} + \frac{\rho D}{2} Cd_2 |u_1| u_1$$

where u_1 = the first order velocity calculated from linear wave theory. This model can be used in the design office.

3. Horizontal velocity and accelerations calculated using second order wave theory, the flow properties being again based on the measured wave amplitude and period. The expression for the force is

$$F_3 = \rho \frac{\pi D^2}{4} Cm_3 \left(\frac{\partial u_1}{\partial t} + \frac{\partial u_2}{\partial t}\right) + \frac{\rho D}{2} Cd_3 |u_1 + u_2| (u_1 + u_2)$$

where u_1 = first order velocity and u_2 = second order velocity, both are calculated using Stokes theory. This model can also be used in the design office. By comparing F_2 and F_3 it is possible to assess the effect of including second order terms.

4. Horizontal velocities and accelerations obtained from measured values of these quantities by assuming that third and higher order components are negligible, and that the first and second order

components can be obtained from the measured values by using equations 3.69 and 3.70. The expression for the force is

$$F_4 = \rho \frac{\pi D^2}{4} Cm_4 \frac{\partial u_{1m}}{\partial t} + \frac{\rho D}{2} Cd_4 \, |u_{1m}| \, u_{1m}$$

where u_{1m} = first order velocity calculated in accordance with equation 3.69. Note that u_{1m} and $\partial u_{1m}/\partial t$ are not true first order components, since by the manner of their calculation they include in fact contributions of higher order components. Nevertheless, this model is based on the measured value of the velocities, and is likely to be more realistic than the second model, which is based on theoretical rather than actual flow properties.

5. The velocity is equal to u_{1m} as defined above. However, the acceleration is assumed to be equal to the sum of the first order and the second order components. The expression for the force is

$$F_5 = \rho \frac{\pi D^2}{4} Cm_5 \left(\frac{\partial u_{1m}}{\partial t} + \frac{\partial u_{2m}}{\partial t}\right) + \frac{\rho D}{2} Cd_5 \, |u_{1m}| \, u_{1m}$$

where u_{2m} = second order velocity calculated in accordance with equation 3.70. Since the Lighthill correction consists of second order terms (see equation 3.55), it is deemed that the presence of the second order acceleration provides for a more consistent formulation of the force to a second order approximation.

Least squares analyses were performed to obtain the time invariant coefficients Cd_i and Cm_i ($i = 1,2,..5$). Separate analyses were performed as follows:

(a) For each of the seven individual waves in each run. All five models were evaluated.

(b) For the whole run. Only the first model was evaluated. Justification for this will be presented later.

For the first model figures 5.1 to 5.3 plot the drag coefficients for each individual wave, showing their variation with Keulegan-Carpenter number (KC), Reynolds number (Re) and the frequency parameter (β), respectively. The drag coefficients show a large variability at low KC. This may be expected because the drag term is small relative to the inertia term and instabilities occur in its calculation. Note that above KC $\simeq$ 4 the drag term is more significant and shows little variation with increasing KC. It is noted that the dependence of the drag coefficient on KC is similar to that reported by Sarpkaya (1976a).

Figures 5.4 to 5.6 plot the inertia coefficients for each individual wave against KC, Re and β, respectively. It is seen in figure 5.4 that at low KC numbers the inertia coefficient is greater than the ideal potential flow value of 2.0. This is in agreement with results obtained by Chakrabarti (1976,1980), who also reported values of Cm significantly greater than 2.0. To some extent the results are also similar to those obtained by Keulegan and Carpenter (1958) and Sarpkaya (1976a,1976b,1976c). In the circular cylinder data obtained by Keulegan and Carpenter at low KC (KC < 4.5) all the estimated inertia coefficients had values greater than the ideal potential flow value of 2.0. Sarpkaya had few results in the low KC region, but for the flows where KC < 4.5 the inertia coefficients were greater than 2.0. Differences may be noted between the results obtained by Chakrabarti and from the NCEL tests on the one hand, and by Keulegan and Carpenter and by

Sarpkaya on the other. These may be explained by the fact that the flow in the NCEL and Chakrabarti's tests is two-dimensional under a changing free surface, whereas in the Keulegan and Carpenter and Sarpkaya tests the flow is one-dimensional.

The variation of Cd and Cm with Reynolds number has the same general trend as the variation with KC. Neither Cd or Cm varies greatly with the frequency parameter. It is noted that the range of Re and β numbers covered by this investigation is small.

Figures 5.7 and 5.8 plot, against the Keulegan-Carpenter number, the averages of the drag and inertia coefficients, respectively. These are defined as the averages of the coefficients of the seven individual waves of each run. The drag and inertia coefficients estimated from the total run are plotted in figures 5.9 and 5.10, respectively, against the Keulegan-Carpenter number for the total run. No significant difference is observed between the coefficients calculated from the total history and those calculated by averaging the individual wave results. Therefore, testing all five models on the total run is not necessary; averaging individual results provides a very good estimate of the results that would be obtained for the total run.

The second model is now discussed briefly. Figures 5.11 and 5.12 show the variation with KC number, of the drag and inertia coefficients, respectively. From figure 5.11 it can be seen that there is more scatter in the drag coefficients at low KC for the second model than for the first model (figure 5.1). Again, at higher KC numbers there is slightly more scatter but the difference is not significant. Figure 5.12 shows that, for low KC, the inertia

coefficients for the second model are closer to the ideal potential flow value of 2.0 than is the case for the first model (based on total measured flow properties). In general, inertia coefficients calculated using the second model are smaller and exhibit more scatter than those based on the total measured flow properties.

Figures 5.13 and 5.14 show the variation of the drag and inertia coefficients with KC, respectively, for the third model. When comparing figures 5.11 and 5.13 it can be seen that the addition of the second order term does not change the drag coefficient significantly over the range of KC considered. Also, when comparing figures 5.12 and 5.14 the same can be said for the inertia coefficients. The main noticeable difference between first and second order results occurs at higher KC numbers where the model including the second order properties exhibits slightly less scatter.

In figures 5.15 and 5.16 the variation of the drag and inertia coefficients with KC, respectively, is plotted for the fourth model. The results shown in figure 5.15 differ very little from the results for the first model (figure 5.1). Also there is little difference between the inertia coefficients based on the fourth model (figure 5.16) and those based on the first model (figure 5.4), the largest difference occurring at the higher KC numbers. It is seen from the comparison of the first and fourth models that the inclusion of the second order measured terms has a negligible effect on the drag and inertia coefficients. This was also observed in the comparison of the results for the second and third models.

However, the difference between the coefficients for the first and fourth models on the one hand, and the second and third models on the other, is quite significant. This difference may be explained by remembering that, as indicated previously, the fourth model is not a true first order model, that is u_{1m} and $\partial u_{1m}/\partial t$ each represent a sum of infinitely many harmonic components multiplied by a factor. Also, as stated in section 4.2, the second order components obtained by Fourier decomposition of the measured time histories were, especially at low KC numbers, significantly greater than the calculated second order components based on Stokes second order wave theory. Indeed it is noted in figure 5.12 (inertia coefficients for the second model), that at higher KC numbers the mean values do not differ significantly from the corresponding values in figure 5.16. However, at lower KC numbers the difference is quite significant. The same comment can be made when comparing the drag coefficients for the fourth model (figure 5.15) and the drag coefficients for the second model (figure 5.11). It is the difference between the measured and theoretical second order components, stated above, that leads to the discrepancy between the coefficients based on the measured flow properties and those based on the Stokes theory.

Figures 5.17 and 5.18 show the variation of the drag and inertia coefficients with KC, respectively, for the fifth model. A comparison of the drag coefficient based on the first model (figure 5.1), the fourth model (figure 5.15), and the fifth model (figure 5.17) shows that as the model flow properties approach the total measured properties the drag coefficient has less scatter at

higher KC numbers. The same pattern is seen for the inertia coefficients shown in figure 5.4 (based on the first model), figure 5.16 (based on fourth model) and figure 5.18 (based on fifth model).

From the analysis of the five different models a few observations can be made:

1) The use of second order velocity and acceleration terms or approximations thereof in the Morison equation does not alter the drag and inertia coefficients significantly.

2) The inertia and drag coefficients calculated by averaging the individual wave results are good estimates of the coefficients for the whole run. Therefore, each model did not need to be evaluated for the whole run.

3) The inertia coefficients based on the measured flow properties are greater than the ideal potential flow value of 2.0 and are greater than the values predicted by Sarpkaya (1986) and Bearman et al. (1985). This will be discussed in more detail in the following section.

5.2 Theoretical Analysis of the Force Coefficients

The Stokes theory reviewed in Section 2.3.3 predicts values of $Cm > 2.0$ for flows with low Keulegan-Carpenter numbers. If that theory were applicable to the NCEL flows with low KC numbers then it could be expected that, for these flows, the Cm and Cd values obtained by using the Morison equation would be identical or close to the values obtained using equations 2.12 and 2.13.

Calculations were conducted to ascertain whether this is so. It was found that for all low KC flows the inertia coefficients were at least 10% greater than the value yielded by equation 2.12. For example, for β = 40163 and KC = 1.049 equations 2.12 and 2.13 yielded Cm = 2.011 and Cd = 0.125. The values calculated from the measured flow properties were Cm = 2.34 and Cd = 0.163. For β = 17372 and KC = 1.83 equations 2.12 and 2.13 yielded Cm = 2.017 and Cd = 0.109. The values based on the measured data were Cm = 2.253 and Cd = 1.006. It is therefore concluded that equation 2.12 is not an acceptable model for the inertia coefficients in the case of the NCEL low KC flows. A similar statement cannot be made confidently for equation 2.13 which yields the drag coefficient, owing to the instabilities that occur when estimating Cd by the least squares method for the NCEL data at low KC numbers.

Equations 2.12 and 2.13 were derived under the assumption that fluctuating flow velocities are very small, so that it is allowable to neglect the terms which involve the square of the velocity [Stokes (1850), p. 12]. The equations were rederived in Bearman et al. (1985) again on the basis of the assumption that the boundary layer equations (derived from the Navier-Stokes equations) may be linearized. In light of the discrepancies between the results obtained from the tests and those based on equations 2.12 and 2.13 it is in order to verify the extent to which the linearization is acceptable for low Keulegan-Carpenter number wave flows. In Lin (1957) it is suggested that linearization is acceptable for oscillatory flows with frequencies of, say, 5000 Hz. In the case

of the NCEL data, however, the frequencies are of the order of 0.5 Hz. We now show that for the NCEL data, and possibly for other data to which an attempt to apply Stokes theory was reported [Bearman et al. (1985), Sarpkaya (1986)], the nonlinear terms neglected in Stokes theory are relatively large compared to the linear and viscous terms rather than being negligible.

Assume, for the order of magnitude analysis in the boundary layer equation, that the mean flow is zero, that is, the flow comprises only the oscillatory components in equations 2.14a to 2.14d. Assume also that the oscillatory component is equal to that obtained from linear wave theory. In order to have a useful comparison of terms all velocities are nondimensionalized by the free stream velocity, U_0, all linear dimensions are nondimensionalized by the cylinder diameter, D, and time is nondimensionalized by D/U_0. The nondimensionalized velocities U and u are then both of order 1. The ratio of the boundary layer thickness to the cylinder diameter is denoted by δ. As noted by Schlichting (1960), in the boundary layer v is of the order δ, and since the component of velocity parallel to the wall increases from zero at the wall to the value 1 in the free flow, across the boundary layer we get

$$\frac{\partial u}{\partial y} \approx \frac{1}{\delta}, \text{ and } \frac{\partial^2 u}{\partial y^2} \approx \frac{1}{\delta^2} \text{ whereas } \frac{\partial v}{\partial y} \approx \frac{\delta}{\delta} = 1$$

Equation 2.15 then becomes

$$\frac{\partial u_1}{\partial t} + u_1 \frac{\partial u_1}{\partial x} + v_1 \frac{\partial u_1}{\partial y} +$$

$$\omega D/U_0 \quad 1 \quad k\,D \quad \delta \quad 1/\delta$$

$$\overline{u_1 \frac{\partial u_1}{\partial x}} + \overline{v_1 \frac{\partial u_1}{\partial y}} =$$

$$1 \quad k\,D \qquad \delta \quad 1/\delta$$

$$\frac{\partial U_1}{\partial t} + U_1 \frac{\partial U_1}{\partial x} - \overline{U_1 \frac{\partial U_1}{\partial x}} + \nu \frac{\partial^2 u_1}{\partial y^2}$$

$$\omega\,D/U_0 \quad 1 \quad k\,D \quad 1 \quad k\,D \quad (1/R_e)\ 1/\delta^2$$

The orders of magnitude are shown in the version of equation 2.15 given above under each individual term; ω = circular frequency of the circular flow, k = wavenumber of the flow, and R_e = Reynolds number. Definitions of u_1, v_1 and U_1 can be found in section 2.3.3. The orders of magnitude shown are valid if, as stated previously, the flow is approximately described by linear wave theory. In most wave tank tests and in the ocean environment the circular frequency is of the order 0 to 5. The corresponding value of the wavenumber can be obtained from the dispersion relation (equation 3.23) and gives $k \simeq 0$ to 2.5. From Schlichting the nondimensionalized boundary layer thickness is of the order $(1/R_e)^{1/2}$, therefore, it can be seen in the comparison above, that all terms are of the same order of magnitude. This simple analysis shows that the nonlinear terms cannot be considered insignificant.

Research appears to be in order on the extent to which the nonlinear terms neglected in Stokes and Bearman et al. might be capable of explaining the large values of Cm, as well as the values of Cd, corresponding to low KC flows of interest in ocean engineering.

5.3 Calculation of Forces Using the Morison Equation

The force time histories based on the Morison equation with time invariant coefficients were calculated for both the full time history and each individual wave of the full record. Figures 5.19 to 5.22 show measured and calculated full force time histories for the lowest KC (KC = 0.32), as well as for KC = 4.41, KC = 10.26 and the highest KC (KC = 15.31). The dominant harmonic of the residue for all the force histories appears to be close to the second harmonic of the force. It is noted that the Lighthill correction term which is a second order term also has frequencies equal to twice the fundamental frequency. On the other hand the Sarpkaya residue terms described in section 2.7 have frequencies equal to odd multiples of the fundamental frequency.

Results corresponding to typical individual waves from each of the runs plotted in figures 5.19 to 5.22 are given in figures 5.23 to 5.26. These individual waves were typical of all the individual wave results and it was found that for all waves the dominant harmonic of the residue appears to be close to the second harmonic of the force (see residue curve in figures 5.23 to 5.26). Figure 5.27 shows the root mean square error, normalized by the maximum force for the individual wave, versus the Keulegan-Carpenter number for each of the individual waves. The results are based on time invariant drag and inertia coefficients and the total measured flow properties. The normalized error is relatively constant for the range of KC considered, that is for these data the Morison equation fits the data well in the inertia dominated and drag-inertia regimes. No comment can be made on the drag dominated

regime because the KC numbers for these tests do not fall in the normally accepted drag dominated regime (that is, KC > 20, see section 2.3.1). It should be noted, in figure 5.27, that six points at KC ≃ 12 to 14 are significantly different from the rest of the data points in the same region. This run (NCEL16) was found to give unrealistic results including the results concerning inertia coefficients, see, for example, figures 5.4, 5.8, 5.10. The reason for the deviation is not understood and might be attributed to experimental factors.

5.4 Force Coefficients and the Lighthill Correction Term

This section deals with the Lighthill correction term, its effect on the force coefficients, Cd and Cm, and the effect the Lighthill correction has on reducing the error between the measured and calculated forces.

Three different force models were tested to determine which would give the best fit of the calculated forces to the measured forces for the individual waves. Only the first two models were tested on the total time histories. The force models were:

(1) The Morison equation with the Lighthill correction, using the total measured flow properties. The drag and inertia coefficients are based on the Morison equation only.

(2) The Morison equation with the Lighthill correction, using the total measured flow properties. The drag and inertia coefficients are based on the Morison equation with the Lighthill correction.

(3) A true second order analysis, that is, only using terms up to and including second order. That is, $\partial u/\partial t = \partial u_1/\partial t + \partial u_2/\partial t$; and

$u\,|u| = u_1\,|u_1|$. The components u_1 and u_2 are based on the measured flow properties (section 3.5). The drag and inertia coefficients are based on the Morison equation with the Lighthill correction.

The results for the entire time histories will be discussed first. Figures 5.28 to 5.31 plot the total calculated forces using the first model (that is, based on the Morison equation with the Lighthill correction) and the measured forces for the same KC values given in figures 5.19 to 5.22. Comparing figures 5.19 to 5.22 with figures 5.28 to 5.31 it can be observed that there is a minimal difference between the residues (difference between the calculated and measured forces) calculated using the Morison equation on the one hand, and the residues calculated using the Morison with the Lighthill correction on the other. This is more apparent in figure 5.32, which plots the rms error for the forces calculated using the Morison equation with the Lighthill correction versus the rms error for the forces calculated from the Morison equation (without correction). It can be seen that there is very little deviation from the line of equal error, indicating that the Lighthill correction is insignificant for this set of data.

The second series of plots are again for the the entire time histories (figures 5.33 to 5.36) and show the measured and calculated forces based on the second model above. When figures 5.33 to 5.36 are compared to figures 5.19 to 5.22 or figures 5.28 to 5.31, it can be seen that again the difference between the residues is minimal. This can be seen more clearly in figure 5.37 where the rms errors for the Morison equation are compared with

those for the second model given above. The force coefficients based on the Morison equation with the Lighthill correction are therefore not significantly different from those calculated using just the Morison equation. This can be seen more clearly in figures 5.38 and 5.39 where the drag and inertia coefficients, respectively, are shown for the individual wave results. These two figures plot the force coefficients based on the second model, with the force coefficients based on the Morison equation superimposed. It can be seen that there is very little difference in the drag coefficients over the whole range of KC numbers considered. For the inertia coefficients the largest error, although still small occurs at the higher KC numbers. Hence, it can be concluded that for the NCEL data the addition of the Lighthill correction does not decrease the drag coefficient significantly.

Results of the analysis of the force time histories for individual waves with the Lighthill correction are now discussed. Figures 5.40 to 5.51 show the measured and calculated forces for the three models described at the beginning of the section. The same individual waves as used in the previous section are analysed. From all the figures it can be seen that the addition of the Lighthill correction does not change the total forces significantly. It can be noted that at low KC numbers the results based on a true second order analysis (model 3) are not significantly different from the results based on the total measured flow properties (model 1 and model 2). This could be expected since at low KC numbers the second order components are much smaller than the first order components. The Lighthill

correction becomes larger with increasing KC numbers though it is still negligible for practical purposes.

An overall assessment of the three models can be made by comparing the rms error for each model against the rms error for the Morison equation. Figure 5.52 plots the rms error for each individual wave of the NCEL record for the first model against the rms error for the Morison equation. It is seen that the Lighthill correction does not improve on the Morison equation; in fact in most cases the Morison equation without correction provides a better fit to the measured forces. Figures 5.53 and 5.54 plot the rms errors for the second and third models respectively, against the rms error for the Morison equation. Again these figures show that the effect of the Lighthill correction is negligible.

Calculations were also performed to examine the effect of the Lighthill correction on the drag and inertia coefficients using different models for the flow parameters. The calculations showed that this effect was negligible in all cases. Thus the addition of the Lighthill correction did not improve the Morison equation for the range of KC and Re numbers covered by the NCEL tests. Also, the addition of the Lighthill correction term did not alter the drag coefficient to any significant extent. Both conclusions are at variance with those suggested in Lighthill's 1979 BOSS keynote address.

5.5 Sarpkaya's Correction Term

The NCEL data was also analyzed according to the procedure adopted by Sarpkaya (1981a, 1981b), in which the total force was

divided into a drag force, inertia force and a residual force. For data obtained in one-dimensional flow Sarpkaya found from a Fourier analysis of the force residue ($F_{measured} - F_{Morison}$) that the third and fifth harmonics were dominant. The analysis for the NCEL data which corresponds to a two-dimensional flow showed that the second and third harmonics were generally dominant. It was seen in Section 3.7 that if instead of a harmonic wave there are higher frequency components, then the residue comprises all harmonics and not just the odd ones as derived by Keulegan and Carpenter (1958) and Sarpkaya (1981a, 1981b). From the previous section outlining the results of the Lighthill analysis it was seen that the force residues are not accounted for by the Lighthill correction. Therefore, an approach similar to the one proposed by Sarpkaya was used to see whether this would provide a better fit to the measured force data.

Typical results for the Fourier components of the residue for different KC values are given in Tables 5.1 to 5.5. Tables 5.1 to 5.5 give results for waves with a KC = 0.39 (inertia dominated), KC = 2.36 (inertia dominated), KC = 6.24 (inertia/drag-inertia transition), KC = 10.12 (drag-inertia regime), and KC = 14.93 (drag-inertia regime), respectively. Although all harmonics from one through ten are present the second and third are dominant.

Sarpkaya formulated his residue in terms of a constant, Λ, which is the ratio of the deviation of the maximum inertial force from its ideal value to the maximum drag force. In Sarpkaya's data the value attained a maximum at about KC = 12.5. Figure 5.55 plots Λ against the KC number for the NCEL data. The scatter in Λ for

low KC can be attributed to the uncertainty in the drag coefficient at low KC. The value of Λ is constant for all KC values greater than approximately 8.0 and does not have the variability between KC = 6 and KC = 20 that was observed in the Sarpkaya results.

Two residue models were tested: 1) same model as Sarpkaya (that is, residue comprising third and fifth harmonics see equation 2.54), and 2) based on the results obtained from the Fourier analysis of the force residues of the NCEL data. For this data the residues second and third harmonics were dominant. Coefficients were averaged over the seven individual waves from each run.

Figures 5.56 to 5.61 show the variation of each of the six coefficients (Cd, Cm, C_3, Φ_3, C_5, Φ_5 see equation 2.54) with KC number for the first model. Comparing figure 5.56 to figure 5.7 (average drag coefficient calculated using the Morison equation) and figure 5.61 to figure 5.8 (average inertia coefficient calculated using the Morison equation) it can be seen that inclusion of the Sarpkaya correction does not alter the drag or the inertia coefficients significantly. The coefficient C_3 (figure 5.58) does show significant variability for KC > 5, and the results are not as well behaved as those obtained by Sarpkaya (see figure 2.10). The other three coefficients showed even more variability with KC and none of the coefficients followed the pattern obtained by Sarpkaya (which is similar to that of figure 2.10).

Figures 5.62 to 5.67 give the variation of the six coefficients (Cd, Cm, C_2, Φ_2, C_3, Φ_3) with KC for the second model. As with the first Sarpkaya model, the addition of the two correction terms does not alter the magnitude of the drag and

inertia coefficients significantly. This can be seen by comparing the drag coefficients in figures 5.62 and 5.7 (coefficients based on the Morison equation) and the inertia coefficients in figures 5.67 and 5.8 (based on the Morison equation). Also the coefficients in the correction terms (C_2, Φ_2, C_3, Φ_3) showed more variability with KC number than would be expected if the Sarpkaya residue model were valid.

Figure 5.68 compares the root mean square error values for the two different models. From this figure it can be seen that in all cases the rms error for the first model is greater than the rms error for the second model. In figures 5.69 and 5.70 the rms errors for the two models are compared with the rms error for the Morison equation. The second model leads to a significant reduction in the error and the first model gives results that are not significantly different from the Morison equation results, that is the second model is significantly better than the Morison equation. Note that all of the coefficients were obtained by least squares curve fitting. These values are only applicable to the present set of data, and the results should not be generalized to other types of flow.

From the analysis of the Sarpkaya correction terms a few observations can be made:

1. The force coefficients Cd and Cm do not vary significantly with the model chosen.

2. There is no clear variation of the ratio Λ as shown in the results obtained by Sarpkaya for $6 < KC < 20$.

3. The residue coefficients do not have the consistency of the values obtained by Sarpkaya, and there is no distinct maximum at KC = 12.5, as observed in Sarpkaya's and Keulegan and Carpenter's results.

4. The universal constants and the Sarpkaya distribution (see Sarpkaya (1981a), equation 66) relating the coefficients to the KC number are not valid for the NCEL wave data. This is attributed to the fact that, unlike the experimental flows analyzed by Sarpkaya, which are one-dimensional, the NCEL flows are two-dimensional wave flows under a changing free surface.

N	A(N)	B(N)	C(N)	PHASE
1	-0.897	-0.165	0.912	1.389
2	-1.528	-1.658	2.255	0.745
3	0.924	0.342	0.985	1.216
4	0.305	0.129	0.331	1.172
5	0.234	0.066	0.243	1.296
6	0.185	0.037	0.189	1.375
7	0.149	0.027	0.151	1.388
8	0.123	0.026	0.125	1.363
9	0.108	0.023	0.111	1.360
10	0.098	0.019	0.100	1.373

Table 5.1. First ten Fourier components of the force residue, KC = 0.39.

N	A(N)	B(N)	C(N)	PHASE
1	-0.138	-0.088	0.164	1.000
2	-0.374	-1.344	1.395	0.272
3	0.159	0.574	0.596	0.271
4	0.053	0.162	0.170	0.319
5	0.044	0.110	0.119	0.380
6	0.038	0.061	0.072	0.559
7	0.032	0.034	0.046	0.758
8	0.025	0.028	0.037	0.734
9	0.021	0.026	0.033	0.674
10	0.019	0.021	0.028	0.758

Table 5.2. First ten Fourier components of the force residue, KC = 2.36.

N	A(N)	B(N)	C(N)	PHASE
1	0.077	0.167	0.184	0.432
2	-0.108	-0.876	0.882	0.123
3	0.238	-0.323	0.402	-0.635
4	0.161	-0.068	0.175	-1.169
5	0.113	0.088	0.143	0.911
6	0.068	0.054	0.087	0.906
7	0.047	0.004	0.047	1.485
8	0.044	0.002	0.044	1.523
9	0.045	0.017	0.048	1.198
10	0.038	0.018	0.042	1.132

Table 5.3 First ten Fourier components of the force residue, KC = 6.24.

N	A(N)	B(N)	C(N)	PHASE
1	-0.310	0.431	0.530	-0.623
2	0.669	-0.617	0.910	-0.826
3	-0.395	-0.710	0.813	0.508
4	-0.139	-0.336	0.364	0.392
5	-0.086	0.006	0.086	-1.503
6	-0.056	0.052	0.076	-0.826
7	-0.041	-0.009	0.042	1.358
8	-0.034	-0.031	0.046	0.841
9	-0.032	-0.011	0.034	1.252
10	-0.029	0.005	0.029	-1.390

Table 5.4. First ten Fourier components of the force residue, KC = 10.12.

N	A(N)	B(N)	C(N)	PHASE
1	0.297	1.464	1.494	0.199
2	-0.104	-3.052	3.054	0.034
3	0.002	-1.220	1.221	-0.002
4	0.080	-0.734	0.738	-0.108
5	0.091	-0.011	0.092	-1.429
6	0.052	0.142	0.151	0.348
7	0.028	0.024	0.037	0.857
8	0.024	-0.046	0.052	-0.476
9	0.030	-0.019	0.036	-0.989
10	0.032	0.019	0.037	1.013

Table 5.5. First ten Fourier components of the force residue, KC = 14.93.

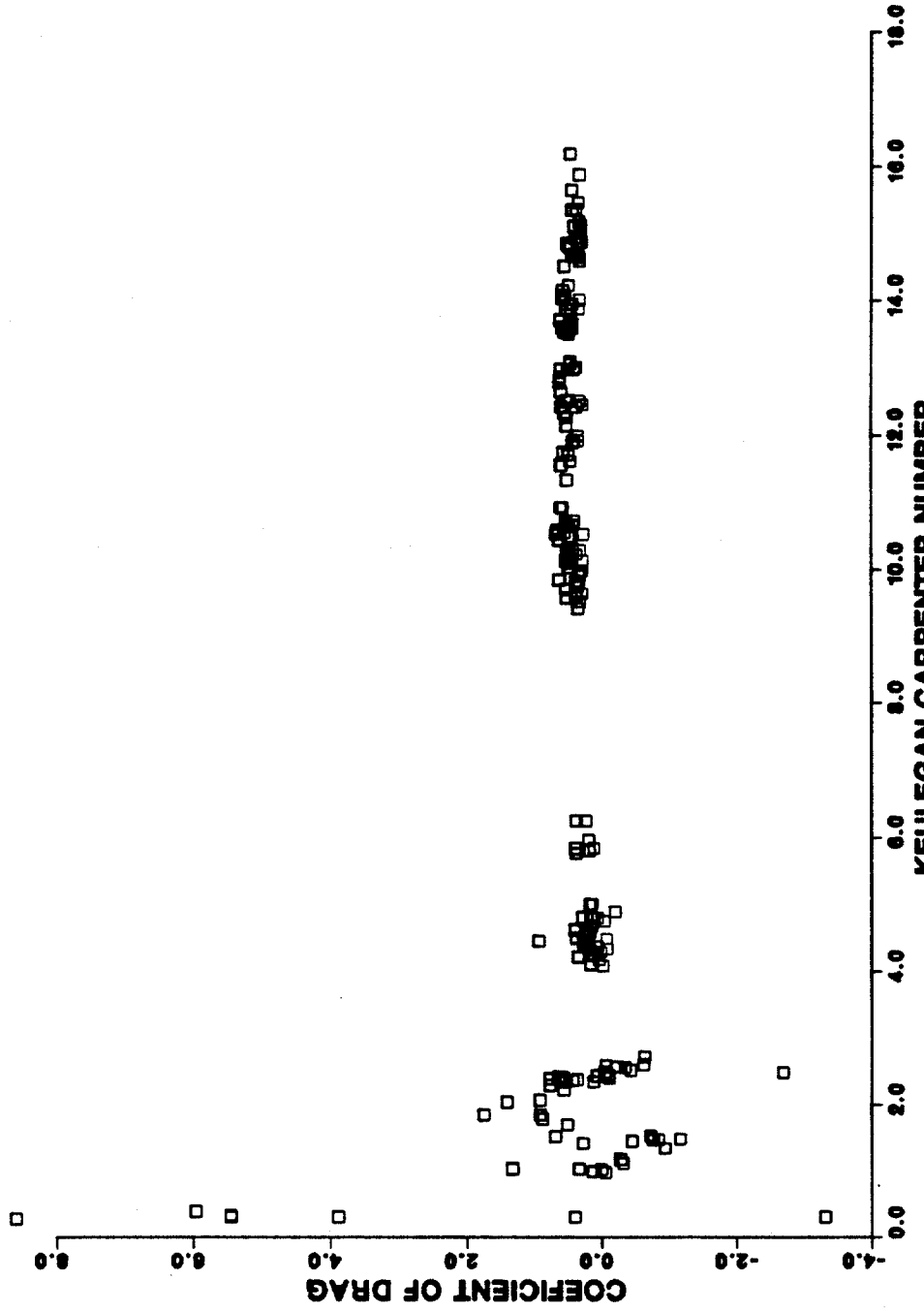

Figure 5.1. Coefficient of drag versus Keulegan-Carpenter number.

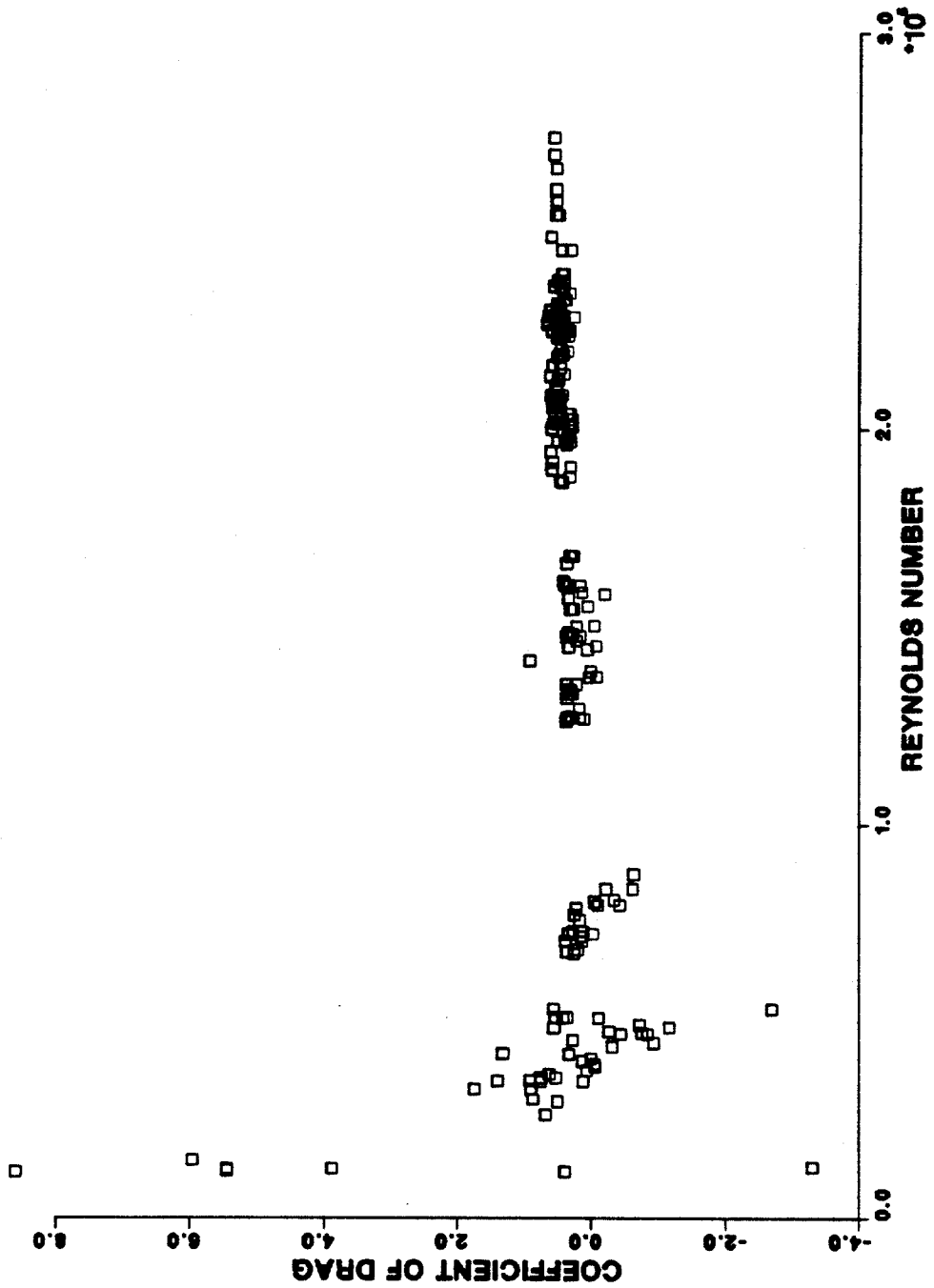

Figure 5.2. Coefficient of drag versus Reynolds number.

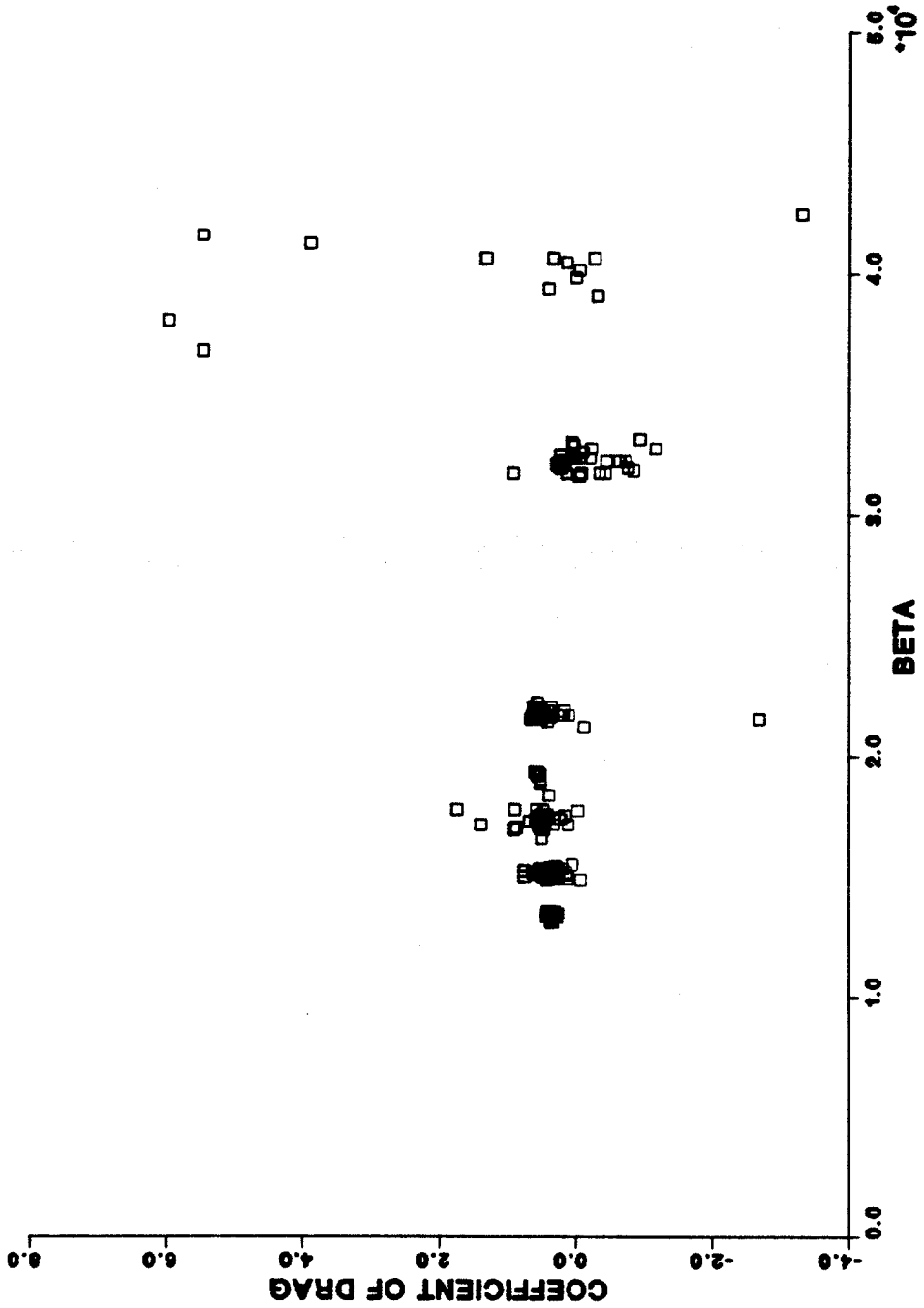

Figure 5.3. Coefficient of drag versus frequency parameter, β.

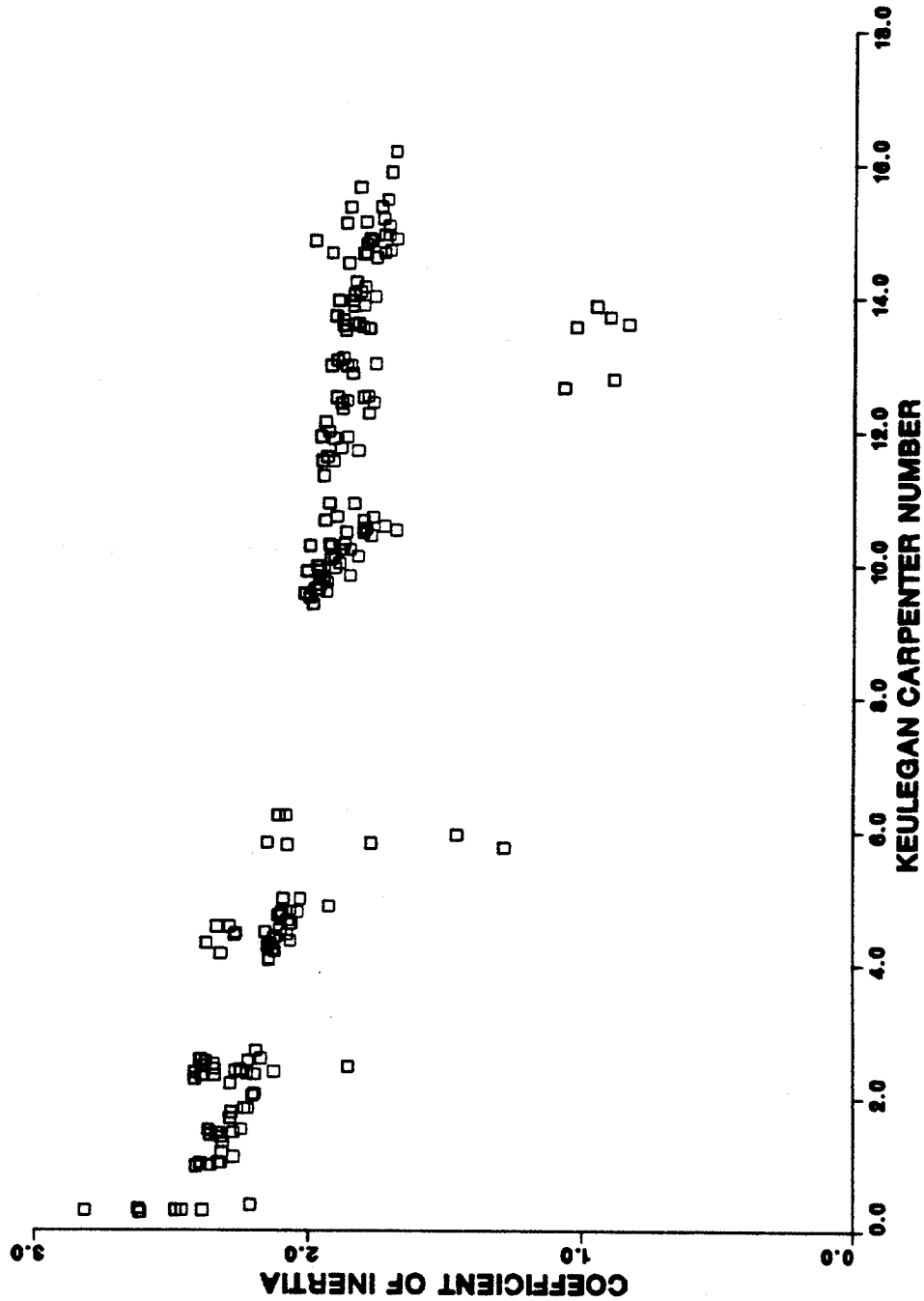

Figure 5.4. Coefficient of inertia versus Keulegan-Carpenter number.

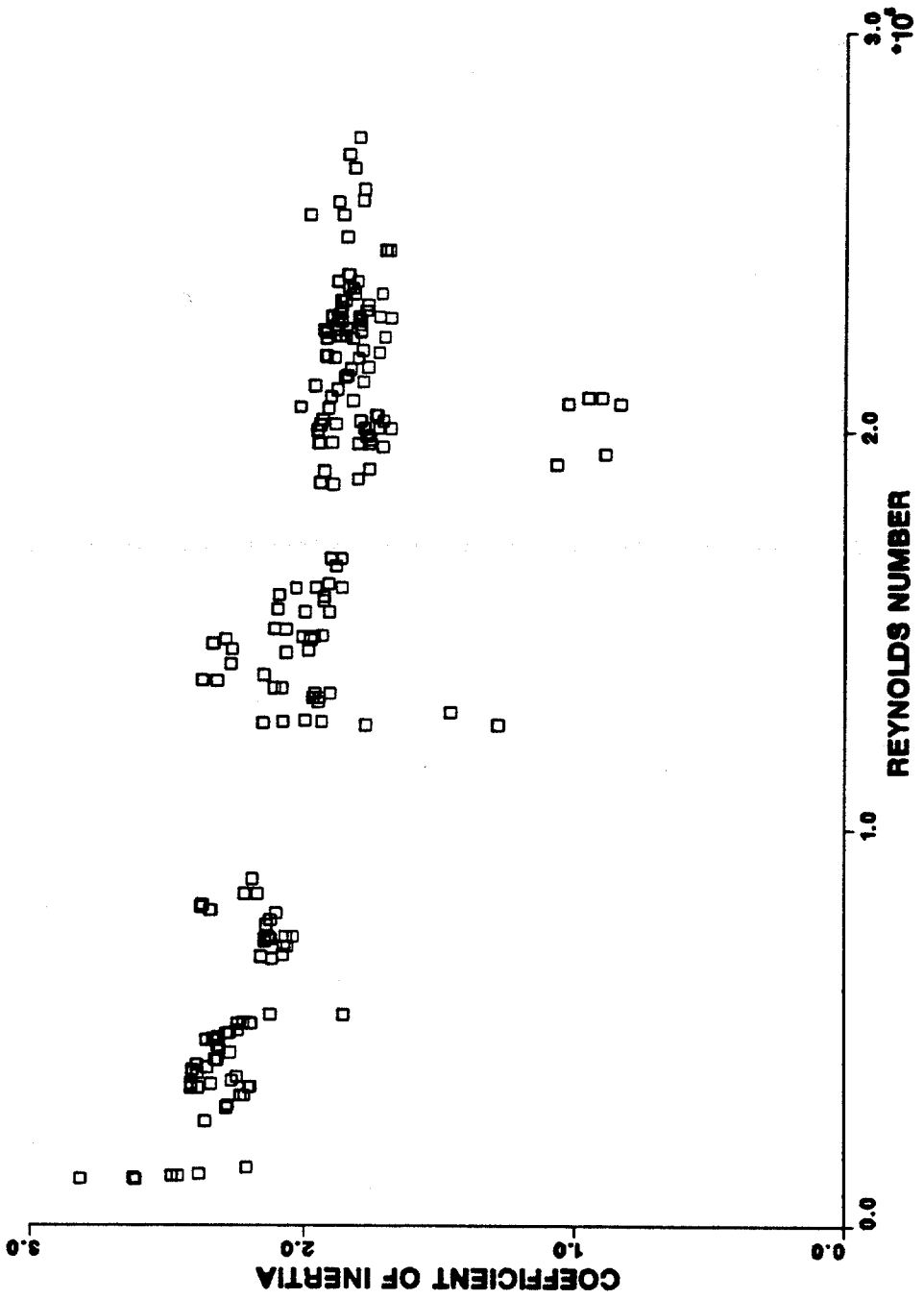

Figure 5.5. Coefficient of inertia versus Reynolds number.

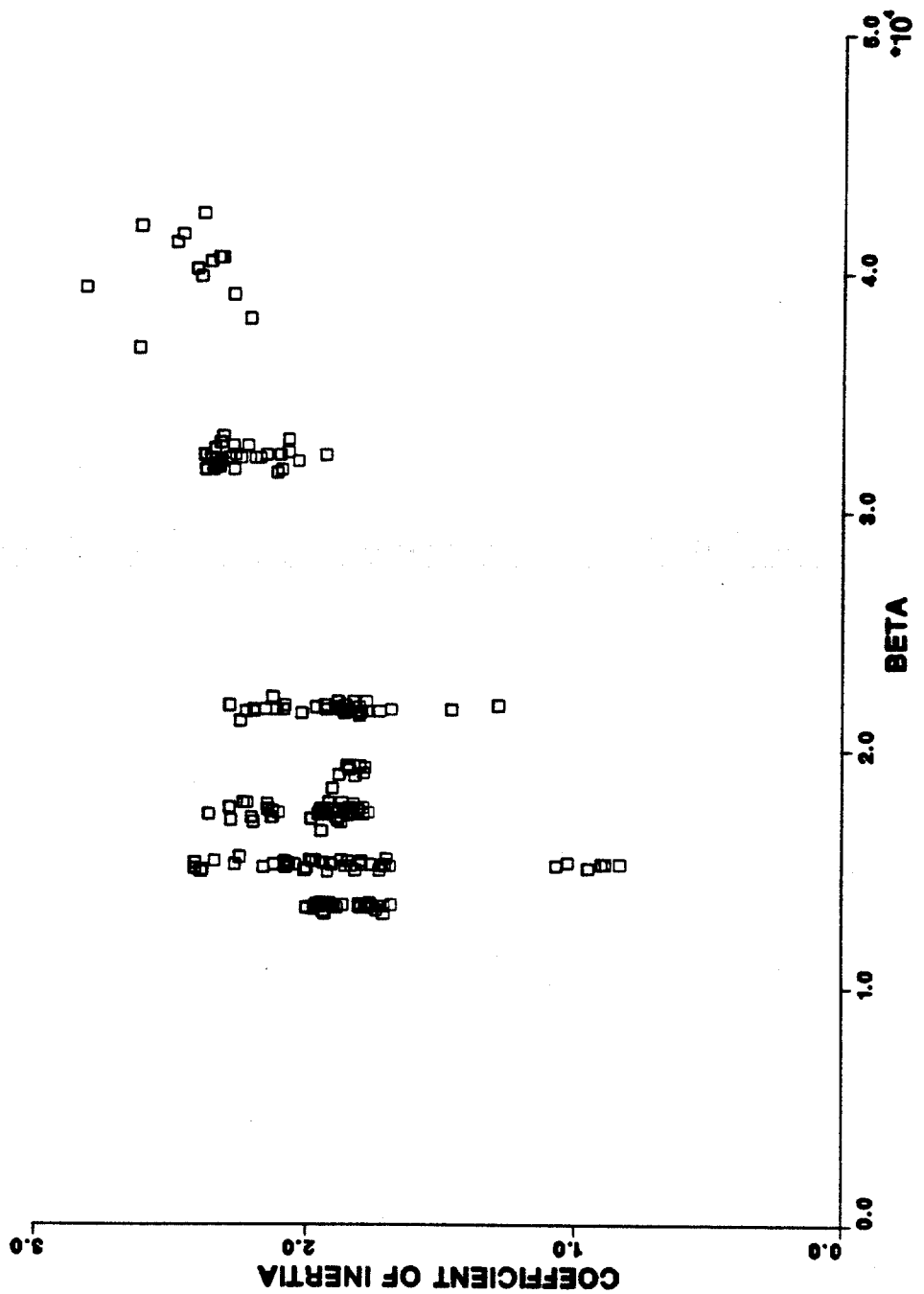

Figure 5.6. Coefficient of inertia versus frequency parameter, β.

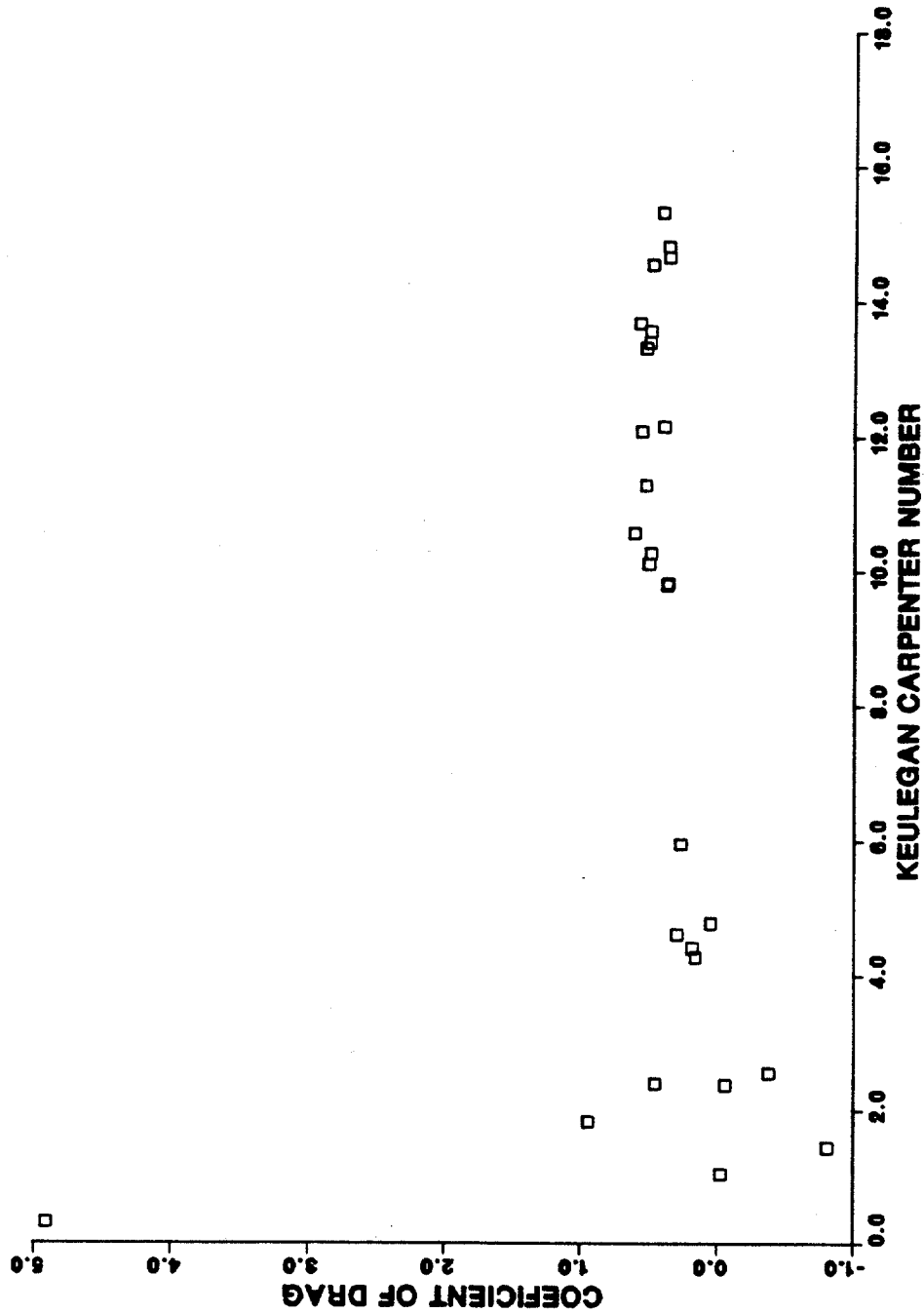

Figure 5.7. Coefficient of drag versus Keulegan-Carpenter number.
Average of individual results, model 1.

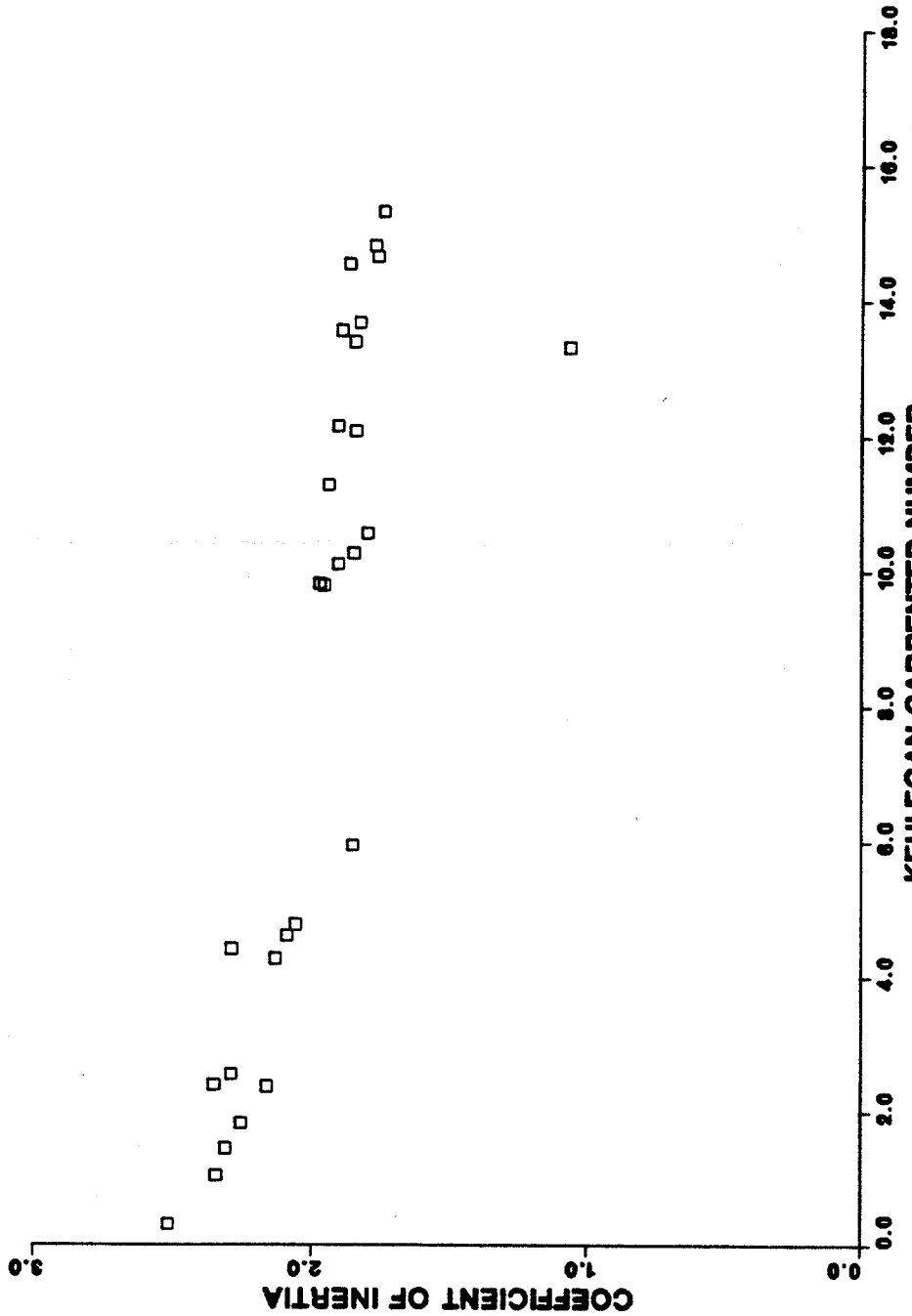

Figure 5.8. Coefficient of inertia versus Keulegan-Carpenter number.
Average of individual results, model 1.

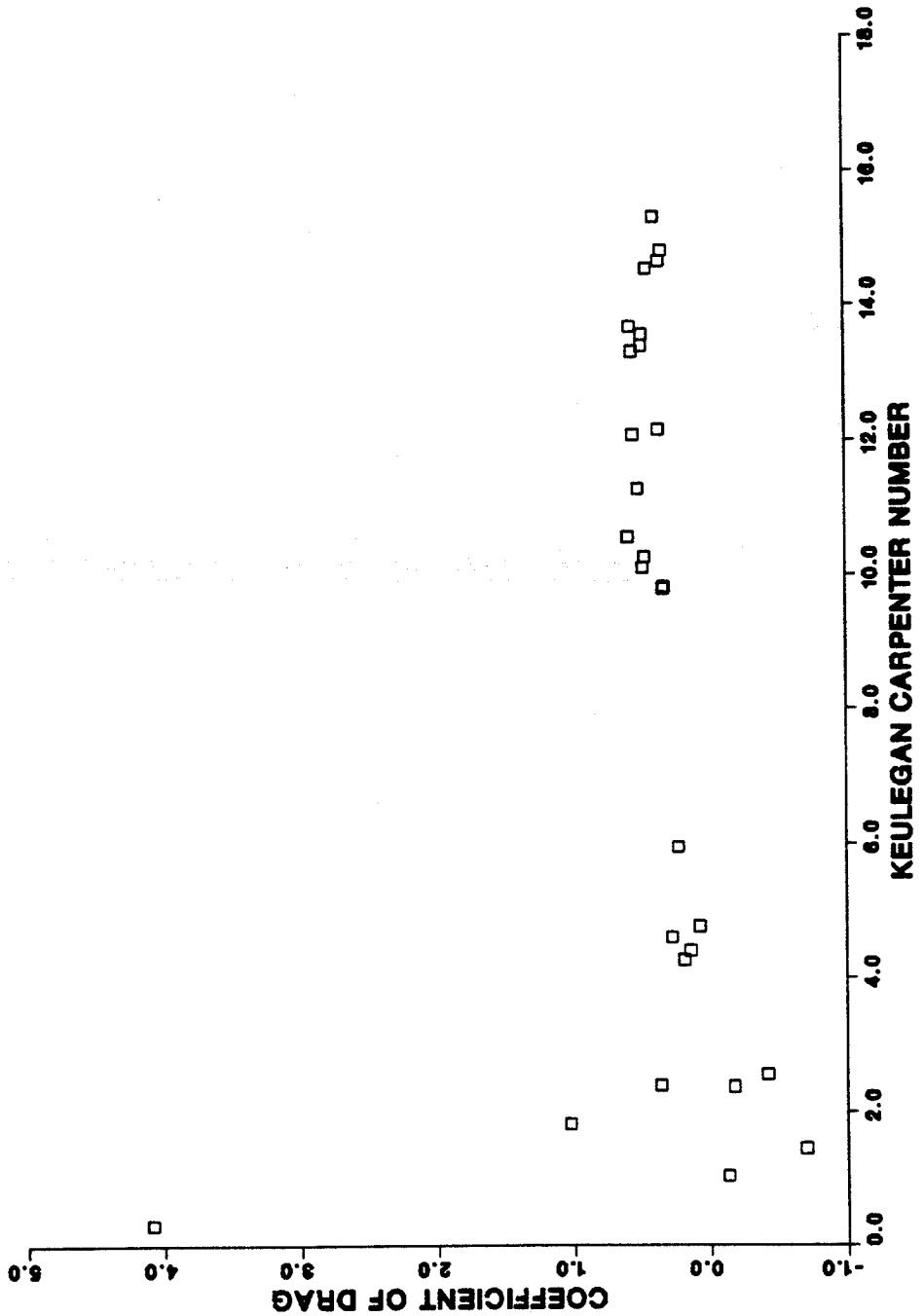

Figure 5.9. Coefficient of drag versus Keulegan-Carpenter number.
Total run results, model 1.

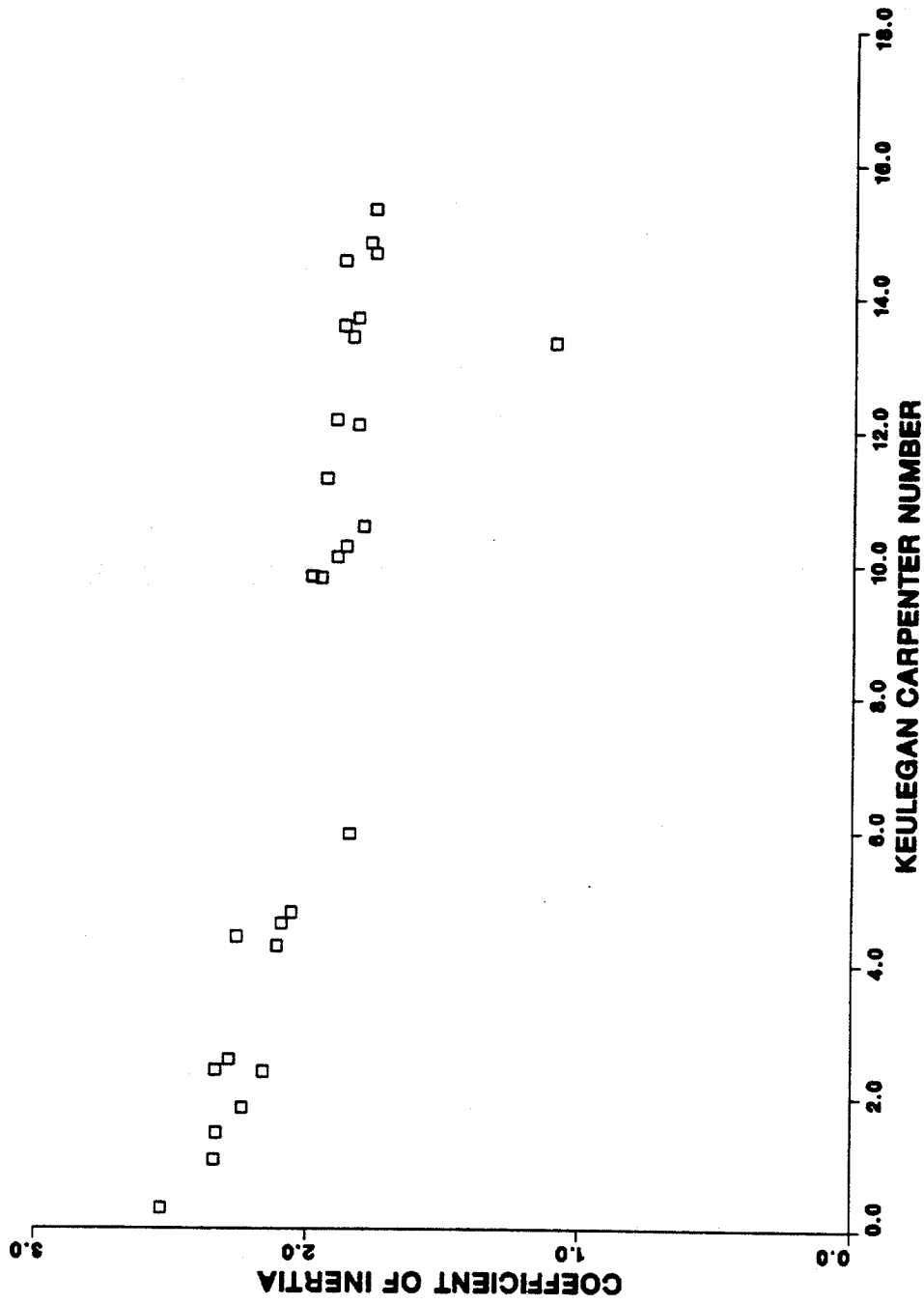

Figure 5.10. Coefficient of inertia versus Keulegan-Carpenter number.
Total run results, model 1.

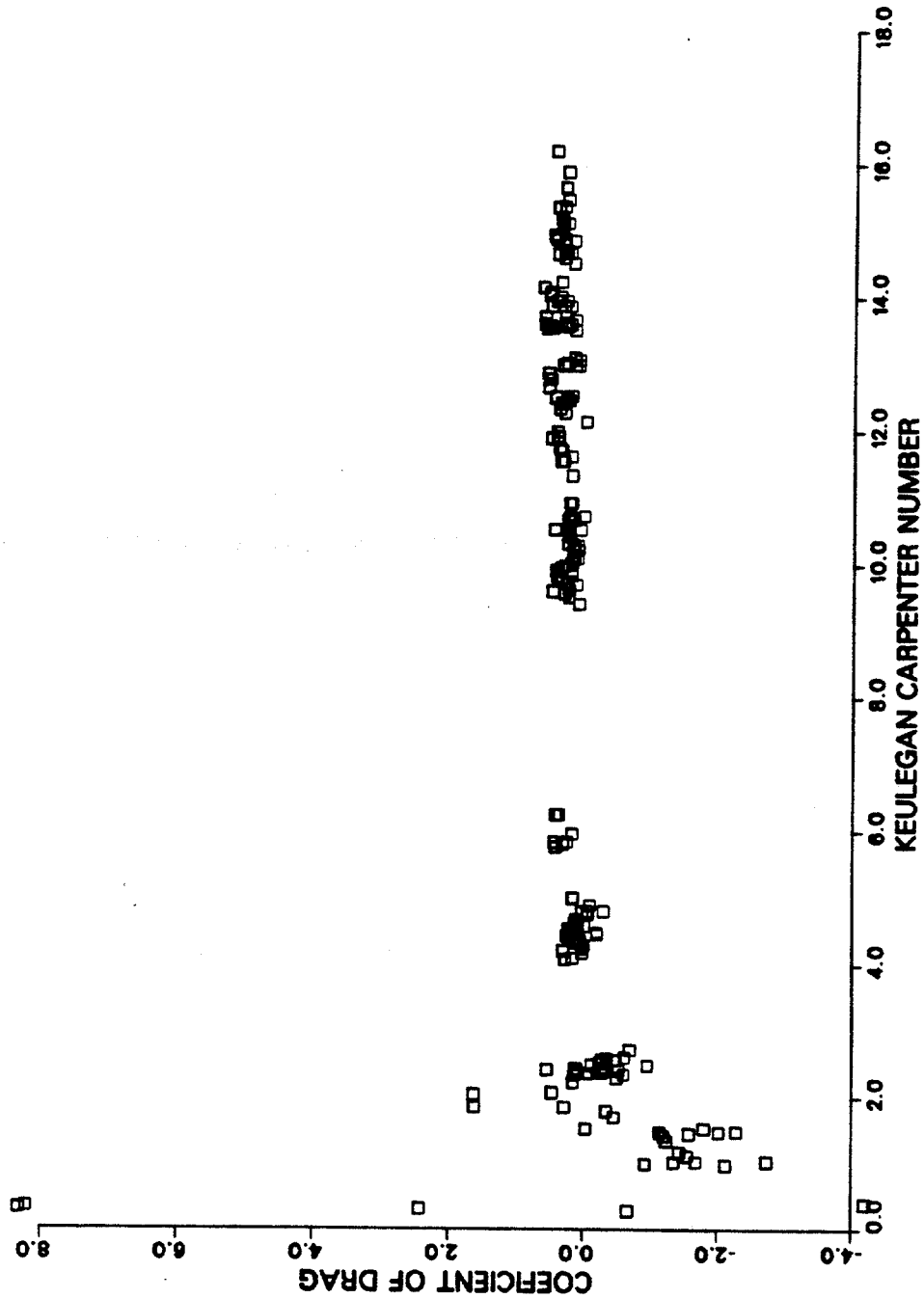

Figure 5.11. Coefficient of drag versus Keulegan-Carpenter number.
Individual wave results, model 2.

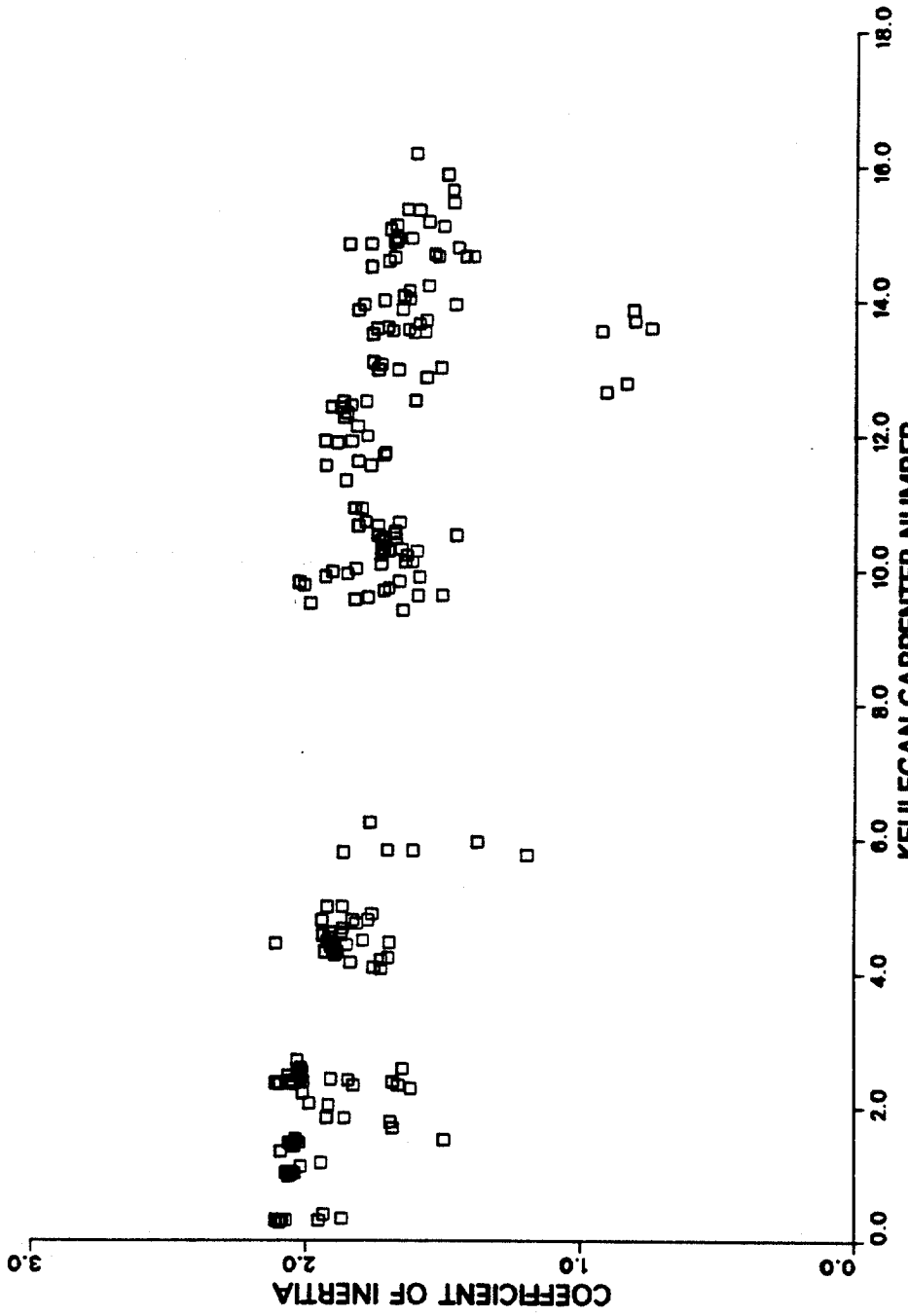

Figure 5.12. Coefficient of inertia versus Keulegan-Carpenter number. Individual wave results, model 2.

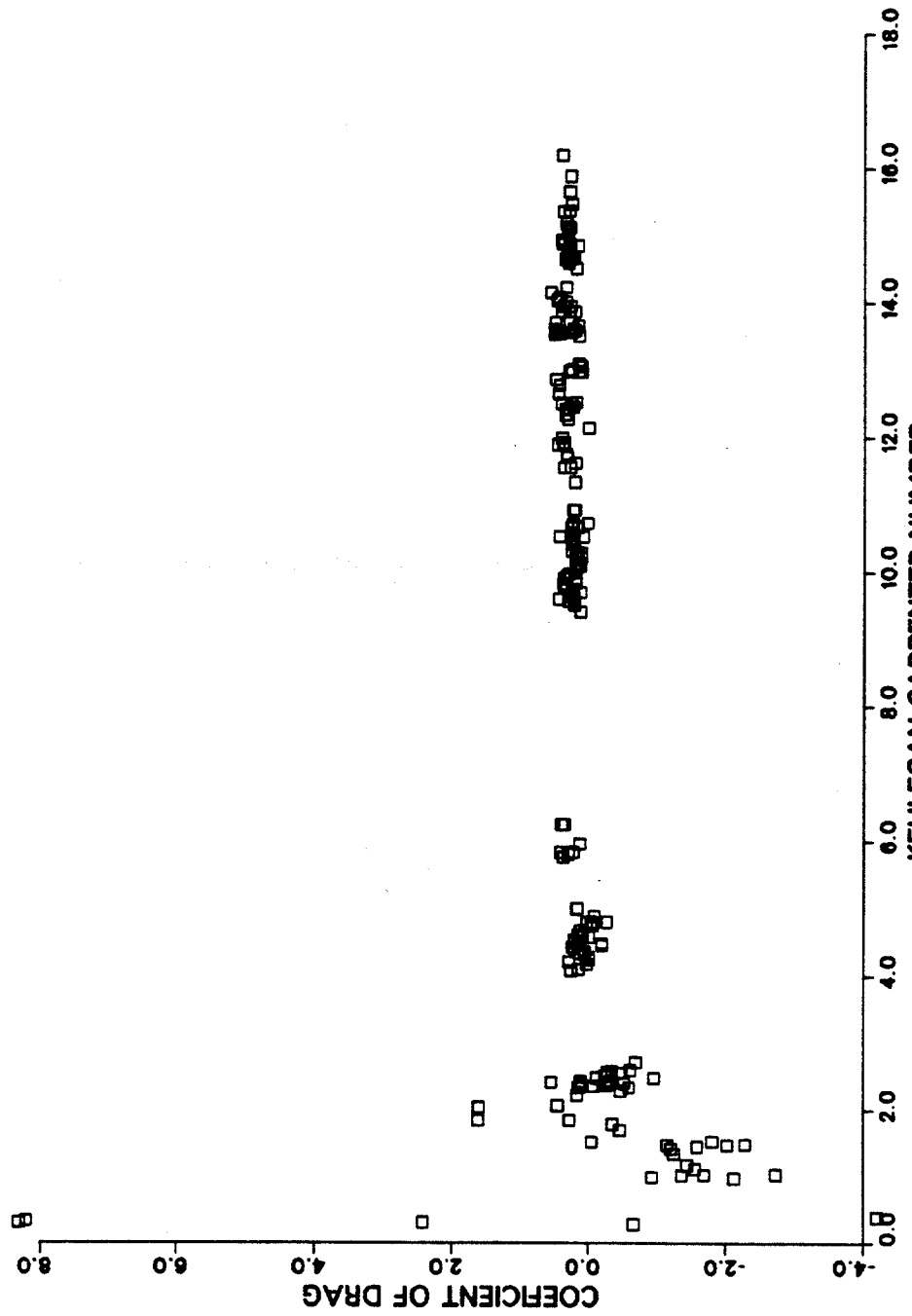

Figure 5.13. Coefficient of drag versus Keulegan-Carpenter number.
Individual wave results, model 3.

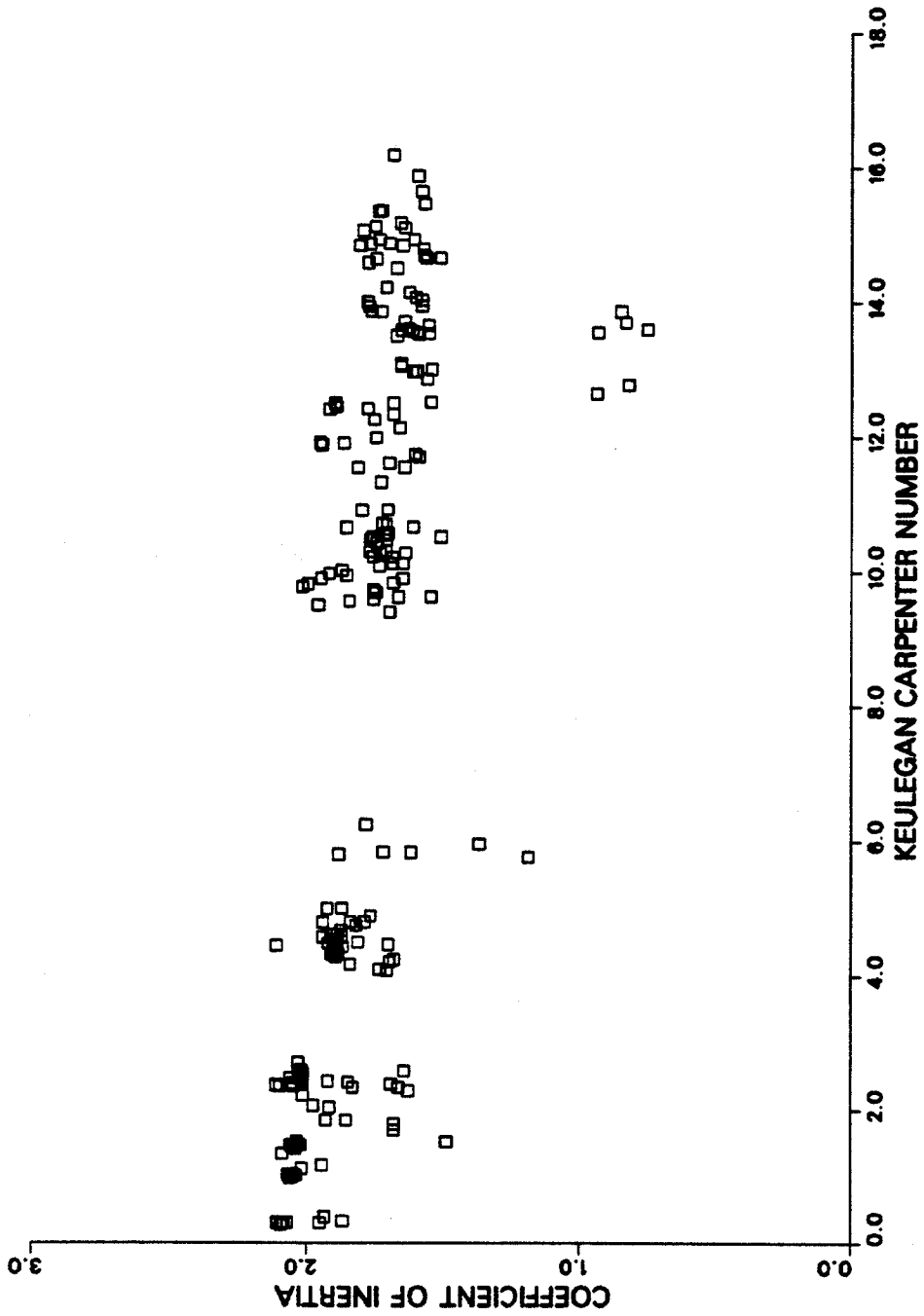

Figure 5.14. Coefficient of inertia versus Keulegan-Carpenter number. Individual wave results, model 3.

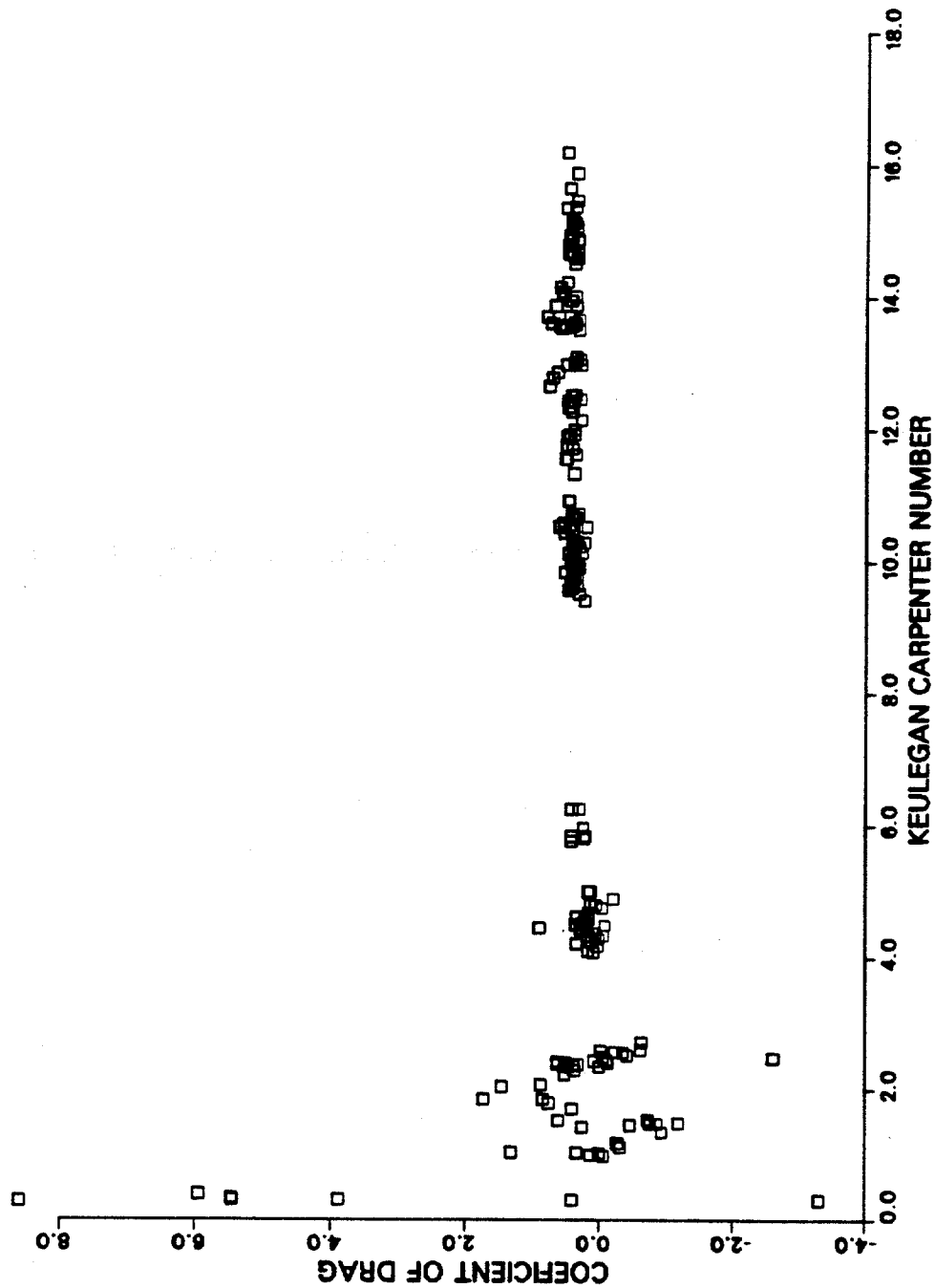

Figure 5.15. Coefficient of drag versus Keulegan-Carpenter number.
Individual wave results, model 4.

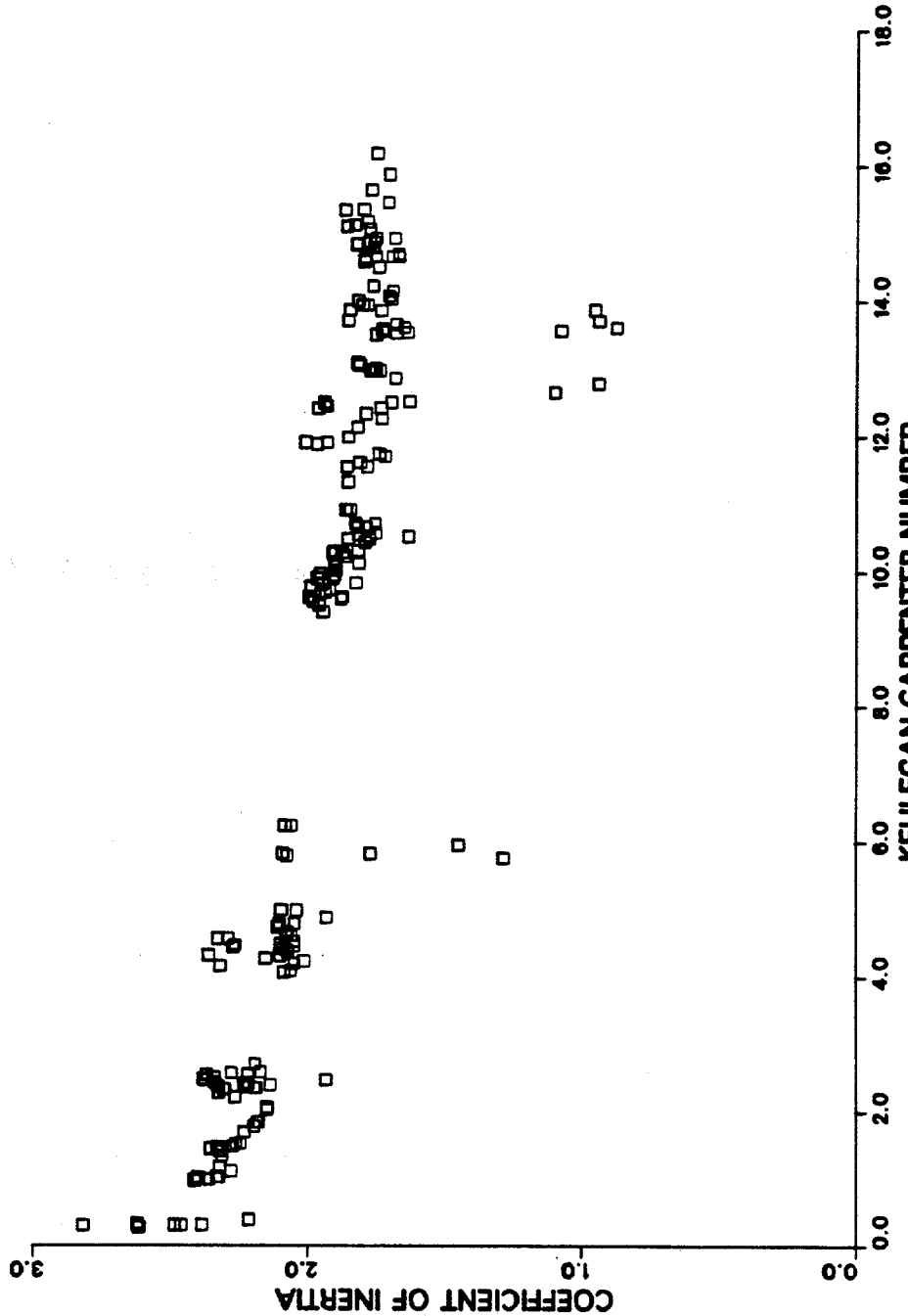

Figure 5.16. Coefficient of inertia versus Keulegan-Carpenter number. Individual wave results, model 4.

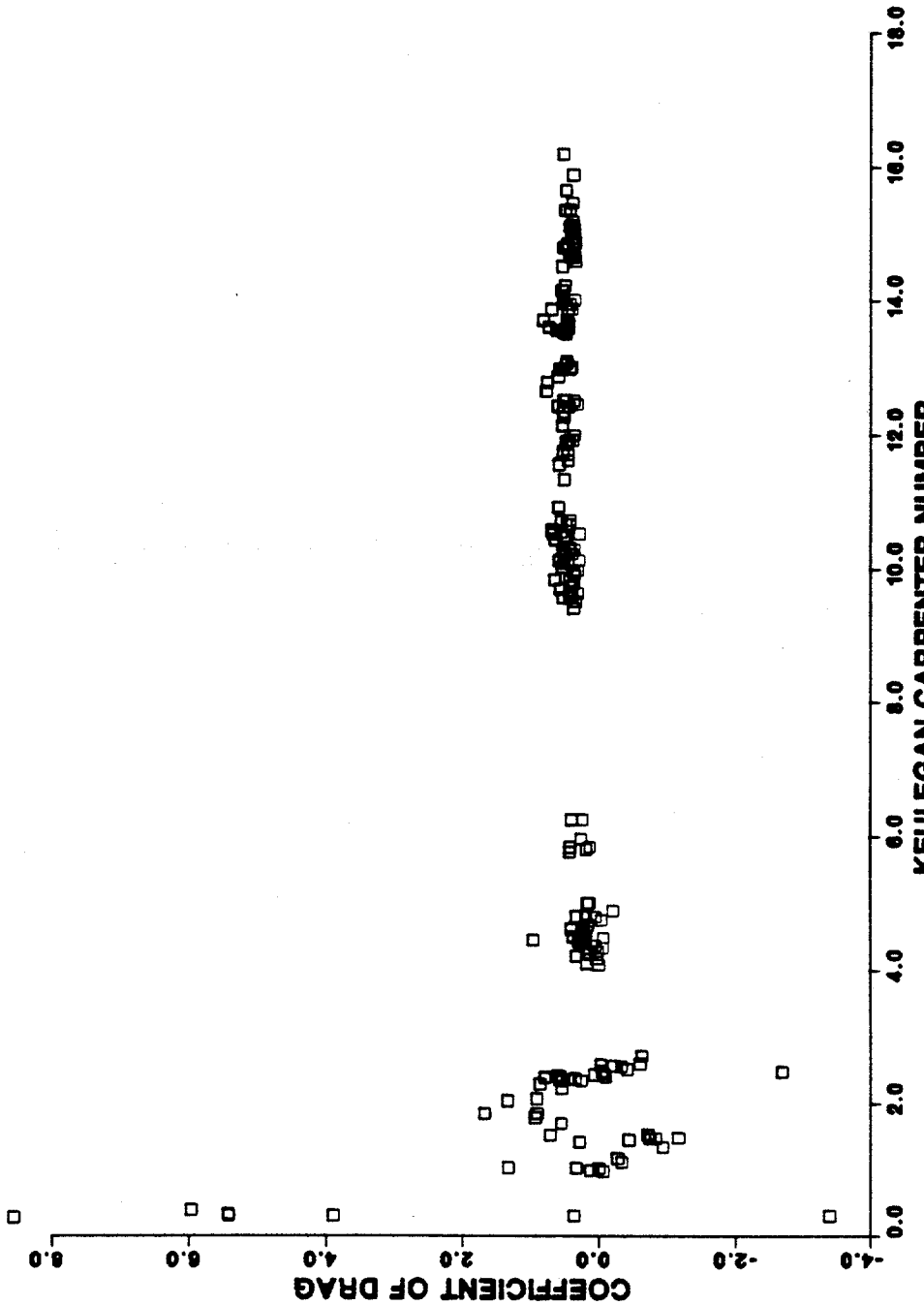

Figure 5.17. Coefficient of drag versus Keulegan-Carpenter number. Individual wave results, model 5.

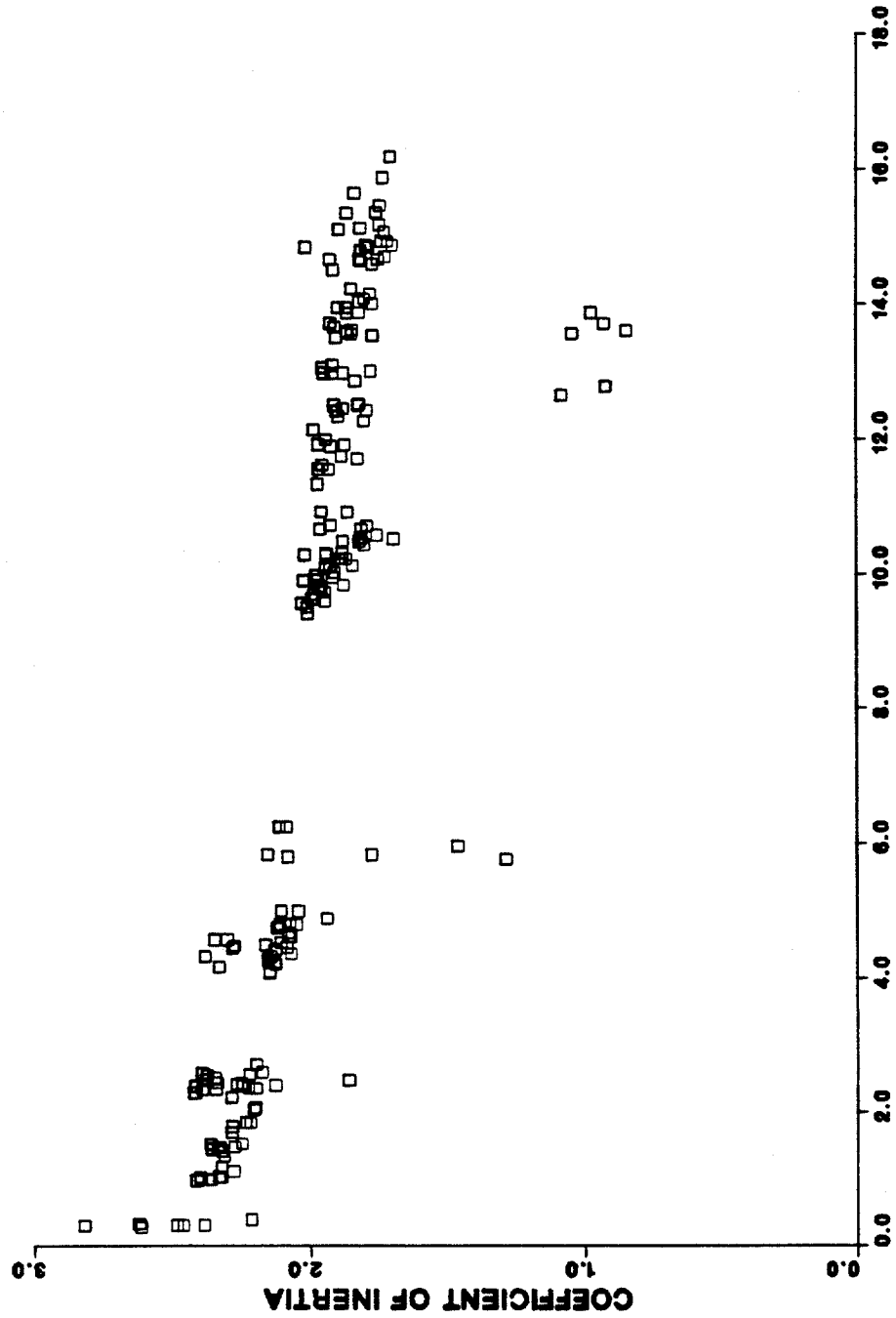

Figure 5.18. Coefficient of inertia versus Keulegan-Carpenter number. Individual wave results, model 5.

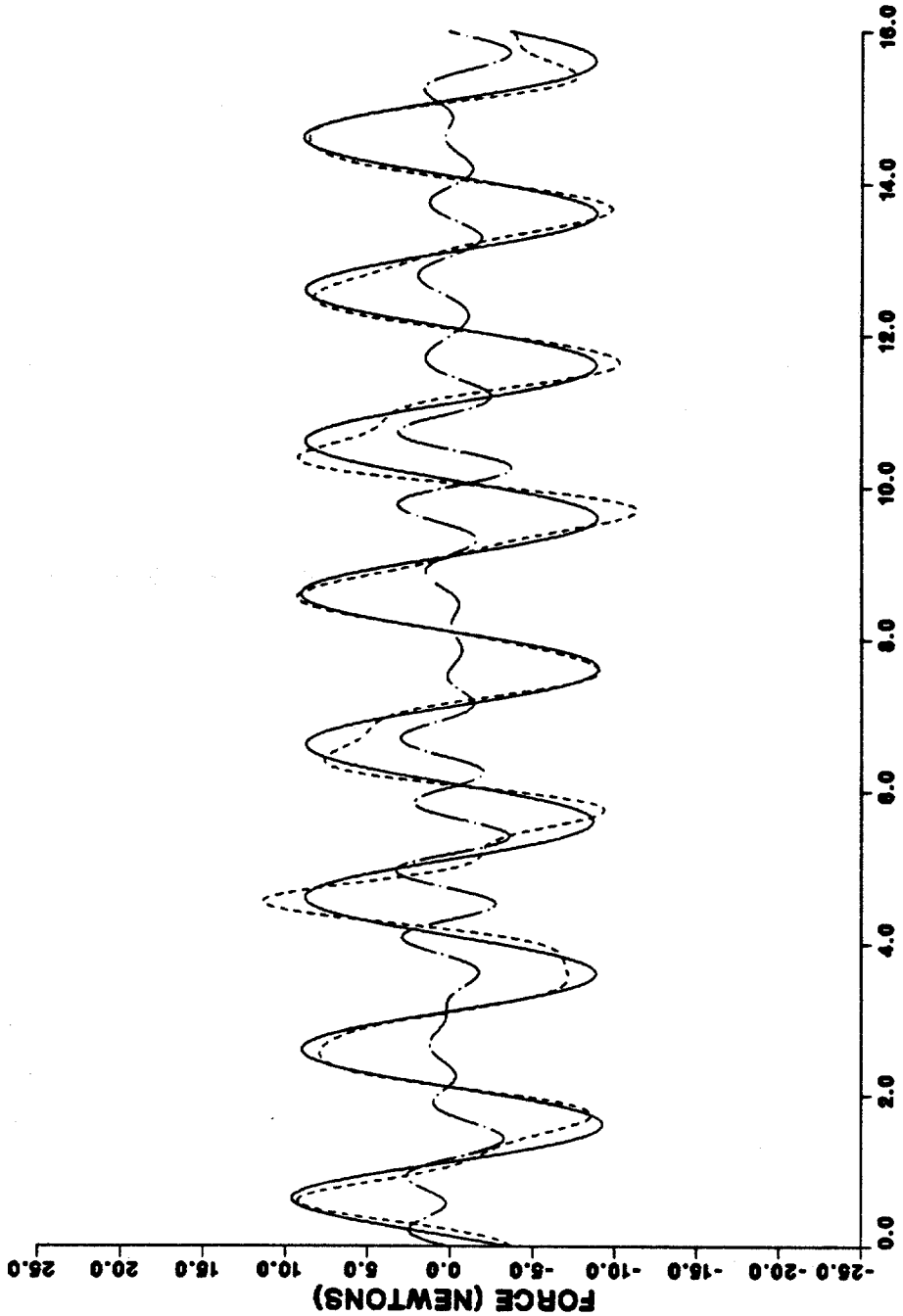

Figure 5.19. Comparison of measured and Morison forces, KC = 0.32.
[Measured ——; Morison force - - -; difference between measured and calculated force (force residue) —·—·—].

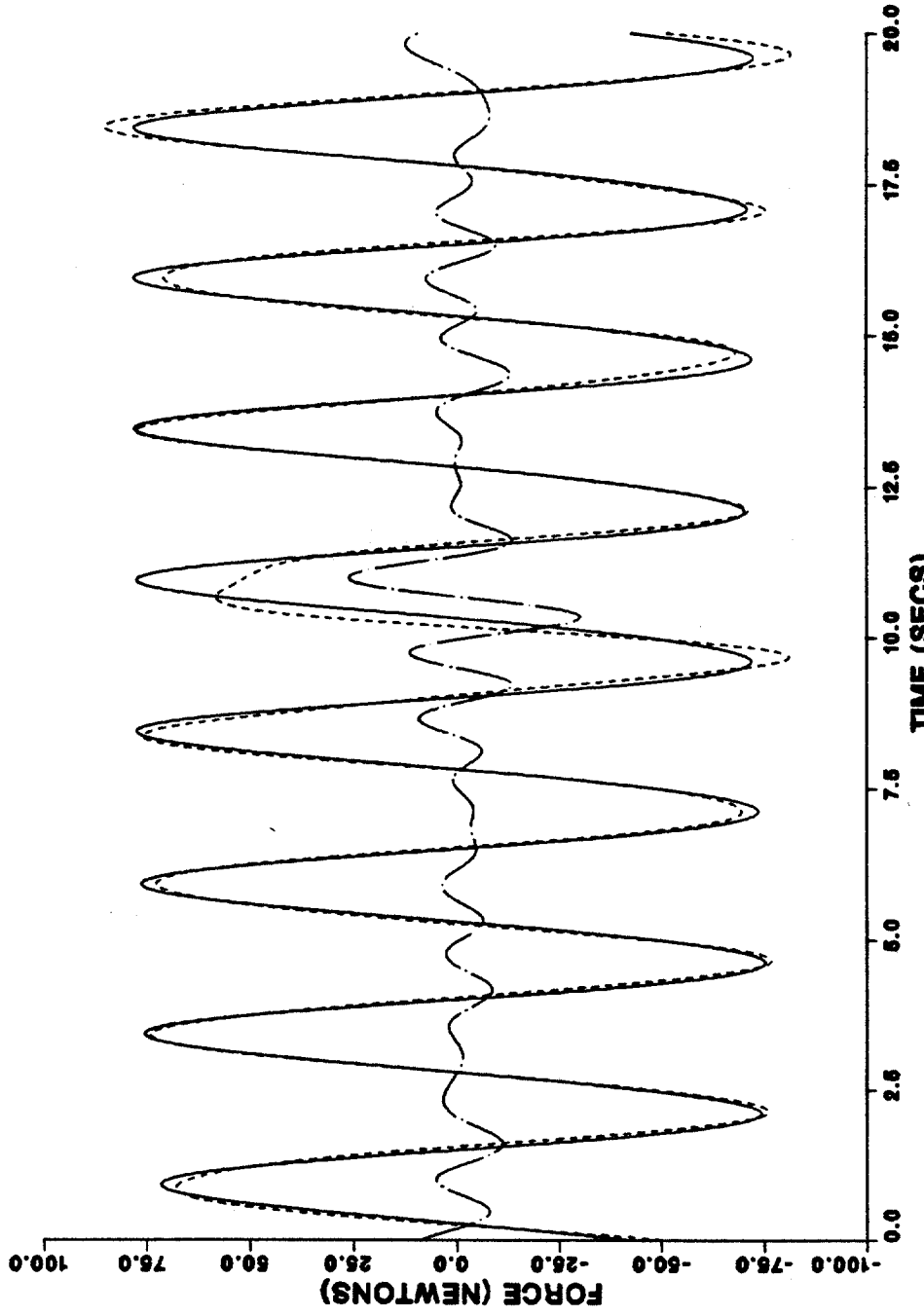

Figure 5.20. Comparison of measured and Morison forces, KC = 4.41.
[Measured ——; Morison force ---; difference between measured and calculated force (force residue) —·—·—].

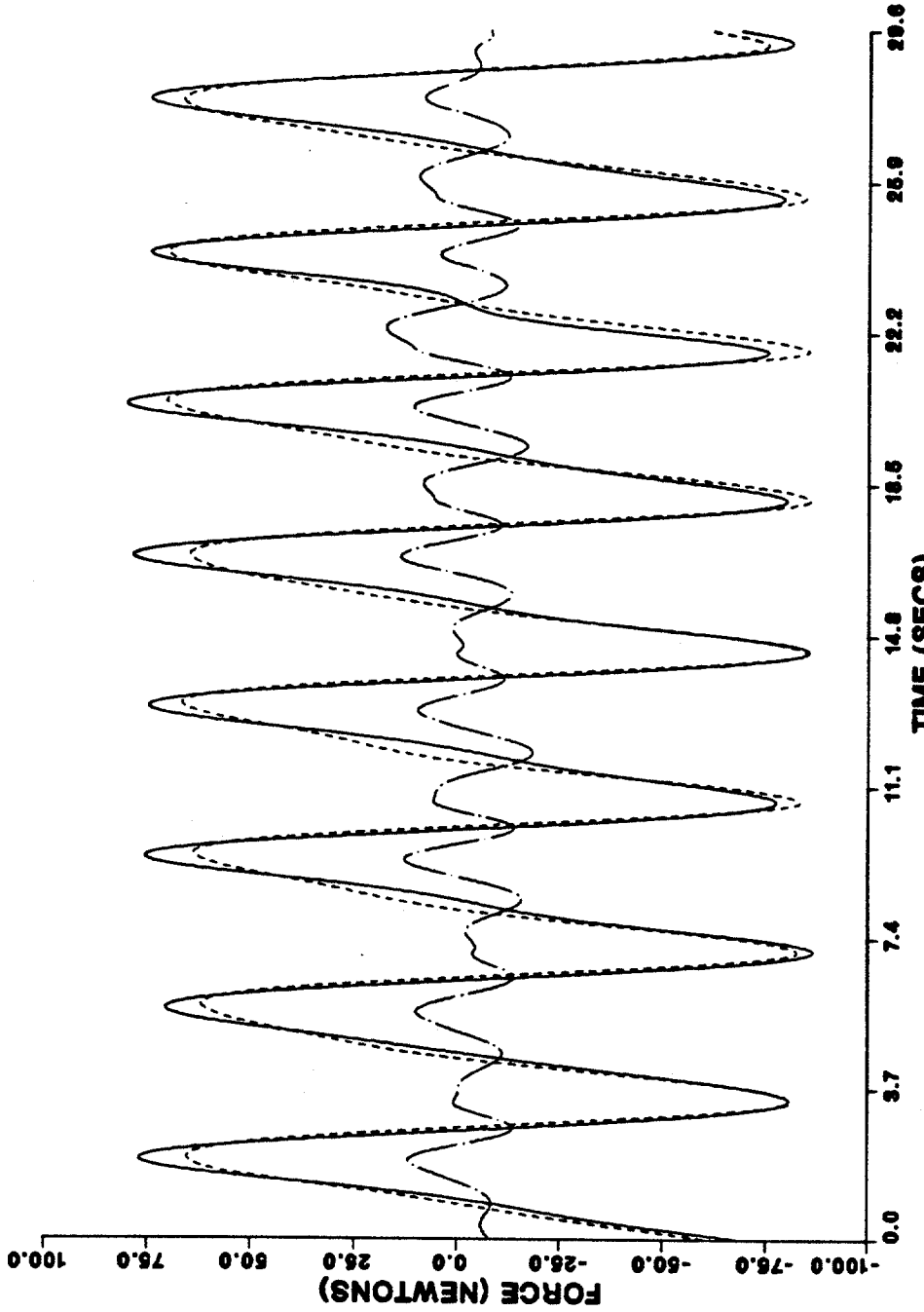

Figure 5.21. Comparison of measured and Morison forces, KC = 10.26.
[Measured ——; Morison force - - -; difference between measured and calculated force (force residue) —·—·—].

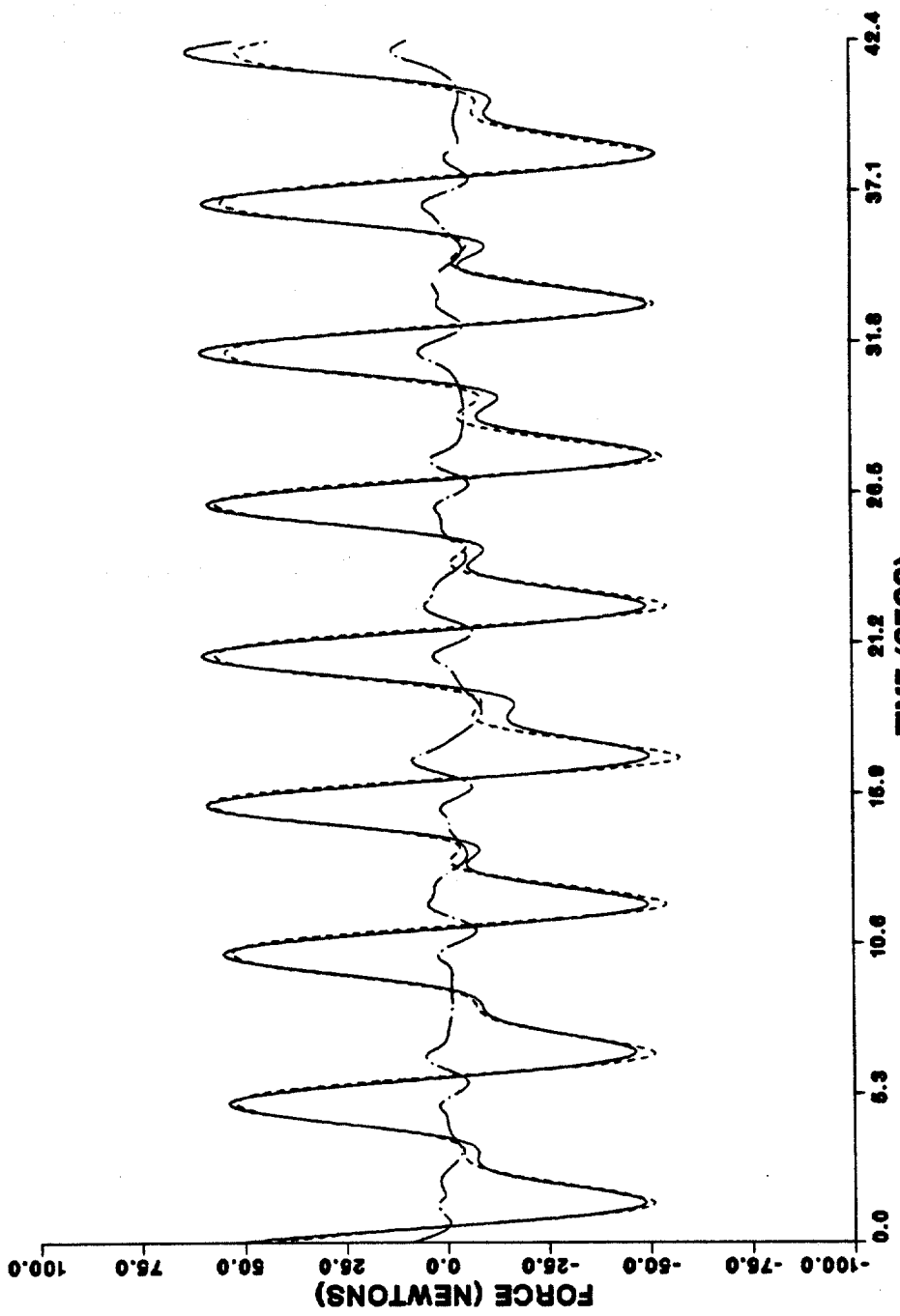

Figure 5.22. Comparison of measured and Morison forces, KC = 15.31.
[Measured ——; Morison force - - -; difference between measured and calculated force (force residue) —·—·].

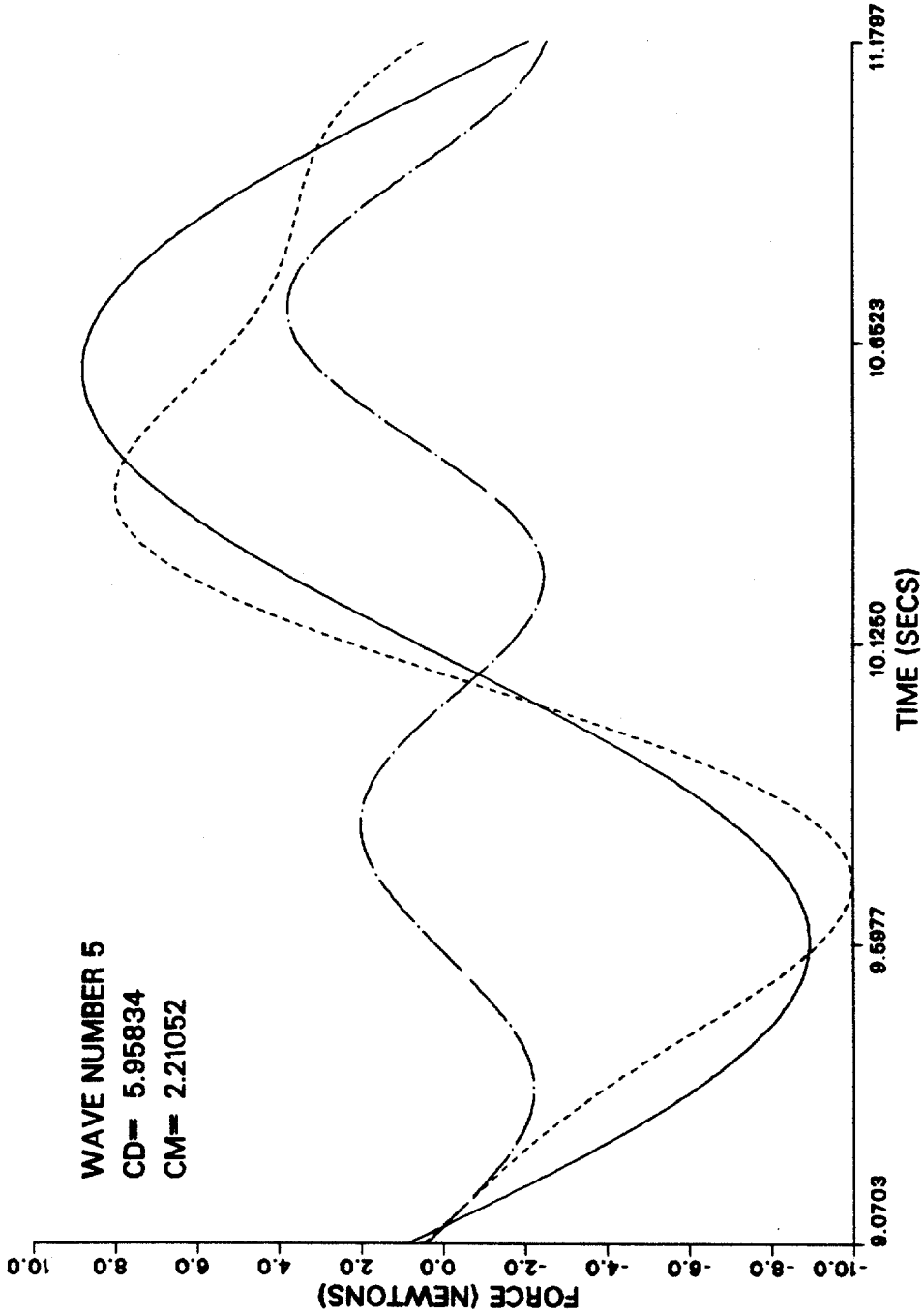

Figure 5.23. Comparison of measured and Morison force for an individual wave, wave 5, run 2. [Measured ——; Morison force - - -; difference between measured and calculated force (force residue) —·—·].

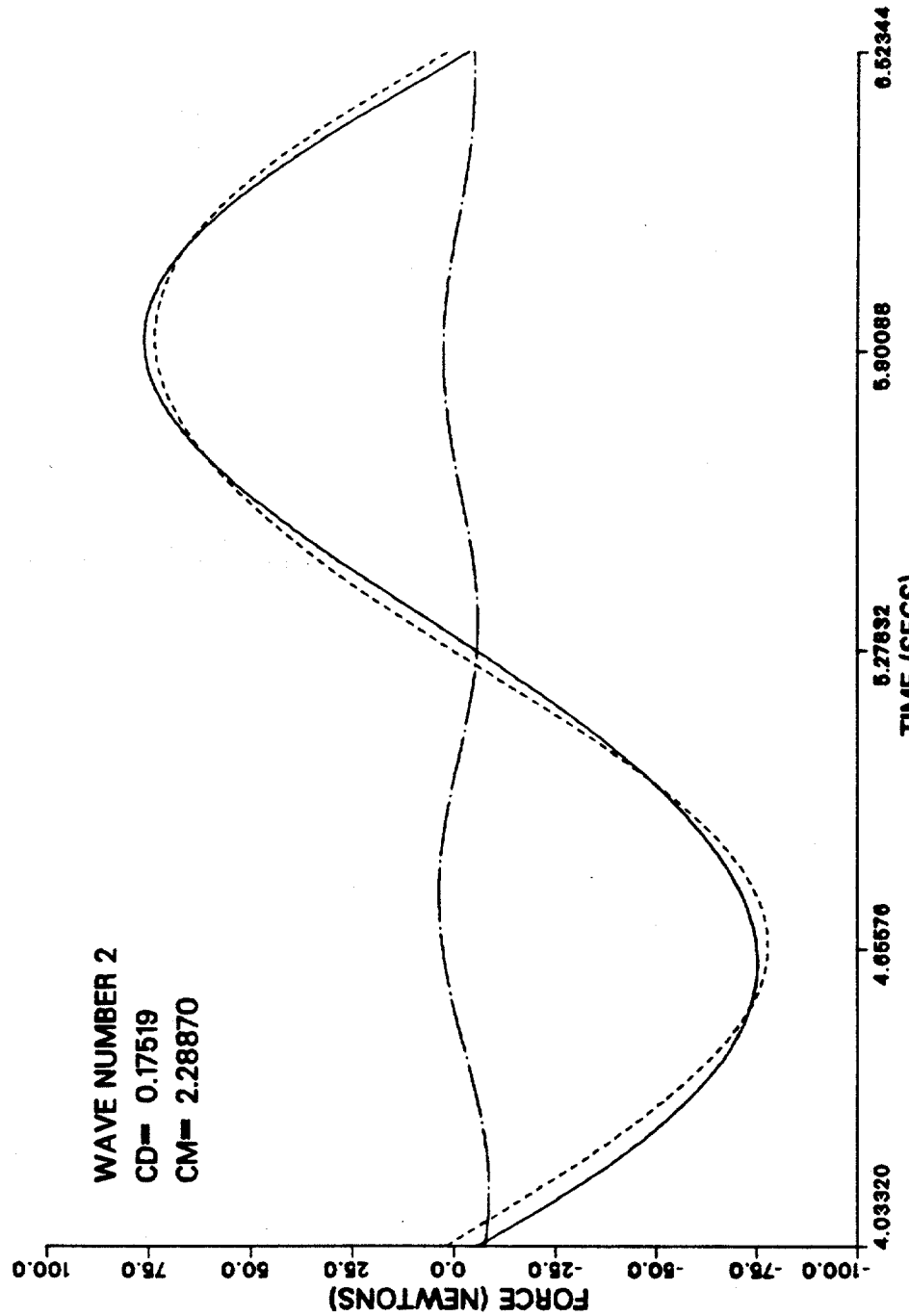

Figure 5.24. Comparison of measured and Morison force for an individual wave, wave 2, run 5. [Measured ——; Morison force - - -; difference between measured and calculated force (force residue) —·—·].

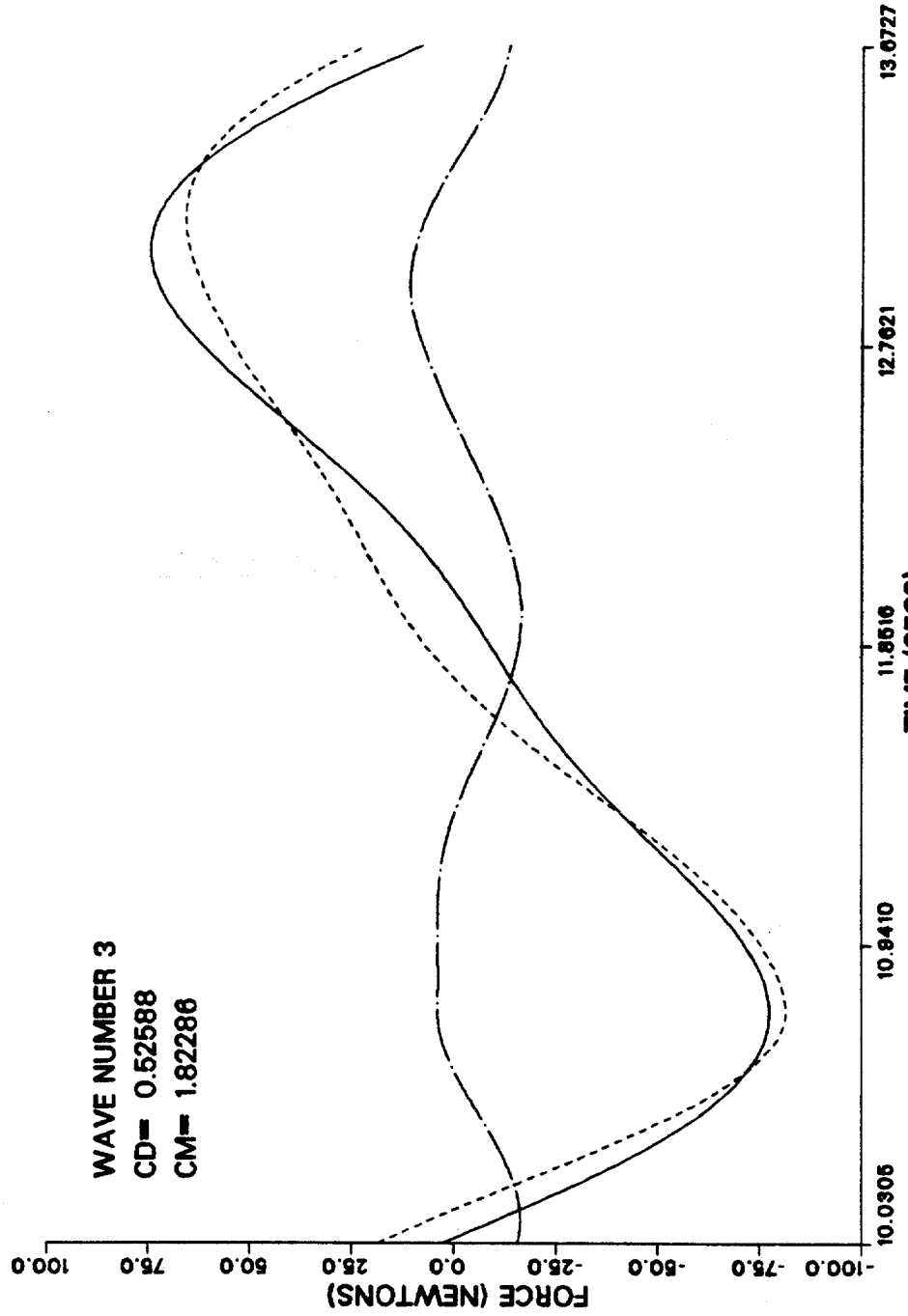

Figure 5.25. Comparison of measured and Morison force for an individual wave, wave 3, run 22. [Measured ——; Morison force - - -; difference between measured and calculated force (force residue) —·—·].

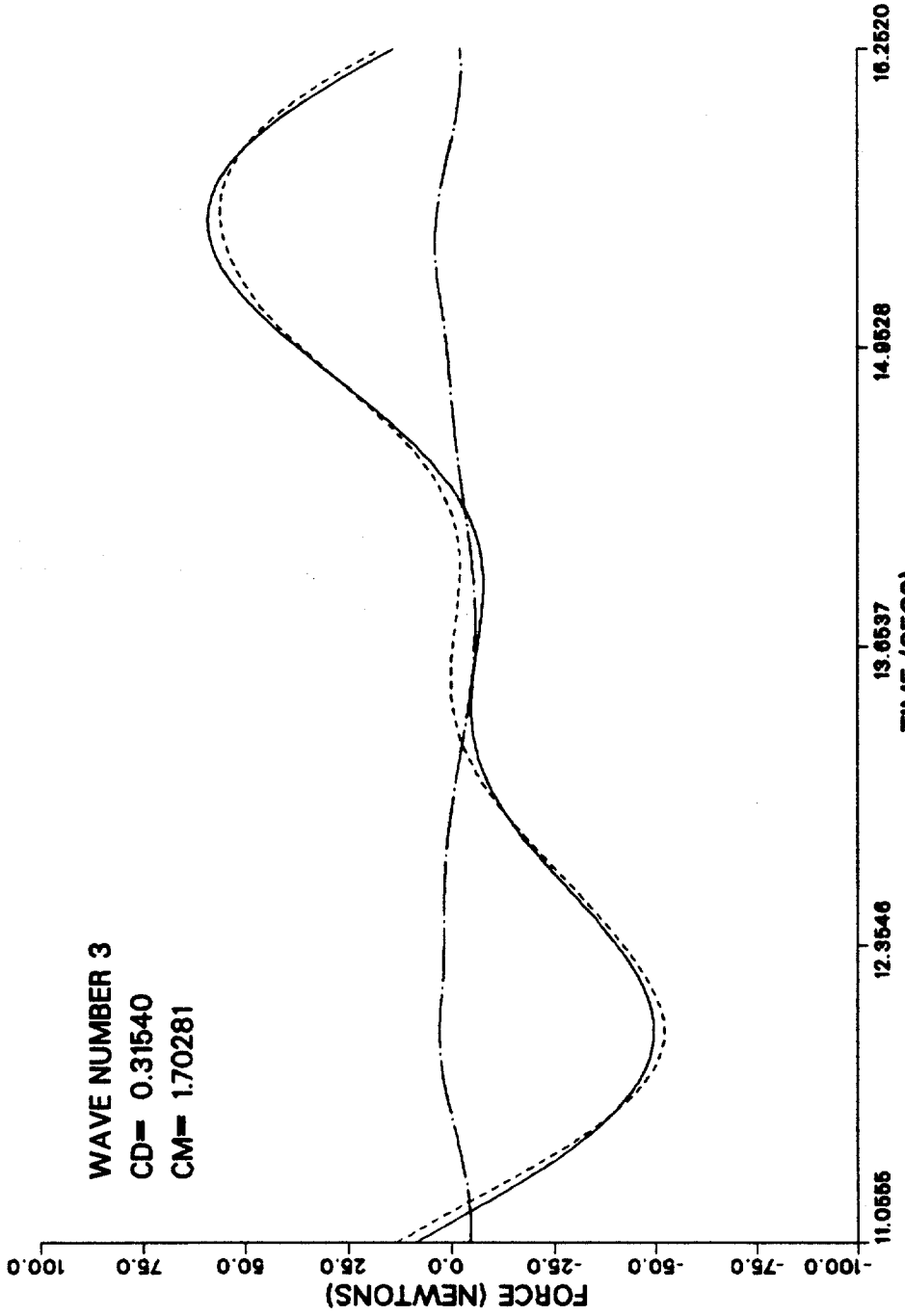

Figure 5.26. Comparison of measured and Morison force for an individual wave, wave 3, run 20. [Measured ——; Morison force - - -; difference between measured and calculated force (force residue) —·—·].

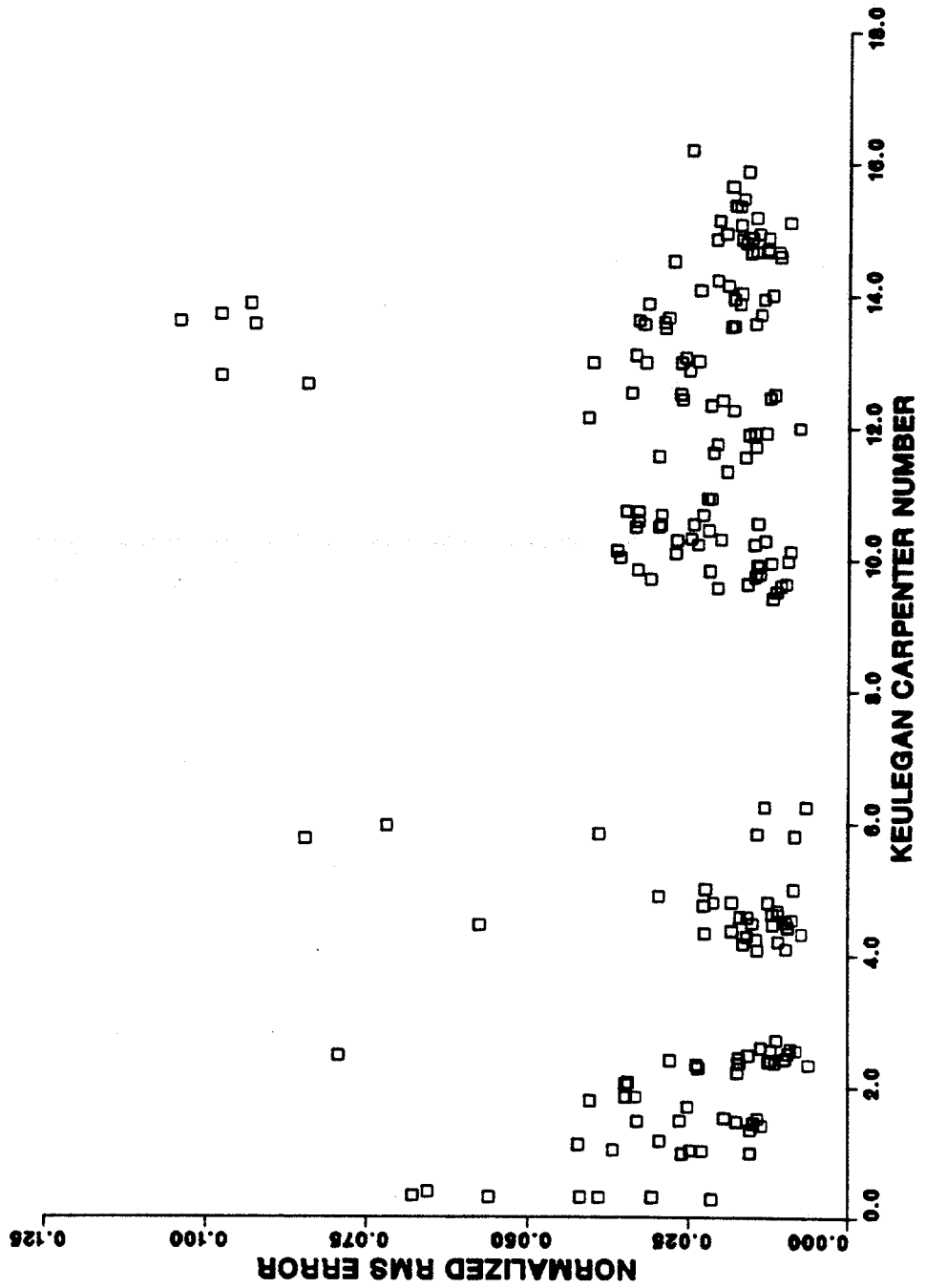

Figure 5.27. Normalized rms error versus the Keulegan-Carpenter number.

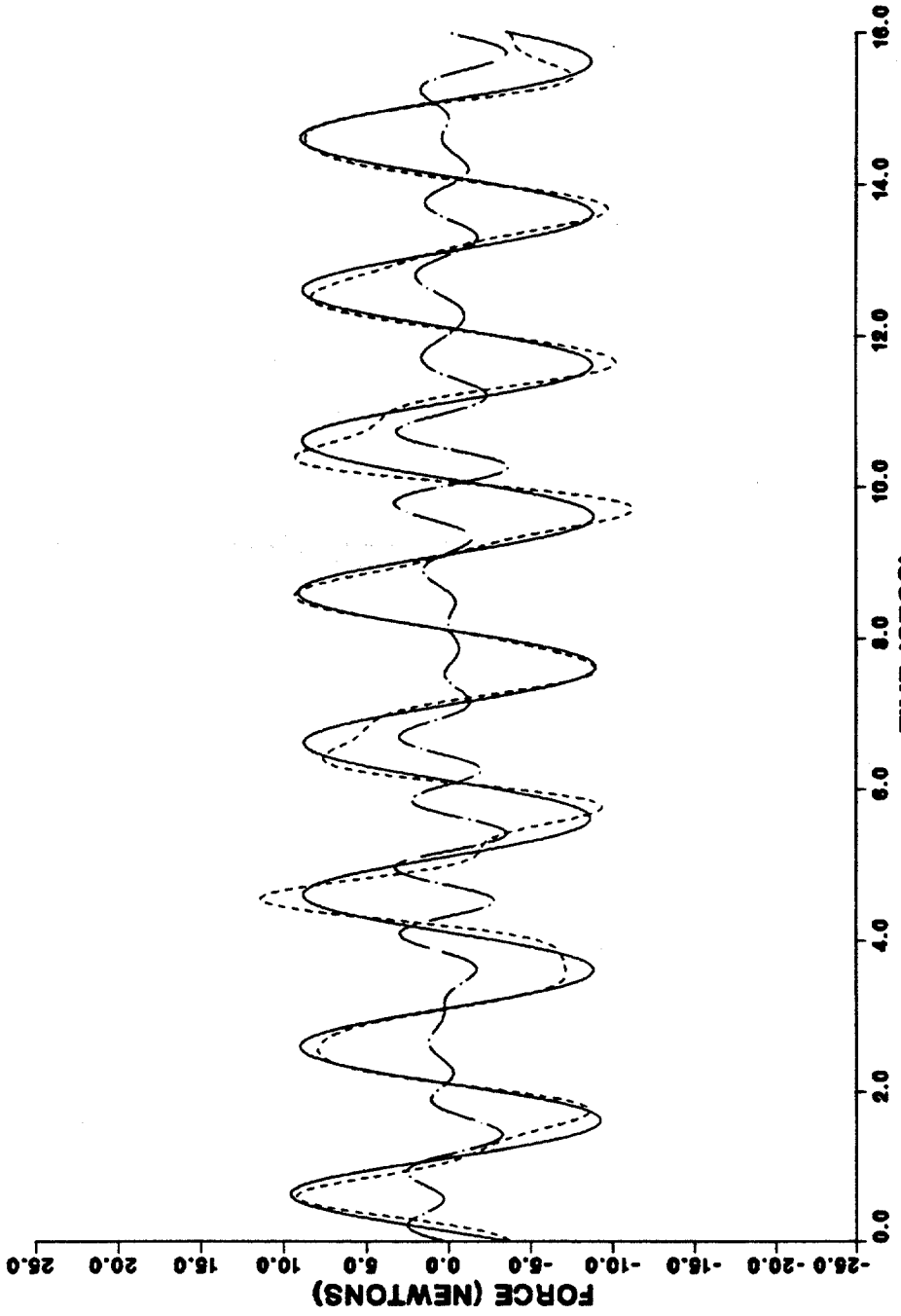

Figure 5.28. Comparison of measured and Morison with Lighthill correction force, model 1, KC = 0.32. [Measured ——; Morison with Lighthill correction - - -; force residue —·—·].

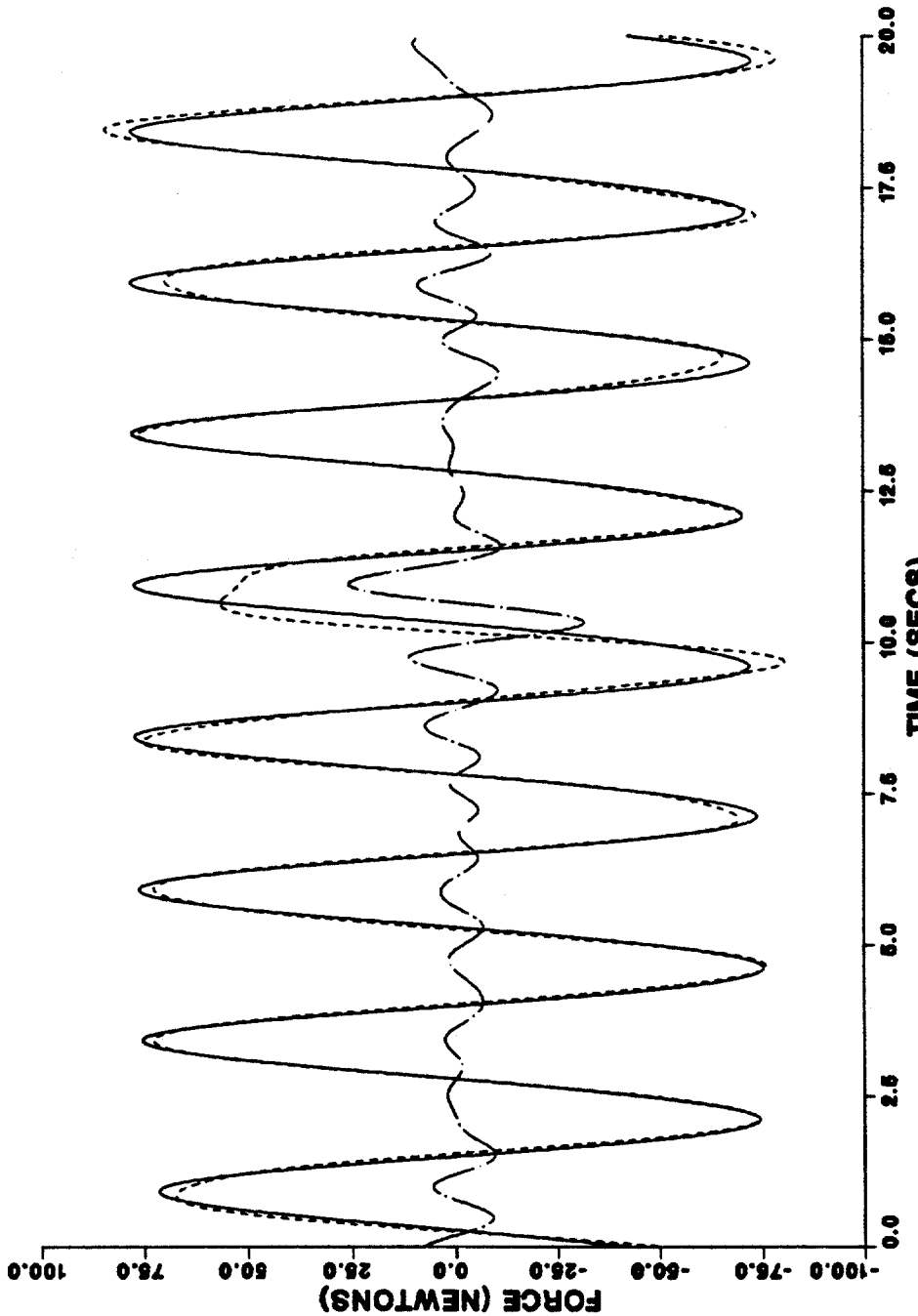

Figure 5.29. Comparison of measured and Morison with Lighthill correction force, model 1, KC = 4.41. [Measured ——; Morison with Lighthill correction ---; force residue —·—·].

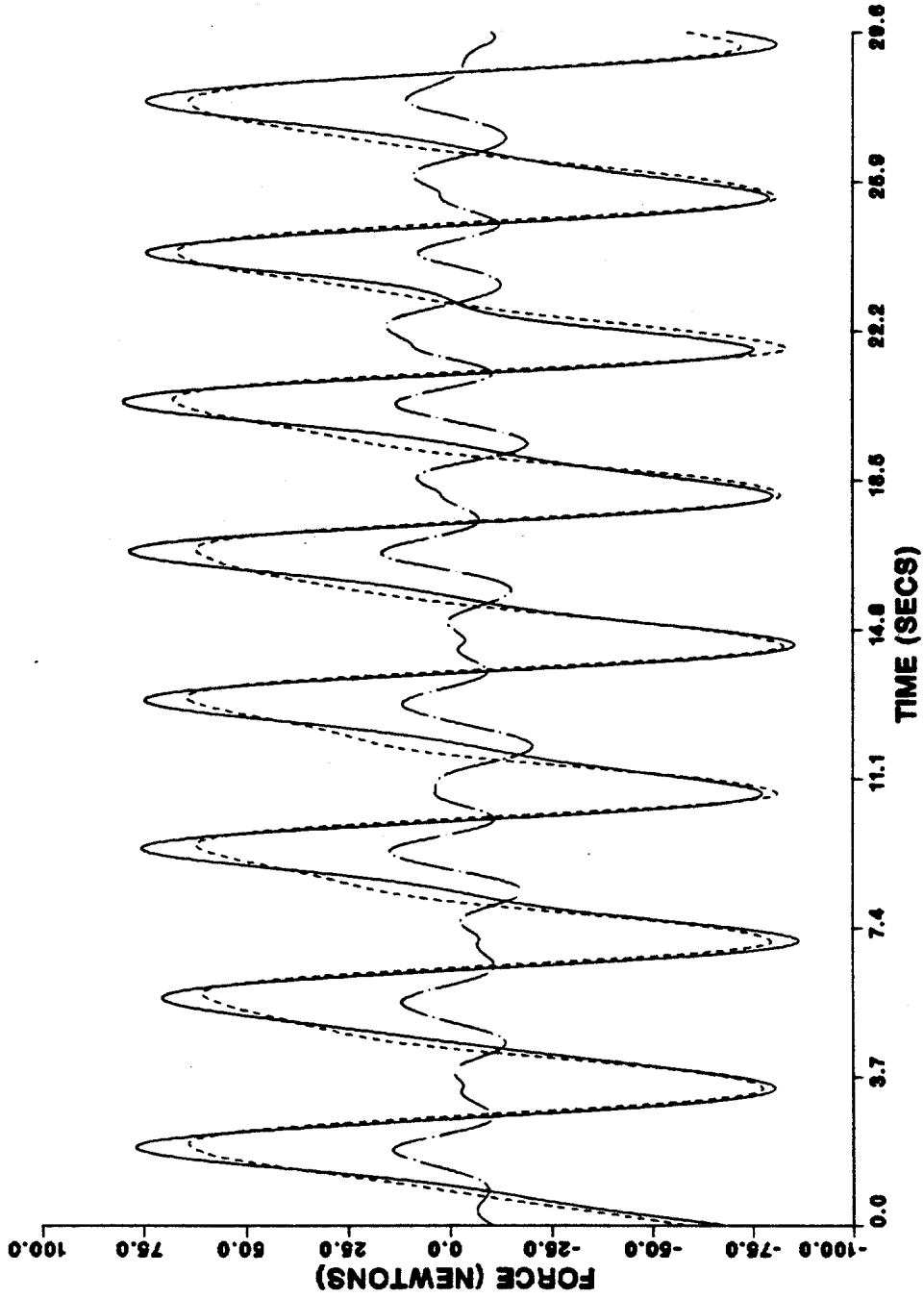

Figure 5.30. Comparison of measured and Morison with Lighthill correction force, model 1, KC = 10.26. [Measured ——; Morison with Lighthill correction ---; force residue —·—·—].

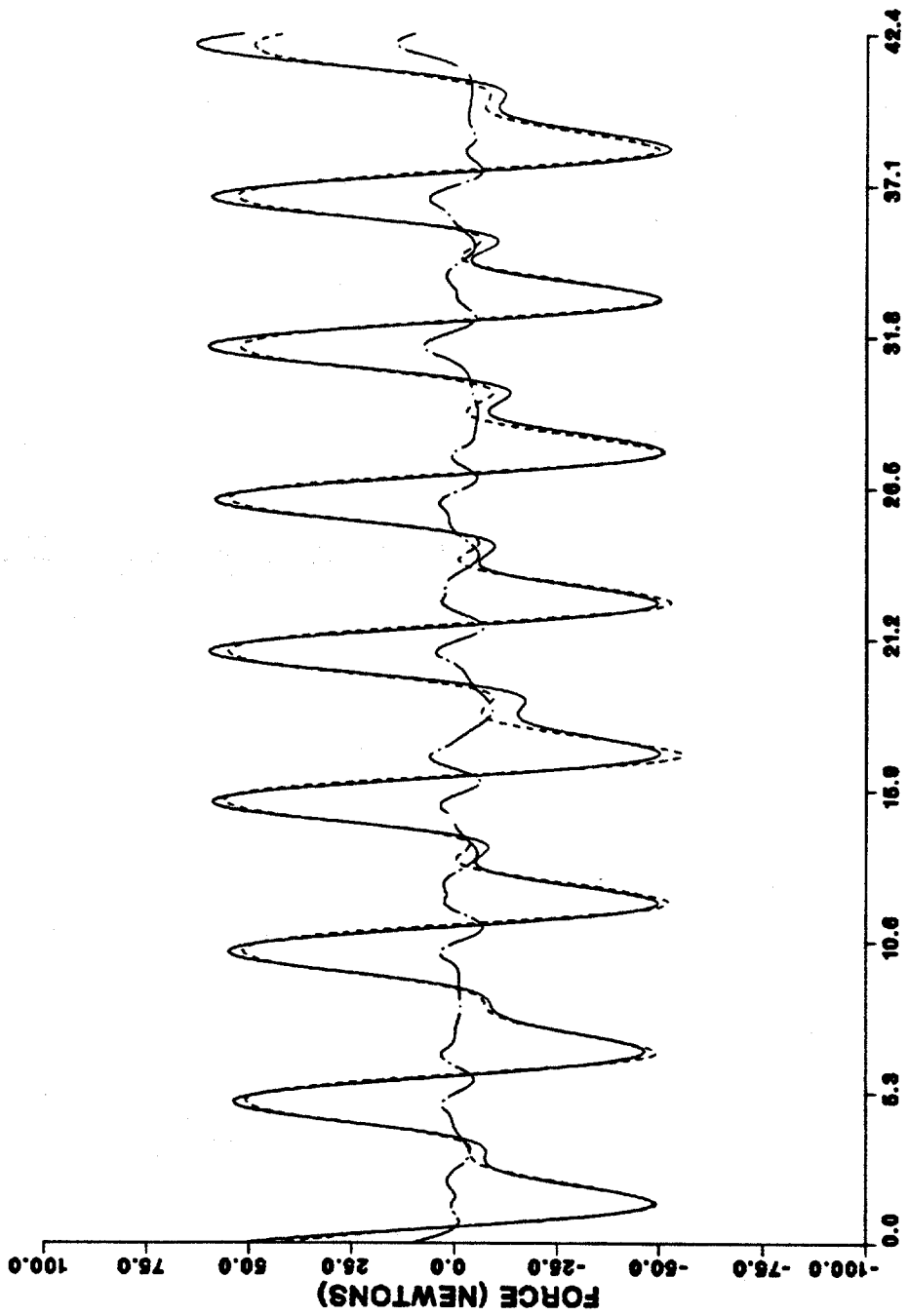

Figure 5.31. Comparison of measured and Morison with Lighthill correction force, model 1, KC = 15.31. [Measured ——; Morison with Lighthill correction ---; force residue —·—·—].

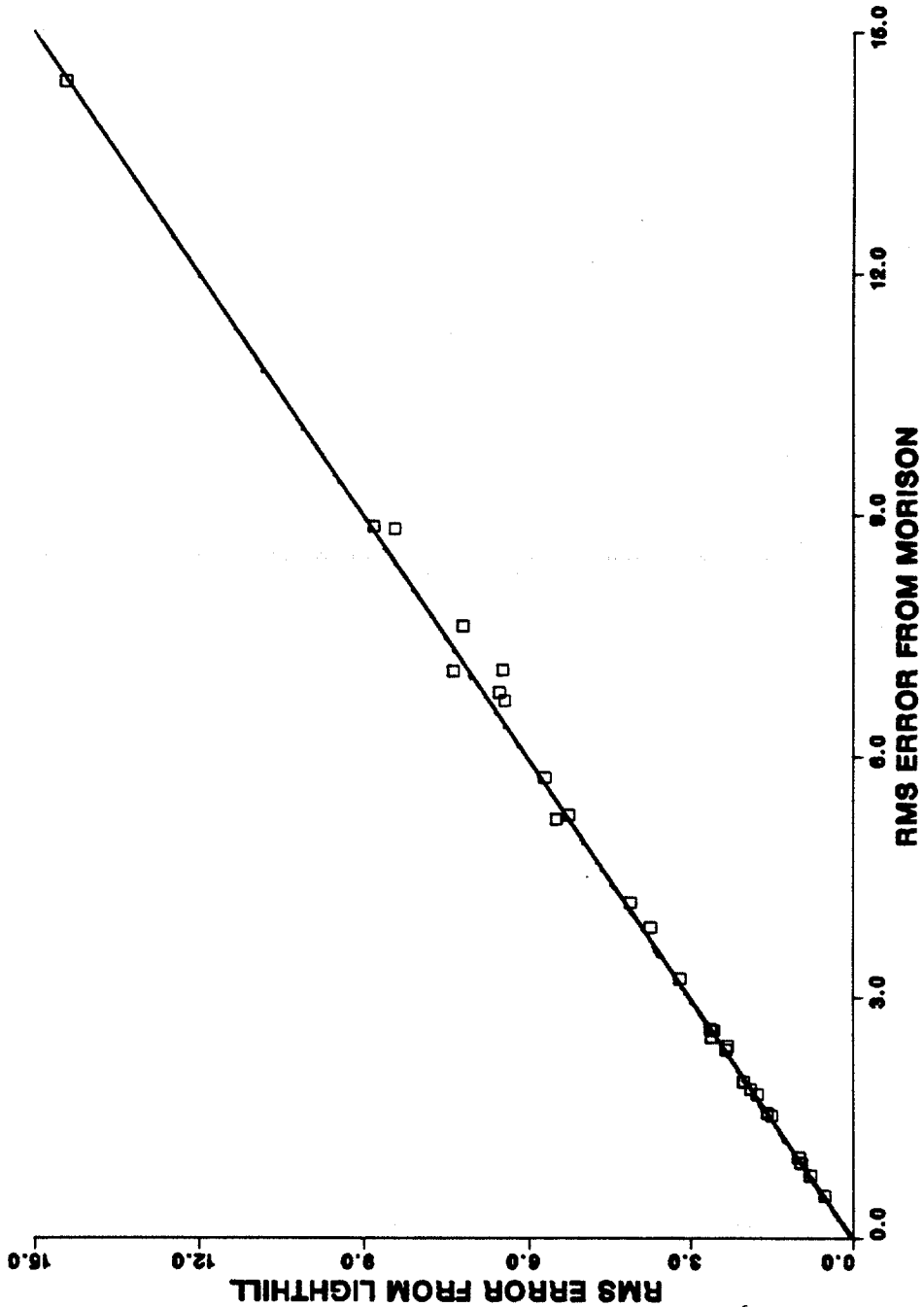

Figure 5.32. rms error from Morison with the Lighthill correction (model 1) versus the rms error from Morison alone for the total run.

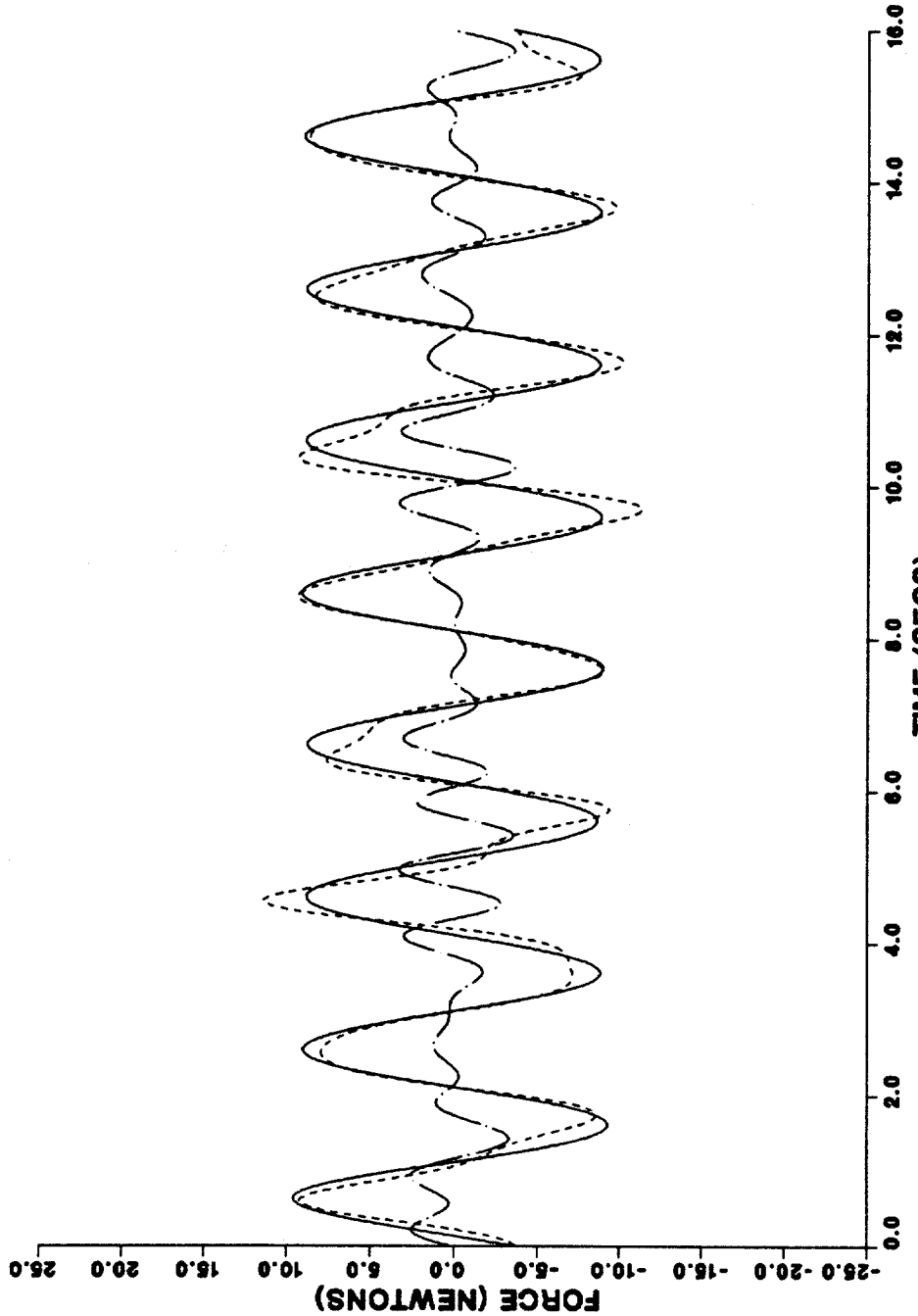

Figure 5.33. Comparison of measured and Morison with Lighthill correction force, model 2, KC = 0.32. [Measured ——; Morison with Lighthill correction ---; force residue —·—·].

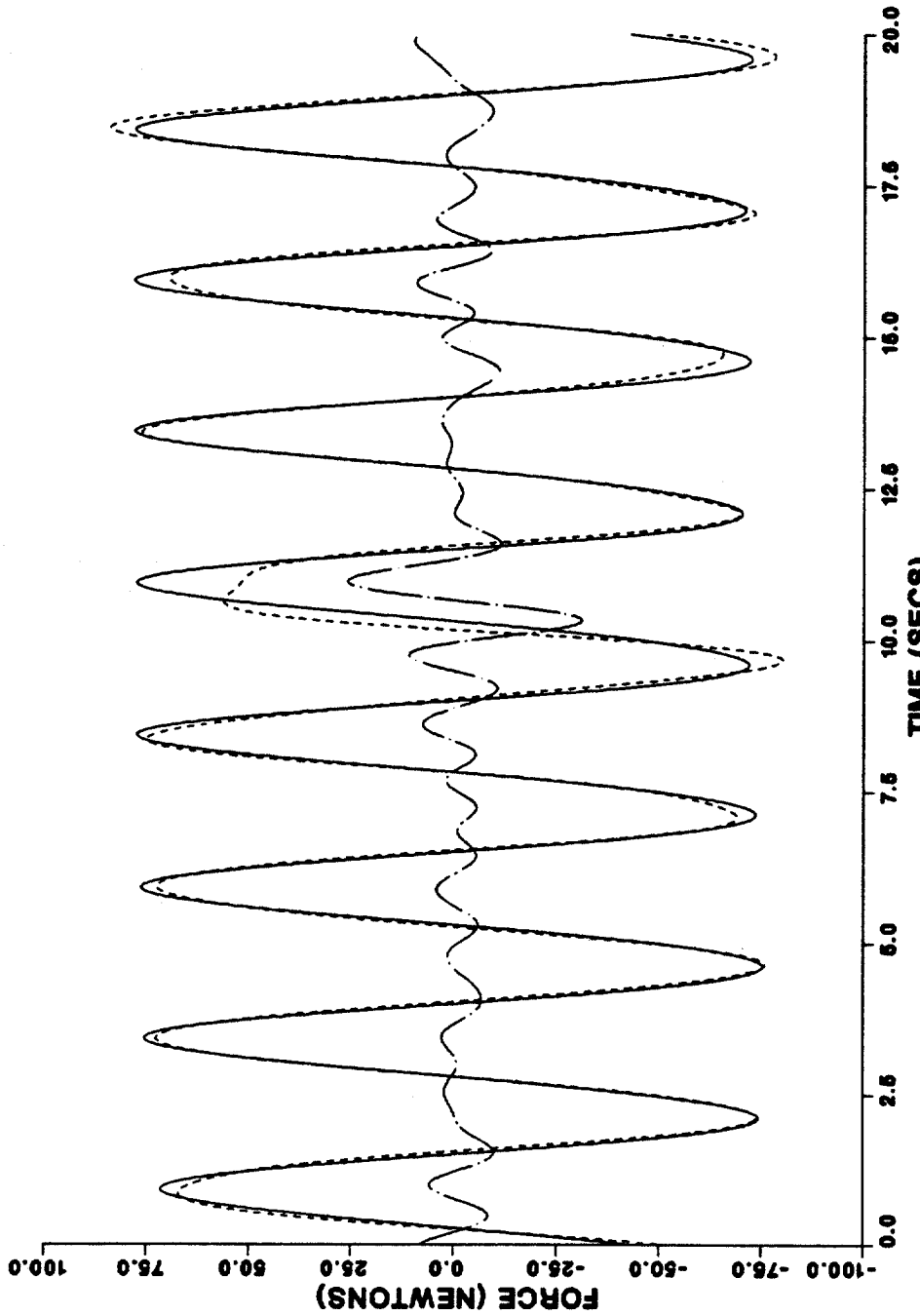

Figure 5.34. Comparison of measured and Morison with Lighthill correction force, model 2, KC = 4.41. [Measured ——; Morison with Lighthill correction ---; force residue —·—·—].

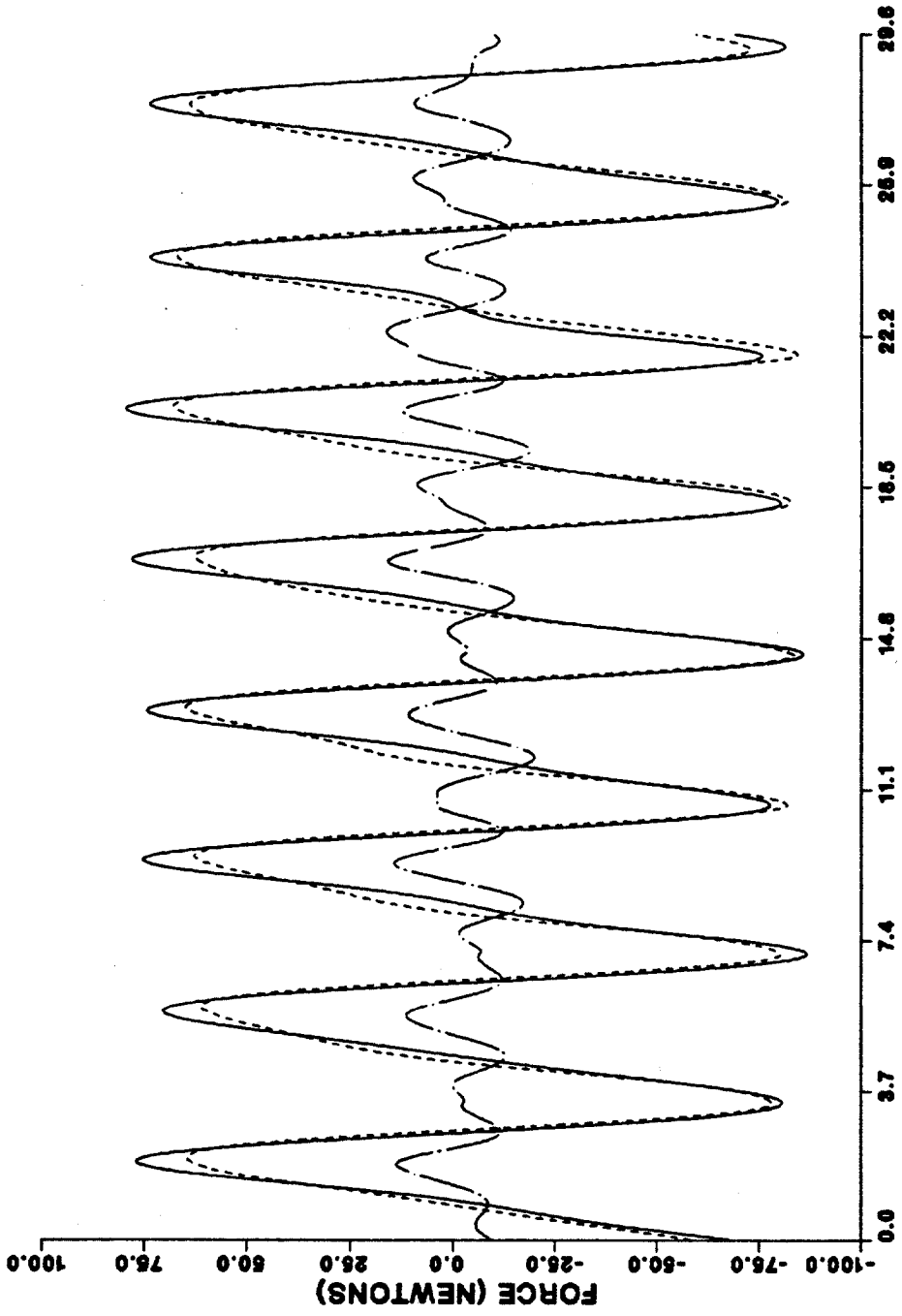

Figure 5.35. Comparison of measured and Morison with Lighthill correction force, model 2, KC = 10.26. [Measured ——; Morison with Lighthill correction - - -; force residue —·—·—].

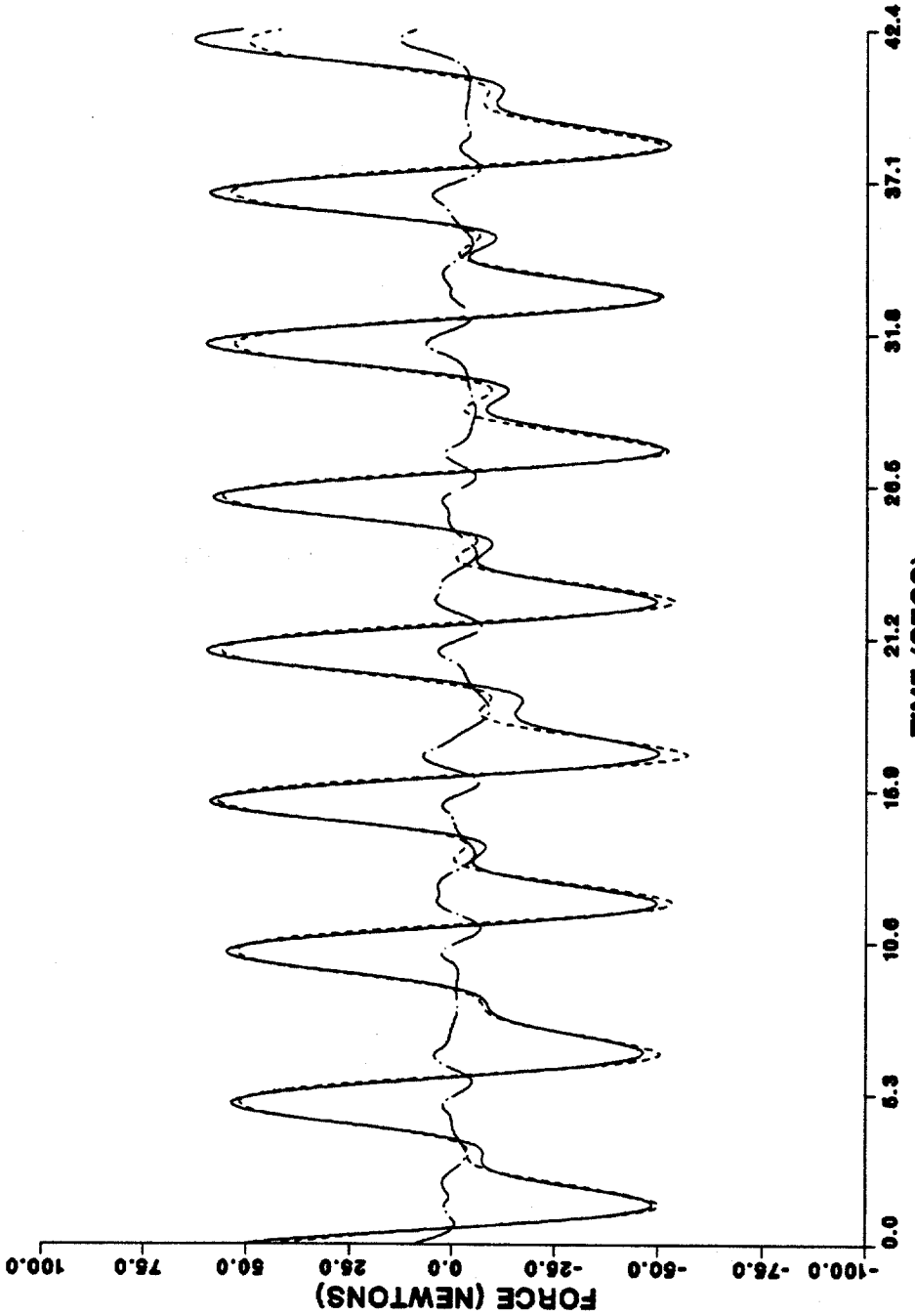

Figure 5.36. Comparison of measured and Morison with Lighthill correction force, model 2, KC = 15.31. [Measured ——; Morison with Lighthill correction ---; force residue —·—·].

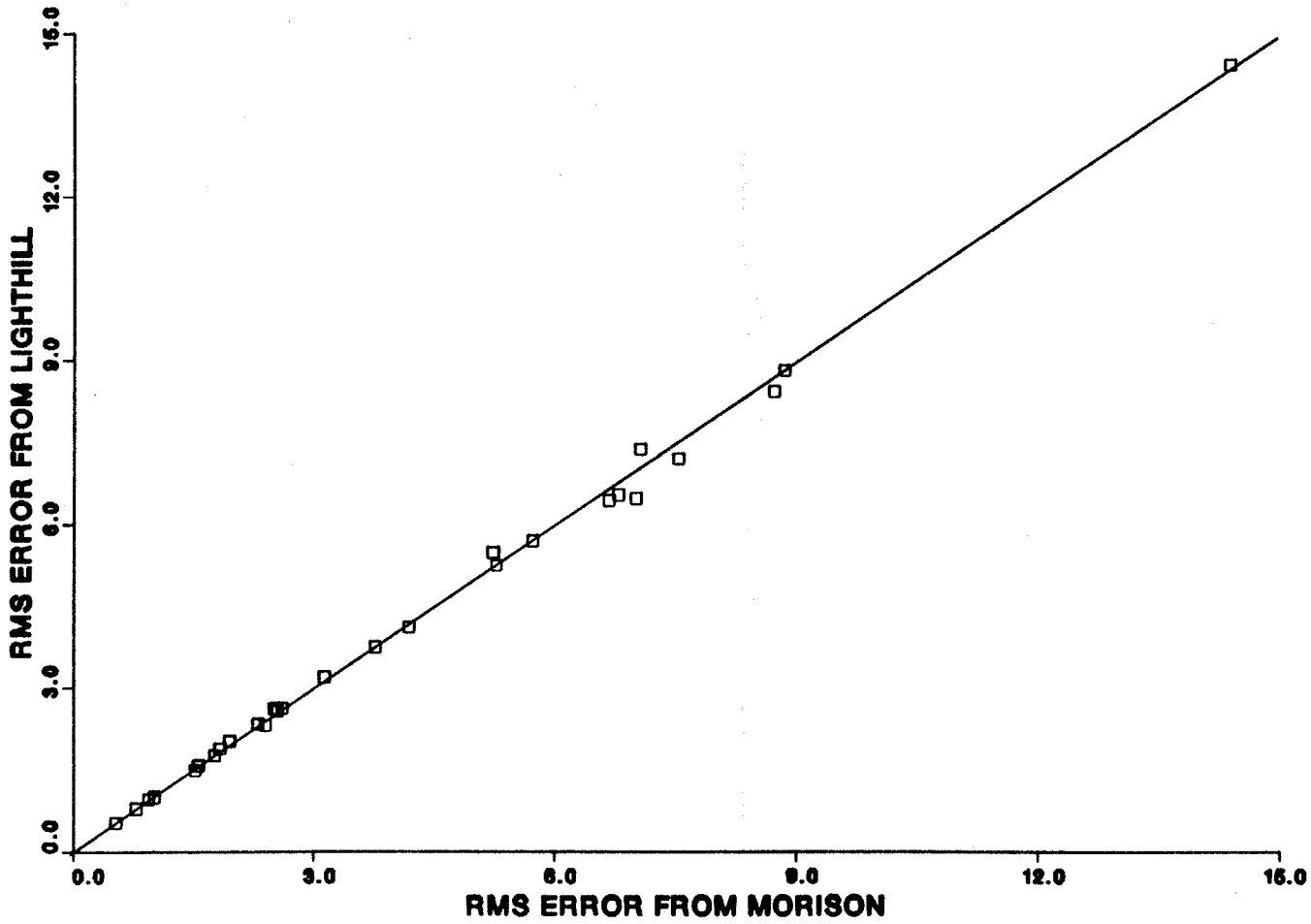

Figure 5.37. rms error from Morison with the Lighthill correction (model 2) versus the rms error from Morison alone for the total run.

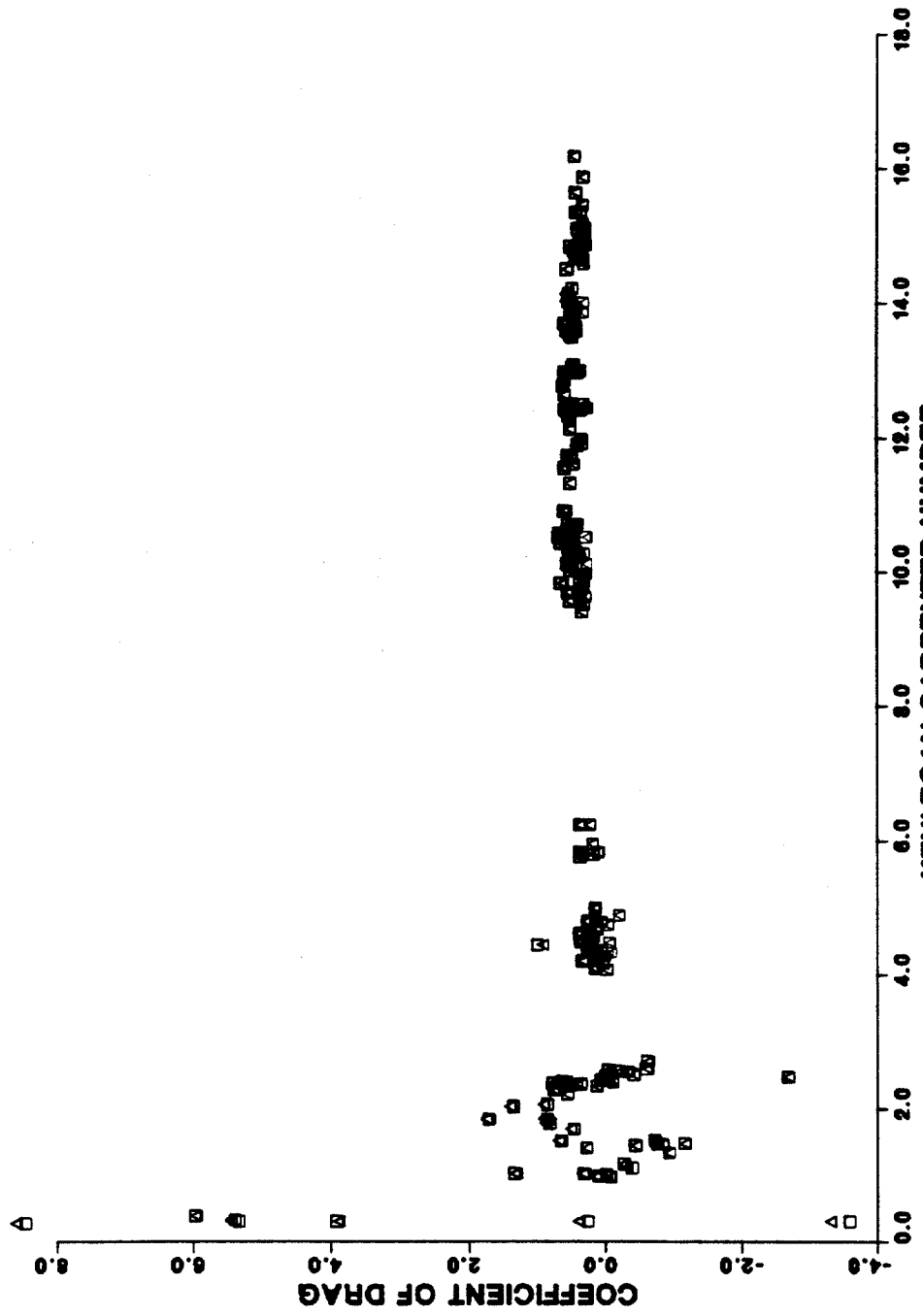

Figure 5.38. Comparison of drag coefficients calculated using the Morison equation (Δ) and the Morison equation with the Lighthill correction (□).

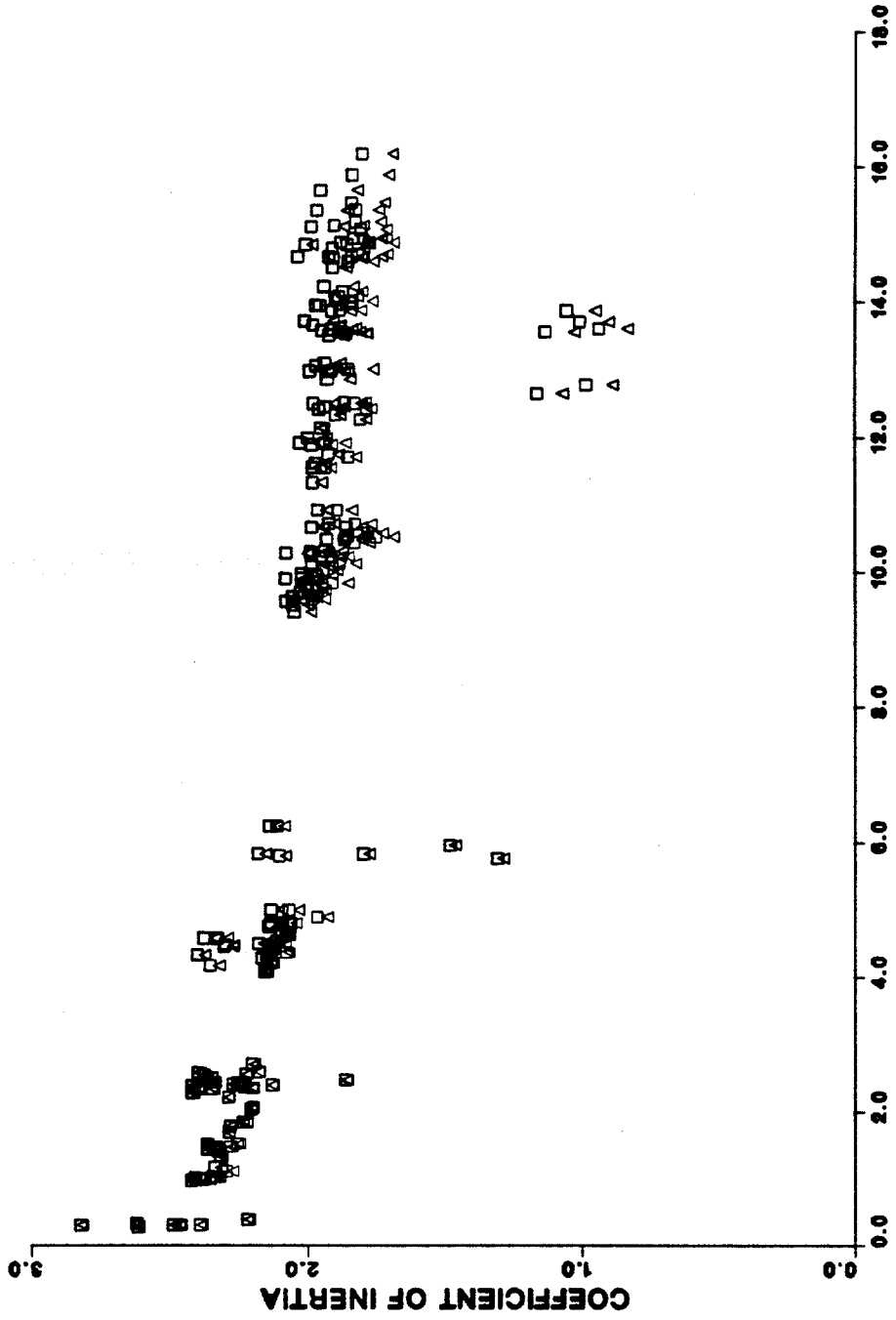

Figure 5.39. Comparison of inertia coefficients calculated using the Morison equation (Δ) and the Morison equation with the Lighthill correction (□).

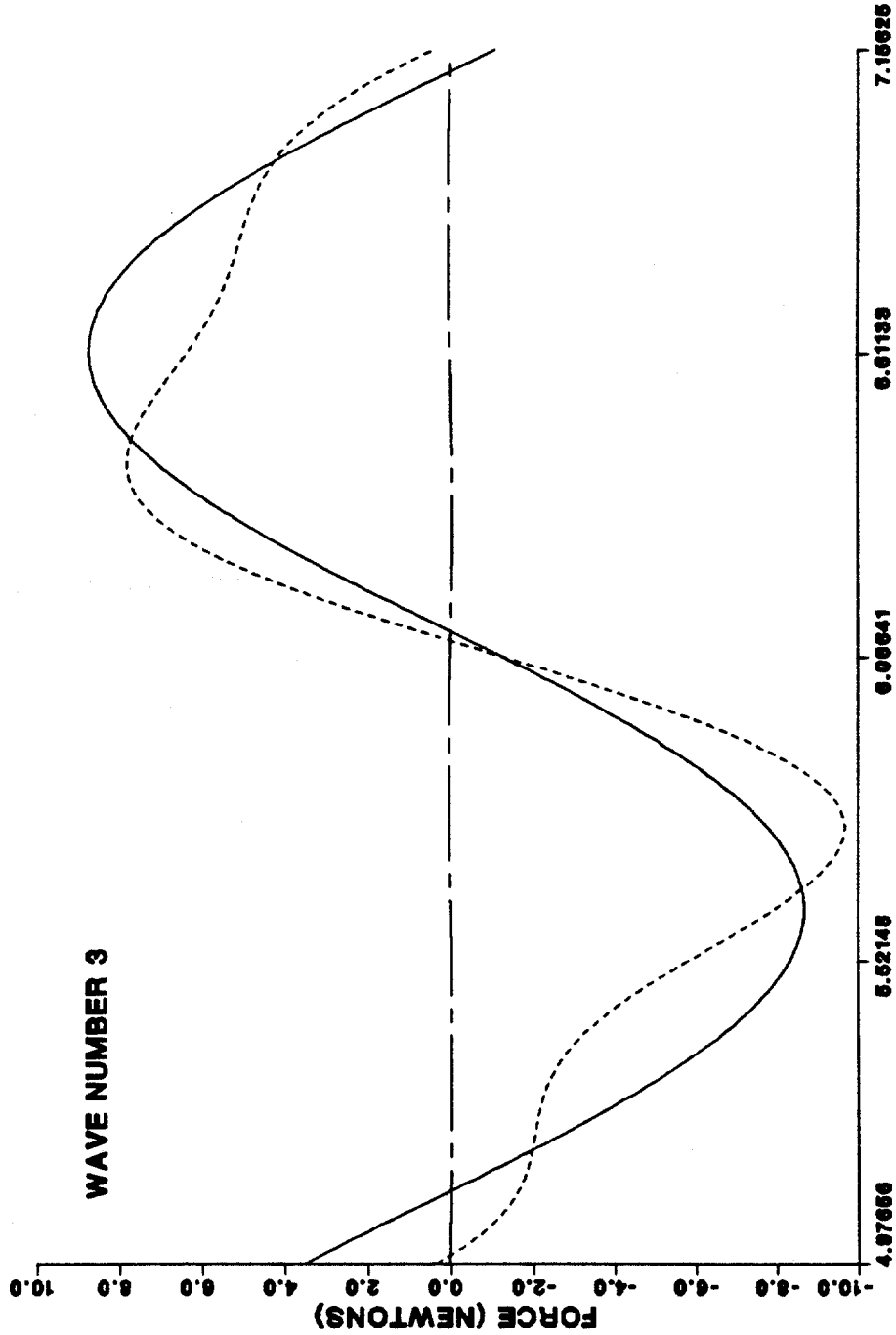

Figure 5.40. Comparison of measured and calculated forces (based on the first model), wave 3 run 2. [Measured ——; Morison with Lighthill correction - - -; force residue —·—·—].

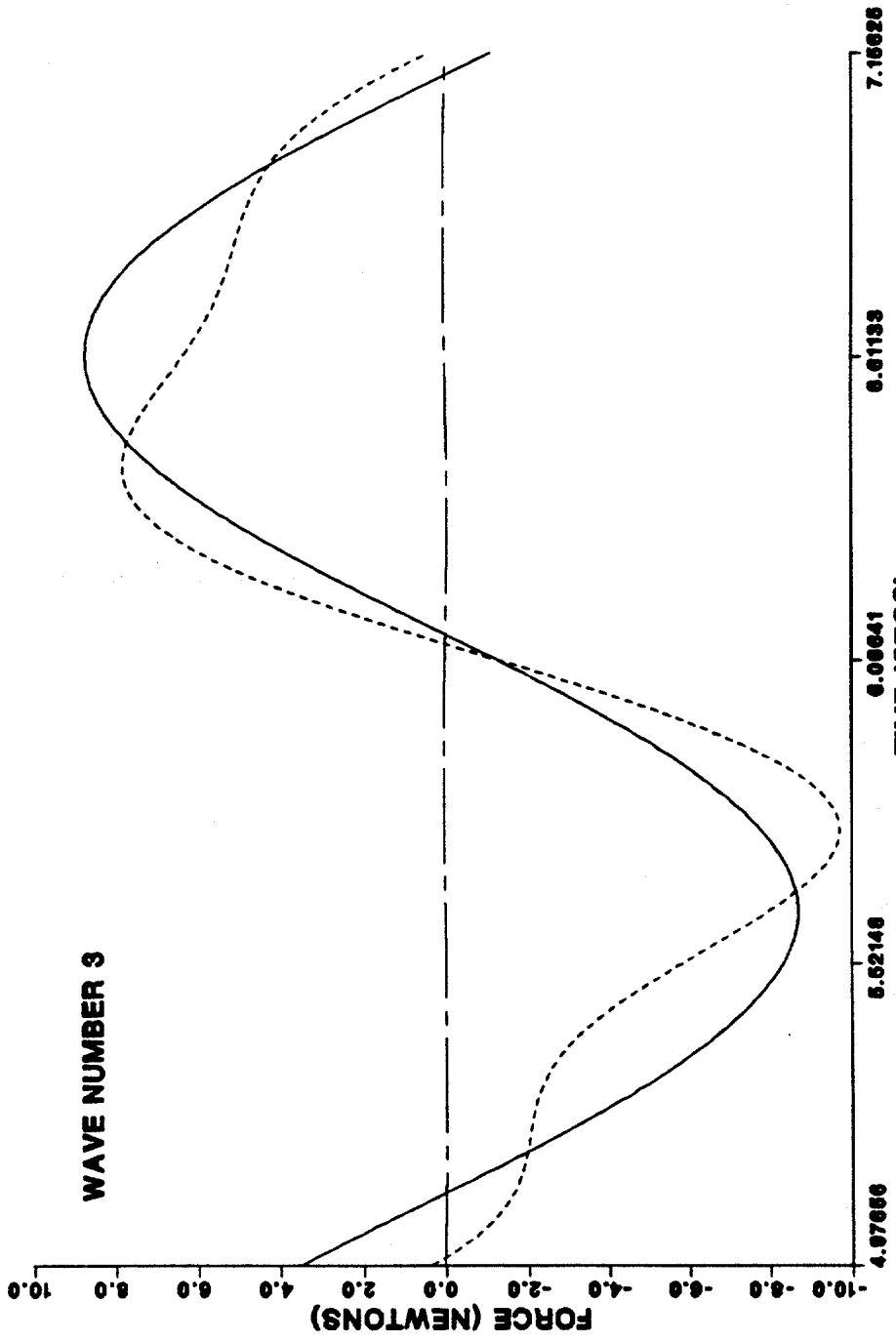

Figure 5.41. Comparison of measured and calculated forces (based on the second model), wave 3 run 2. [Measured ——; Morison with Lighthill correction ---; force residue —·—·—].

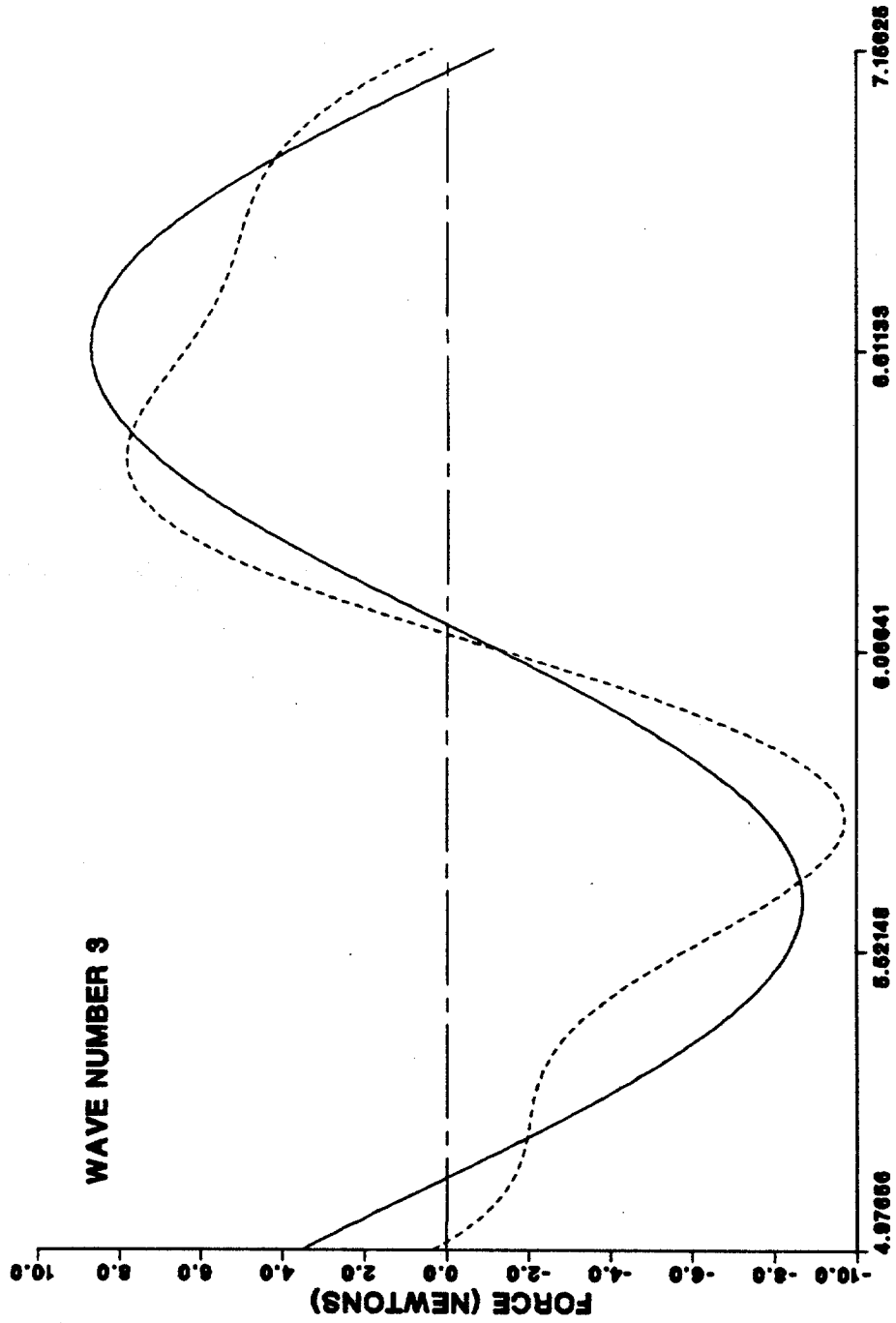

Figure 5.42. Comparison of measured and calculated forces (based on the third model), wave 3 run 2. [Measured ——; Morison with Lighthill correction - - -; force residue —·—].

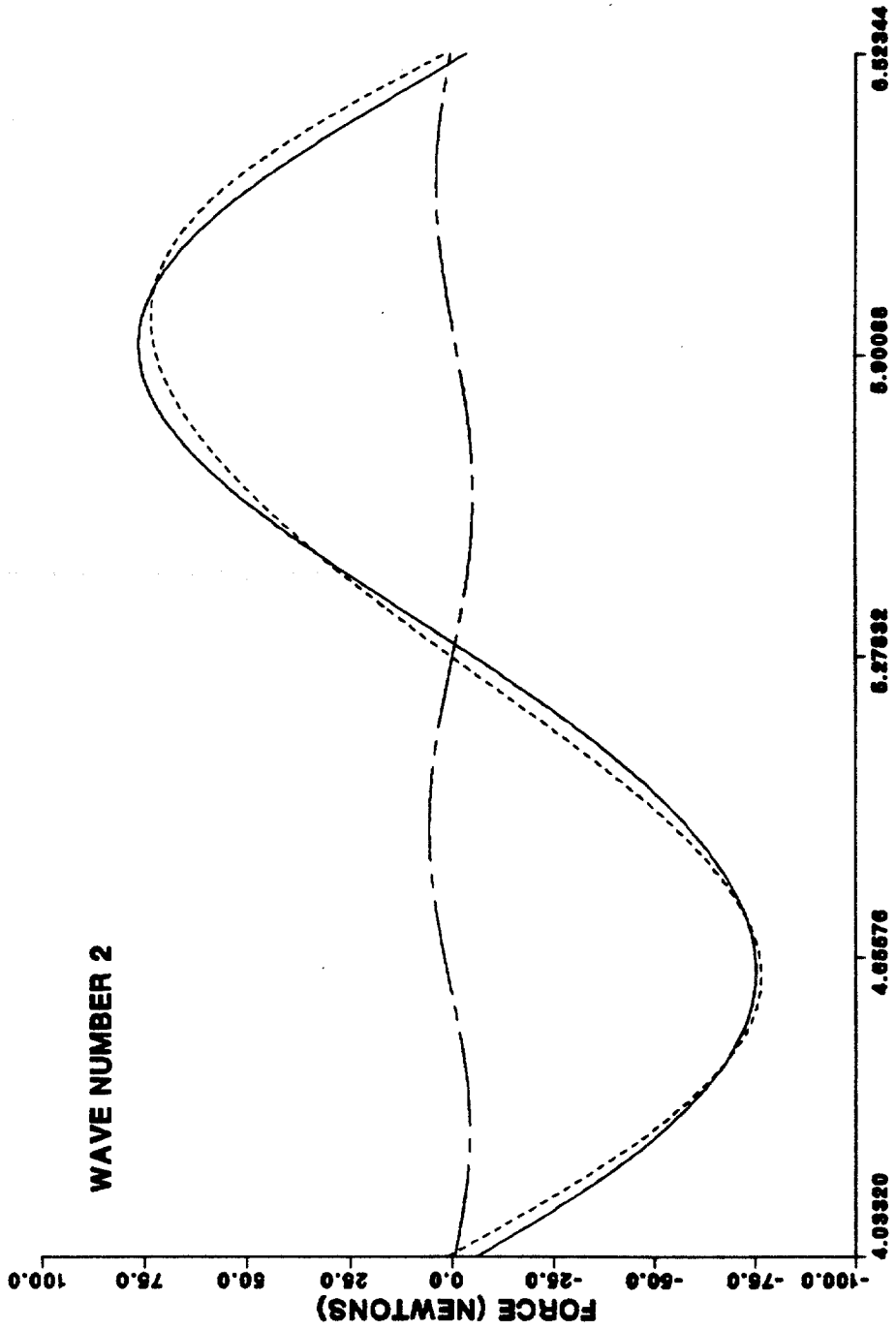

Figure 5.43. Comparison of measured and calculated forces (based on the first model), wave 2 run 5. [Measured ——; Morison with Lighthill correction ---; force residue ——·——].

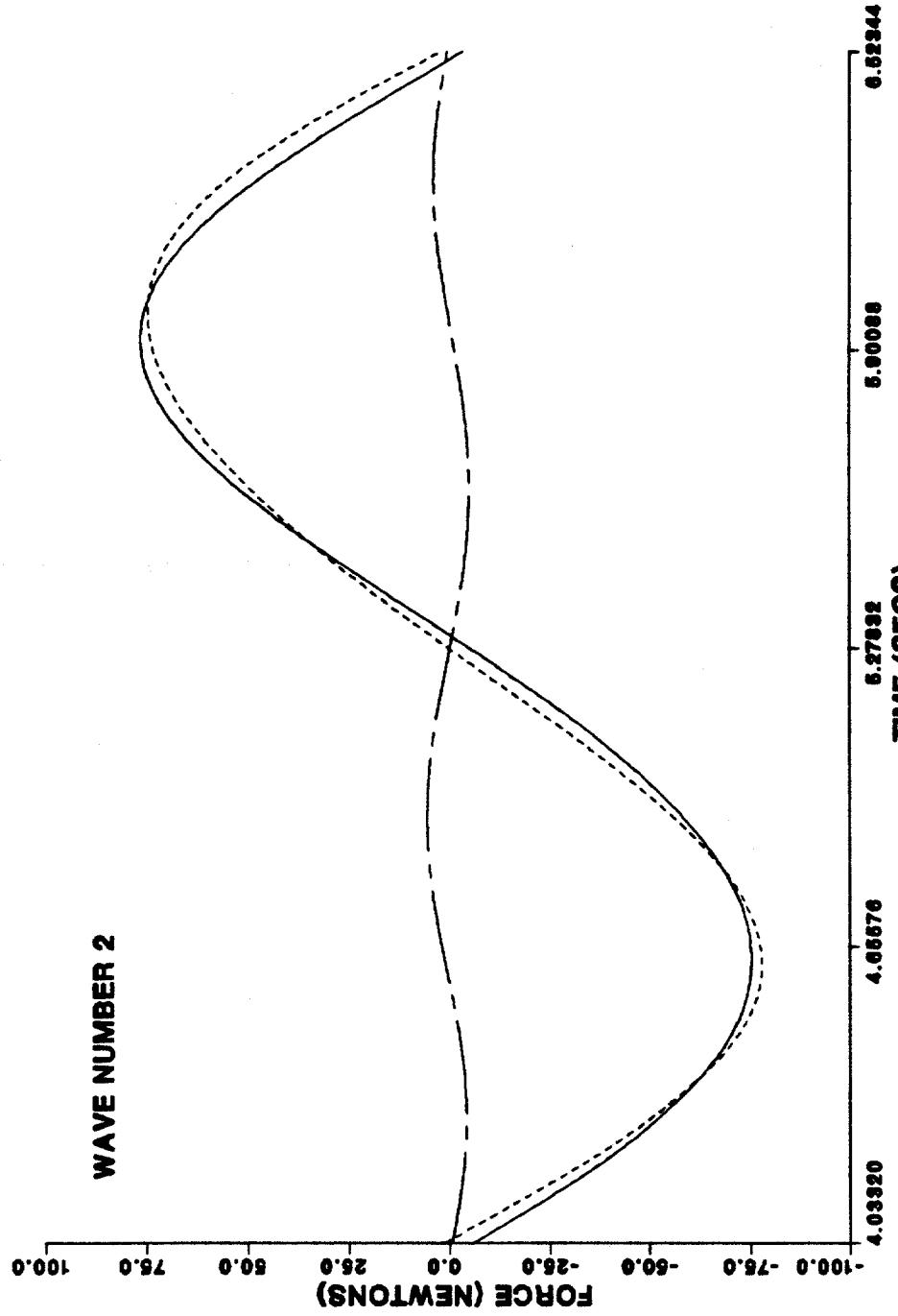

Figure 5.44. Comparison of measured and calculated forces (based on the second model), wave 2 run 5. [Measured ——; Morison with Lighthill correction ---; force residue —·—·—].

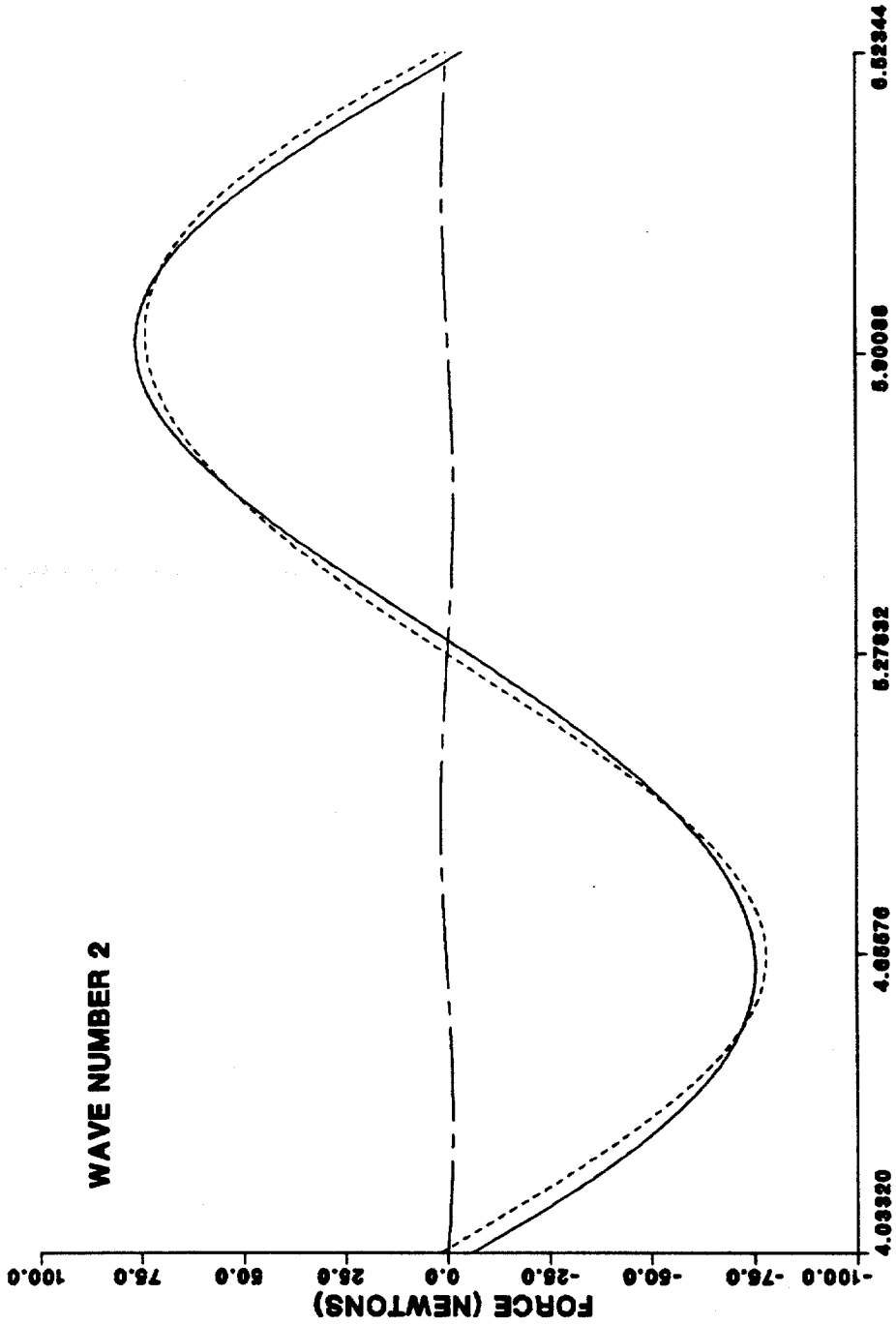

Figure 5.45. Comparison of measured and calculated forces (based on the third model), wave 2 run 5. [Measured ——; Morison with Lighthill correction ---; force residue —·—].

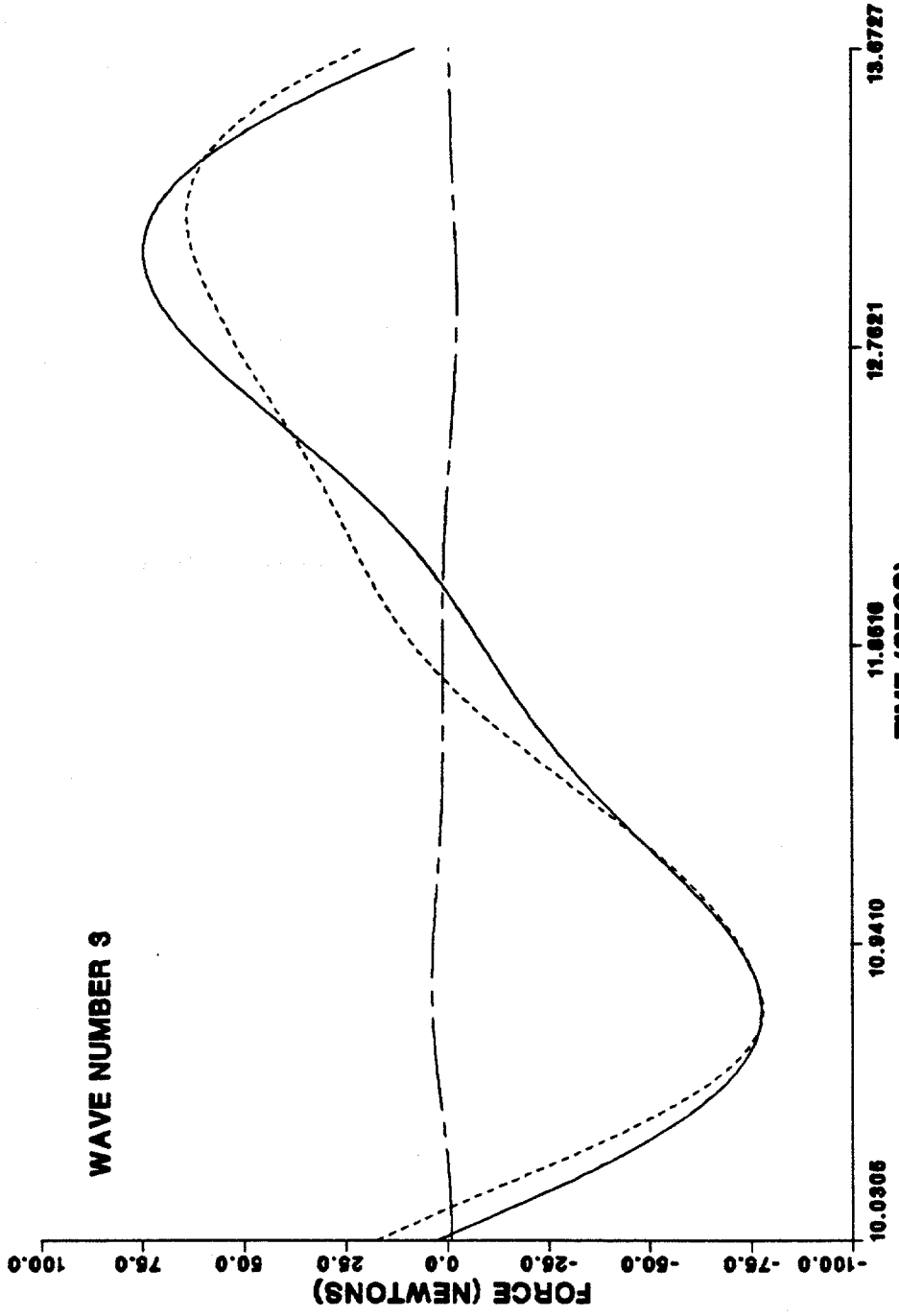

Figure 5.46. Comparison of measured and calculated forces (based on the first model), wave 3 run 22. [Measured ——; Morison with Lighthill correction ---; force residue —·—].

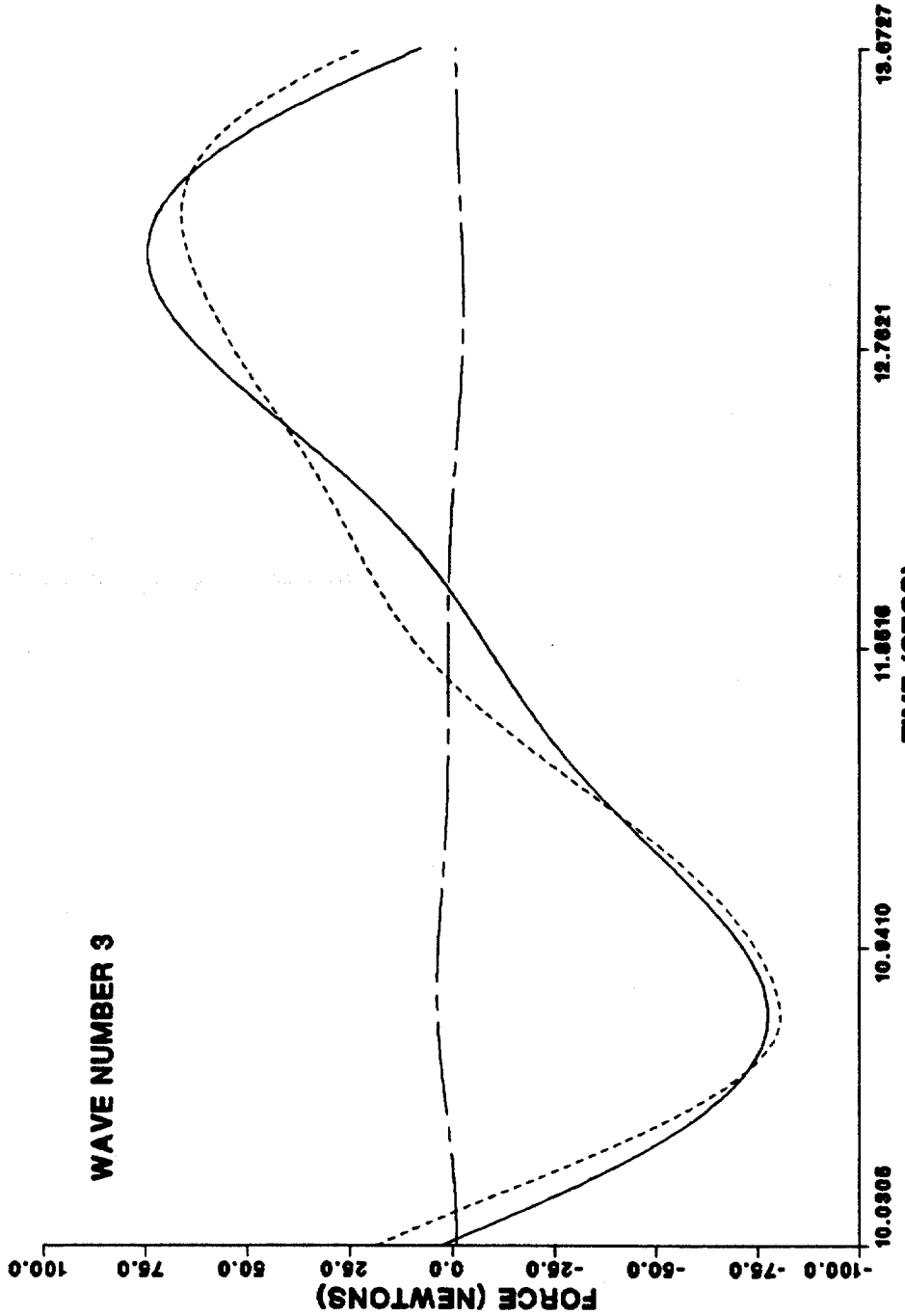

Figure 5.47. Comparison of measured and calculated forces (based on the second model), wave 3 run 22. [Measured ——; Morison with Lighthill correction ---; force residue —·—].

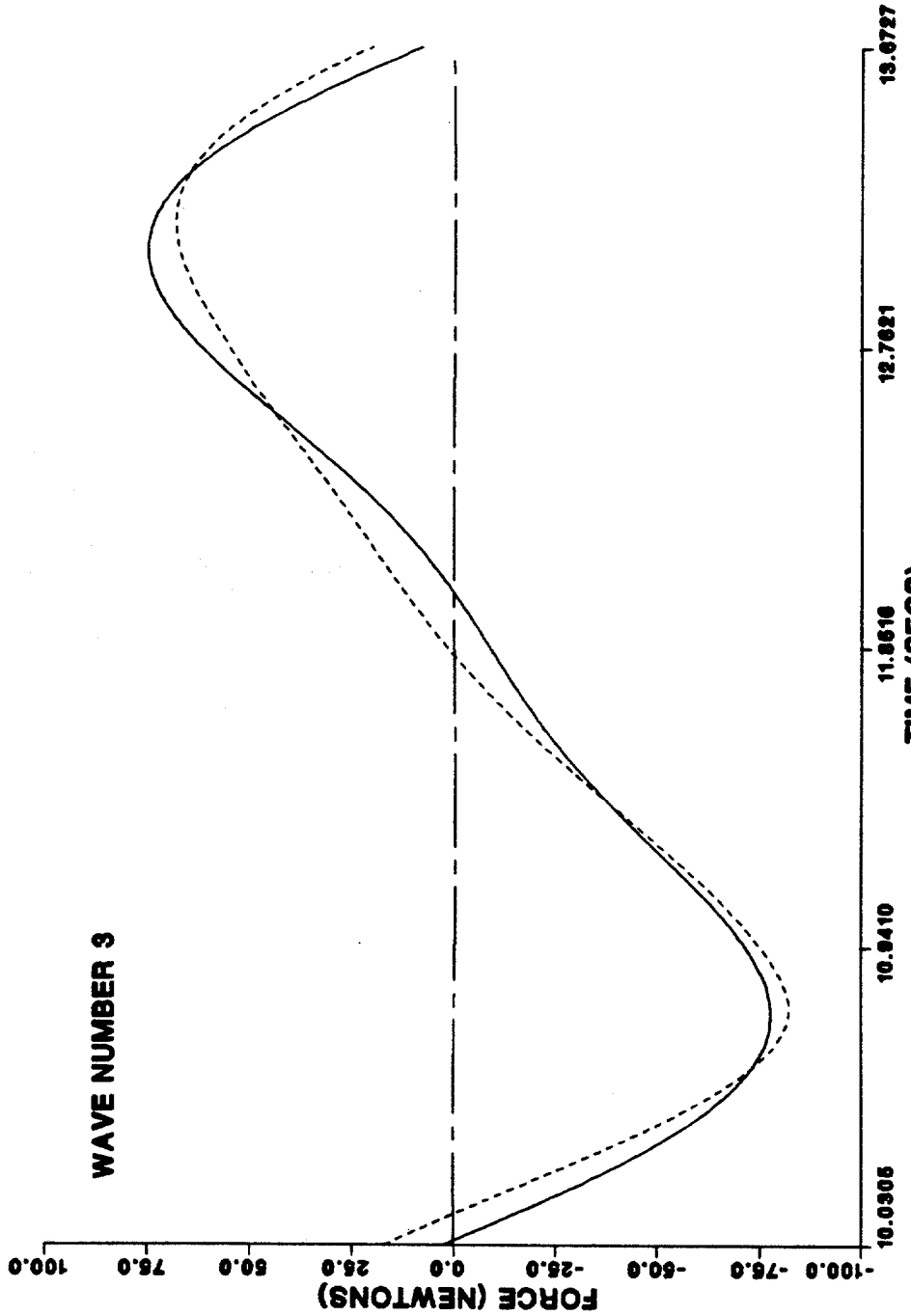

Figure 5.48. Comparison of measured and calculated forces (based on the third model), wave 3 run 22. [Measured ——; Morison with Lighthill correction - - -; force residue —·—·—].

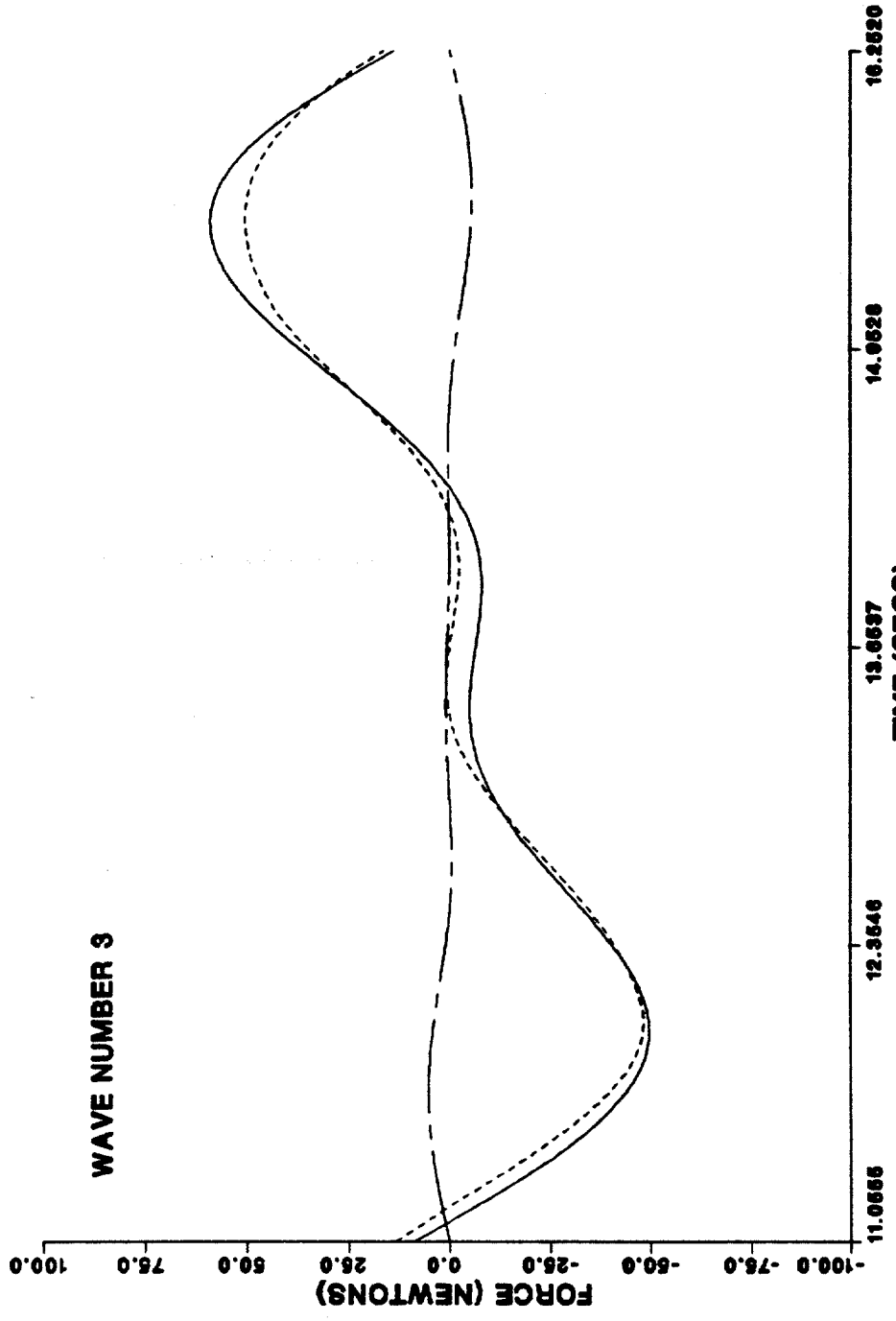

Figure 5.49. Comparison of measured and calculated forces (based on the first model), wave 3 run 20. [Measured ——; Morison with Lighthill correction ---; force residue —·—·—].

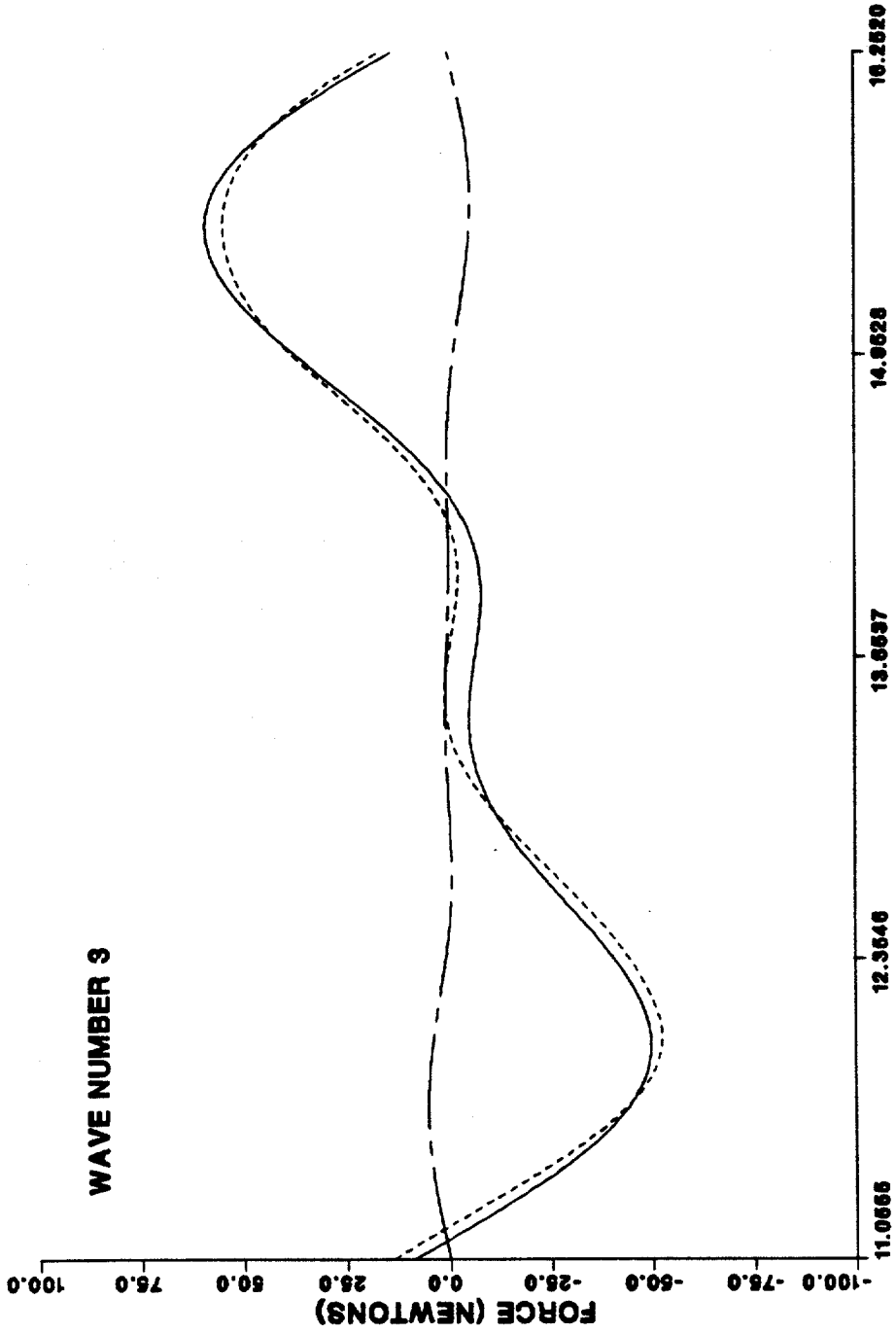

Figure 5.50. Comparison of measured and calculated forces (based on the second model), wave 3 run 20. [Measured ——; Morison with Lighthill correction ---; force residue —·—].

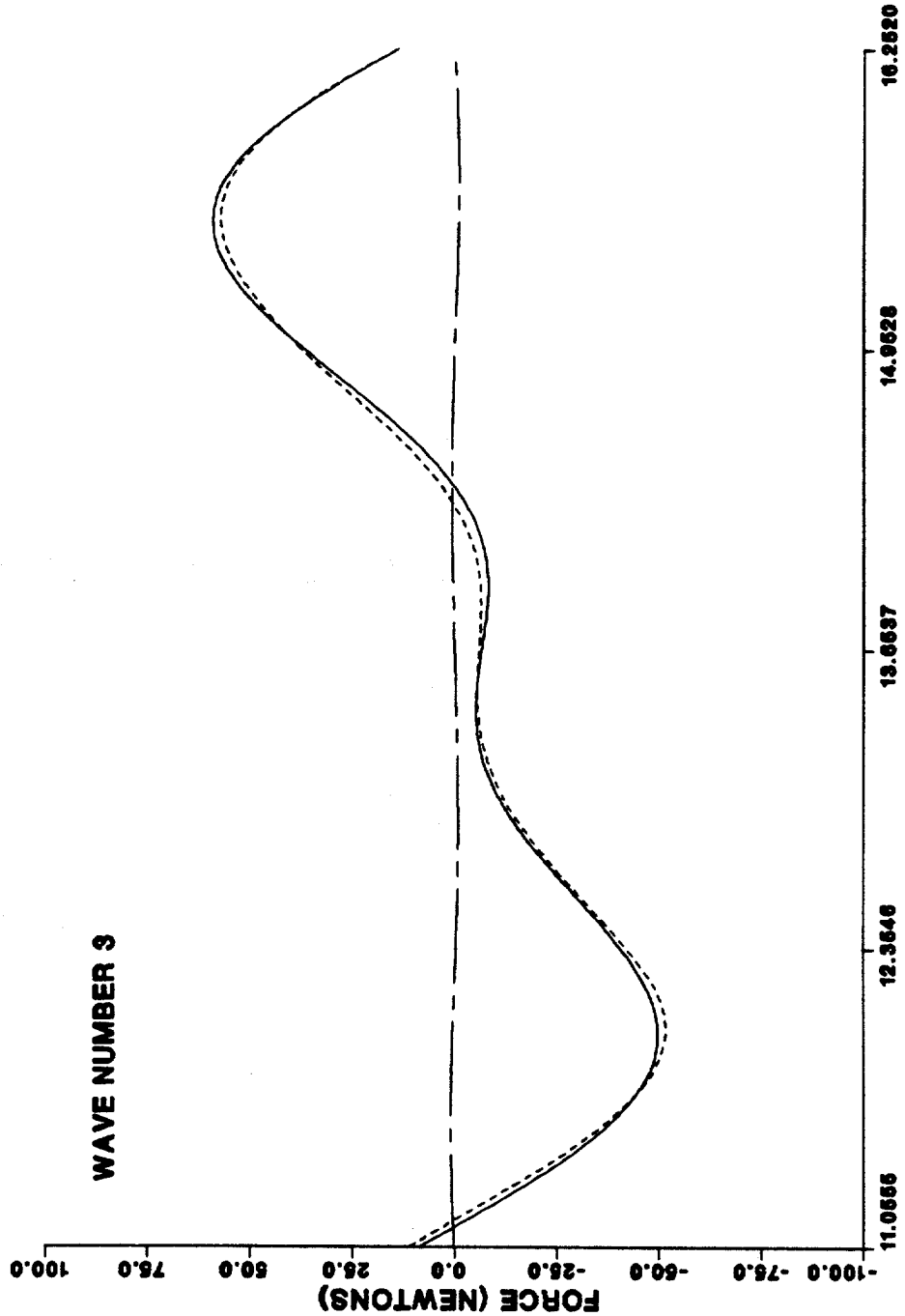

Figure 5.51. Comparison of measured and calculated forces (based on the third model), wave 3 run 20. [Measured ——; Morison with Lighthill correction ---; force residue —·—·—].

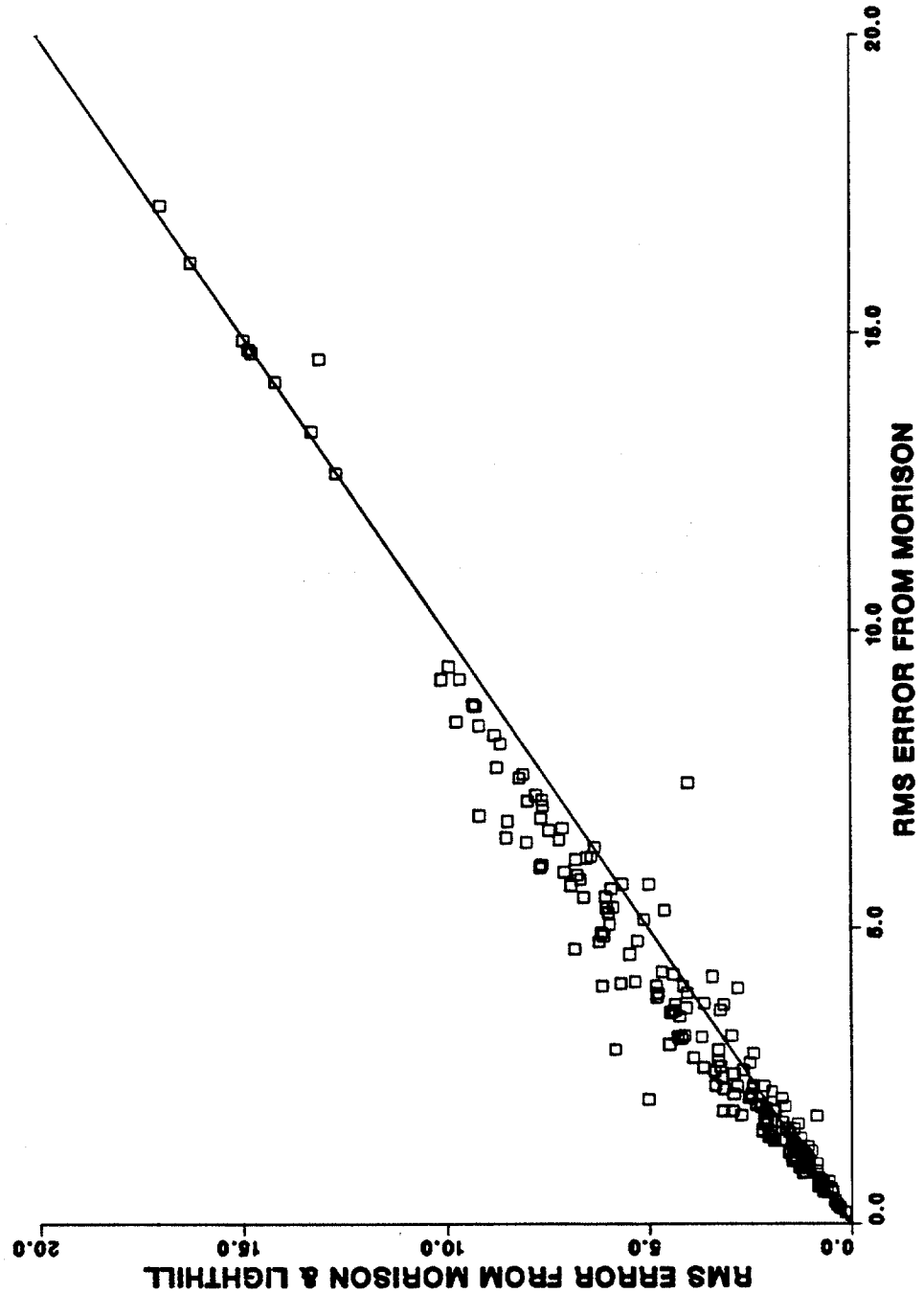

Figure 5.52. rms error from model 1 versus rms error from Morison.

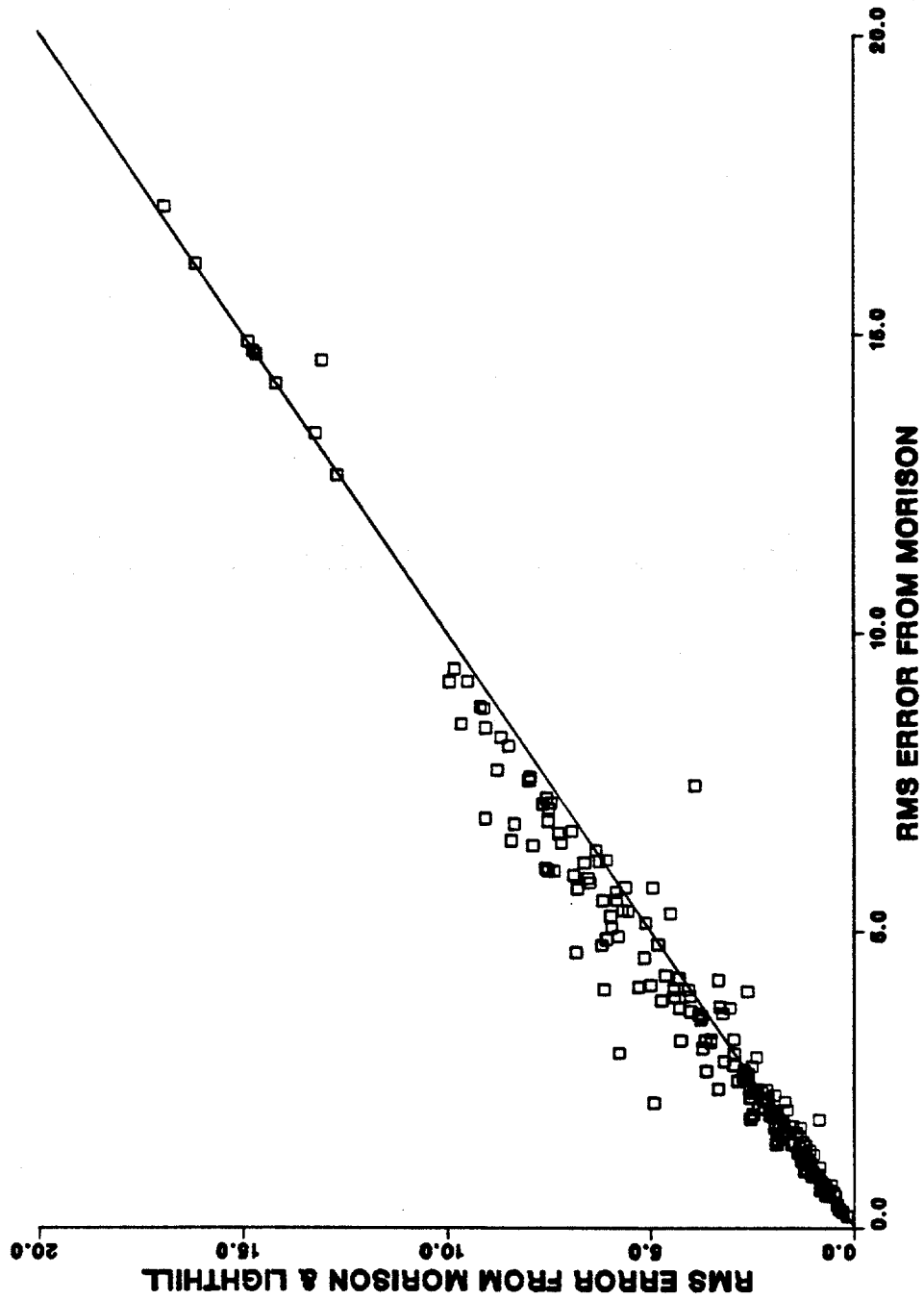

Figure 5.53. rms error from model 2 versus rms error from Morison.

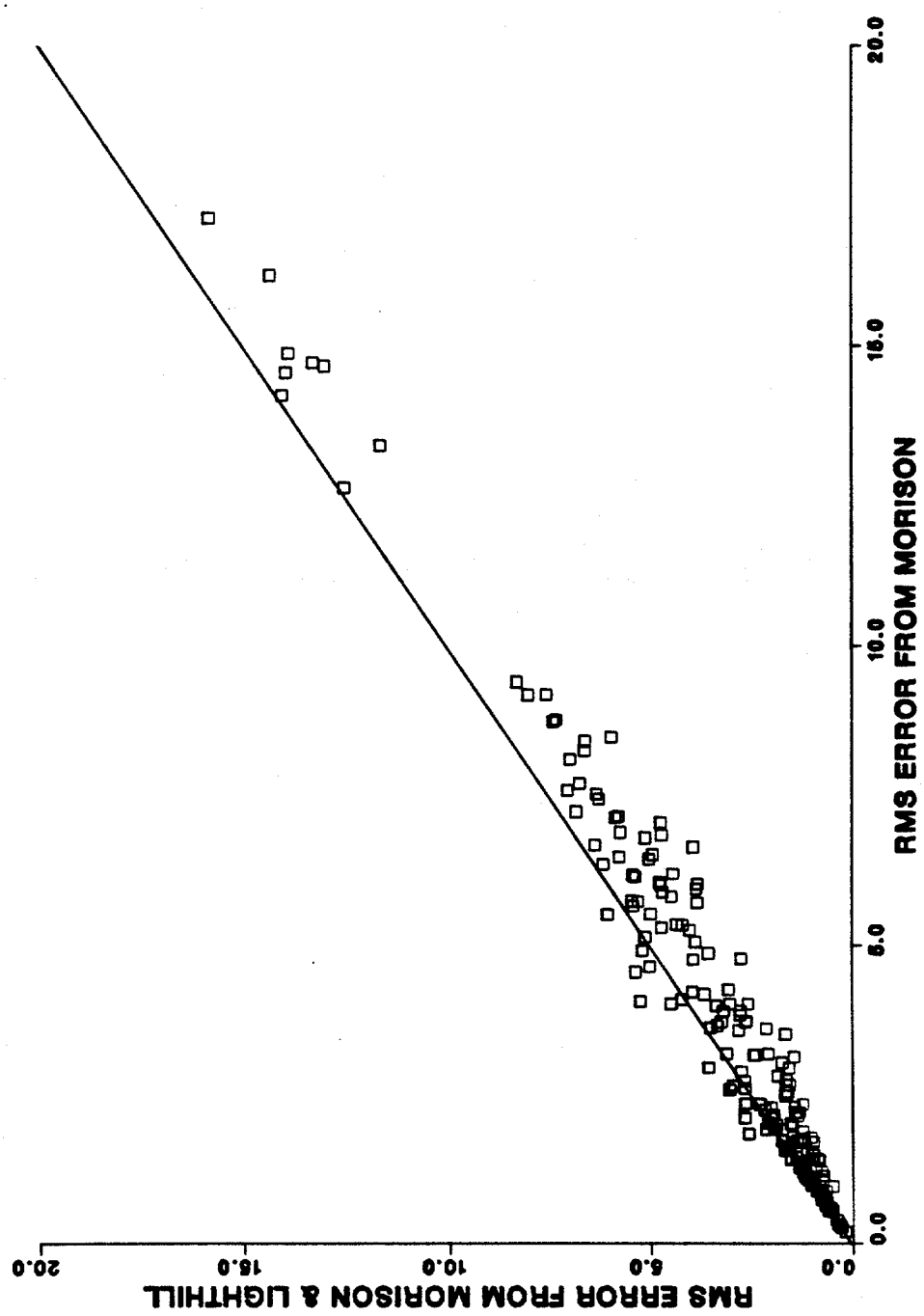

Figure 5.54. rms error from model 3 versus rms error from Morison.

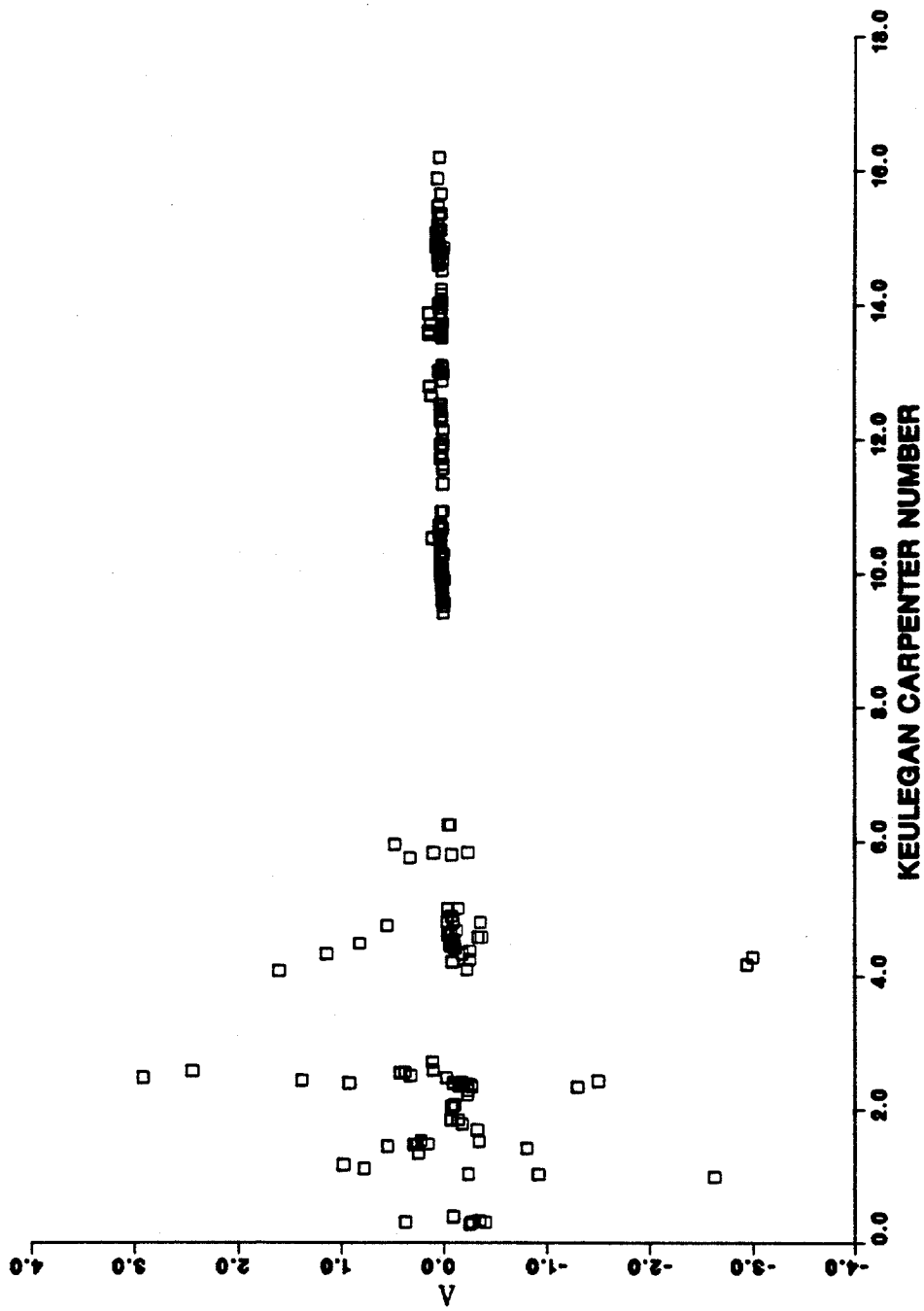

Figure 5.55. Sarpkaya constant Λ versus the Keulegan-Carpenter number.

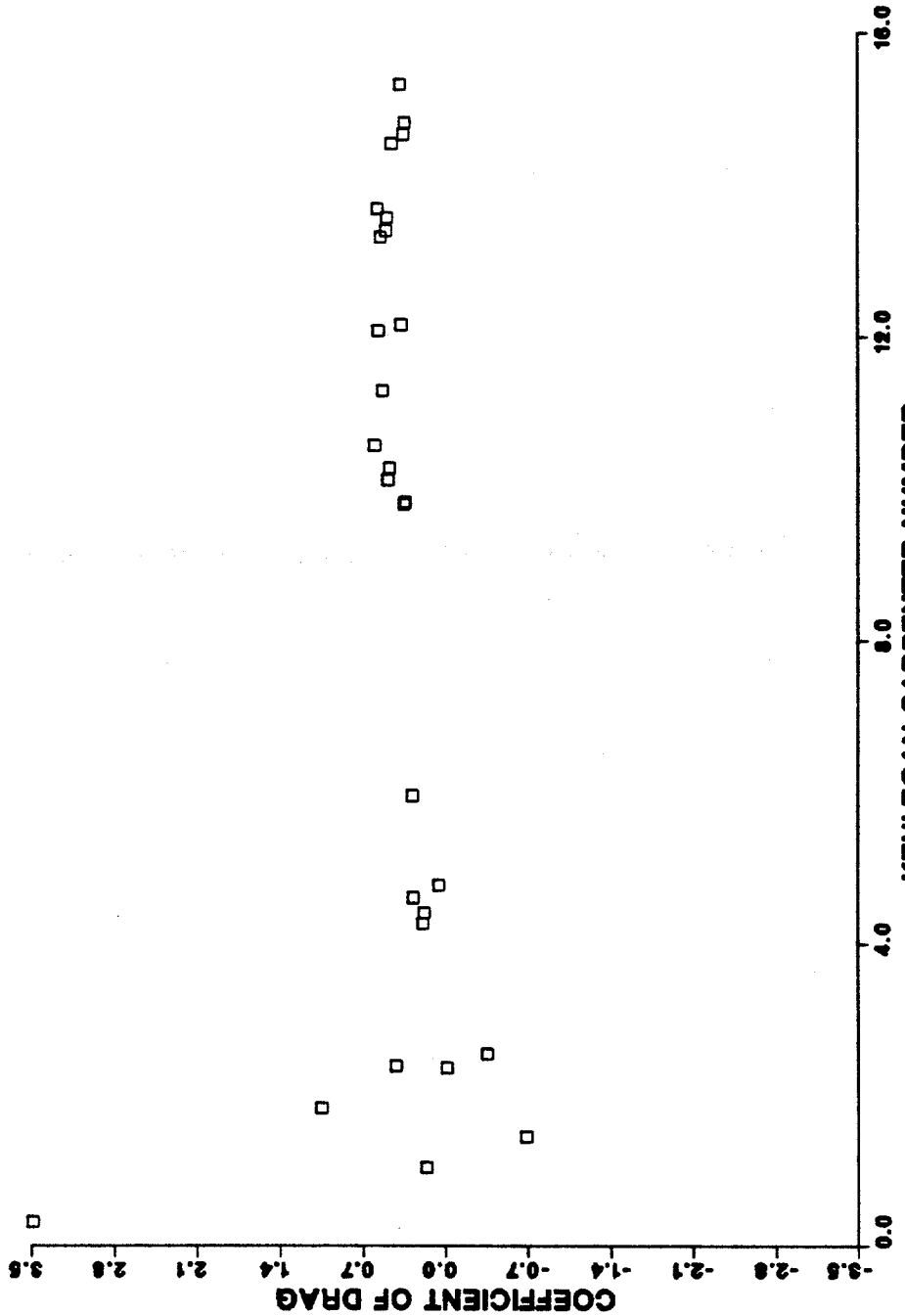

Figure 5.56. Average drag coefficient for each run versus the Keulegan-Carpenter number, from the first Sarpkaya model.

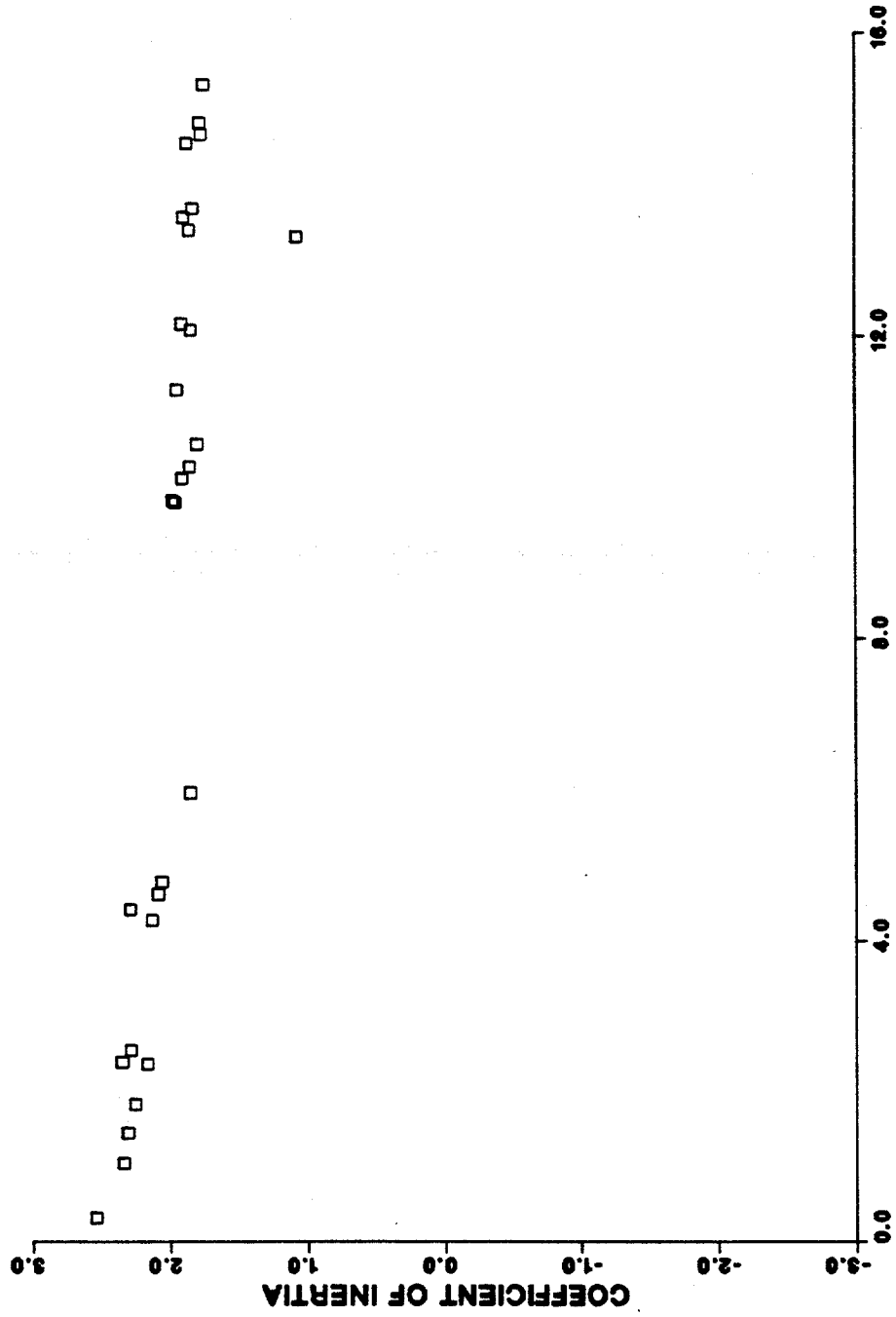

Figure 5.57. Average inertia coefficient for each run versus the Keulegan-Carpenter number, from the first Sarpkaya model.

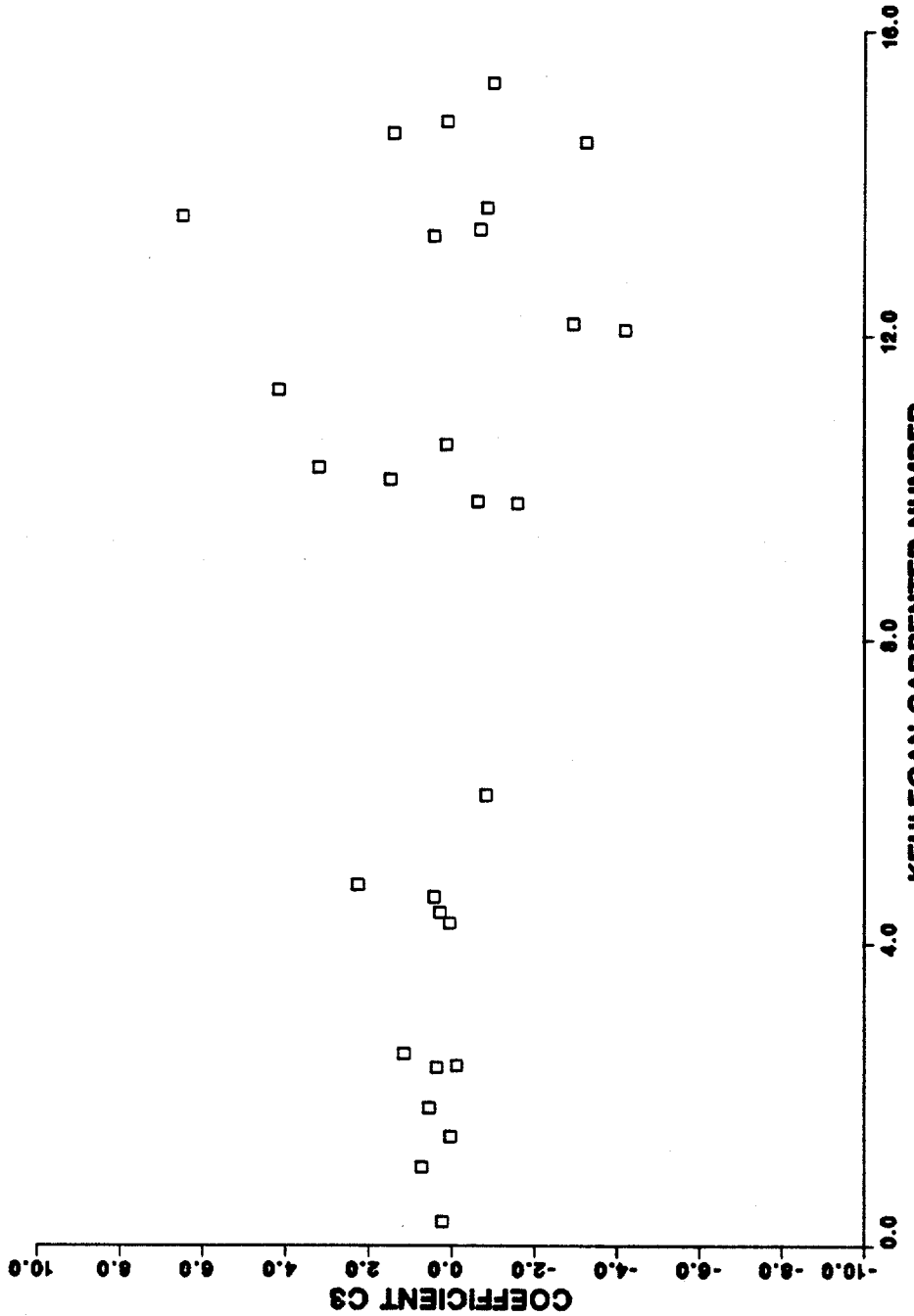

Figure 5.58. Average coefficient C_3 for each run versus the Keulegan-Carpenter number, from the first Sarpkaya model.

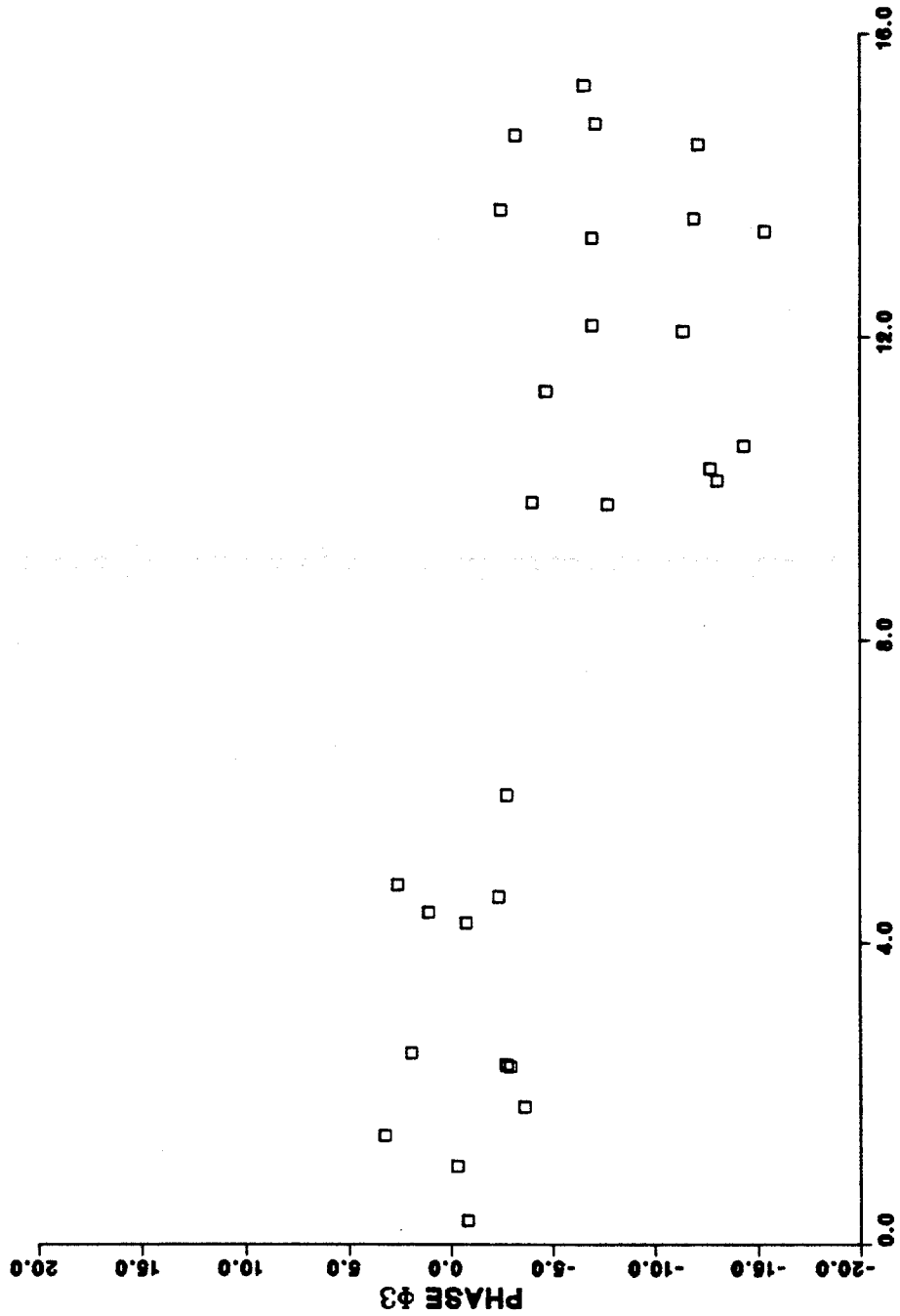

Figure 5.59. Average coefficient Φ_3 for each run versus the Keulegan-Carpenter number, from the first Sarpkaya model.

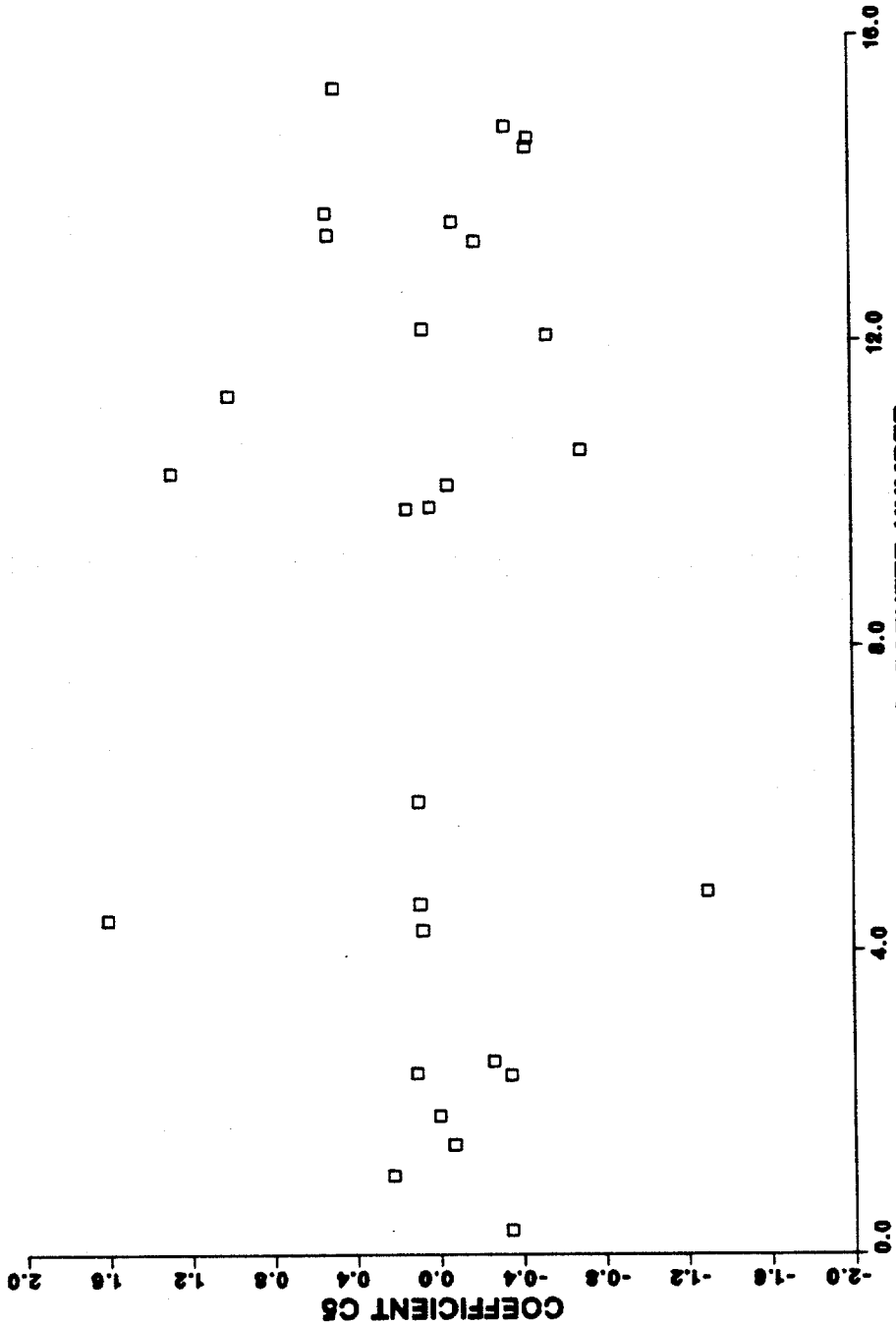

Figure 5.60. Average coefficient C_5 for each run versus the Keulegan-Carpenter number, from the first Sarpkaya model.

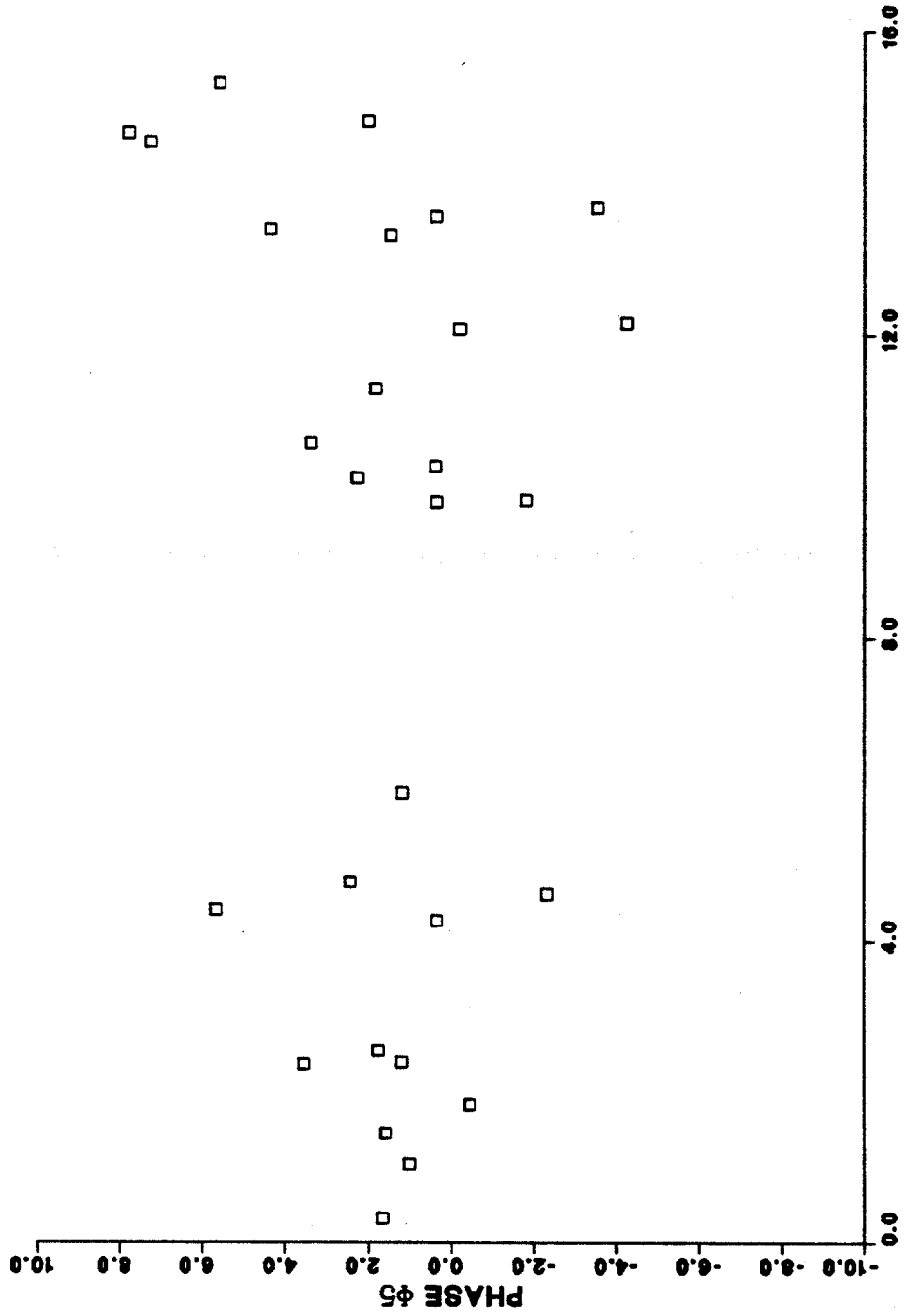

Figure 5.61. Average coefficient Φ_5 for each run versus the Keulegan-Carpenter number, from the first Sarpkaya model.

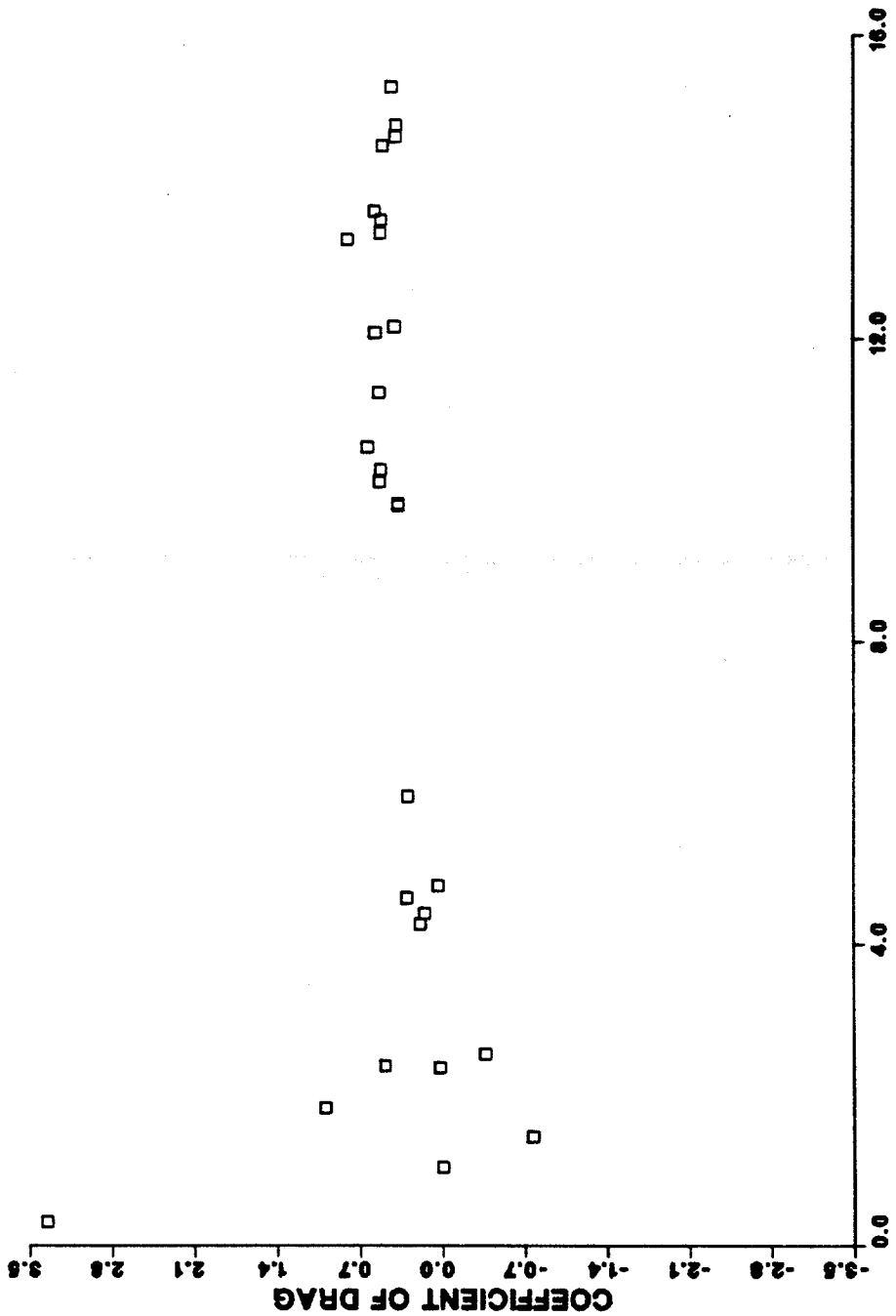

Figure 5.62. Average drag coefficient for each run versus the Keulegan-Carpenter number, from the second Sarpkaya model.

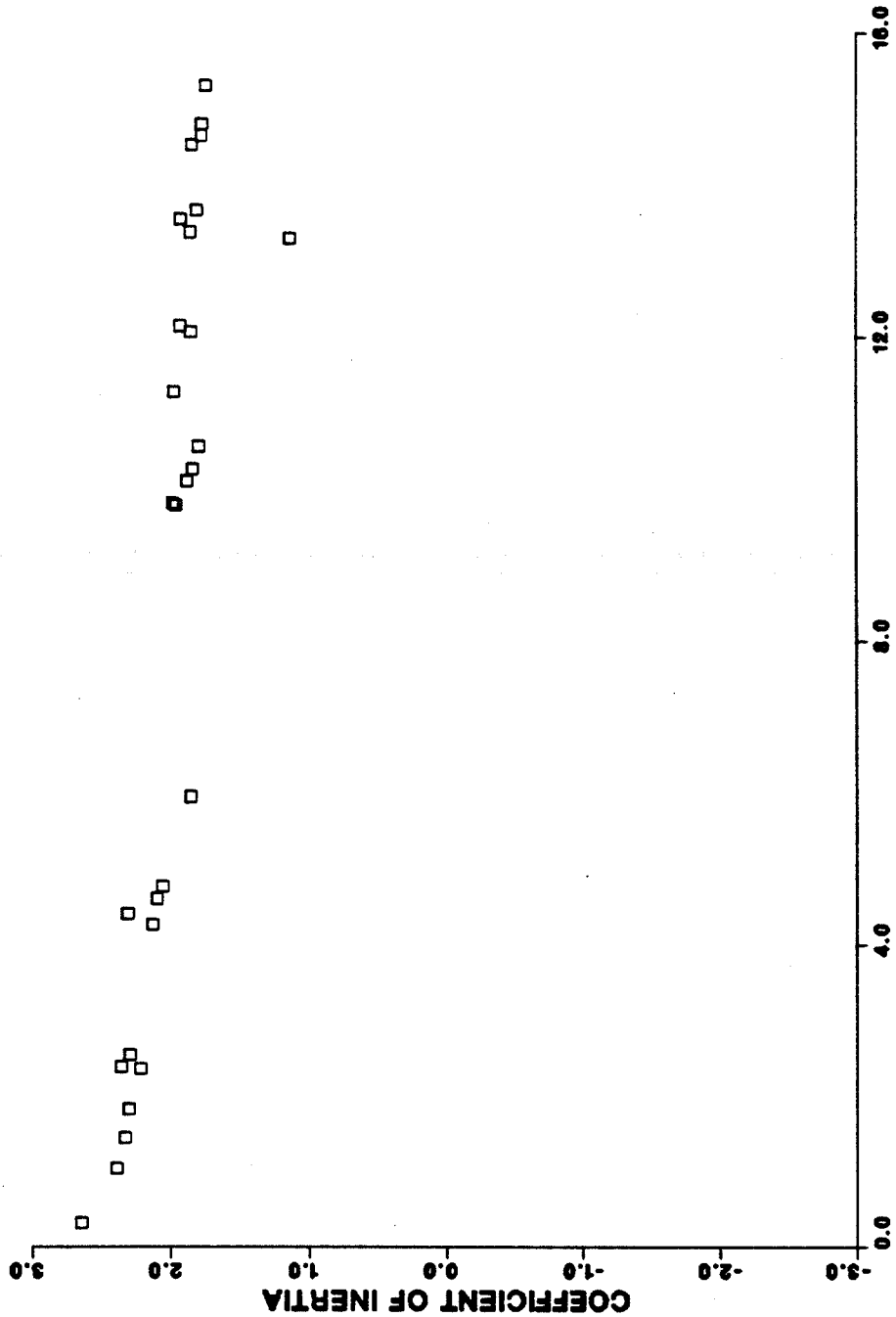

Figure 5.63. Average inertia coefficient for each run versus the Keulegan-Carpenter number, from the second Sarpkaya model.

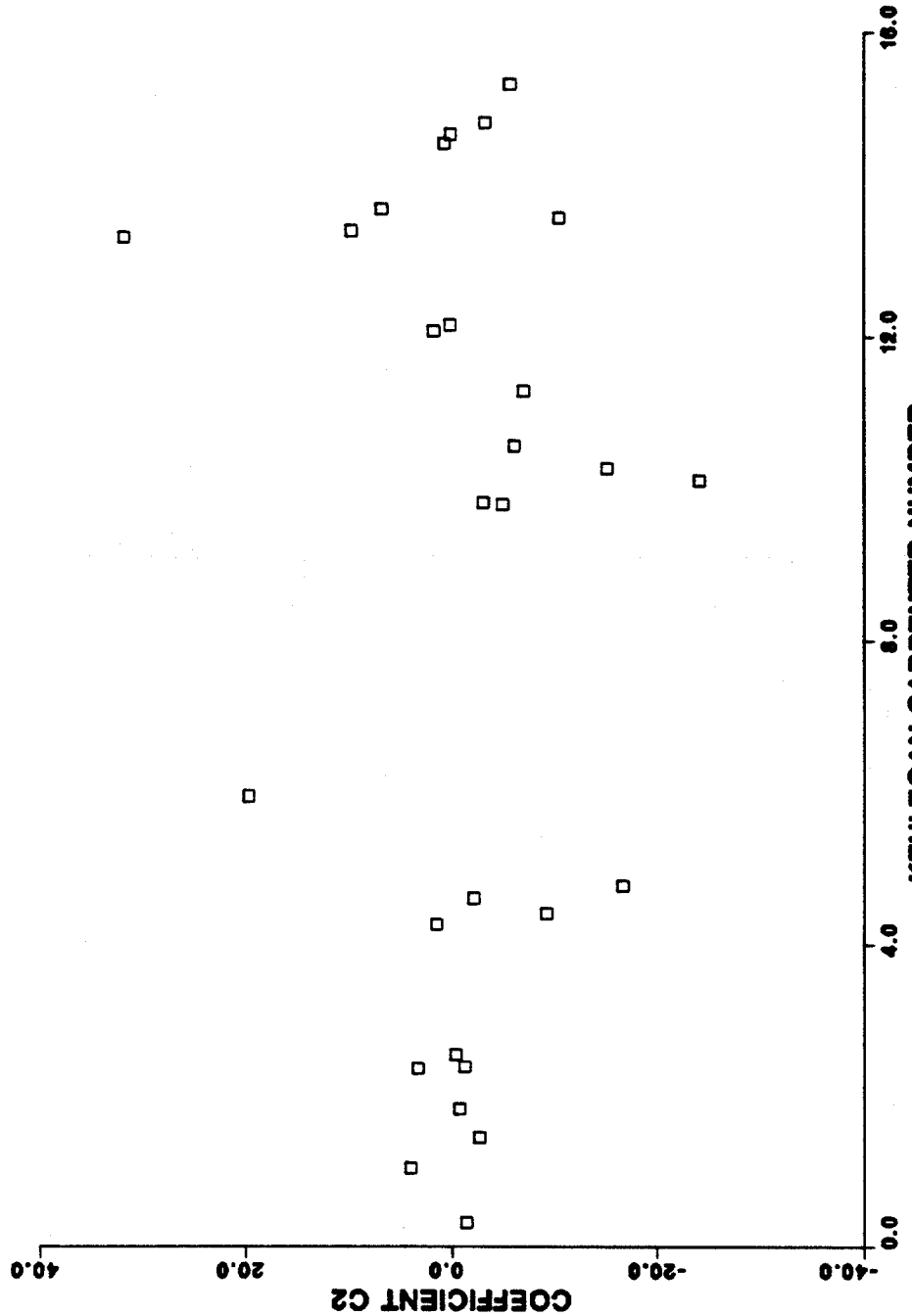

Figure 5.64. Average coefficient C_2 for each run versus the Keulegan-Carpenter number, from the second Sarpkaya model.

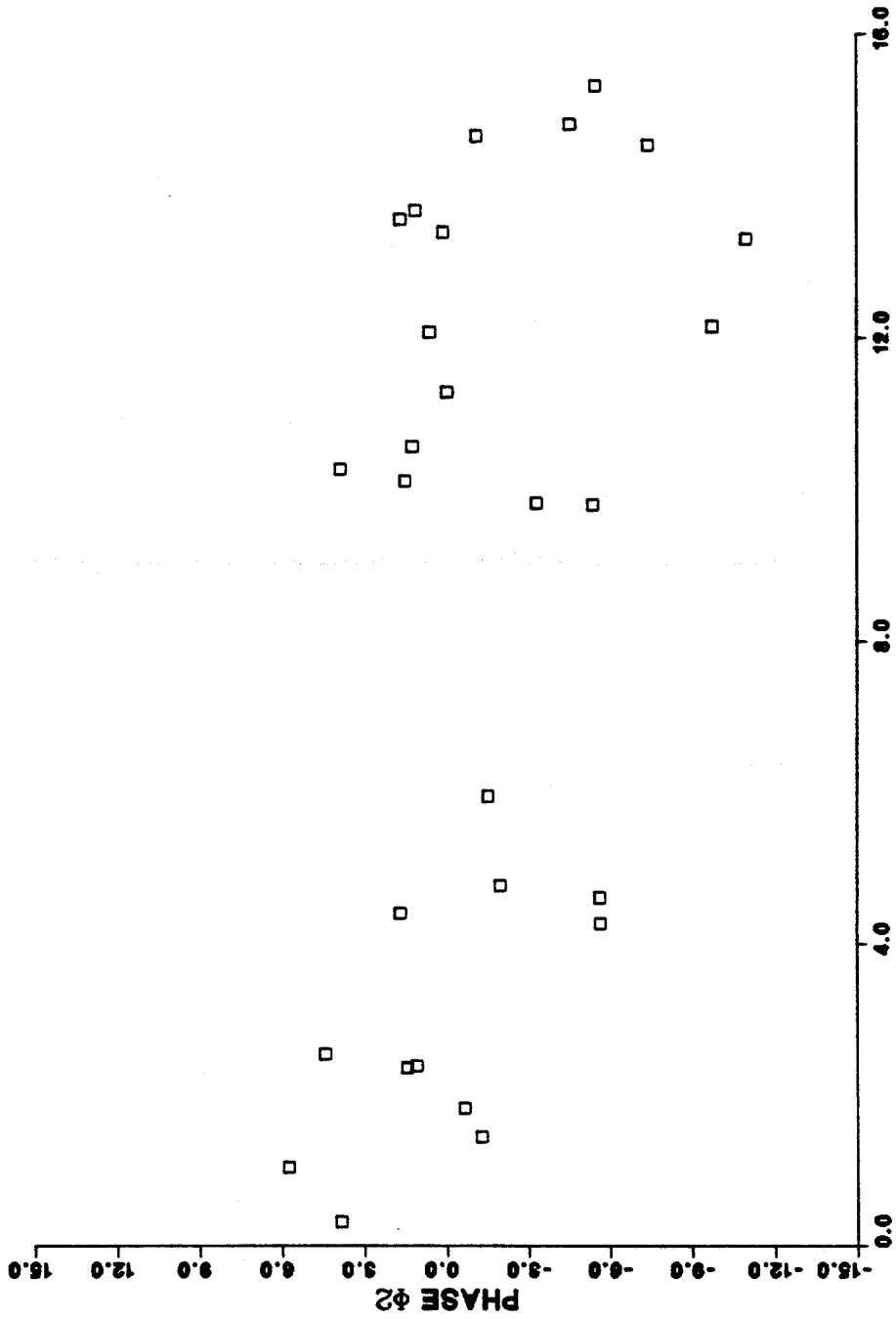

Figure 5.65. Average coefficient Φ_2 for each run versus the Keulegan-Carpenter number, from the second Sarpkaya model.

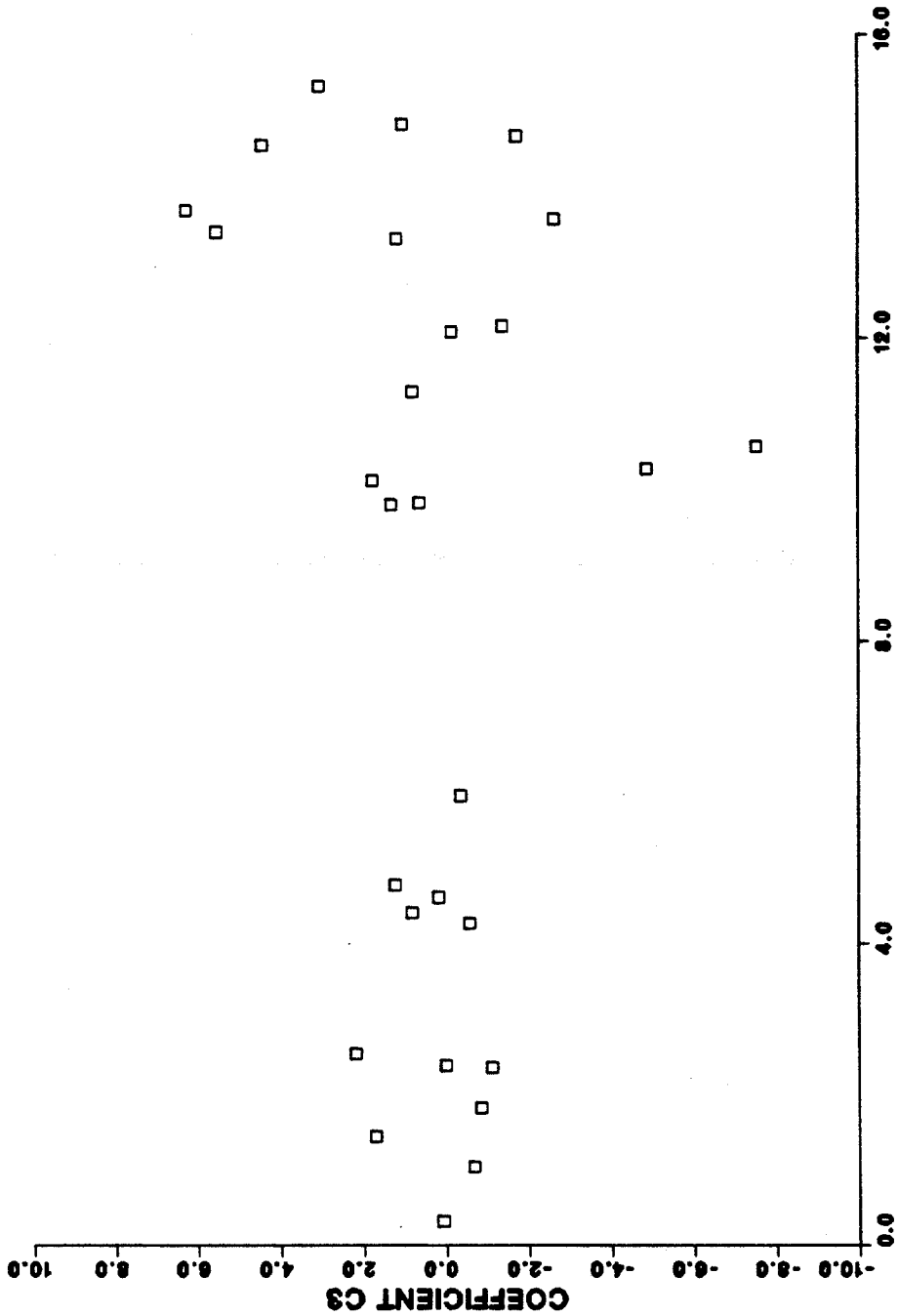

Figure 5.66. Average coefficient C_3 for each run versus the Keulegan-Carpenter number, from the second Sarpkaya model.

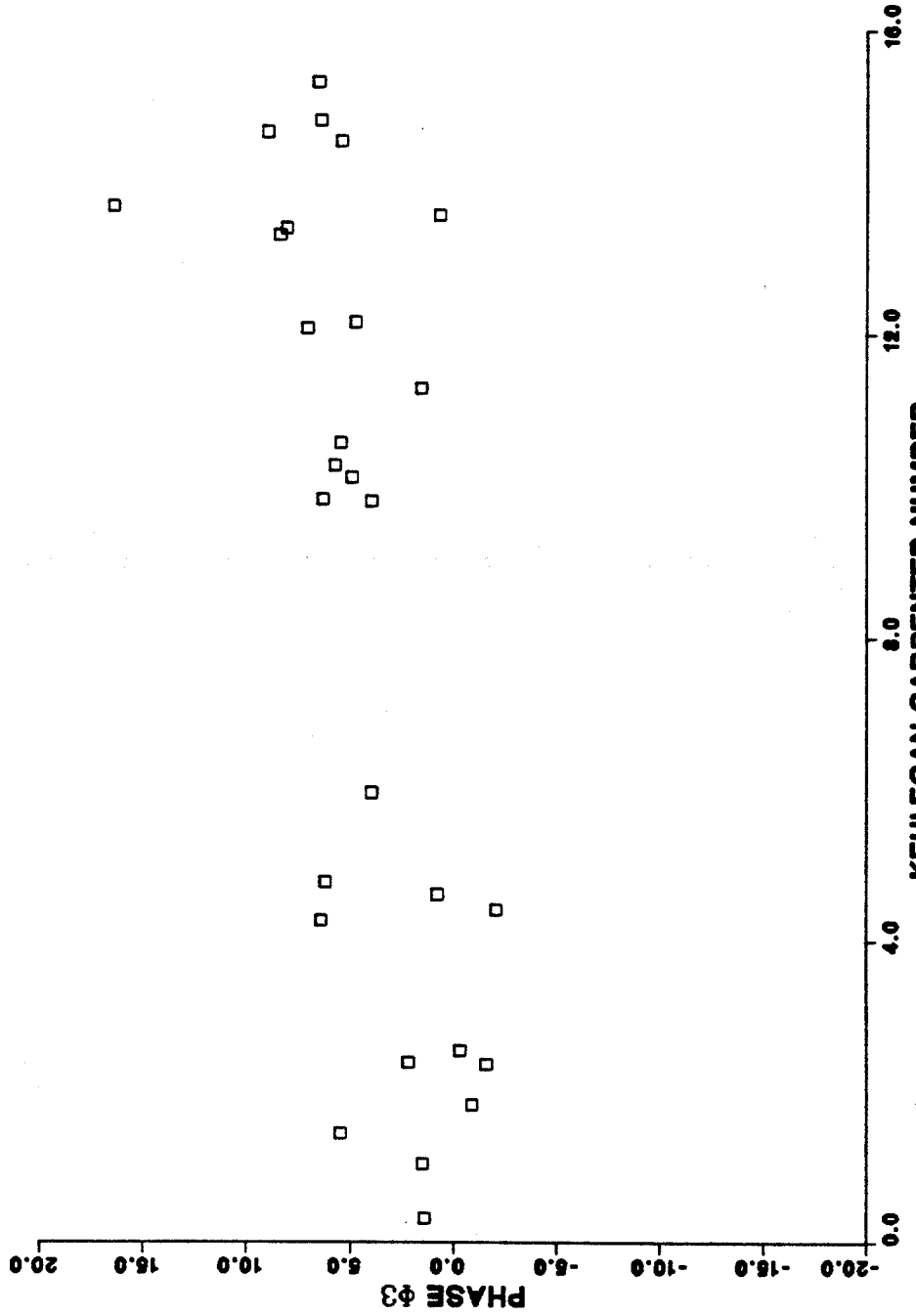

Figure 5.67. Average coefficient Φ_3 for each run versus the Keulegan-Carpenter number, from the second Sarpkaya model.

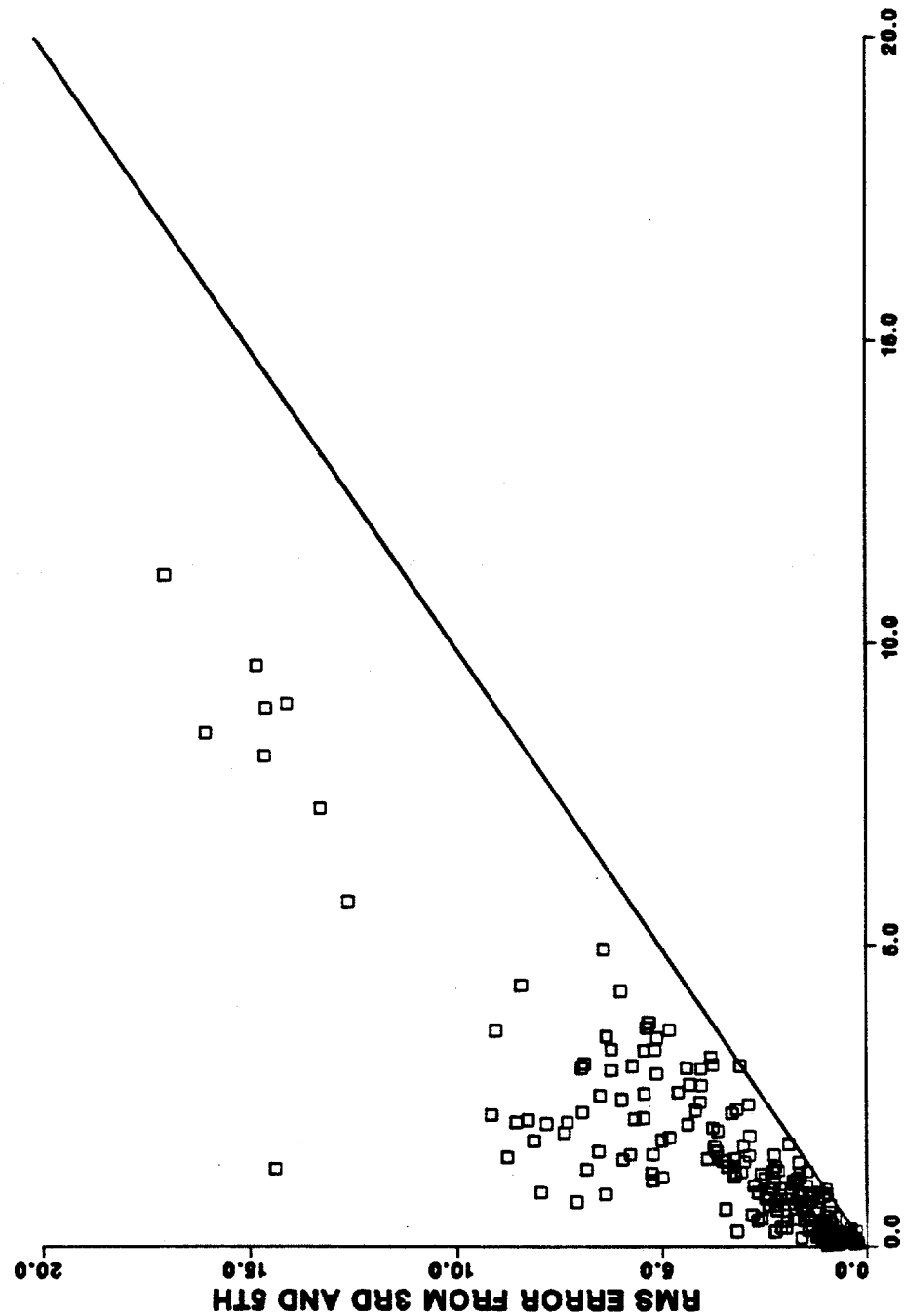

Figure 5.68. rms error from the first Sarpkaya model versus the rms error from the second Sarpkaya model.

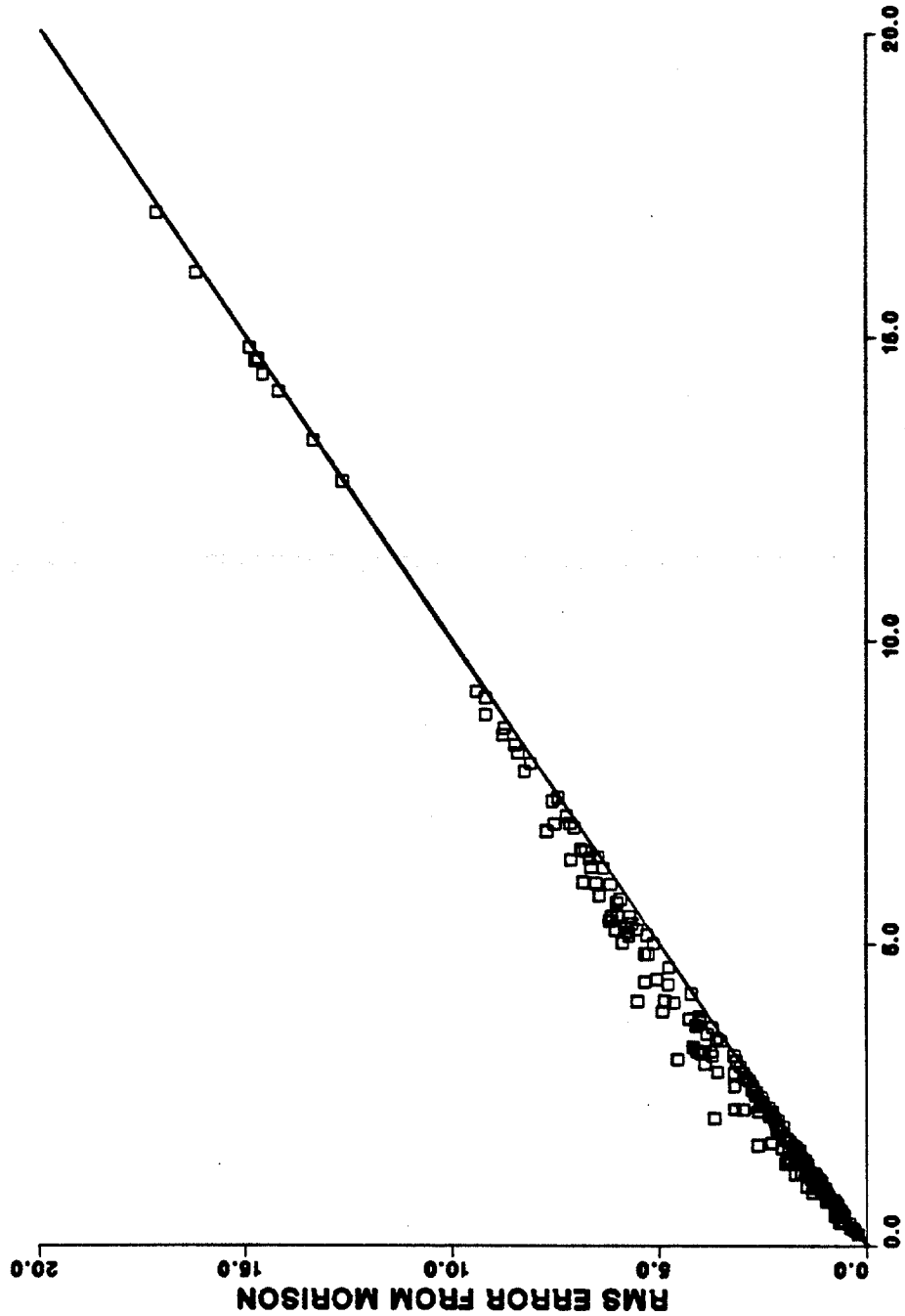

Figure 5.69. rms error from the Morison equation versus the rms error from the first Sarpkaya model.

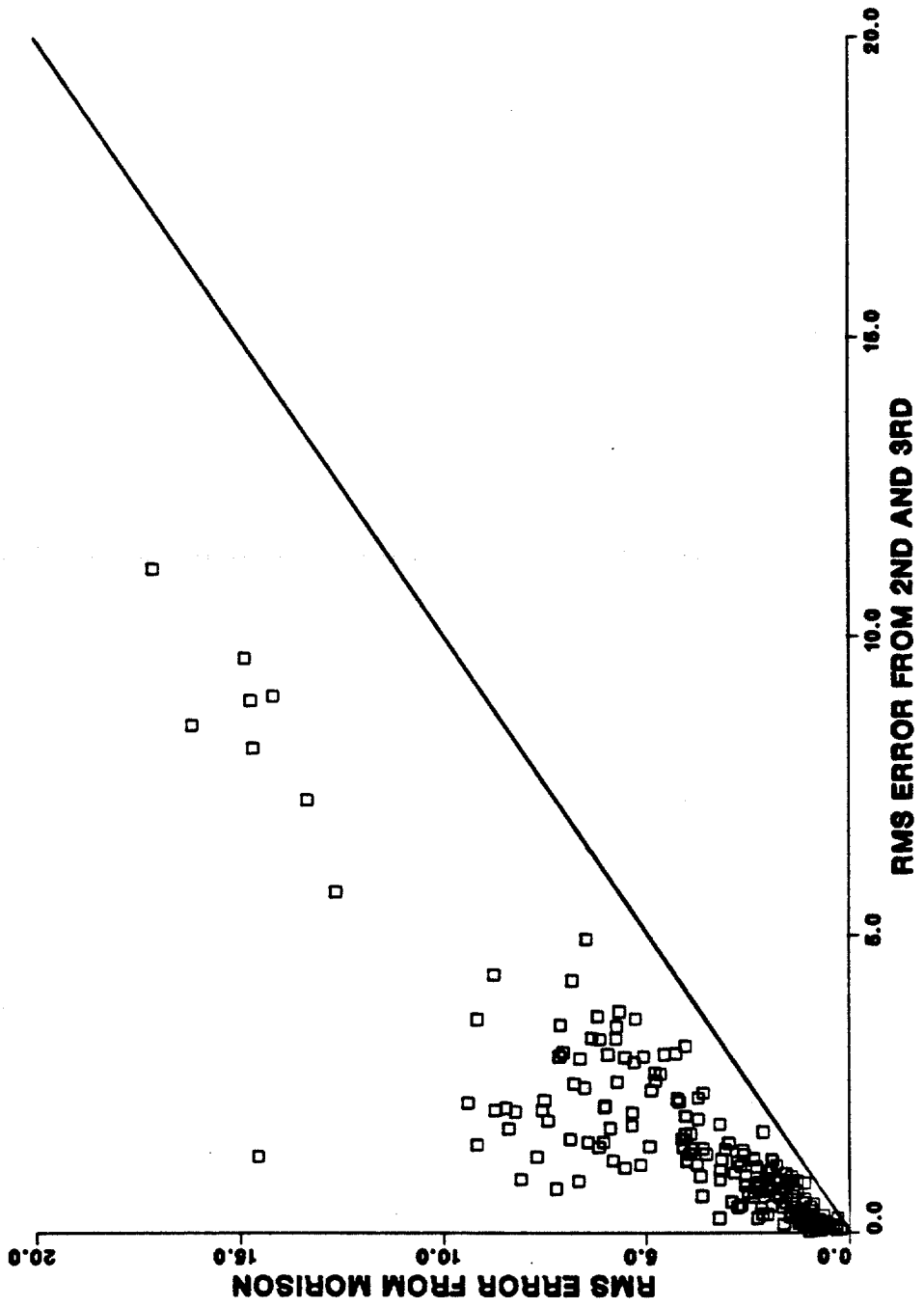

Figure 5.70. rms error from the Morison equation versus the rms error from the second Sarpkaya model.

CHAPTER SIX

DATA ANALYSIS AND ESTIMATION OF CORRECTION TERMS FOR THE RANDOM FLOW

This chapter deals with the analysis of the random experimental data described in Section 4.3 and the evaluation of the Lighthill correction for these data.

6.1 Estimates of the Forces Based on the Morison Equation

Least squares analyses of the total smoothed time histories of the measured forces, velocities, and accelerations were performed to estimate the drag and inertia coefficients in the Morison equation. The values so obtained were Cd = 0.2345 and Cm = 1.8295 for the lower level and Cd = 0.5393 and Cm = 2.0502 for the upper level. Using these time invariant drag and inertia coefficients the force time histories were regenerated using:

1. The Morison equation in conjunction with the total measured horizontal velocity and acceleration.
2. The Morison equation in which the drag term was linearized (equation 2.47), in conjunction with the total measured velocity and acceleration.
3. The Morison equation in which the drag term was neglected, in conjunction with the total measured acceleration.
4. The Morison equation in terms of the wave elevation and linear wave theory (equation 2.48), in conjunction with the total measured wave elevation.

The regenerated force time histories are shown in figures 6.1 to 6.8, where the full lines represent the measured force spectra and the dash lines represent the calculated force spectra. The spectra were obtained by using IMSL routine FTFPS which calculates the spectrum by fast Fourier transformation of the autocorrelation function. The analysis of the data showed that the effective Keulegan-Carpenter number was 5.75 for the lower level and 6.00 for the upper level (see section 4.3). From these KC numbers it would be expected that the flow conditions would be inertia-dominated approaching the inertia/inertia-drag transition (see section 2.3.1).

Figure 6.1 shows the measured force spectrum at the lower level and the calculated force spectrum based on the first force model. It is seen that the Morison equation with time invariant coefficients provides an excellent fit to the measured force history at the first level. A similar conclusion for the upper level follows from figure 6.2, which shows that the largest discrepancy is about 5% and occurs at the spectral peak. It is concluded that, for the Delft data, the Morison equation with time invariant coefficients provides an excellent fit to the measured forces.

Figure 6.3 shows the measured force spectrum and the force spectrum calculated using the linearized version of the Morison equation (equation 2.47). There is excellent agreement between the measured and calculated spectra. The linearization does not seem to alter the Morison equation spectrum drastically. This was expected because figures 4.65 and 4.66 showed that linearization

provided an excellent fit to the nonlinear drag term. The largest difference is about 3% and occurs at the spectral peak frequency. The same result can be observed in figure 6.4 for the upper level.

Figures 6.5 and 6.6 show the measured force spectra and the force spectra calculated by neglecting the drag term. Very little difference can be observed between the calculated inertia spectrum and the total Morison spectrum (figure 6.1) for the lower level. At the upper level the difference is more noticeable at the spectral peak frequency. This was expected, since at this level the drag is more significant.

Figures 6.7 and 6.8 show the measured spectra and the calculated spectra based on equation 2.48. For the lower level the forces calculated using linear wave theory are in excellent agreement with the measured forces. The result for the upper level based on linear wave theory still provides a reasonable estimate for the total measured forces but the difference between the measured and calculated spectra is in this case more noticeable.

6.2 Estimates of the Forces Based on the Morison Equation with the Lighthill Correction Term

Least squares analyses were also performed to obtain the drag and inertia coefficients when the Lighthill correction term was included in the calculation of the forces. The coefficients obtained from the analyses were Cd = 0.2341, Cm = 1.8343 for the lower level and Cd = 0.5403, Cm = 2.0587 for the upper level. When these results are compared to the values obtained by using the Morison equation alone it can be seen that the Lighthill correction

term has very little effect on the magnitudes of the drag and inertia coefficients. This result would indicate that the Lighthill correction is not a significant proportion of the total force. This is also borne out by the measured force spectra (full line) and the calculated force spectra (dashed lines) shown in figure 6.9 for the lower level and figure 6.10 for the upper level. Indeed, it can be seen that the addition of the Lighthill correction does not change significantly the calculated spectra with respect to their values based on the Morison equation with no correction (see figures 6.1 and 6.2).

In conclusion it is seen that the Morison equation provided an excellent model for the Delft measured forces. The inclusion of the Lighthill correction term made very little difference to both the force coefficients and the calculated force spectra.

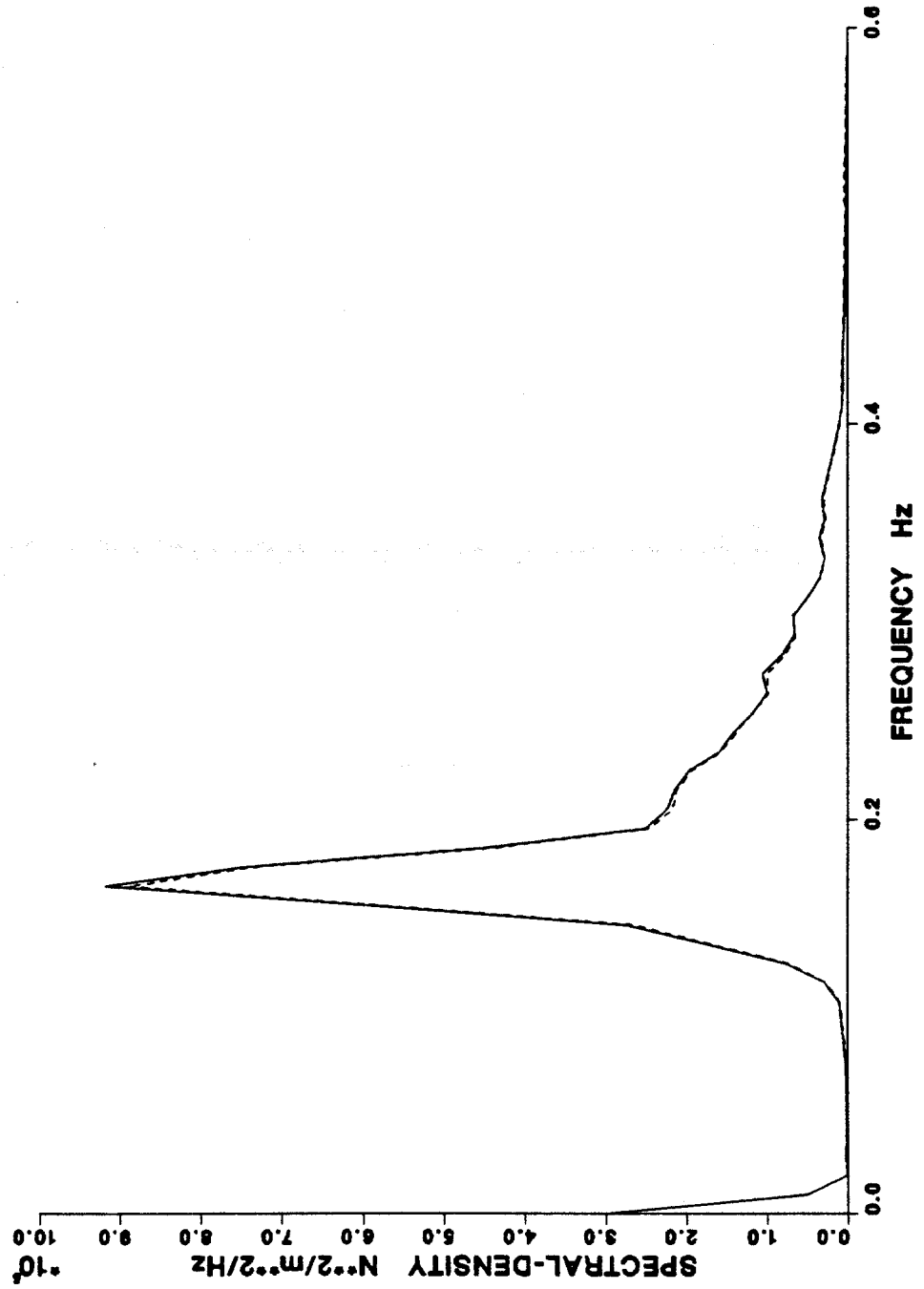

Figure 6.1. Comparison of force spectra, lower level.
[Measured ——, Morison ---].

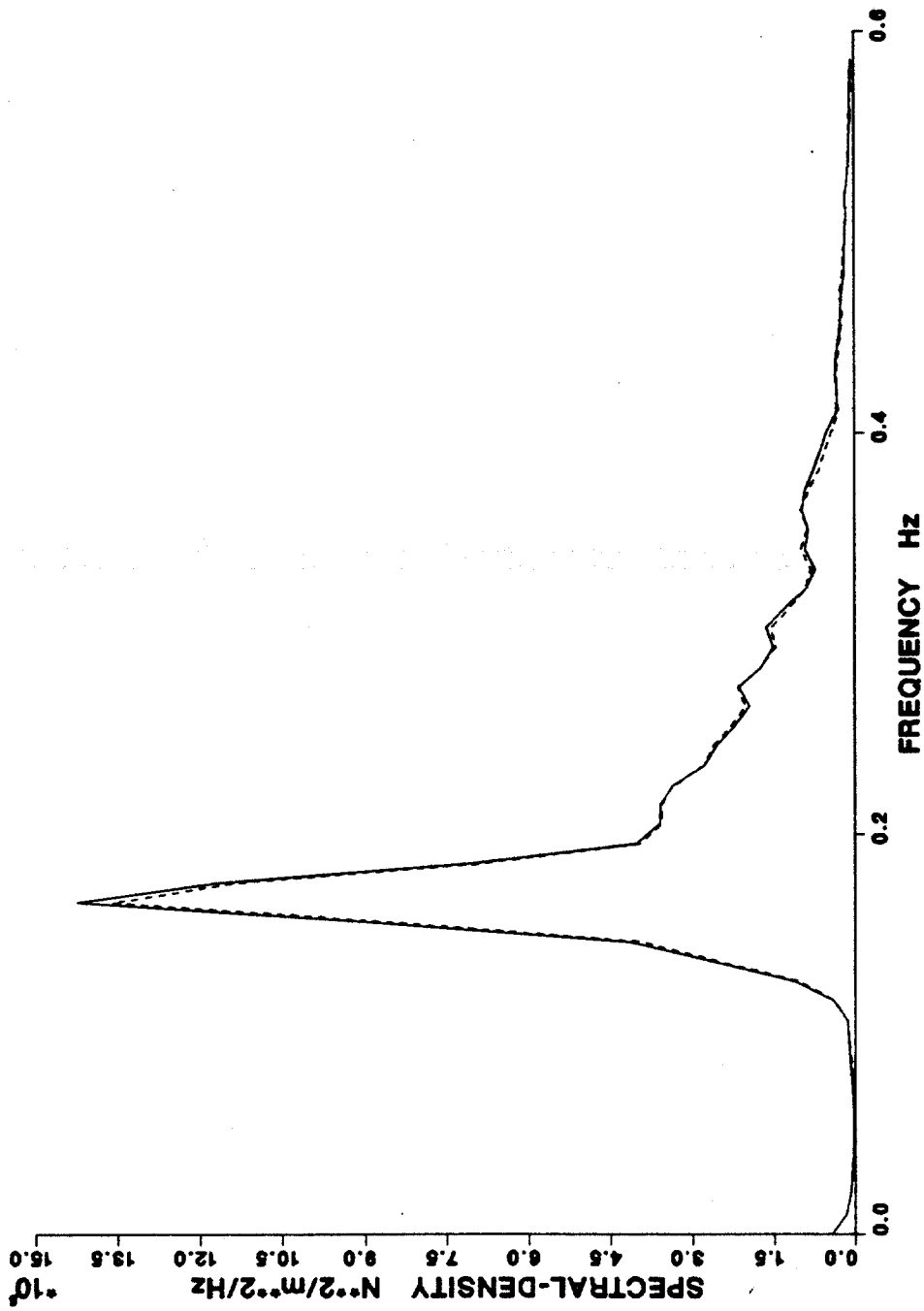

Figure 6.2. Comparison of force spectra, upper level.
[Measured ——, Morison - - -].

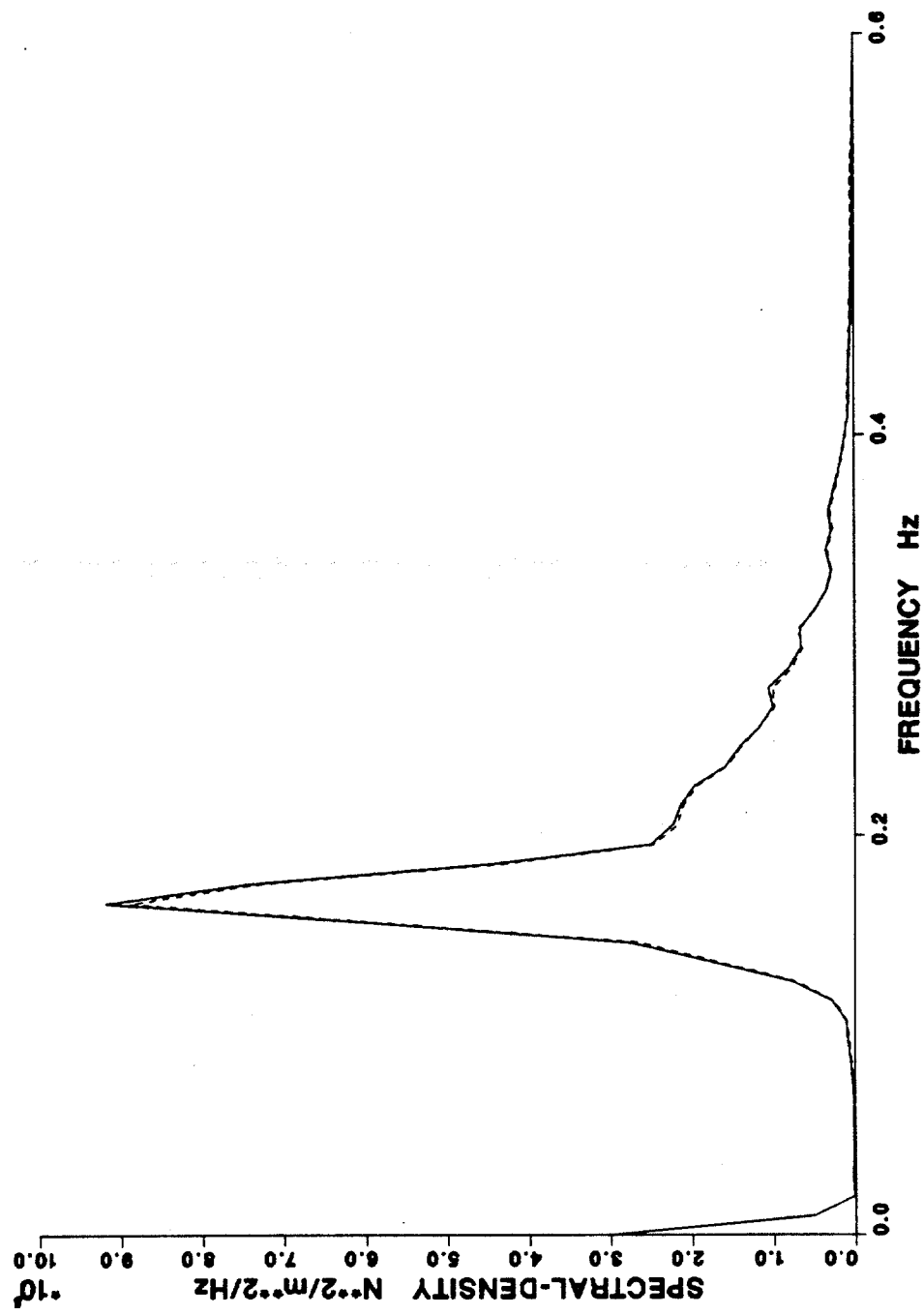

Figure 6.3. Comparison of force spectra, lower level.
[Measured ——, linearized Morison - - -].

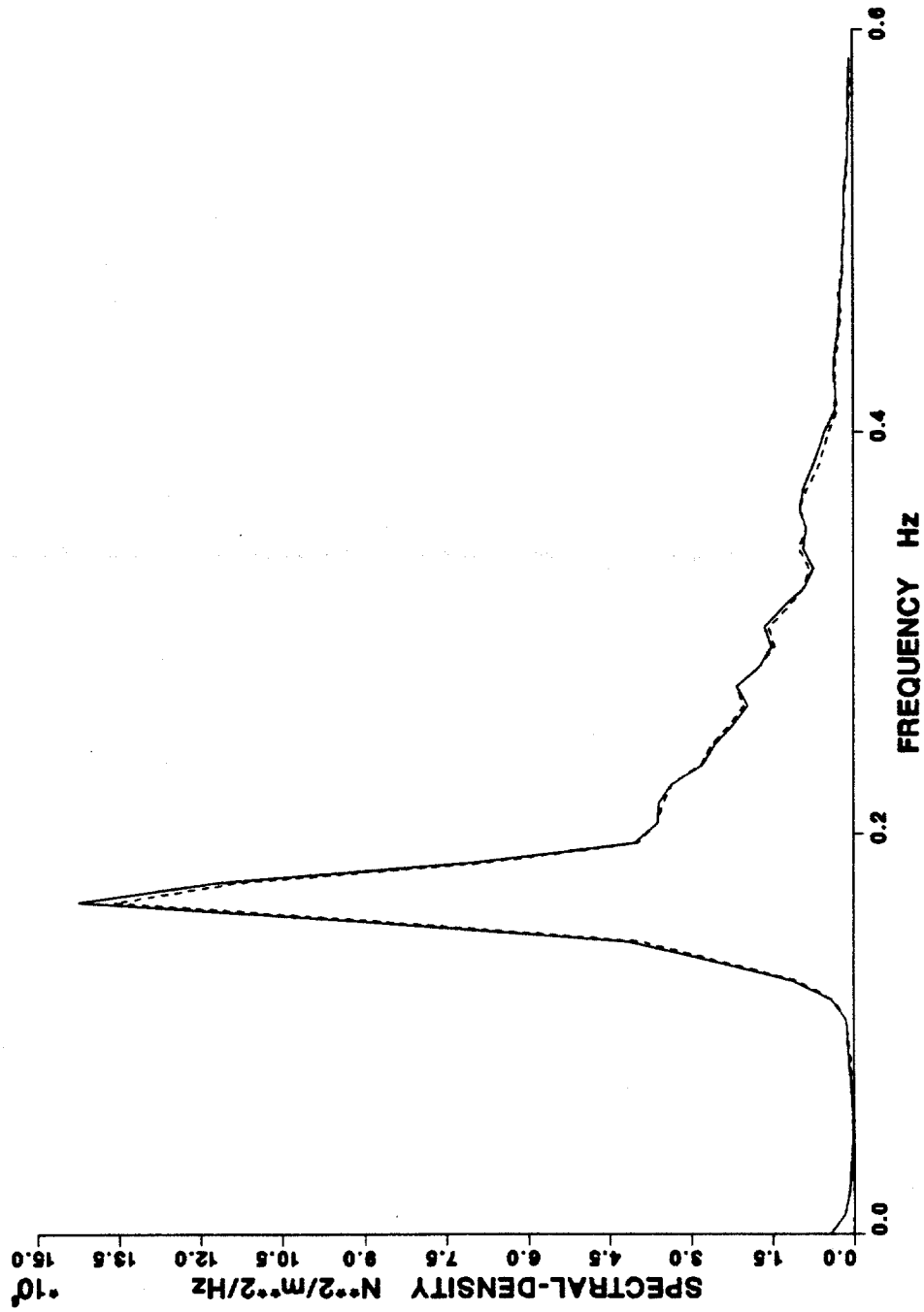

Figure 6.4. Comparison of force spectra, upper level.
[Measured ——, linearized Morison ---].

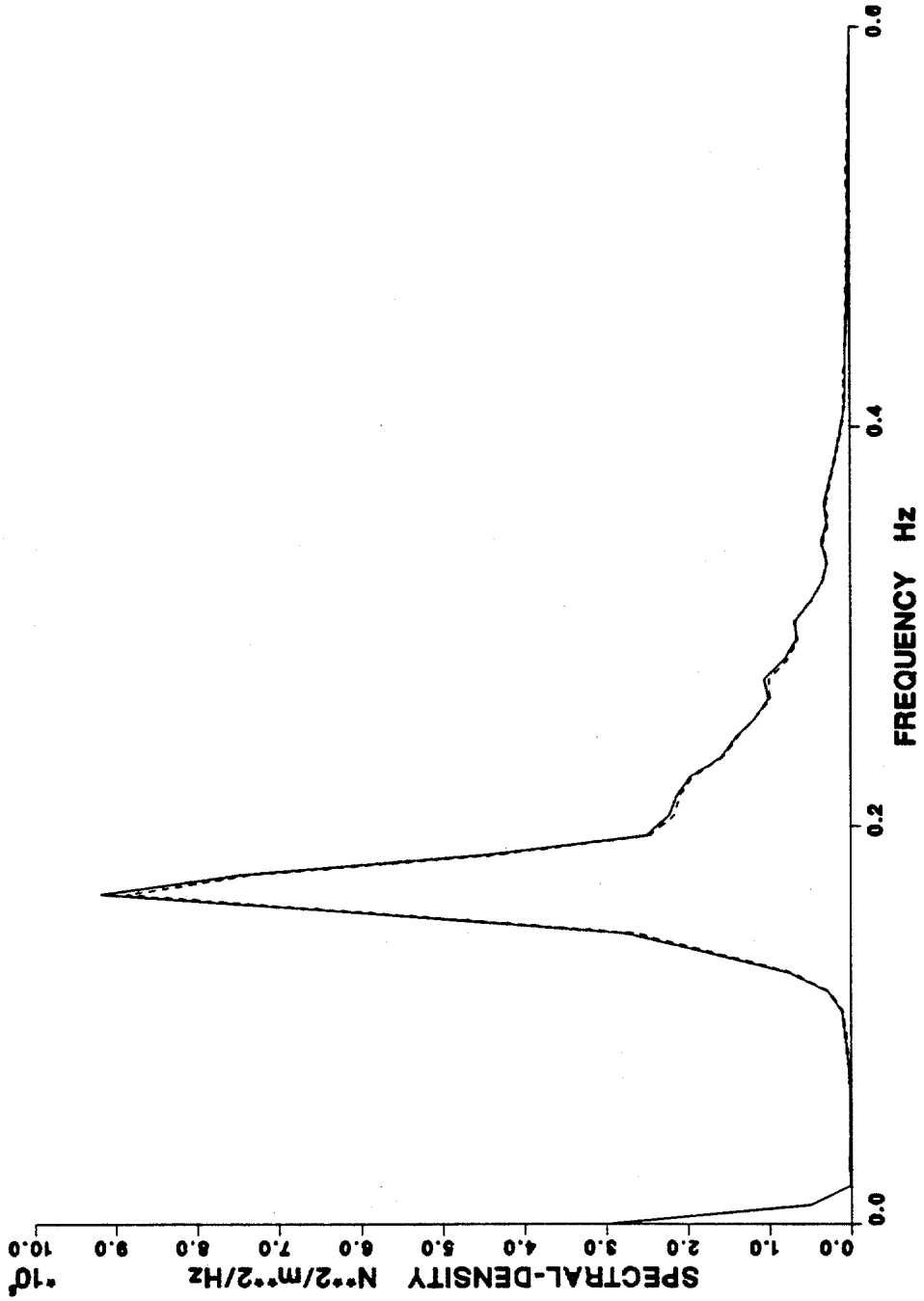

Figure 6.5. Comparison of force spectra, lower level.
[Measured ——, Morison inertia only ---].

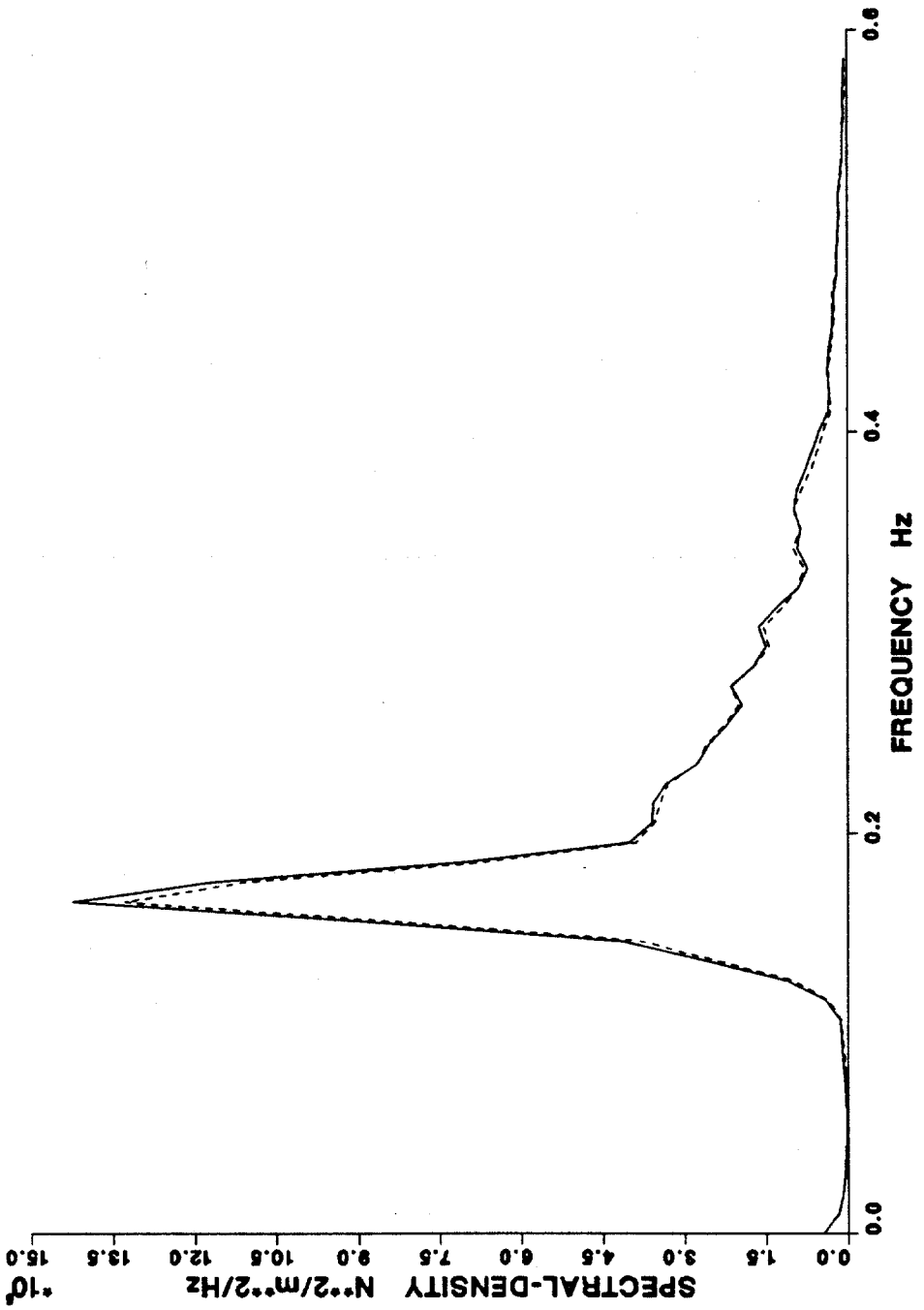

Figure 6.6. Comparison of force spectra, upper level.
[Measured ——, Morison inertia only ---].

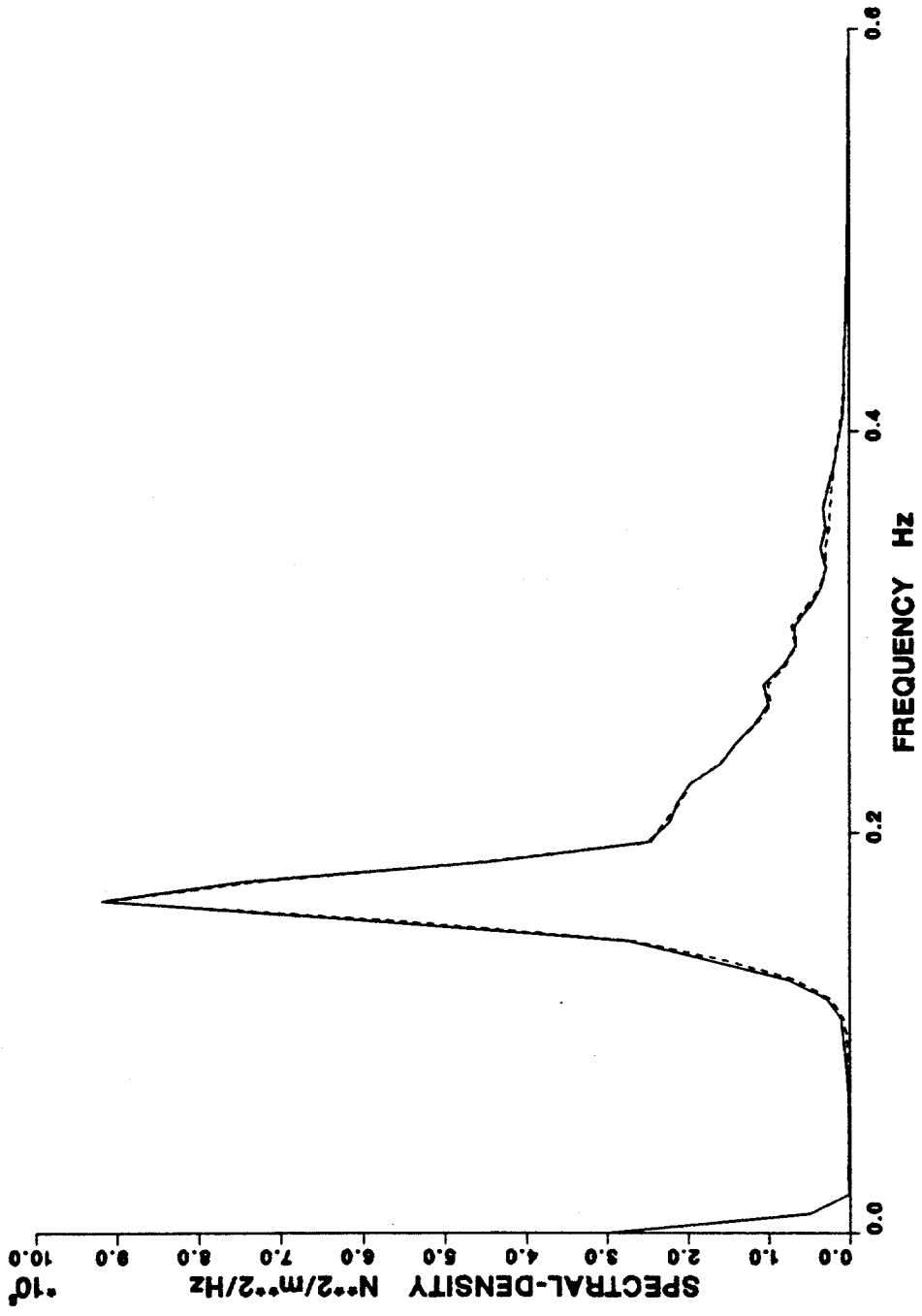

Figure 6.7. Comparison of force spectra, lower level.
[Measured ——, linearized Morison in terms of wave elevation ---].

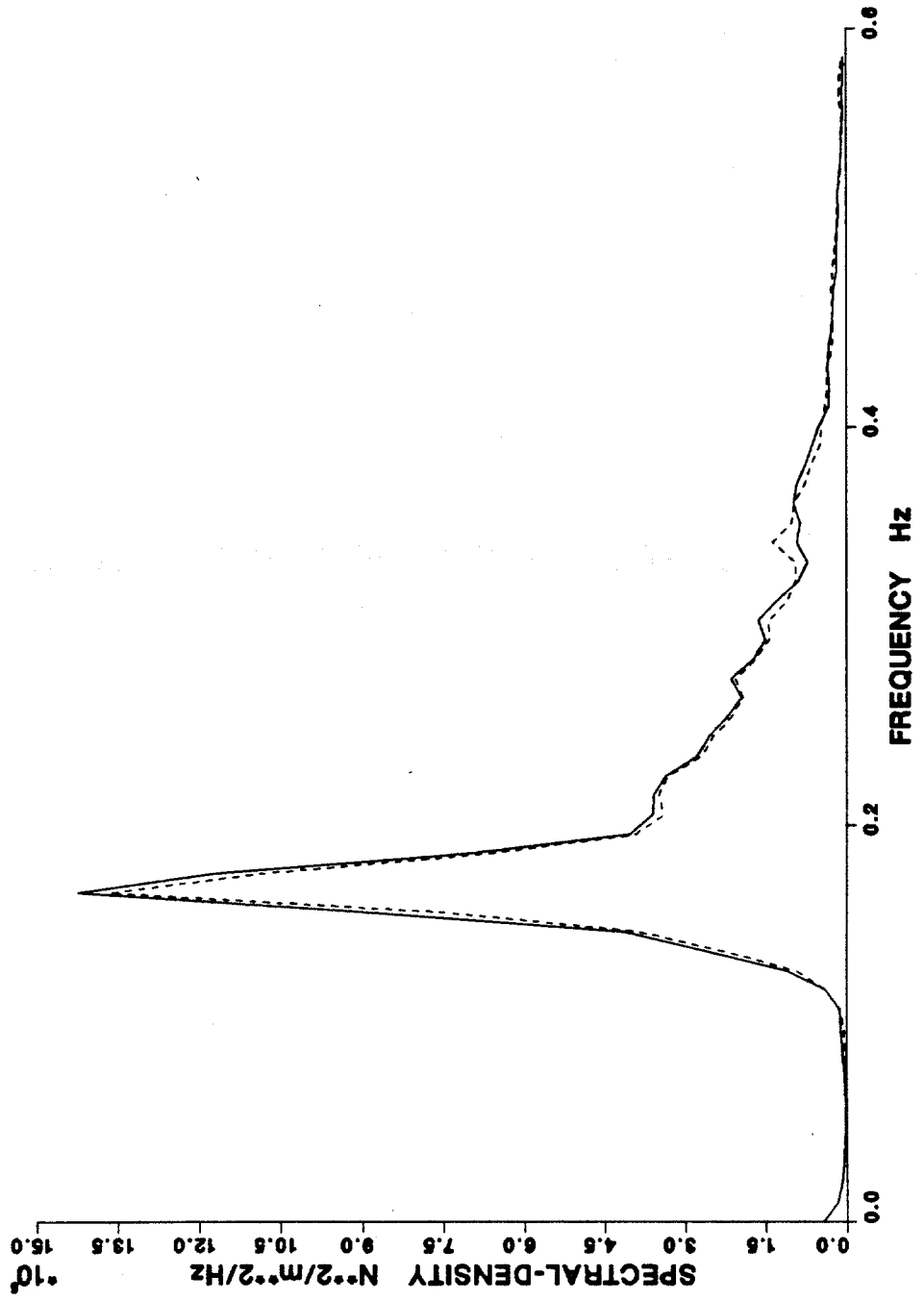

Figure 6.8. Comparison of force spectra, upper level.
[Measured ——, linearized Morison in terms of wave elevation ---].

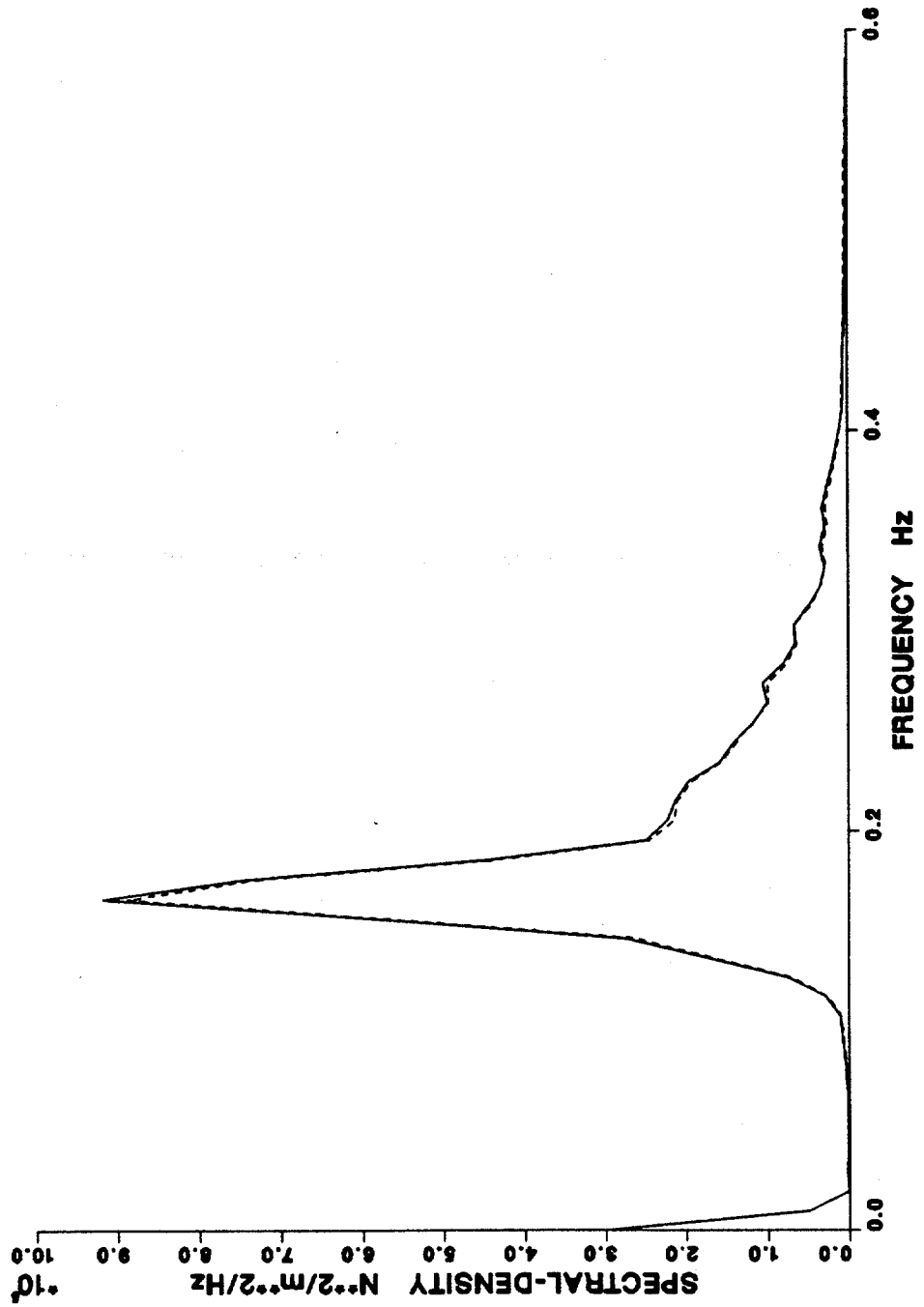

Figure 6.9. Comparison of force spectra, lower level.
[Measured ——, Morison with the Lighthill correction ---].

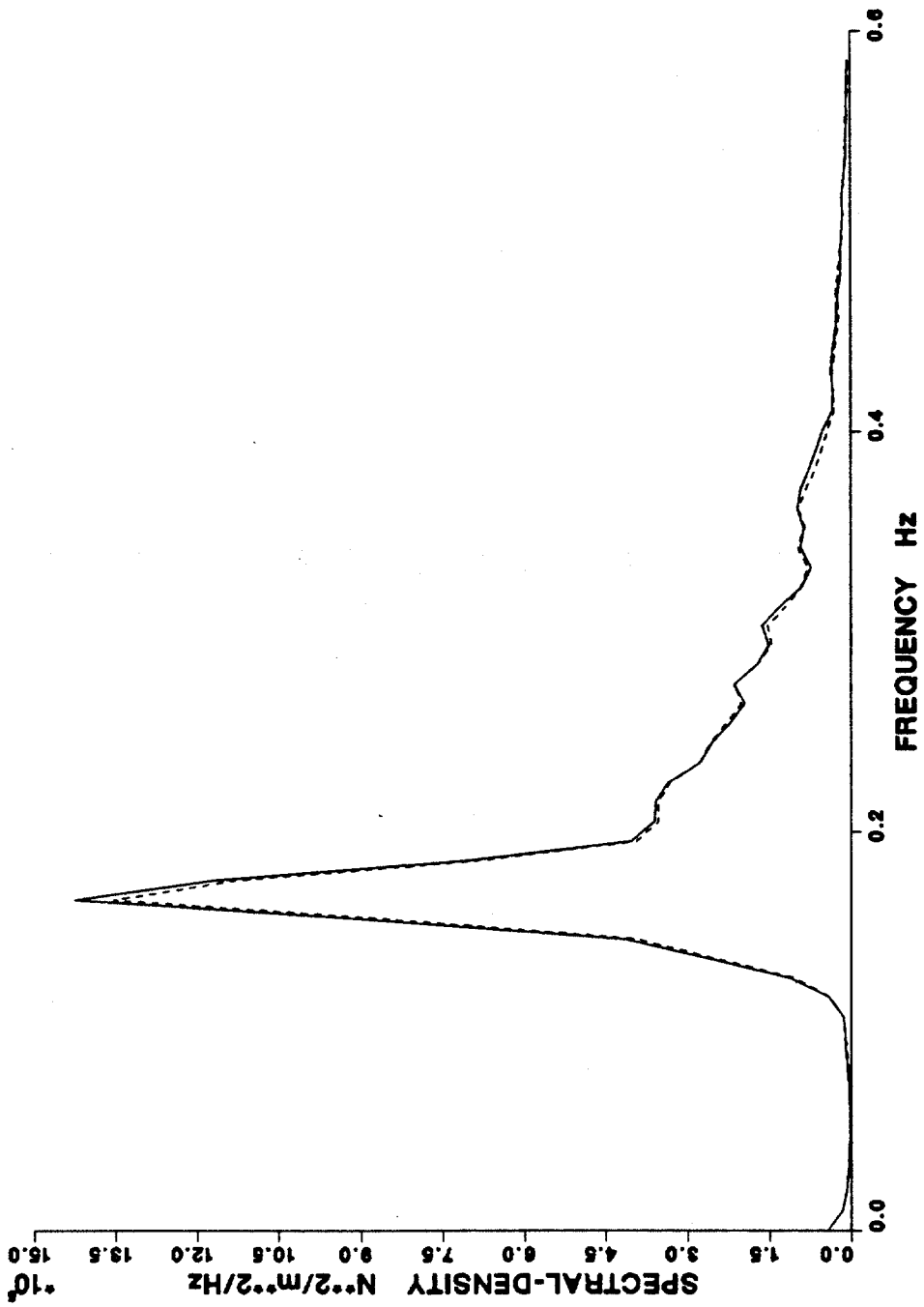

Figure 6.10. Comparison of force spectra, upper level.
[Measured ——, Morison with the Lighthill correction ---].

CHAPTER SEVEN

SUMMARY, CONCLUSIONS AND RECOMMENDATIONS

7.1 Summary and Conclusions

This work presented theoretical and experimental studies of hydrodynamic forces on submerged, slender circular cylinders. The study was undertaken to obtain an improved model for the hydrodynamic forces. Such a model is needed because the extent to which dynamic amplification of tension leg platform motions is significant depends on the hydrodynamic damping supplied by the fluid-structure interaction. Sir James Lighthill argued that the hydrodynamic damping might be estimated incorrectly if the hydrodynamic forces are described by the Morison equation. He developed the outline of a theory for the estimation of a nonlinear correction term of potential origin, that could affect the estimation of the viscous force. This work investigates the significance of the Lighthill correction in quantitative terms and its effect on the viscous and total force on the cylinder.

For non-surface piercing structural elements the Lighthill correction is associated with the dynamic pressure calculated from the Bernoulli equation. The Lighthill correction is derived for the condition of finite water depth in Chapter Three.

Three sets of data were obtained for the analysis. Only two of the sets were sufficiently complete to allow a conclusive analysis to be performed. These two sets of data comprised in-line velocities, in-line forces, transverse forces and wave elevation

for both periodic and random wave flows. The periodic data and the random data were obtained from the Naval Civil Engineering Laboratory (NCEL) and the Delft Hydraulics Laboratory (DHL), respectively.

For the periodic data it was found that both the drag and inertia coefficients had a strong dependence on the Keulegan-Carpenter number. The ranges of the Reynolds number and the β parameter were limited. At low Keulegan-Carpenter numbers the inertia coefficients based on the measured flow properties were greater than the ideal potential flow value of 2.0. The experimental values were also greater than the theoretical values predicted by Sarpkaya (1986) and Bearman et al. (1985).

For both the periodic data and the random data the Morison equation with time invariant coefficients fits the data well over the range of conditions covered in these tests. For the periodic data the Morison equation provided an equally good fit over the whole range of Keulegan-Carpenter numbers investigated. This result is at variance with most other experimental work which has found that the Morison equation is less applicable in the inertia-drag regime ($KC > 6$) where fractional shedding of vortices occurs.

For both the periodic and the random data the Lighthill correction did not improve the performance of the Morison equation significantly and did not alter the drag coefficient to any significant extent for either set of data. For most of the periodic data tests the Morison equation without the Lighthill correction provided a better fit to the measured forces.

A correction for flow separation effects of the type described by Sarpkaya (1981a, 1981b) is also considered. The analysis of the periodic data showed that the difference between the measured and calculated forces (the residue) did not have the third and fifth harmonics of the force being dominant that were identified for one-dimensional flows by both Keulegan and Carpenter (1958) and Sarpkaya (1981). Instead, the best fit for the NCEL data was observed when the residue comprised the second and third harmonics of the force. A significant improvement over the Morison equation was thus achieved but because all coefficients in the correction terms were obtained by a least squares analysis they are only applicable to the NCEL data and cannot be generalized to other types of flow. Conversely, it was found that the universal constants in Sarpkaya's four term Morison equation, which were obtained for one-dimensional flow were not valid for the NCEL tests.

7.2 Future Research

Areas of future research identified in the course of this investigation are:

1) The theoretical estimation of the drag and inertia coefficients at low Keulegan-Carpenter number flows of interest in ocean engineering. A cylinder immersed in an oscillatory flow experiences a force opposing the motion which is usually considered to be composed of three parts, due to

i) the inertia of the accelerating flow (of potential origin),

ii) the influence of the viscous boundary layer and

iii) separation of the boundary layer which leads to the shedding of vortices. This third part is negligible for flows with low Keulegan-Carpenter numbers.

The estimation of the drag and inertia coefficients in this low Keulegan-Carpenter number case involves analytical modeling of the nonlinear boundary layer equation (equation 2.15). At present the theory has only been applied to high frequency flows where the boundary layer equation can be linearized. This linearization has also been used in the work of Sarpkaya (1986) and Bearman et al. (1985) even though it appears that it is not acceptable in the case of ocean flows. The investigation outlined here is expected to explain the large values of the inertia coefficient Cm, and to provide realistic information on the values of the drag coefficient Cd, for low Keulegan-Carpenter numbers.

2) The analysis of pressure distributions around a vertical cylinder immersed in a wave flow. Theoretical expressions and experimental data (such as are provided by the Delft measurements) may be used to investigate pressure distribution patterns inherent in various models and in the data and possible differences between theory and experiment.

3) A statistical analysis of random wave flow data aimed at finding an optimal force model. This can be attempted by using an all-possible-subsets regression analysis on various plausible models, for example by using the Mallows C_p method.

BIBLIOGRAPHY

Batchelor, G.K. (1970). An Introduction to Fluid Dynamics. Cambridge University Press.

Bearman, P. W., Chaplin, J. R., Graham, J. M. R., Kostense, J. K., Hall, P. F. and Klopman, G. (1985). "The Loading on a Cylinder in Post-Critical Flow Beneath Periodic and Random Waves." Behaviour of Offshore Structures (BOSS '85), The Netherlands.

Bearman, P. W., Downie, M. J., Graham, J. M. R. and Obasaju, E.D. (1985). "Forces on Cylinders in Viscous Oscillatory Flow at Low Keulegan-Carpenter Numbers." Journal of Fluid Mechanics, Vol. 154.

Bearman, P. W., Graham, J. M. R. and Singh, S. (1979). "Forces on Cylinders in Harmonically Oscillating Flows." Mechanics of Wave-Induced Forces on Cylinders, (ed. T. L. Shaw), Pitman Advanced Publishing Program, London.

Bendat, J. S. (1983). "Statistical Errors for Nonlinear System Measurements Involving Square-Law Operations." Journal of Sound and Vibration, Vol. 90(2).

Bendat, J. S. and Piersol, A. G. (1982). "Spectral Analysis of Nonlinear Systems Involving Square-Law Operations." Journal of Sound and Vibration, Vol. 81(2).

Bendat, J. S. and Piersol, A. G. (1986). "Decomposition of Wave Forces into Linear and Nonlinear Components." Journal of Sound and Vibration, Vol. 106(3).

Bidde, D. D. (1971). "Laboratory Study of Lift Forces on Circular Piles." Journal Waterways, Harbors and Coastal Engineering Div., ASCE, Vol. 97, No. WW4.

Bishop, J. R. (1978). "The Mean Square value of Wave Force Based on the Morison Equation." National Maritime Institute Report NMI-R-40.

Bishop, J. R. (1979). "R.M.S. Force Coefficents Derived from Christchurch Bay Wave Force Data." National Maritime Institute Report NMI-R-62.

Borgman, L. E. (1967a). "Random Hydrodynamic Forces on Objects." Ann. Math Statist., Vol. 38.

Borgman, L. E. (1967b). "Spectral Analysis of Ocean Wave Forces on Piling." Journal Waterways and Harbors Div., ASCE, Vol. 93, No. WW2.

Borgman, L. E. (1969). "Ocean Wave Simulation for Engineering Design." Journal Waterways and Harbors Div., ASCE, Vol. 95, No. WW4.

Borgman, L. E. (1972). "Statistical Models for Ocean Waves and Wave Forces." Advances in Hydroscience, Vol. 8.

British Ship Research Association (BSRA) (1976). " A Critical Evaluation of the Data on Wave Force Coefficients." BSRA, Wallsend upon Tyne, Contract Report W.278.

Chakrabarti, S. (1980). "In-line Forces on Fixed Vertical Cylinders in Waves." Journal Waterways, Port, Coastal and Ocean Div., ASCE, Vol. 106, No. WW2.

Chakrabarti, S., Wolbert, A. and Tam, W. (1976). "Wave Forces on a Vertical Cylinder." Journal Waterways, Harbor and Coastal Engineering, ASCE, Vol. 102, No. WW2.

Cook, G. R., Kumarasena, T. and Simiu, E. (1986). "Amplification of Wind Effects on Compliant Platforms." Proceedings of a session at Structures Congress '86, ASCE.

Dean, R. G. (1965). "Stream Function Representation of Nonlinear Ocean Waves." J. Geophys. Res., Vol. 70.

Ellix, D. M. (1984). "Second Order Wave Loading on Vertical Cylinders." Ph.D. Thesis, The City University, London.

Ellix, D. M. and Arumugum, K. (1985). "Second Order Wave Loading on Surface Piercing Cylinders." Behaviour of Offshore Structures (BOSS '85), The Netherlands.

Funke, E. R. and Mansard, E. P. D. (1979). "On the Synthesis of Realistic Sea States in a Laboratory Flume." National Research Council Canada (NRCC), Report No. LTR-HY-66.

Funke, E. R. and Mansard, E. P. D. (1984). "The NRCC "Random" Wave Generation Package." National Research Council Canada (NRCC), Report No. TR-HY-002.

Garrison, C., Field, J. and May, M. (1977). "Drag and Inertia Forces on a Cylinder in Periodic Flow." Journal Waterways, Port, Coastal and Ocean Div., ASCE, Vol. 103, No. WW2.

Gaston, J. D. and Ohmart, R. D. (1979). "Effects of Surface Roughness on Drag Coefficients." Civil Engineering in the Oceans IV, ASCE.

Gerstner, F. (1802). "Theorie Der Wellen." Abhandlungen der Koniglichin Bohimschen Gesellschaft der Wissenschaften, Prague.

Hall, P. (1984). "On the Stability of the Unsteady Boundary Layer on a Cylinder Oscillating Transversely in a Viscous Fluid." Journal of Fluid Mechanics, Vol. 146.

Heideman, J. C., Olsen, O. A. and Johansson, P. I. (1979). "Local Wave Force Coefficients." Civil Engineering in the Oceans IV, ASCE.
Hogben, N., Miller, B. L., Searle, J. W. and Ward, G. (1977). "Estimation of Fluid Loading on Offshore Structures." Proc. Institution of Civil Engineers, Vol. 63, Part 2.

Honji, H. (1981). "Streaked Flow Around an Oscillatory Circular Cylinder." Journal of Fluid Mechanics, Vol. 107.

Houmb, O. G. and Overvik, T. (1976). "Parameterization of Wave Spectra and Long Term Joint Distribution of Wave Height and Period." Proc. Behaviour of Offshore Structures (BOSS '76), Trondheim, Vol. 1.

Huang, N. E., Chen, D. T., Tung, C. C. and Smith, J. R. (1972). "Interactions Between Steady Non-Uniform Currents and Gravity Waves with Applications for Current Measurements." Journal of Physical Oceanography, Vol. 2.

Hudspeth, R. T. and Nath, J. H. (1985). "High Reynolds Number Wave Force Investigation in a Wave Flume." Report No. CR 85.004, Naval Civil Engineering Laboratory, Port Hueneme, CA.

Isaacson, M. (1979). "Nonlinear Inertia Forces on Bodies." Journal of Waterways, Port, Coastal and Ocean Div., ASCE, Vol. 105, No. WW3.

Keulegan, G. H. and Carpenter, L. H. (1958). "Forces on Cylinders and Plates in an Oscillatory Fluid." Journal of Research of the National Bureau of Standards, Vol. 60, No. 5.

Korteweg, D. J. and DeVries, G. (1895). "On the Change of Form of Long Waves Advancing in a Rectangular Canal, and on a New Type of Long Stationary Waves." Phil. Mag., 5th Series, Vol. 39.

LeMehaute, B. (1969). "An Introduction to Hydrodynamics and Water Waves, Vol. 2: Water Wave Theories." U.S. Dept. of Commerce, Environmental Science Series Administration, Essa Technical report ERL 118-POL-3-2, Pacific Oceanographic Laboratories, Miami, Fla.

LeMehaute, B. (1976). An Introduction to Hydrodynamics and Water Waves. Springer Verlag, Dusseldorf.

Lighthill, J. (1979). "Waves and Hydrodynamic Loading." Proc. 2nd Int. Conf. on the Behaviour of Offshore Structures BOSS '79, London, Vol. 1.

Lin, C. C. (1957). "Motion in the Boundary Layer with a Rapidly Oscillating External Flow." Proc. 9th International Congress of Applied Mechanics, Brussels, Vol. 4.

McCormick, M. (1973). Ocean Engineering Wave Mechanics. Wiley-Interscience, Wiley.

Milne-Thomson, L. M. (1960). Theoretical Hydrodynamics. (4th edition). The MacMillan Co., New York.

Morison, J. R., O'Brien, M. P., Johnson, J. W. and Schaaf, S. A. (1950). "The Forces Exerted by Surface Waves on Piles." Petroleum Trans., AIME, Vol. 189.

Paterson, A. R. (1983). A First Course in Fluid Dynamics. Cambridge University Press.

Pearcey, H. H. and Bishop, J. R. (1979). "Wave Loading in the Drag and Drag-Inertia Regimes; Routes to Design Data." Proc. of the Behaviour of Offshore Structures Conference (BOSS '79), Vol. 1, London.

Peregrine, D. H. (1976). "Interaction of Water Waves and Currents." Advances in Applied Mechanics, Vol. 16, Academic Press, New York.

Rayleigh, Lord. (1876). "On Waves." Phil. Mag., Vol. 1.

Sarpkaya, T. (1976a). "Vortex Shedding and Resistance in Harmonic Flow About Smooth and Rough Circular Cylinders at High Reynolds Numbers." Report No. NPS-59SL76021, Naval Postgraduate School, Monterey, CA.

Sarpkaya, T. (1976b). "In-Line and Transverse Forces on Smooth and Sand Roughened Cylinders in Oscillatory Flow at High Reynolds Numbers." Report No. NPS-69SL76062, Naval Postgraduate School, Monterey, CA.

Sarpkaya, T. (1976c). "Vortex Shedding and Resistance in Harmonic Flow About Smooth and Rough Circular Cylinders." Proceedings of the International Conference on the Behavior of Offshore Structures (BOSS '76), Vol.1.

Sarpkaya, T. (1976d). "In-Line and Transverse Forces on Cylinders in Oscillatory Flow at High Reynolds Numbers." Proc. of the Offshore Technology Conference, Vol. II, (OTC-2533).

Sarpkaya, T. (1981a). "A Critical Assessment of the Morison Equation." International Symposium on Hydrodynamics in Ocean Engineering, Trondheim.

Sarpkaya, T. (1981b). "Morison Equation and the Wave Forces on Offshore Structures." Report No. CR 82.008, Naval Civil Engineering Laboratory, Port Hueneme, CA.

Sarpkaya, T. (1986). "Force on a Circular Cylinder in Viscous Oscillatory Flow at Low Keulegan-Carpenter numbers." Journal of Fluid Mechanics, Vol. 165.

Sarpkaya, T., and Isaacson, M. (1981). Mechanics of Wave Forces on Offshore Structures. Van Nostrand Reinhold Co., New York.

Schlichting, H. (1960). Boundary Layer Theory. McGraw-Hill Book Co., New York, 4th ed.

Schwartz, L. W. (1974). "Computer Extension and Analytic Continuation of Stokes' Expansion for Capillary-Gravity Waves." Journal of Fluid Mechanics, Vol. 95, No. 1.

Shinozuka, M. and Jan, C. -M. (1972). "Digital Simulation of Random Processes and Its Applications." Journal of Sound and Vibration, Vol. 25(1).

Simiu, E. and Leigh, S. D. (1983). "Turbulent Wind Effects on Compliant Platforms." NBS Building Science Series 151.

Skjelbreia, L. and Hendrickson, J. A. (1960). "Fifth Order Gravity Wave Theory." Proc. 7th Coastal Eng. Conf., The Hague.

Standing, R. G. (1980). "Wave by Wave Analysis of Data from the Christchurch Bay Wave Force Experiment." National Maritime Institute, Report NMI R 86.

Stoker, J. J. (1957). Water Waves. Interscience Publishers, New York.

Stokes, G. G. (1847). "On the Theory of Oscillatory Waves." Trans. Camb. Phil. Soc., Vol. 8, Also Math Phys. Papers, Vol. 1, Camb. Univ. Press, 1880.

Stokes, G. G. (1851). "On the Effect of the Internal Friction of Fluids on the Motion of Pendulums." Camb. Phil. Trans., Vol. IX. Pt. 2.

Tung, C. C. and Huang, N. E. (1973). "Statistical Properties of Wave-Current Force." Journ. of Waterways, Harbors and Coastal Eng. Div., ASCE, Vol. 99, WW3.

Tung, C. C. and Huang, N. E. (1976). "Interactions Between Waves and Currents and Their Influence on Fluid Forces." Behaviour Of Offshore Structures Conference BOSS '76, Tronheim, Vol. I.

Verley, R. (1975). "Wave Forces on Structures - an Introduction." B.H.R.A., Report No. TN 1319.

Vugts, J. H. and Bouquet, A. G. (1985). "A Non-Linear, Frequency Domain Description of Wave Forces on an Element of a Vertical Pile in Random Seas." Behaviour of Offshore Structures (BOSS '85), The Netherlands.

Wang, C. -Y. (1968). "On High Frequency Oscillatory Viscous Flows." Journal of Fluid Mechanics, Vol. 32.